Universita Karlova v Praze

Přírodovědecká fakulta

Studijní program: Imunologie

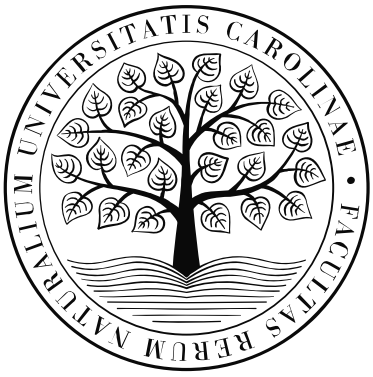

Mgr. Šimon Borna

Regulation of leukocyte signal transduction by membrane adaptor proteins and kinases

Regulace signální transdukce leukocytů membránovými adaptorovými proteiny a kinázami

Doktorská dizertační práce

Školitel:

Mgr. Tomáš Brdička, Ph.D.

Laboratoř leukocytární signalizace

Ústav molekulární genetiky, AV ČR

Praha, 2020

Prohlášení

Prohlašuji, že jsem dizertační práci vypracoval samostatně a že jsem uvedl všechny použité zdroje. Tuto práci, ani žádné její části, jsem nepoužil k získání jiného nebo stejného akademického titulu. Pouze dva experimenty, které jsou uvedené v mé diplomové práci jsou pro úplnost problematiky zahrnuty i zde a je to u nich zřetelně uvedeno.

V Praze, dne 26.02.2020 Šimon Borna

Acknowledgement

I would like to thank to all the people who helped me during my Ph.D. studies. Especially, I would like to thank to Tomáš Brdička for supervising my work on the projects and the thesis. I acknowledge his patience, courage and attitude, which made the time of my Ph.D. study exciting and joyful! Big thank also belongs to all my present and past collages from Laboratory of Leukocyte Signaling and Meri Alberich Jorda and people from her team for help, their contributions to the publications and for making such a great working environment. I would also like to acknowledge people, which collaborated on the projects and people from service groups, who are indispensable for our work. Finally, I would like to thank to my friends and family for your support.

1. Contents

2. Abstract

Signaling pathways must be finely tuned to assign a signal of appropriate strength and duration to the receptor stimulation. Their dysregulation can be very harmful. The consequences of dysregulated signaling pathways vary from autoimmunity, immunodeficiency, and autoinflammation to abnormal proliferation and cancer. In my thesis I aimed to characterize the roles of kinases and membrane associated or transmembrane adaptor proteins in signaling pathways downstream of different receptors.

First, I was comparing the roles of SRC family kinases (SFK) in the initiation of antigen receptor signaling in B cells and in T cells. This effort resulted in the manuscript where we re-evaluated current data, which suggested that SYK can initiate BCR signaling independently of SFK. We show that much lower SFK activity is required for the initiation of BCR signaling than for TCR signaling, but we did not find any evidence for SFK-independent signal transduction. We also found that multiple factors are responsible for setting the higher threshold for SFK activity required to initiate signaling by TCR, including differences between SYK and ZAP-70, structure of the antigen receptor itself and separation of the receptor from transmembrane adaptor LAT, which is a major hub coordinating the formation of TCR signalosome. Based on our data, we propose that TCR detects the SFK activity at multiple levels. We further discuss how multiple level SFK kinase sensing model fits to the current model of TCR signaling and antigen discrimination.

Chemokine receptor CXCR4 is another key leukocyte receptor. It regulates homing and retention of leukocytes and their progenitors in the bone marrow and is essential for proper hematopoiesis. We found that it is negatively regulated by a novel previously uncharacterized transmembrane adaptor protein WW binding protein 1 like (WBP1L) also named Outcome predictor of acute leukemia 1 (OPAL1). WBP1L expression was reported to be upregulated in the most common type of childhood acute lymphoblastic leukemia but its function has been unknown. In the work presented in this thesis, we show that via the recruitment of NEDD4-family ubiquitin ligases WBP1L regulates the expression and activity of CXCR4 and very likely other CXCR4-independent pathways. This way it contributes to the control of migration and other functions of hematopoietic stem cells and hematopoietic progenitors, and to their ability to reconstitute hematopoiesis after bone marrow transplantation. Collectively, our data show that WBP1L regulates hematopoietic processes, which are clinically relevant and may also have consequences for the biology of leukemia.

I have also contributed to the work aiming to characterize the mechanism of how another membrane-associated adaptor protein PSTPIP2 regulates inflammation. Absence of PSTPIP2 in mice leads to the development of autoinflammatory disease chronic multifocal osteomyelitis (CMO). It appears to be caused by dysregulated production of proinflammatory cytokine IL-1β by neutrophils. We found that reactive oxygen species (ROS) production by NADPH oxidase is also severely deregulated in neutrophils from these animals and that blocking NADPH oxidase by genetic deletion of its gp91phox subunit almost completely prevents the bone damage accompanying this disease. These data suggested that dysregulated ROS production is among the major pathophysiological mechanisms behind the autoinflammatory disease in PSTPIP2-deficient mice and may also be relevant for autoinflammatory bone diseases in humans.

Finally, for parts of these projects it was important to have a reliable method for expression of various cDNA constructs in hematopoietic progenitors and in dendritic cells and macrophages differentiated from these cells. The reliable cost-effective protocol we developed for this purpose was published separately and it is also a part of this thesis.

Collectively, the data presented in this thesis demonstrate crucial role of membrane adaptor proteins and kinases in the regulation of leukocyte signal transduction through various receptors. Consequently, they also demonstrate the fact that these proteins influence leukocytes at multiple levels, including their development, migration, and participation in the immune response.

3. Abstrakt

Signální dráhy musí být velmi citlivě nastaveny, aby umožnily přiřadit stimulaci receptoru signál o vhodné síle a trvání. Špatně regulované signální dráhy mohou být velmi nebezpečné. V důsledku špatné regulace signálních drah mohou vznikat autoimunitní onemocnění, imunodeficience, sterilní záněty nebo nekontrolovatelná proliferace buněk a vznik nádorů. V mé dizertační práci se soustředím na roli transmembránových a s membránami asociovaných adaptorových proteinů a kináz v receptorových signálních drahách.

Jako první jsem porovnával role kináz z rodiny SRC (SFK) v iniciaci signalizace přes antigenně specifické receptory B a T buněk. Tato práce vedla k vytvoření rukopisu, kde jsme re-evaluovali recentní studie naznačující, že kináza Syk by mohla iniciovat signalizaci BCR nezávisle na SFK. V naší práci ukazujeme, že iniciace signalizace BCR vyžaduje, na rozdíl od TCR, jen velmi nízkou aktivitu SFK. Signalizaci BCR, která by byla nezávislá na SFK jsme však nepozorovali. Dále ukazujeme, že k iniciaci signalizace přes TCR je potřeba překonat vyšší práh aktivity SFK než u signalizace BCR z několika různých důvodů. Těmi jsou zejména rozdíly mezi kinázami SYK a ZAP-70, rozdíly ve struktuře BCR a TCR a separace TCR a adaptorového proteinu LAT, který je kritickým organizátorem TCR signalozomu. Naše data tedy ukazují, že signalizace TCR detekuje aktivitu SFK na několika úrovních. V naší práci dále diskutujeme, jak zapadá náš model víceúrovňové detekce aktivity SFK do současného modelu TCR signalizace a antigenní diskriminace.

Chemokinový receptor CXCR4 je další velmi důležitý receptor leukocytů. CXCR4 reguluje migraci a zadržování leukocytů a jejich progenitorů v kostní dřeni a je tedy nezbytný pro správnou hematopoézu. Naše práce ukazuje, že CXCR4 je regulován novým dříve necharakterizovaným transmembránovým adaptorovým proteinem WBP1L (WW binding protein 1 like), také označovaným jako OPAL1 (Outcome predictor of acute leukemia 1). Zvýšená exprese proteinu WBP1L byla nalezena v buňkách dětský pacientů s nejčastějším typem akutní lymfoblastické leukémie, ale funkce proteinu WBP1L byla neznámá. V naší publikaci zařazené do této dizertační práce ukazujeme, že WBP1L reguluje pomocí interakce s NEDD4 ubiquitin ligázami expresi a aktivitu CXCR4 a velmi pravděpodobně i další signální dráhy na CXCR4 nezávislé. Tím následně ovlivňuje migraci a další funkce hematopoetických progenitorů a kmenových buněk, včetně jejich schopnosti obnovit funkci kostní dřeně po transplantaci. Naše práce tedy ukazuje, že WBP1L

reguluje důležité procesy spojené s hematopoézou, které jsou klinicky relevantní a důležité i z pohledu biologie leukemií.

Dále jsem během doktorského studia přispěl k publikaci, která měla za cíl charakterizovat mechanismus, jakým membránový adaptorový protein PSTPIP2 reguluje zánět. Absence PSTPIP2 v myším modelu vede ke vzniku autoinflamatorního onemocnění nazývaného chronická multifokální osteomyelitida (CMO). Toto onemocnění je způsobené produkcí prozánětlivého cytokinu IL-1β neutrofilními granulocyty. V naší práci se nám podařilo zjistit, že neutrofilní granulocyty z těchto myší mají kromě toho i zvýšenou produkci reaktivních kyslíkových radikálů (ROS). Umlčením enzymu NADPH oxidáza, který je zodpovědný za produkci ROS, genetickým vyřazením jeho podjednotky gp91phox jsme zabránili zánětlivé destrukci kostí, která je s tímto onemocněním spojená. Tato data tedy ukazují, že deregulace produkce ROS je jedním z hlavních patologických mechanismů autoinflamatorního onemocnění CMO a může být relevantní i pro lidská autoinflamatorní onemocnění spojená s poškozením kostí.

Pro výše zmíněné projekty bylo velmi důležité vytvořit metodiku, která by nám umožnila exprimovat různé cDNA konstrukty v hematopoetických progenitorech a v dendritických buňkách a makrofázích diferencovaných z těchto progenitorů. Naši relativně levnou a efektivní metodiku jsme shrnuli v článku, který je také součástí mé dizertační práce.

Data obsažená v mé dizertační práci ukazují zásadní roli membránových adaptorových proteinů a kináz v regulaci signální transdukce rozličnými receptory leukocytů. Tím také demonstrují skutečnost, že tyto proteiny ovlivňují leukocyty na více úrovních, včetně jejich vývoje, migrace a účasti na imunitní odpovědi.

4. Introduction

4.1. Spatial organization of signal transduction

Cells in every organism represent autonomous units isolated from their surroundings by plasma membrane. In order to communicate with each other or to sense changes in the extracellular space, cells have developed complicated system of receptors and signaling pathways, which translate the information from the extracellular space to the cellular responses such as changes in gene expression, protein stability or cytoskeleton arrangement. Evolution of signal transduction apparats gave rise to many different mechanisms of signal transduction. In immune cells, the signal transduction often uses the system of tyrosine and serine/threonine kinases to transfer the signal over rather short distances and combines this system with enzymes that produce and release messengers such as Ca^{2+}, cAMP or IP_3, which spread the signal throughout the cell.

A spatial organization of molecules participating in signal transduction is a critical mechanism of the regulation of this process. The system is based on highly evolutionarily conserved domains and interacting motifs. Here, I would like to briefly introduce you to several examples relevant for my thesis.

One of these conserved domains is SRC homology domain 2 (SH2) [1-3]. It is a small domain composed of central beta sheet surrounded by two alpha helices on each side, which together form a binding groove with two pockets. The first pocket interacts with phosphorylated tyrosine and the second pocked usually with an amino acid positioned tree residues in the C-terminal direction from the phosphotyrosine [4-7]. Consequently, SH2 domains recognize phosphorylated tyrosines in the context of surrounding residues.

Another typical domain necessary for proper spatial organization of signaling molecules is SRC homology domain 3 (SH3). It is also a relatively small domain, which recognizes and binds to proline rich sequences (PRR) [8, 9]. The interaction is of a rather low affinity [10]. It has been suggested that the lower affinity of SH3 - PRR interaction can be beneficial. It enables short transient interactions, which can mediate first contact between the molecules. The interaction can be further enforced via for example SH2 or another SH3 domain. Alternatively, it can dissociate and immediately interact with other molecules, which can be an advantage if the signal has to be quickly spread [11].

The next example of protein interacting domains are WW binding domains. They are named based on two conserved tryptophan residues present in the sequence [12, 13]. Similarly to SH2 and SH3 domains, they are also relatively small. They are composed of three antiparallel beta sheets [14, 15]. There are four classes of WW binding domains, which interact with slightly different motifs. However, the motifs always contain proline. It is important to note that WW binding motifs are present in immunologically important family of NEDD4 E3 ubiquitin ligases, which regulate protein stability. This represents another mechanism by which signal transduction is regulated [16].

4.2. Antigen specific receptors

4.2.1. Overview

Vertebrates have two types of antigen specific receptors B cell and T cell antigen receptor (BCR and TCR, respectively). In contrast to other immunoreceptors, their specifity is not completely encoded in the genome. The genes coding for antigen specific receptors are composed of several segments, which are assembled in a process of gene rearrangement [17]. The connection of two individual segments is associated with insertion of short random sequences in between them, which increases the variability of the antigen receptor specificity [18-20]. In contrast to majority of TCRs, BCR is able to further undergo process of somatic hypermutation [21-24]. In this process, activation induce deaminase (AID) deaminates cytosine and thus converts it to uracil [25, 26]. The mismatch between uracil and guanine and the presence of uracil in DNA induce error prone DNA repair, which results in changes of the original sequence [27].

Therefore, the process of antigen specific receptor assembly and editing gives rise to an enormous amount of receptors with broad range of specificities. It enables the organism to fight against the wide range of pathogens. Nevertheless, the process of antigen receptor assembly and thus the T or B cell development has to be tightly regulated to prevent autoimmunity. Cells, which successfully rearrange their receptors and prove them to be functional are controlled for reactivity against self-antigens. The autoreactive clones are then deleted in the process of negative selection [28, 29]. This process is particularly important in T cells, because they control B cell responses to antigens, as well as immune responses of many other cell types [30]. Consequently, signaling pathways,

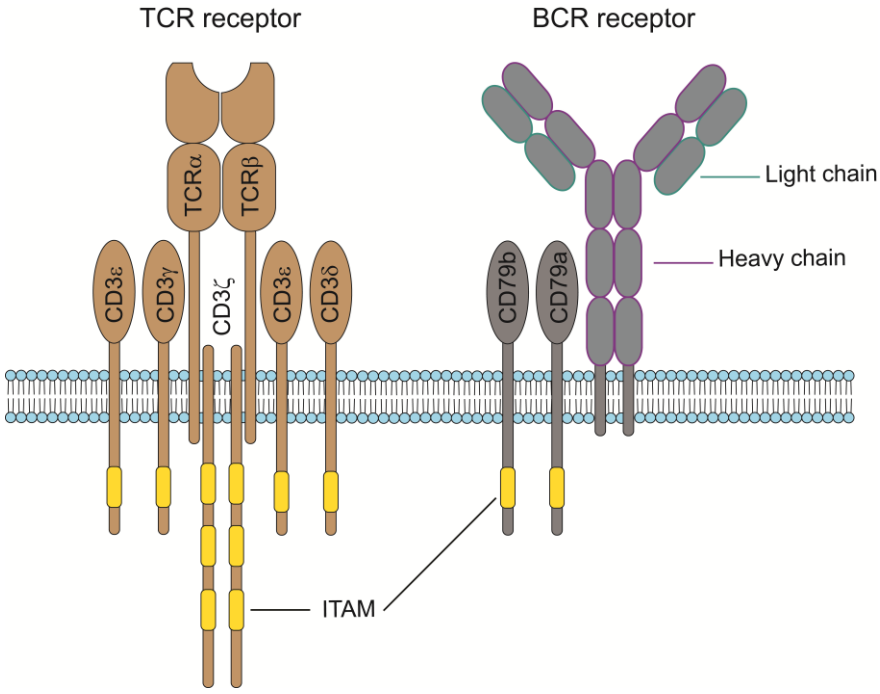

which integrate and translate the signal from the receptors to the immune responses must be precisely regulated.

Figure 1. Composition of BCR and TCR.

4.2.2. BCR and TCR composition

BCR is composed of a surface receptor and non-covalently associated transmembrane adaptor proteins CD79a and CD79b, also known as Igα and Igβ [31]. CD79a and CD79b have similar structure and form disulfide linked heterodimer (Figure 1.) [32]. They have an extracellular immunoglobulin like domain, a transmembrane domain and a cytoplasmic domain containing immunoreceptor tyrosine-based activation motifs (ITAM) [33, 34].

TCR is formed by a surface receptor, which contains two subunits TCRα and TCRβ (in my theses I will focus only on TCRαβ and not on TCRγδ) and non-covalently associated transmembrane adaptor proteins (Figure 1.). These are covalent dimers of CD3γε, CD3δε and TCRζζ, which form barrel like structure around the surface receptors [35]. All CD3δ, γ, ε molecules have similar structure to CD79 molecules. They have an extracellular immunoglobulin-like domain, a transmembrane domain and a cytoplasmic domain with a single ITAM motif. In contrast to CD3 molecules, TCRζ has different structure. It has only a negligible extracellular domain, a transmembrane domain and a longer cytoplasmic domain containing three ITAM motifs [34, 36-39].

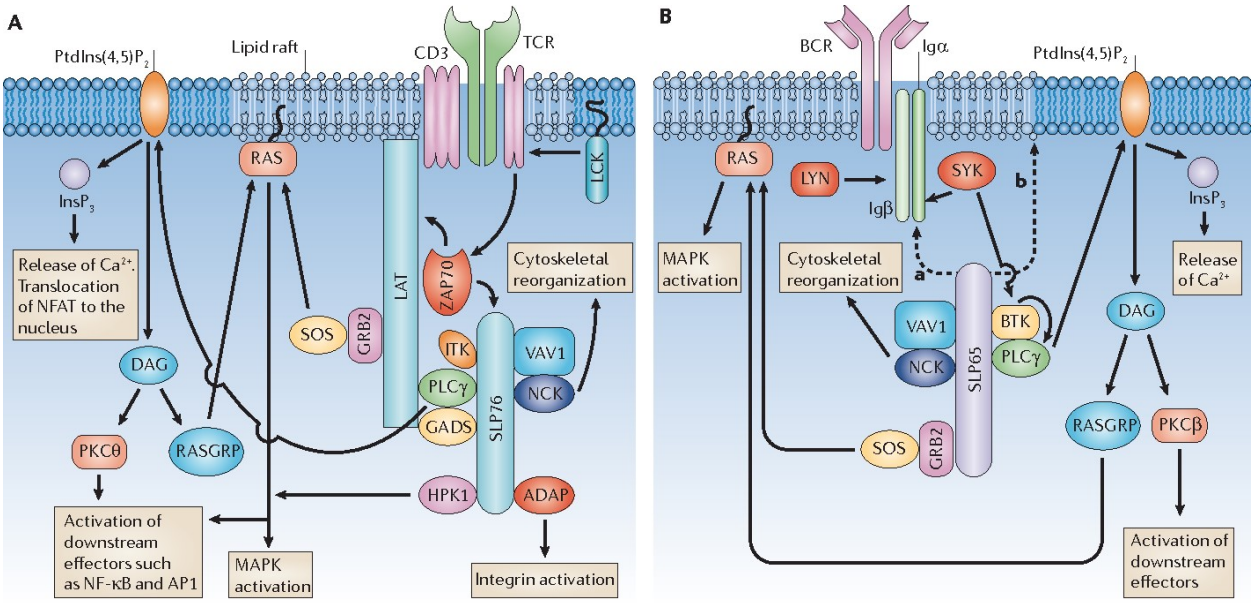

Figure 2. Basic scheme of BCR and TCR signaling. The scheme was adopted from [40].

4.2.3. TCR proximal signaling

TCRs recognize complexes of peptide-MHC molecules on the surfaces of antigen presenting cells. Recent evidence suggests that binding of the peptide-MHC complex induces conformation changes in TCR, which result in an exposure of ITAM motifs [41, 42]. CD4 or CD8 co-receptors also bind to the MHC molecules. Both co-receptors interact with SRC-family kinase (SFK) LCK and via interaction with MHC they bring LCK to the close proximity of the exposed ITAMs [43, 44]. Mainly LCK but also other members of SRC family such as FYN phosphorylate ITAMs. Phosphorylated ITAMs (pITAMs) serve as docking domains for SYK family kinases [45].

This family consists of only two members SYK and ZAP-70. Although ZAP-70 is the main T cell kinase, SYK is also expressed in developing thymocytes and in some T cell populations [46, 47]. They are close homologs with similar structure [48]. They have two tandem SH2 domains connected with a kinase domain by a linker region. In the steady state they are in closed and inactive conformation. Binding to pITAMs leads to a conformational change, which results in their opening and activation. However, to become fully active they have to be further phosphorylated. They are phosphorylated by SFK or by trans-autophosphorylation [49-52]. There are two main regions of their phosphorylation: activation loop of the kinase domain and the linker region. Phosphorylation in the activation loop positively contributes to the kinase activity and

phosphorylation of the linker region stabilizes open conformation [51, 53-56]. Consequently, as it has been reported, the phosphorylation of linker region of ZAP-70 prolongs the interaction of ZAP-70 with pITAMs [57].

Activation of ZAP-70 is crucial for TCR signal transduction [58]. It phosphorylates an accessory transmembrane adaptor protein LAT, which serves as a platform for assembly of PLCγ containing signalosome. Moreover, recent evidence suggests that ZAP-70 in cooperation with LCK brings LAT to the close proximity of TCR [59]. The assembly of signalosome on LAT is the final step of proximal TCR signaling and it results in further propagation of the signal from plasma membrane to the inside of the cell (Figure 2.) [60].

4.2.5. BCR proximal signaling

In contrast to TCR, BCR recognizes soluble antigens. Although the basic scheme of the signaling is very similar to the TCR signaling, there are some interesting differences. According to the current dissociation activation model of BCR signaling, BCRs are present on the plasma membrane in a form of tightly packed oligomers. Antigen stimulation of BCRs leads to their dissociation and exposure of ITAM motifs, which are in turn phosphorylated by SFK [61, 62].
However, the necessity of SFK in the initiation of BCR signaling is not unequivocally established. It is certain that BCR signaling can be initiated even with very low SFK kinase activity. It is well documented on SFK-deficient B cells. Three most expressed SFK in B cells are LYN, BLK and FYN. However, it is important to note that B cells also express small amounts of other SFK members, which could potentially contribute to the BCR signal transduction. LYN deficient B cells respond to BCR stimulation but the signaling is delayed [63]. Moreover, triple deficient $LYN^{-/-}$, $BLK^{-/-}$, and $FYN^{-/-}$ B cells have severe block in early stage of development but they respond to antibody stimulation of CD79 by ITAM and SYK phosphorylation [64]. In line with these experiments, inhibition of SFK activity by small molecular inhibitor PP2 leads to a delay in BCR signaling but does not completely inhibit it. The requirements for SFK activity in the initiation of BCR signaling are dependent on the type or strength of stimulation. When B cells are stimulated with monovalent or weak antigen, the signaling can be inhibited by PP2, while stimulation with more potent antigen cannot be blocked this way [65, 66]. Under some experimental conditions, it has been shown that SYK can phosphorylate ITAM motifs independently of SFK [66-68]. Based

on these observations, it has been suggested that if the stimulation of BCR is multivalent, SYK can activate itself in a trans manner, phosphorylate ITAM motifs and initiate the signaling independently of SFK [66]. Similarly to TCR signaling, activation of SYK is a crucial step in the initiation of BCR signaling, which results in an assembly of complex signalosome on the platform of CD79a and CD79b heterodimer (Figure 2.). Notably, unlike TCR, BCR does not use an accessory transmembrane adaptor protein, which would be similar to LAT, to facilitate assembly of this signalosome [69].

4.3. Adaptor proteins in leukocyte signaling

4.3.1. Transmembrane adaptor proteins

Transmembrane adaptors are group of proteins, which lack enzymatic activity. They are used by other proteins such as kinases or lipases as scaffolds or platforms for assembly of signalosomes of varying complexity. They can be divided into two main groups. The first group contains proteins, which directly associate with receptors such as CD3, CD79, DAP10 or DAP12 [31, 36-39, 70, 71]. The second group is composed of proteins, which do not appear to be directly associated with any particular receptor in the steady state. Those are mainly LAT, PAG, LIME, LAX, NTAL, LST1, SCIMP, PRR7 or WBP1L [72-88]. Nevertheless, it is not always completely clear whether and how tightly are some of these proteins bound to receptors. For example SCIMP has been shown to regulate DECTIN-1 signaling without directly interacting with the receptor. It has been suggested that it interacts with DECTIN-1 only indirectly via tetraspanin-enriched microdomains [89]. On the other hand, it has also been reported that after stimulation with TLR2, TLR3 and TLR4 ligands SCIMP directly interacts with these receptors and regulates their signaling. However, prior to activation, in the steady state, interaction of SCIMP with these receptors is rather weak or non-detectable [90, 91].

All transmembrane adaptor proteins, which do not directly associate with the receptors have very similar structure. They are rather small, monomeric (with the exception of LST1), single membrane spanning molecules. They have very small or no extracellular domain, followed by transmembrane and most likely disordered cytoplasmic domain. Majority of them also have conserved palmitoylation motif CXXC or CXC in the close proximity of the transmembrane domain [74-80, 85-88]. Palmitoylation affects trafficking and localization of these proteins within

the plasma membrane [92-94]. Although cytoplasmic domain is very variable among the members of transmembrane adaptor family, some common types of motifs can be distinguished. LAT, LAX, SCIMP, NTAL, PAG and LIME have tyrosine containing motifs recognized by SH2 domains, as well as proline containing sequences, typical ligands for SH3 domains [74-80, 85, 88]. In contrast, WBP1L and PRR7 have WW domains binding motifs PPXY, which are typically recognized by WW domains of NEDD4 family ubiquitin ligases [86, 87, 95-97].

Although the structure of the transmembrane adaptor proteins is very similar, they participate in different signaling pathways. For example, the best known adaptor protein LAT have a critical role in T cell signaling as discussed above. PAG regulates SFK kinase activity by bridging SFK with their negative regulator CSK kinase [75, 76]. SCIMP is positive regulator of pattern recognition receptors TLR 2,3,4,9 and DECTIN-1 [89-91]. Interestingly, NTAL was reported to have both positive and negative roles in TCR signaling. It was shown that when LAT is present, NTAL acts as negative regulator of TCR signaling and its loss leads to T cell mediated autoimmunity [98]. On the other hand, when LAT is absent NTAL can partially substitute for its loss [99]. Notably, the list of the transmembrane adaptors may be still incomplete and new possible transmembrane adaptor proteins involved in leukocyte signaling may still be identified in protein sequence databases.

4.3.2. WBP1L, ETV6 and human diseases

In my thesis we aimed to discover the function of WBP1L, one of the poorly characterized transmembrane adaptor proteins. Therefore, I would like to highlight previous findings connected to WBP1L that served as initial clues and motivations for the study.

Expression of Outcome predictor of acute leukemia (OPAL1) also known as WW binding protein 1 like (WBP1L) was initially reported to correlate with good prognosis of acute lymphoblastic leukemia in children [100]. Later, it was shown that WBP1L is not an independent marker of good prognosis but its expression rather correlates with *ETV6-RUNX1* translocation [101, 102], which had already been established as a marker of favorable prognosis in leukemia [103]. Nevertheless, if the *ETV6-RUNX1* patients were treated with less aggressive treatment, WBP1L expression still positively correlated with the prognosis [102].

ETV6 gene is coding for transcriptional repressor and *WBP1L* was proven to be its target gene [104, 105]. Interestingly, *ETV6-RUNX1* translocation leads to the disruption of one allele of ETV6 and the second allele is commonly also deleted or inactivated [106, 107]. The loss of function of ETV6 repressing ability explains overexpression of WBP1L in *ETV6-RUNX1* positive leukemias. Notably, *ETV6* mutations are not restricted to acute lymphoblastic leukemia. *ETV6* is also mutated in patients with myelodysplastic syndrome, acute myeloid leukemia or thrombocytopenia [108-112]. Apart from pathological hematopoiesis, ETV6 also has an important function in normal hematopoiesis. This is well documented in ETV6 deficient mice. These mice are dying between embryonic day 10.5 and 11.5. The reasons for premature embryonic death are most likely defects in angiogenesis and intra embryonic apoptosis. However, the embryonic hematopoiesis doesn't seem to be affected by the loss of ETV6 [113]. In order to dissect the role of ETV6 in adult hematopoiesis, Wang et al studied the contribution of ETV6 deficient cells to the development of hematopoiesis in chimeric mice. These mice were prepared by injection of ETV6 deficient stem cells to the blastocyst of wild type animals. Remarkably, ETV6 deficient cells completely failed to contribute to the adult hematopoiesis [114]. Later, the same group further studied the role of ETV6 in hematopoiesis using inducible knock out mice. By several elegant experiments, they demonstrated that ETV6 is a critical regulator of hematopoietic stem cell survival [115].

Sequence analysis of WBP1L revealed similar architecture as structural protein family referred to as Shisa or Shisa-like proteins. The family is composed of proteins, which have conserved unique cysteine-containing motifs in the extracellular domain. WBP1L and other proteins identified by an *in silico* screening approach based on sequence similarities were grouped and named single transmembrane proteins with conserved 6 cysteines. Interestingly, several of these proteins such as WBP1 also have WW binding motifs, which may be recognized by NEDD4 family ubiquitin ligases. Nevertheless, there is little evidence so far about the structure of the extracellular domains or the function of these proteins [116].

4.3.3. Cytoplasmic adaptor proteins

Similarly to transmembrane adaptor proteins, cytoplasmic adaptors have no enzymatic activity and serve as connectors between other proteins. They feature remarkable structural and functional diversity and contribute to signaling pathways of majority if not all known surface receptors. In the following paragraphs I will briefly describe several examples of adaptor proteins that are relevant for publications presented in this thesis.

4.3.3.1. SLP76 and SLP65

SLP76 and SLP65 adaptors are mainly participating in signal transduction downstream of immunoreceptors such as TCR, BCR, NK receptors or Fc receptors. Although they share only 33% sequence homology, they have similar domain organization, starting with several SH2 binding motifs followed by proline rich region and an SH2 domain at the C-terminus [40, 117-121]. In addition, SLP65 has at the N terminus a leucine zipper like domain, not present in SLP76, which is important for SLP65 binding to the plasma membrane [122]. Both SLP65 and SLP76 interact with PLCγ [123, 124]. The interaction is necessary for bringing PLCγ to the proximity of immunoreceptors and consequently for the initiation of calcium response [124-126]. Apart from PLCγ they also interact with several other proteins involved in signal transduction and thus participate as accessory scaffold proteins in the assembly of complex signalosome associated with the immunoreceptors, which is illustrated in detail in Figure 2. [40].

4.3.3.2. MyD88 and TRIF

Other adaptor proteins, including MyD88 and TRIF participate in pattern recognition receptor signaling. Pattern recognition receptors (PRR) recognize structural motifs of both exogenous origin present in molecules associated with pathogens and of endogenous origin present in molecules associated with tissue damage [127-129]. The first identified and the most studied family of PRRs are Toll like receptors (TLR) [129-132]. TLR signaling pathways are initiated through binding of MYD88 and/or TRIF cytoplasmic adaptor proteins to the receptors. Both of them contain Toll/IL-1 receptor (TIR) domains, which mediate the homotypic interaction with the

TIR domain of the receptor. Binding of these adaptors to the receptor mediates signalosome assembly and activation of downstream signaling pathways [133-137].

4.3.3.3. PSTPIP2

In our work we focused on cytoplasmic adaptor protein PSTPIP2, which have not yet been directly connected to any receptor signaling pathway and its loss leads to severe disease in mice. It is a cytoplasmic adaptor protein expressed in myeloid cells [138-140]. However, its protein expression in lymphoid cells have not yet been thoroughly tested. Expression of PSTPIP2 is upregulated by stimulation with proinflammatory molecules such as LPS, INFγ or TNFα [138, 141].

PSTIP2 belongs to the family of proteins containing F-bar domain. It's a curved, banana-shaped domain, which mediates interaction with cellular membranes [142-144]. The remaining part of PSTPIP2 protein contains several interaction motifs, which were shown to mediate interaction with PEST family phosphatases, CSK kinase and SHIP1 phosphatase (Figure 3.) [138, 139, 144]. Nevertheless, till now it has not been clear how are the PSTPIP2 interacting proteins connected to PSTPIP2 function.

The indispensability of PSTIP2 adaptor for the regulation of proinflammatory leukocyte signaling has been well demonstrated in murine models. Two independent papers have described mice, which suffered from autoinflammatory disease caused by the loss or substantially reduced expression of PSTPIP2 [141, 145, 146]. These animals had point mutations in *Pstpip2* gene, either spontaneous [147] or induced by chemical mutagenesis [141]. The mouse strain with the complete loss of PSTPIP2, named *Pstpip2*^{cmo}, was further used in the majority of experiments reported in the literature. The *cmo* abbreviation in the strain's name stands for chronic multifocal osteomyelitis, the name of the disease these mice suffer from. It is manifested by sterile inflammation of paws, tails and occasionaly ears, and severe bone destruction in the affected tissues. The disease can be transferred by bone marrow transplantation, which proves its hematopoietic origin. It also develops in RAG deficient mice, which lack adaptive immunity. These data suggests that its primarily induced by myeloid cells [141, 146].

Pstpip2^{cmo} mice have elevated levels of several proinflamatory cytokines and among them IL-1β was shown to play crucial role in disease development. The major source of active form of IL-1β

in CMO mice are neutrophils [148-150]. However, it is unclear what receptor, if any, stimulates these cells to produce excessive amounts of IL-1β. Recent evidence suggest that microbiota play a role in priming of CMO neutrophils, since CMO disease can be prevented by microbiota-affecting diet, antibiotics or microbiota transplantation [148].

PSTPIP2 was shown to negatively regulate Fc- receptor and TLR signaling pathways as well as signaling initiated by silica treatment [138]. Nevertheless, there is no evidence of direct or indirect interaction of PSTPIP2 with these receptors. Therefore, the precise mechanism of how PSTPIP2 regulates signaling pathways and thus prevents autoinflammation remains to be discovered.

4.4. NEDD4 family ligases in leukocyte signaling

NEDD4 family ligases are a group of proteins, which share similar domain organization. They are composed of N terminal C2 domain, which mediates interaction with lipids, several WW binding domains and C terminal HECT catalytic domain. Similarly, to other E3 ubiquitin ligases, they transfer ubiquitin to the lysines of targeted proteins or to another ubiquitin to generate polyubiquitin chains. There are several different types of ubiquitin chains based on the position, where additional ubiquitins are added to the growing polyubiquitin chain. However, NEDD4 family ligases seem to make predominantly chains, which tag proteins for the proteasome degradation [151].

The family of NEDD4 ubiquitin ligases is composed of 9 members in humans, of which 8 are also conserved in mice. The NEDD4 family members are NEDD4, NEDD4L, NEDL1, ITCH, WWP1, WWP2, SMURF1 and SMURF2 [97]. Several reports suggest that they share common mechanisms of regulation, though not all of the mechanisms have been shown in each member of the family and, thus, several related models of their regulation have been suggested (Figure 3.) [151].

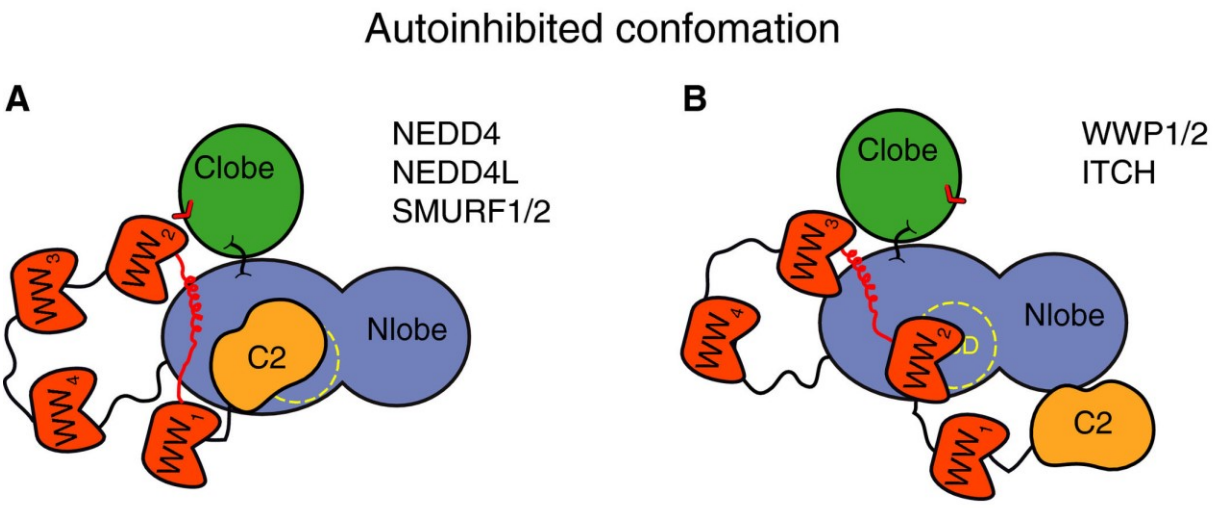

Figure 3. Visualization of two models of autoinhibited conformation of NEDD4 family ubiquitin ligases. Each model lists members, which are suggested to adopt the particular conformation. Image was adopted from [151].

In the steady state, they are in the cytoplasm in closed and inactive conformation. The closed conformation is maintained by the interaction between the linker region separating neighboring WW binding domains and a HECT domain [152]. The C2 domain has also been suggested to participate in this intramolecular interaction by binding the HECT domain [153, 154]. Moreover, the closed conformation can be further stabilized by an intermolecular interaction of WW binding domain with LPXY motif or other motifs within the HECT domain (Figure 3.) [155, 156]. Binding of WW domains to their binding motifs present in substrates, C2 binding to lipids or phosphorylation can induce separation of WW domains and C2 domain from HECT domain and a switch to active open conformation [152, 153, 155-158]. The active NEDD4 ligases ubiquitinate substrates. Often, they also undergo auto-ubiquitination, which couples their activation to their own degradation [151, 152].

The function of NEDD4 family ligases is pleotropic, ranging from neuromuscular development to immune cell signaling [159, 160]. Moreover, several members were suggested to have overlapping functions. For example, expression of a chemokine receptor CXCR4 was shown to be regulated by at least two members of NEDD4 family ligases ITCH and WWP1 [161-163]. Deficiencies of NEDD4 family E3 ligases in mouse models result in varied phenotypes. Probably the most striking immunologically relevant one has been observed in mice lacking NEDD4 family member ITCH.

These mice develop autoimmune condition characterized by pulmonary inflammation and constant itching. The chronic inflammation leads to premature death [164, 165]. Similarly to other E3 ligases, ITCH has numerous substrates and, thus, the autoimmunity does not seem to have a single disease causing mechanism [166]. However, at least part of the mechanism was explained by ITCH ability to ubiquitinate and thus mark for the degradation transcriptional factor JunB in T cells. Loss of ITCH and thus upregulation of JunB leads to T cell polarization to Th2 phenotype observed in Itchy mice. Th2 T cells produce IL-4 and IL5, which stimulate B cells to produce IgE and IgG1 antibodies, which can cause allergy like response presented with skin itching via Fc- receptor induce degranulation of myeloid cells such as mast cells, basophils or eosinophils [167].

4.5. CXCR4 signaling and biology

CXCR4 is a G-protein coupled chemokine receptor, which seven times spans plasma membrane. It also is one of the receptors used by HIV virus to enter the cell [168-170]. Its canonical ligand is stromal cell derived factor 1 (SDF-1) also known as CXCL12 [171-173]. Alternative spicing of *SDF-1* gene gives rise to six different isoforms of the protein named SDF-1α, SDF-1β, SDF-1γ, SDF-1δ, SDF-1ε and SDF-1φ [174, 175]. They have different properties, including different life span and expression pattern [176]. However, they all stimulate CXCR4 [175].

CXCR4 stimulation leads to an activation of several signaling pathways, which are usually divided into two groups. The first group of signaling pathways are initiated via activation of trimeric G proteins, which activate PLCβ and thus induce calcium response, inhibit adenylate cyclase or activate PIP3 kinases and, consequently, AKT signaling pathway. The second group of signaling pathways are G protein independent. These are JAK/STAT or MAPK signaling pathways [177, 178].

Experiments with CXCR4 deficient mice revealed pivotal role of CXCR4 in homing and retention of hematopoietic cells in the bone marrow. However, these mice died perinatally, because of cardiac defects, which made research on the role of CXCR4 in adult hematopoiesis difficult [179]. Initially, it could only be studied in animals transplanted with fetal liver cells from CXCR4 deficient mice. The resulting chimeras were not able to retain immature progenitors in the bone marrow and consequently increased numbers of progenitors were found in blood [180].

Interestingly, the number of hematopoietic stem cells in CXCR4 deficient mice was increased. Moreover, these cells were shown to be hyperproliferative in culture and this hyperproliferation could be inhibited by addition of SDF-1 [181]. Further experiments with SDF-1 and CXCR4 deficient mice or WHIM mice (discussed below) have also shown that CXCR4 regulates early B cell development [182, 183]. These data suggest that CXCR4 signaling also has functions independent of cell migration.

Opposite effect on hematopoietic cell migration is observed in patients with mutations of C terminal tail of CXCR4 [184]. These mutations can prevent internalization and desensitization of CXCR4 required for proper termination of its signaling. Consequently, the patients have low blood cell counts and particularly profound defect in B cell mediated immune response [185]. It leads to the development of Warts, Hypogammaglobinemia, Infections and Myelokathexis (i.e. retention of myeloid cells in the bone marrow), collectively reffered to as WHIM syndrome [186]. However, WHIM syndrome should be rather understood as an extreme example of CXCR4 hyperactivation. Milder upregulation of CXCR4 activity does not necessarily lead to such a strong phenotype. For example, mice deficient in adaptor protein MIM, which have upregulated CXCR4 expression, show enhanced leukocyte migration toward SDF-1 but no peripheral lymphopenia [187, 188]. It should be noted that MIM affects not only CXCR4 signaling but also several other signaling pathways [188]. Therefore, the phenotype of these mice may be also affected by CXCR4 independent mechanisms.

5. Aims of the study

In my thesis, I aimed to characterize the roles of adaptors and kinases in signal transduction of immune cells. Clearly, in a single thesis one cannot cover all the adaptors, kinases and signaling pathways regulating immune system. Therefore, I together with my colleagues and collaborators focused on those that are part of the long term research line of our laboratory. I believe that understanding the molecular mechanisms behind the immune system regulation is the basic prerequisite for the development of therapies to human diseases. In the following text, I will describe questions and problems we wanted to solve and also briefly clarify the connections to their potential impact on human medicine, before discussing individual projects in more detail.

The first project aimed to characterize the role of SFK in the initiation of BCR and TCR signaling. As mentioned in the introduction, TCR and BCR have different requirements regarding the amount of SFK activity necessary to initiate the signaling. It is particularly interesting, because both signaling pathways use similar scheme or mechanisms of signal transduction. It has been believed that in contrast to ZAP-70, SYK kinase can phosphorylate ITAMs and thus initiate the signaling independently of SFK. However, this hypothesis has not yet been sufficiently supported by the experimental evidence. Therefore, the main questions behind this project were: Can SYK phosphorylate ITAMs and thus induce signaling independently of SFK? If not, what are the other mechanisms responsible for the resistance of BCR signaling to SFK inhibition? Or if we look at the same issue from the different angle. What are the SFK-sensing mechanisms in TCR signaling, which make the TCR signaling hypersensitive to SFK inhibition? Detailed understanding of antigen specific receptor signaling is the basic perquisite for the development of therapy of B and T cell-mediated autoimmunity and immunodeficiency or for the development of chimeric antigenic receptors for cancer therapy.

The second project aimed to discover the function of previously uncharacterized gene *WBP1L*. It codes for transmembrane adaptor protein overexpressed in the most common type of acute lymphoblastic leukemia in children. Its expression is regulated by ETV6 repressor, which regulates stem cell survival and is often mutated in cancer. Moreover, analysis of *WBP1L* coding sequence predicts several binding sides for NEDD4 family ubiquitin ligases. Therefore, the main question of this projects were: Does WBP1L interact with NEDD4 family ubiquitin ligases? What are the signaling pathways regulated by WBP1L? Does WBP1L regulate hematopoiesis? Does WBP1L

functions overlap with the function of ETV6 in hematopoietic stem cells? What is the potential impact of WBP1L function on the biology of leukemia?

The third project focuses on the role of cytoplasmic adaptor protein PSTPIP2 in the development of chronic multifocal osteomyelitis (CMO). It is well documented that the loss of PSTPIP2 causes the CMO disease in mice. However, it is not completely clear, what signaling pathways apart from pathways downstream of inflammasome/IL-1β cause the disease and how they are regulated by PSTPIP2. In our work, we aimed to connect PSTPIP2 to the signaling pathways regulating neutrophil biology and analyze the impact of this regulation on the disease development. We believe, that connecting neutrophil signaling pathways to the disease manifestation can help us find targets for therapy in related autoinflammatory diseases in humans.

In the fourth project, we aimed to establish and optimize a method allowing expression of fluorescently tagged proteins in macrophages and dendritic cells. We do not expect any clinical impact of his method. Nevertheless, we have successfully used this method in both PSTPIP2 and WBP1L projects and it continues being indispensable in our studies of localization of intracellular proteins in living cells.

6. Results and discussion

6.1. Differential threshold for sensing Src-family kinase activity by B cell and T cell antigen receptors.

This study is a continuation of my previous work summarized in my diploma thesis. Since majority of the experiments described here and in the manuscript attached below were completed during my Ph.D. studies, I have included the manuscript in my doctoral thesis. Here I am briefly clarifying which of the experiments described below were part of my diploma thesis and what is their relationship to my Ph.D. work. First, in my diploma thesis, I have selected suitable cell lines that show similar resistance/sensitivity to SFK inhibition as cells used in earlier studies and I measured sensitivity of their calcium response to PP2 (chapter 6.1.1. below). I also generated Jurkat-derived P116 cells expressing SYK and ZAP-70 and performed calcium response measurements with these cells. However, because of the instability of the constructs presented in the diploma thesis, I had to make new cDNA constructs coding for SYK and repeat all these experiments within my Ph.D. work. Thus, the original diploma thesis data are not included in the manuscript (chapter 6.1.2., first paragraph). Finally, the experiments with CD16-TCRζ fusion protein (chapter 6.1.4., first paragraph) were part of my diploma thesis and remained in the manuscript. For the sake of clarity and comprehensibility, I have included descriptions of all these data in the following chapters. There were additional data on this topic in my diploma thesis that did not become part of the manuscript and these are not described here.

6.1.1.Experimental model

In this study we have decided to perform all the experiments in human T cell line Jurkat and B cell line Ramos. The main reason for using cell lines and not primary cells was that cell lines enable us to better distinguish true causes from mere correlations, because it is possible and affordable to delete genes in these cells as required and transduce these cells with variety of different constructs. Moreover, both cell lines are well established in the field of TCR and BCR signaling. Our initial experiments demonstrated that the results of earlier studies on other cell lines and primary T cells and B cells [65, 66] can also be reproduced in Ramos B cell line and Jurkat T cell line. TCR signaling initiated by antibody mediated TCR crosslinking in Jurkat cells was inhibited by 2μM

concertation of PP2, while BCR signaling in Ramos cells was resistant to at least ten times higher concentration, though the signaling had delayed kinetics. The delay was proportionate to increasing concentration of PP2.

6.1.2. SYK expression lowers the dependence of TCR and BCR signaling on SFK

To test whether SYK can induce signaling independently of SFK. We took advantage of Jurkat derived T cell line P116, which is deficient in expression of both SYK and ZAP-70 [189]. We transduced these cells with retroviral vectors coding for SYK or ZAP-70. Throughout the study we used the constructs where the cDNA of the gene of interest was attached to a reporter gene via internal ribosomal entry side (IRES). Thus, the reporter gene expression allowed us to indirectly gate and sort for cells with particular expression of the gene of our interest. We stimulated the P116 SYK and P116 ZAP-70 cells with anti TCR antibody in the presence or absence of different concentrations of PP2 and monitored the calcium response by flow cytometry (FACS). We gated on similar expression of SYK and ZAP-70 as we found in Ramos and Jurkat cells. Interestingly, P116 SYK cells were more resistant to SFK inhibition than P116 ZAP-70 cells but the standard dose of PP2 (10μM), which is commonly used to prove involvement of SFK in signaling pathways, completely inhibited TCR signaling in these cells.

Next, we complemented these results with a similar experiment in B cells. However, SYK deficient B cell line had never been prepared before. Therefore, we inactivated SYK-coding gene in Ramos cells using CRISPR-Cas9, which we delivered to the cells by lentivirus, generating R.SYK^{KO} cells. We transduced R.SYK^{KO} cells with ZAP-70 or CRISPR-Cas9 resistant SYK, which we prepared by codon optimization. Similarly to previous experiment we stimulated R.SYK^{KO}-SYK or R.SYK^{KO}-ZAP-70 cells with anti BCR antibody in the presence or absence of different concentrations of PP2. R.SYK^{KO}-SYK cells reacted to SFK inhibition similarly as Ramos cells, showing resistance to at least 20μM PP2. In contrast, R.SYK^{KO}-ZAP-70 cells were resistant to 10μM concentration of PP2, but 20μM concertation of PP2 completely inhibited the signaling. Collectively, these data show that in contrast to ZAP-70, SYK can partially compensate for the loss of SFK activity. However, it cannot fully explain the different level of SFK activity required to initiate BCR or TCR signaling.

6.1.3. SYK ability to phosphorylate ITAMs does not contribute to the increased resistance of SYK expressing cells to SFK inhibition.

The previous studies have suggested that SYK can phosphorylate ITAMs and thus initiate signaling independently of SFK [66-68]. To test whether the difference between SYK and ZAP-70 expressing cells in their resistance to SFK inhibition is caused by the ability of SYK to phosphorylate ITAMs, we probed CD79a phosphorylation in R.SYK^{KO}-SYK, R.SYK^{KO}-ZAP-70 or control R.SYK^{KO} cells transduced with empty vector stimulated by anti BCR antibody in the presence or absence of 20μM concentration of PP2. We used concentration of PP2, which inhibited R.SYK^{KO}-ZAP-70 cell signaling but not R.SYK^{KO}-SYK cell signaling. We used two independent methods to probe CD79a phosphorylation. We immunoprecipitated CD79a and stained for all phosphotyrosines present in the immunoprcipitate (i.e. presumably also those of CD79b, which forms covalent dimers with CD79a) or we probed phosphorylation of one of the CD79a ITAM tyrosines by phosphospecific antibody in total cell lysates. Both approaches resulted in similar outcome. CD79 phosphorylation was higher in the cells transduced with SYK or ZAP-70 than in control cells. Interestingly, this phosphorylation was consistently higher in BCR stimulated R.SYK^{KO}-ZAP-70 than in R.SYK^{KO}-SYK regardless of the presence of PP2. Since PP2 treated R.SYK^{KO}-ZAP-70 cells had more phosphorylated ITAMs than PP2 treated R.SYK^{KO}-SYK cells, SYK ability to phosphorylate ITAMs could not explain the enhanced resistance of SYK expressing cells to SFK inhibition.

These results can also be affected by higher expression of ZAP-70 compared to SYK in the transduced R.SYK^{KO} cells. However, expression of SYK and ZAP-70 in R.SYK^{KO}-SYK and R.SYK^{KO}-ZAP-70 cells was similar to the previous experiment, where signaling in R.SYK^{KO}-ZAP-70 cells could be inhibited by 20μM concentration of PP2, while R.SYK^{KO}-SYK cells were resistant to the same PP2 concentration. Though the mechanism of how SYK is able to partially compensate for the loss of SFK activity could not be completely elucidated by these experiemtns, it is plausible to speculate that higher kinase activity of SYK [190], its ability to bind hemi ITAMs [191] or better ability to autophosphorylate can play a role in the process [192, 193]. Importantly, the increased phosphorylation of CD79 in ZAP-70 and SYK expressing cells is not necessarily the result of direct phosphorylation by these kinases. It is also possible that their tandem SH2 domains

binding to the phosphorylated ITAMs protect ITAM phosphotyrosines from dephosphorylation by phosphatases.

Remarkably, we have observed mild increase in CD79a phosphorylation after BCR stimulation in R.SYK^{KO} control cells in the presence of 20μM PP2, which suggests that even the high dose of PP2 is not able to completely inhibit SFK activity or that there are other kinases, which can phosphorylate ITAMs.

6.1.4. Structure or composition of BCR and TCR affects the sensitivity of the signaling to SFK inhibition

To further explore the mechanism responsible for the differences in the requirement for SFK kinase activity in BCR and TCR signaling, we expressed TCR signaling module in Ramos B cells. The TCR signaling module was a chimeric protein composed of full length TCRζ tagged for the purpose of antibody recognition by extracellular domain of CD16. Importantly, signaling initiated by antibody crosslinking of CD16-TCRζ in Ramos B cells induced relatively strong calcium response, which could be inhibited by standard dose of PP2 (10μM). This result had several important implications. It suggested that composition or structure of BCR and TCR affects the sensitivity to SFK inhibition. It also showed that the resistance of BCR signaling to SFK inhibition is not the result of cell-specific background but that it is dependent on the architecture of particular signaling pathway.

To complement this result, we also expressed BCR in T cells. In line with previous observations, BCR signaling in T cells was slightly but significantly more resistant to SFK inhibition than TCR signaling in the same cells. Interestingly, both TCR signaling in B cells and BCR signaling in T cells were delayed even without the PP2 treatment. We speculated that it could be the result of different specificity of SFK members expressed in B and T cells. To test this hypothesis, we transduced BCR positive T cells with LYN kinase, the prototypic B cell SFK. As we expected, expression of LYN in BCR positive T cells shortened the initial delay in signaling. It suggested certain level of non-redundancy between Src family members. Moreover, expression of LYN also shortened the delay in signaling in PP2-treated cells, which further supports the evidence of incomplete inhibition of SFK by PP2.

6.1.5. Bridging of LAT to TCR decreases dependence of TCR signaling to SFK kinase activity.

Perhaps, the most apparent difference in the composition of BCR and TCR signaling apparatuses is the usage of accessory adaptor protein LAT. Recent paper also suggested that LAT phosphorylation by ZAP-70 is the rate limiting step in TCR activation [194]. It was also shown, that after stimulation LAT becomes physically connected to TCR and that ZAP-70 and LCK are participating in the process [59].

Therefore, we asked whether the separation of LAT from TCR has a role in sensing SFK activity. To test this possibility, we generated another chimeric protein composed of full length LAT tagged with extracellular domain of CD16 to allow for antibody binding. It enabled us to co-crosslink TCR with LAT and thus probe sensitivity of TCR signaling to SFK inhibition independently of the LAT bridging step (Figure 4). We transduced P116 SYK and P116 ZAP cells with CD16-LAT. Next, we stimulated these cells with anti TCR antibody and simultaneously co-crosslinked TCR to LAT by antibodies as shown in Figure 4. Interestingly, co-crosslinking of LAT to TCR substantially increased the resistance of TCR signaling to SFK inhibition. Consistently with previous experiments, this effect was even more profound in the presence of SYK in P116 SYK CD16-LAT cells.

Collectively, our data show that LAT separation from TCR, properties of ZAP-70 and also structure of TCR itself are crucial features of TCR signaling apparat that participate in sensing SFK activity. Although we used the antibody mediated crosslinking of TCR, which is rather rough model of TCR activation our data suggest that TCR signaling apparat have developed multilevel control mechanisms to sense SFK kinase activity. The multi-sensing model of SFK activity well fits to the current model of initiation of TCR signaling and consequently model of the antigen discrimination. It was suggested that the length of the duration of TCR MHC-peptide complex interaction can be interpreted as a time window in which CD4 or CD8 co-receptor recognize MHC molecule and bring the SFK kinase LCK to the close proximity of TCR to phosphorylate ITAMs and thus initiate the signaling [195]. Consistently, high affinity peptides are able to sustain the interaction for longer time than low affinity peptides [196]. Here we show that SFK activity is necessary in several steps of TCR signaling. This likely extends the time, for which TCR MHC-

peptide interaction has to last in order to elicit signaling. It suggests that multi-sensing of SFK activity is a mechanism used to set up signaling threshold necessary for antigen discrimination.

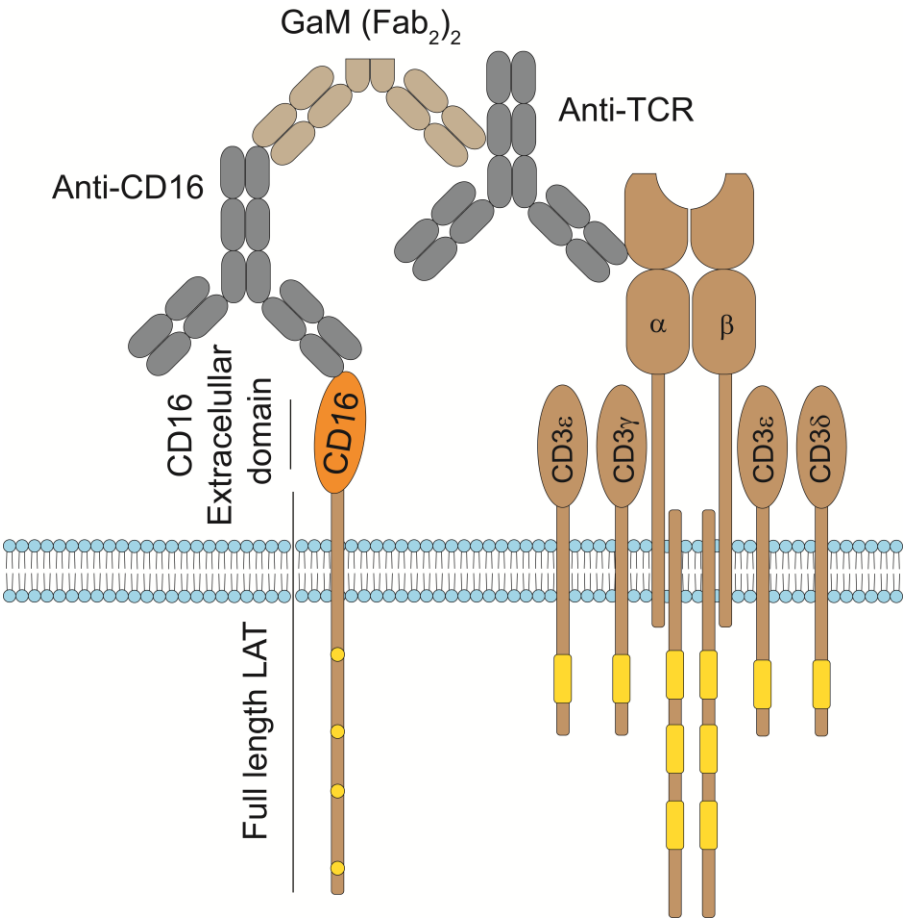

Figure 4. Illustration of experimental setup employed to co-crosslink LAT to TCR.

6.2. Transmembrane adaptor protein WBP1L regulates CXCR4 signaling and murine hematopoiesis

6.2.1. Antibody generation and initial analyses of WBP1L protein

Since WBP1L protein has not been previously studied there were no commercially available antibodies. We developed two types of antibodies recognizing WBP1L. The first was mouse monoclonal antibody against mouse WBP1L, which was suitable for immunoprecipitation but it was suboptimal for western blot staining. The second type of antibody was polyclonal antibody made in rabbit, which showed superior signal on western blot. However, immunoblotting of WBP1L was inefficient and difficult and thus we always had to enrich WBP1L by immunoprecipitation to enable reliable detection.

First, we analyzed expression of WBP1L protein in human and murine leukocyte subsets. We detected the highest expression of WBP1L in monocytes in humans and in macrophages in mice. We also observed relatively high expression of WBP1L in murine B and T lymphocytes in mice but rather lower expression in human lymphocytes. The discrepancy can be caused by different source of the cells, since human lymphocytes were isolated from blood, while murine lymphocytes were isolated from the spleen. We further showed that WBP1L has particularly high expression in *ETV6-RUNX1* positive B cell progenitor cell line REH derived from acute lymphoblastic leukemia compared to *ETV6-RUNX1* negative cell lines of similar origin. However, WBP1L expression was not changed after deletion of *ETV6-RUNX1* fusion gene. It further supports the evidence that WBP1L is downregulated by ETV6 but ETV6-RUNX1 fusion protein is no longer able to suppress WBP1L expression. Since WBP1L appears on the western blot as blurred double band and sequence analyses of extracellular domain revealed putative glycosylation and palmitoylation sites (Figure 5.), we analyzed posttranscriptional modifications of WBP1L. We proved that WBP1L is both palmitoylated and glycosylated. To analyze WBP1L localization within the cell, we transduced WBP1L deficient macrophages with the construct coding for fusion protein WBP1L-GFP that we previously used in our methodical paper (discussed in detail below). We also stained or transduced macrophages with fluorescent markers of cellular compartments and analyzed the co-localization of WBP1L with these markers using a confocal microscope. WBP1L co-localized with the plasma membrane, Golgi apparat, endoplasmic reticulum and partially also with acidic organelles, but it didn’t co-localize with mitochondria.

6.2.2. WBP1L interacts with E3 ubiquitin ligases and regulates CXCR4 expression, ubiquitination and signaling.

In silico analysis of WBP1L sequence revealed putative WW domain binding sides in the intracellular domain. Based on the specific amino acid composition of the WW binding motifs, we speculated that it may serve as an interaction site for NEDD4 family ubiquitin ligases (Figure 5.). To test this hypotheses, we transduced WBP1L deficient immortalized monocyte/macrophage progenitors with a construct coding for WBP1L fused with Strep and Flag tag. We chose this cell type based on a particularly high expression of WBP1L in monocytes and macrophages. We isolated WBP1L and its interacting partners by tandem purification and analyzed this material by tandem mass spectrometry. The data analysis confirmed that WBP1L interacts with several members of NEDD4 family ubiquitin ligases. By comparison of mass spectrometry intensities with mRNA expression analyzed by qPCR we predicted certain level of selectivity for WBP1L interaction with NEDD4 family members. We suggested that WBP1L interacts with WWP2, ITCH, WWP1 and NEDD4L but not with SMURF1, SMURF2 or NEDD4. We further showed by immunoprecipitation experiments with WBP1L, which had WW binding motifs deleted (further referred to as WBP1LΔN) that these motifs are responsible for the interaction with NEDD4 family ligases. Finally, we proved the interaction at the endogenous level by co-precipitation of WBP1L with WWP1 in macrophages.

Since NEDD4 family ligases regulate chemokine receptor CXCR4 [161-163], we speculated that via NEDD4 family ligases WBP1L may regulate expression and ubiquitination of this receptor. To test this hypothesis, we co-transfected WBP1L wild type (WT) form or WBP1LΔN together with CXCR4 to HEK293 cells. As predicted we observed enhanced ubiquitination and reduced expression of CXCR4 when co-transfected with WT WBP1L but the co-transfection of WBP1LΔN had more limited effects.

To test whether WBP1L regulates CXCR4 signaling, we downregulated WBP1L expression by two different shRNAs in human cell line REH and in mouse immortalized monocyte/macrophage progenitors. We stimulated the cells with SDF-1α and monitored the CXCR4 signaling at the level of AKT and ERK phosphorylation. We chose these two signaling pathways, because they represent both G protein dependent and independent signaling [177, 178]. Importantly, we observed enhanced AKT and ERK phosphorylation downstream of CXCR4 after WBP1L downregulation in REH cells, as well as in monocyte/macrophage progenitors.

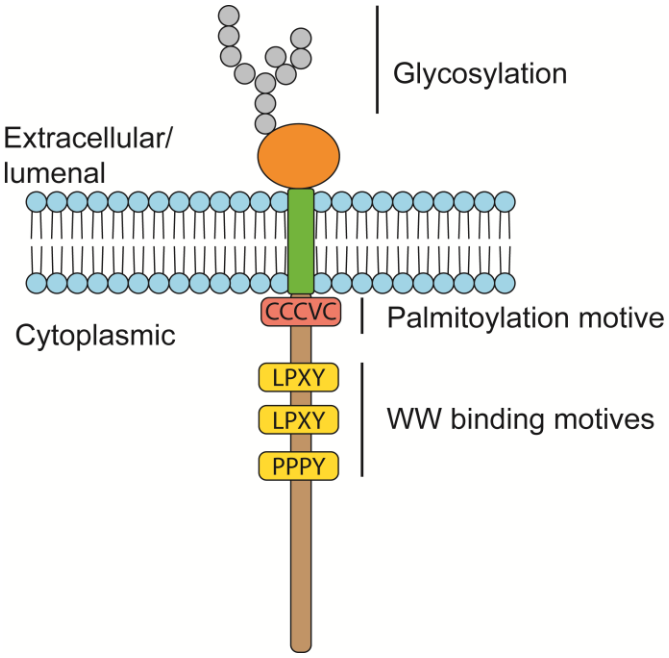

Figure 5. Illustration of WBP1L composition. In the model are highlighted posttranslational modifications and interacting motifs.

6.2.3. Analyses of WBP1L deficient mice

CXCR4 is a key regulator of bone marrow homing and hematopoiesis[180]. To analyze the role of WBP1L in these processes, we obtained WBP1L deficient mice from International Mouse Phenotyping Consortium. First, we confirmed that WBP1L is not expressed in the bone marrow of these mice. Next, we analyzed numbers and percentages of different cell populations in the bone marrow, spleen, lymph nodes, peritoneum and blood. Surprisingly, the overall cellularities of all tested hematopoietic compartments were normal. On the other hand, we observed decreased numbers of pro and pre B cells in the bone marrow and increased numbers of marginal zone B cells in the spleen. This is similar to the phenotype of the WHIM mice, which have, increased CXCR4 signaling and surface expression, similar to what we expected in WBP1L-deficient animals [183]. We have also observed enhanced number of dendritic cells in the spleen and reduced number of B1 cells in the peritoneum. The reason for these differences is unclear but it is very plausible that WBP1L may regulate also other signaling pathways, since NEDD4 family ligases ubiquitinylate multiple proteins and their expression pattern differs among various cell types (discussed in more details in the introduction above).

Interestingly, we also observed enhanced number of Lin^-, $c\text{-}kit^+$, $Sca1^+$ cells. These cells are represent early hematopoietic progenitors and stem cells. To test, whether the WBP1L deficiency also affects function of these cells, we have performed a series of transplantation experiments. We used three congenic mouse strains, which express different variants of CD45 protein and thus the origin of the cells can be easily tracked by flow cytometry. We transplanted bone marrow cells from WT or WBP1L deficient mice mixed with WT competitor bone marrow cells into lethally irradiated recipient mice in a 1:1 ratio. We monitored the engraftment by analysis of blood samples. Remarkably, the WBP1L deficient cells engrafted approximately three times better than the competitor cells, while the WT cells engrafted similarly as the competitor cells. The enhanced engraftment of WBP1L deficient cells was obvious already three weeks after the transplantation at it was sustained for at least four months until we sacrificed the animals. The enhanced engraftment was visible in both lymphoid and myeloid linages, which suggests that WBP1L deficiency affects already early progenitors or stem cells. Since WBP1L deficient mice have increased number of LSK cells, we tested whether the enhanced engraftment is not a simple result of transplanting more hematopoietic stem cells. Therefore, we sorted and transplanted similar numbers of LSK cells using the same set up. The results were the same as when we transplanted the whole bone marrow, showing that the improved engraftment is not the consequence of increased numbers of LSK cells. To test whether the difference is caused by enhanced migration of WBP1L-deficient cells to the bone marrow we performed a homing assay. We transplanted bone marrow cells similarly as in previous experiments but we sacrificed the mice 16 hours after the transplantation and analyzed the ratios of the cells that migrated to the bone marrow. We did not observe any differences in homing abilities between WT and WBP1L deficient cells. Next, we tested proliferation of WBP1L bone marrow cells after transplantation but we did not observe any differences in the proliferation of total bone marrow cells or any of their subsets either. Therefore, the mechanism of how WBP1L affects stem or progenitor cell function remains unclear.

The effect of WBP1L on hematopoietic stem and progenitor cell function has several interesting implications. It was shown that ETV6 is positive regulator of hematopoietic stem cell function but the mechanism of the regulation remains elusive [115]. It is plausible to think that the part of the mechanism how ETV6 regulates hematopoietic stem cell function is mediated by its target gene *Wbp1l* [104]. Moreover, since WBP1L has strong impact on the progenitors and stem cells, it is

plausible that it may affect also cancer stem cells, which have been shown to be a crucial part of leukemia biology.

After publishing this study, we have performed several additional experiments, which are aiming at identifying the mechanism explaining enhanced hematopoietic stem cell function. We have analyzed mRNA expression in WT and WBP1L deficient LSK cells after the transplantation by RNA sequencing. Among other interesting findings we have observed increased expression of metalloproteinase MMP9 in WBP1L deficient cells. Our preliminary data indicate that MMP9 is overexpressed in WBP1L deficient LSK cells also at the protein level. Interestingly, MMP9 was shown to play a positive role in the recovery of hematopoiesis after bone marrow suppression [197].

6.2.4. *WBP1L* has different effects on CXCR4 signaling when it is lost in the germline or when it is inducibly deleted in the adult organism

Although reduced numbers of pre and pro B cells and increased numbers of marginal zone B cells in WBP1L deficient mice are consistent with enhanced CXCR4 signaling, similar homing of bone marrow cells is completely incompatible with this hypothesis. Therefore, we analyzed CXCR4 signaling in WBP1L deficient bone marrow cells but we also did not observe any differences. There are only two possible explanations for this result. Loss of WBP1L is compensated for by other proteins or our shRNA experiments were false positive due to an off-target effect of the shRNA. To distinguish between these two possibilities, we immortalized monocyte/macrophage progenitors from both WT and WBP1L deficient mice. We transduced both cell lines with the same anti WBP1L shRNA as we used previously and analyzed the SDF-1α induced CXCR4 signaling. Interestingly, WBP1L downregulation in WT cells led to an increase in CXCR4 signaling but transduction of WBP1L deficient cells with the same shRNA had no effect. This result is clearly showing that the loss of WBP1L in the germ line can be compensated by other proteins and that WBP1L regulates CXCR4 signaling. Consistently with this conclusion, we observed enhanced bone marrow homing of immortalized progenitors where WBP1L was downregulated by shRNA. Therefore, we generated mice with conditional *Wbp1l* deficiency where *Wbp1l* is deleted by injection of tamoxifen. Interestingly, this acute *Wbp1l* deletion resulted in enhanced CXCR4 signaling in granulocytes, monocytes, T cells and KIT^+ cells. KIT^+ cells represent a mixed population of hematopoietic bone marrow progenitors. Consistently with

previous in vitro experiments, we observed enhanced expression of CXCR4 on KIT^+ cells where *Wbp1l* has been acutely deleted both *in vitro* and *in vivo*. We further showed that these cells migrate faster toward CXCR4 *in vitro* and to the bone marrow *in vivo*. Collectively, these data are showing that the loss of WBP1L in the germ line can be compensated for by currently unknown mechanism but acute loss of WBP1L causes enhanced CXCR4 expression, signaling and CXCR4-mediated migration.

Enhanced CXCR4 signaling was shown to be negative prognostic marker in acute lymphoblastic leukemia. Leukemic cells with high expression of CXCR4 home better to the bone marrow, where they are more protected from chemotherapy [198]. Here, we show that acute loss of WBP1L causes enhanced CXCR4 signaling and bone marrow homing. Therefore, we propose that increase in WBP1L expression in ETV6-RUNX1$^+$ leukemia [102] can attenuate CXCR4 signaling, which may be part of the reason why this type of leukemia responds better to treatment. However, further research on WBP1L function in leukemic cells is necessary to confirm the hypothesis.

6.3. Dysregulated NADPH oxidase promotes bone damage in murine model of autoinflammatory osteomyelitis.

6.3.1. PSTPIP2 regulates NADPH oxidase activity

While trying to discover signaling pathways and receptors regulated by PSTPIP2 we found that PSTPIP2 deficient bone marrow cells have increased production of reactive oxygen species (ROS) in response to treatment with silica particles. These are particles of silicon dioxide. They represent a common environmental agent. For workers generating large amount of dust from silicon dioxide containing materials, exposure to these dust particles represents health hazard, mainly due to their ability to cause chronic inflammation in the lungs [199]. In mice, silica is recognized by SR-B1 receptor and most likely by other receptors, which have not yet been identified. It also activates NLRP3 inflammasome, resulting in IL-1β production and inflammation [200]. Hyperproduction of IL-1β by NLRP3 inflammasome (in part) also drives the disease development in *Pstpip2^{cmo}* mice.

ROS production is one of the mechanisms responsible for pathogen destruction. It is typically elicited in response to PRR receptor stimulation on phagocytes [201]. To identify bone marrow cell population responsible for the increase in ROS production, we isolated monocytes and

granulocytes via magnetic activated cell sorting technique (MACS). While monocyte response to silica was relatively weak and no significant difference between WT and *Pstpip2^{cmo}* cells was observed, granulocytes produced much larger amount of ROS, which was substantially higher in *Pstpip2^{cmo}* cells than in WT.

We further asked, whether the increased ROS production is specific for silica treatment or if other stimulations will have the same effect. We stimulated neutrophils with E. coli bacteria, LPS, fMLP, TNFα and heat aggregated IgG antibodies to stimulate Fc-receptor signaling. Interestingly, all stimulations induced higher production of ROS in PSTPIP2-deficient neutrophils when compared to WT neutrophils, though the response intensity was generally lower than the response to silica. Moreover, we observed increased basal ROS production in bone marrow cells even in the absence of any stimulation. Collectively, these results suggest that PIPSTP2 controls ROS production independently of the type of the stimulation.

Notably, *Pstpip2^{cmo}* neutrophils are exposed to inflammatory environment, which can prime them and thus induce enhanced ROS production. Therefore, the increased ROS production can be an effect extrinsic factors. To test this possibility, we analyzed markers of neutrophil priming. We analyzed CD11b surface expression, activity of IL-1β promoter and cytoskeletal organization [202, 203] . We did not observe upregulation of any marker of neutrophil priming. To further rule out the possibility that the increased ROS production is caused by inflammatory environment, we crossed CMO mice with MYD88 deficient mice. As discussed in the introduction, MYD88 is crucial adaptor protein in TLR signaling but it is also indispensable for IL-1 receptor signaling [204, 205]. Therefore, the PSTPIP2 MYDD88 double deficient mice were healthy. Interestingly, bone marrow cells from these double deficient mice had similarly increased ROS production as CMO bone marrow cells. Together, these data show that the enhanced production of ROS in PSTPIP2 deficient neutrophils is cell intrinsic.

6.3.2. NADPH oxidase activity is responsible for bone destruction in CMO mice

To find out, how NAPDH oxidase activity contributes to the CMO disease development we obtained mice deficient in the gp91PHOX subunit of NADPH oxidase, which is indispensable for NADPH oxidase activity. We crossed this strain to *Pstpip2^{cmo}* mice [206]. Consequently, we observed absence of ROS production in silica treated bone marrow cells from these double deficient mice. We monitored these mice for the disease development and we observed that the

CMO symptoms started to appear with similar kinetic as in *Pstpip2*^{cmo} mice. However, paws from NADPH oxidase deficient *Pstpip2*^{cmo} mice were less swollen than in CMO mice. Moreover, when we performed micro-CT scan of the paws we didn't observe almost any bone destruction in double deficient mice. Therefore, we analyzed also older mice, in which the bone destruction is more substantial. However, even the old mice of the NADPH oxidase deficient *Pstpip2*^{cmo} strain ware almost completely protected from the bone destruction (Figure 6.). Notably, we did not observe any changes in the production of IL-1β in NADPH oxidase deficient *Pstpip2*^{cmo} mice, which suggest that ROS production represents mechanism, which contributes to the disease development independently from IL-1β hyperproduction. Collectively, these data suggest that ROS production by neutrophils is crucial for the development of bone damage in *Pstpip2*^{cmo} model of sterile inflammation.

Neutrophils are not the only cells, which use the same type of NADPH oxidase. Osteoclasts, cells which have a key role in bone remodeling also express the same type of NADPH oxidase and thus they can also be affected by the loss of NADPH activity in our mouse model. However, the loss of NADPH activity in osteoclasts doesn't cause changes in the bone structure or density [207] and therefore it is unlikely that loss of NADPH activity affects the bone destruction in the NADPH oxidase deficient *Pstpip2*^{cmo} mice.

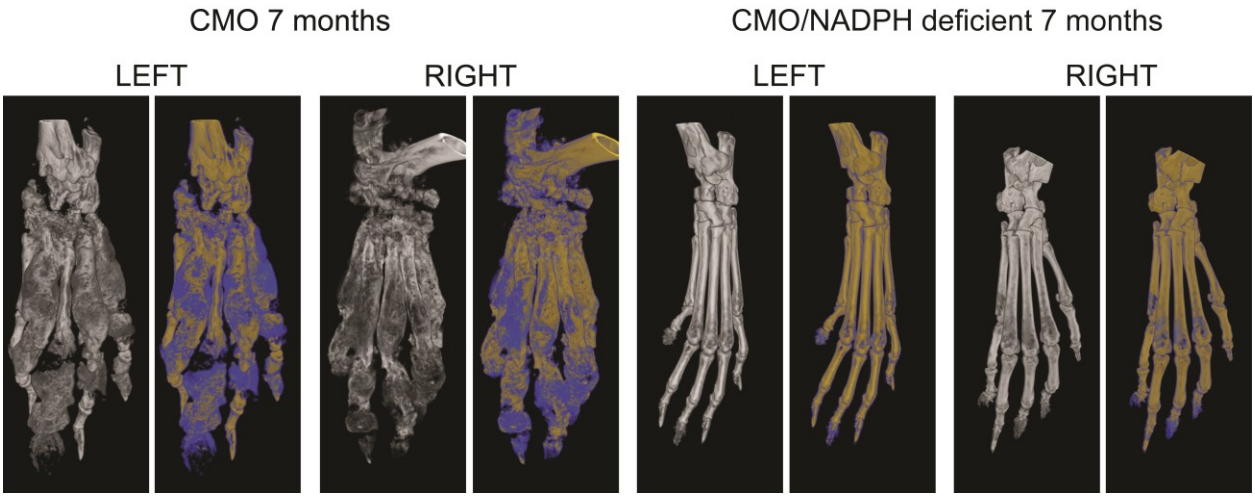

Figure 6. μCT scans from 7 months old CMO or CMO NADPH deficient mice. Blue color represents parts of the bones, which are recently formed.

6.3.3. Loss of PSTPIP2 causes enhanced phosphorylation of NADPH oxidase subunit p47.

In order to dissect the molecular mechanism explaining how PSTPIP2 regulates NADPH oxidase activity we probed the phosphorylation of NADPH oxidase. We isolated the bulk of phosphorylated proteins from silica treated and non-treated granulocytes and detected regulatory p47 subunit of NADPH oxidase by immunoblotting. We observed increased amount of phosphorylated p47 in the cell lysates after silica treatment, which is consistent with observed hyperactivation of NADPH oxidase [208]. We further show that this phosphorylation can be inhibited by protein kinase C inhibitor Gö6976. However, we were not able to explain how PSTPIP2 regulates protein kinase C. Therefore, we speculated that PSTPIP2 can act locally by recruiting phosphatases and CSK kinase to the close proximity of NADPH oxidase. To test this possibility, we transduced KIT^{+} cells with construct coding for PSTPIP2 fused with GFP and transplanted these cells into sub-lethally irradiated recipient mice. Two weeks later we sacrificed the mice and probed PSTPIP2 localization in mature neutrophils by confocal microscopy. In the majority of the cells, PSTPIP2 was diffusely localized in the cytoplasm and treatment with fluorescent silica didn't caused any further changes in its localization. Collectively, these data show that PITPIP2 regulates NADPH phosphorylation through protein kinase C but the precise mechanism is still unknown.

6.4. Expression of fluorescent fusion proteins in murine bone marrow-derived dendritic cells and macrophages.

In this methodical paper, we published a protocol for expression of fluorescent proteins in bone marrow derived macrophages or dendritic cells. The method was indispensable for us, when collecting data for WBP1L publication. The method is basically fusion of two procedures, retrovirus production in Platinum-E cells and preparation of bone marrow derived macrophages and dendritic cells.

It starts by the transfection of Platinum-E cells with retroviral vector MSCV. The Platinum-E cells are 293T cells, which stably express gag-pol and envelope protein of retroviruses and thus enable packaging of the virus and its release to the media [209]. The virus is subsequently collected in the form of culture supernatant. Meanwhile bone marrow cells are isolated, red blood cells are lysed and the cells are placed in the incubator. The disadvantage of the retrovirus, when compared to for example lentivirus is that retroviruses infect only dividing cells [210]. Therefore, after the isolation and before the transduction the cells are left to rest and to start dividing in the media containing M-CSF or GM-CSF, for macrophages or dendritic cells, respectively. The cells are than transduced with the retrovirus containing supernatant in two cycles to obtain maximal level of transduction. The cells are than left in the incubator to differentiate. The presence of M-CSF or GM-CSF growth factors is crucial for proper development of macrophages and dendritic cells from these transduced progenitors.

The method in the publication is well described to the last detail and thus we hope that it will provide the community with relatively low-cost and reliable way to express cDNA constructs in these otherwise hard to transfect cells.

7. Conclusions

In my thesis, I described our effort to characterize the roles of membrane associated or transmembrane adaptor proteins and kinases, which participate in leukocyte signal transduction. Our work on these proteins also gave rise to one methodological paper. I believe, that the results presented here shed a new light on the signaling pathways regulated by these proteins and thus consequently also on the biology of the processes connected with these pathways. To clearly present the conclusions of our work I will list the projects one by one.

In the first project, we studied the roles of SFK in the initiation of BCR and TCR signaling. We did not find any evidence supporting the model of SFK independent BCR signaling. Nevertheless, our data show that to initiate signaling by BCR much lower SFK kinase activity is required than in case of TCR. We demonstrated that SYK is part of the mechanism responsible for the low dependency of BCR signaling on SFK activity. However, the alleged ability of SYK to phosphorylate ITAM motifs cannot explain its role in this phenomenon. In addition we showed that other features of BCR signaling apparat can play a role in the process such as structure or composition of BCR complex and of the SFK members involved in its activation. We further show that in contrast to BCR signaling, TCR signaling senses SFK activity at multiple levels during the initiation of the signaling. Our data suggest that SFK activity is necessary not only for ITAM phosphorylation and activation of ZAP-70 kinase but also for bridging of LAT to TCR. Even though, our model of TCR signaling is somewhat artificial, the results fit well with the current model of TCR signaling initiation. Although additional studies are necessary, our data implicate that multilevel sensing of SFK activity by TCR can contribute to the mechanism of antigen discrimination by setting up the threshold for initiation of TCR signaling.

In the second project, we described previously uncharacterized protein WBP1L. We showed that WBP1L is glycosylated and palmitoylated transmembrane adaptor protein. It regulates CXCR4 signaling in human leukemic cell line REH, as well as in murine monocytes, granulocytes and progenitor cells in the bone marrow. Consequently, it changes the migratory properties of these cells. The molecular mechanism of how WBP1L regulates CXCR4 signaling is likely based on the activation of NEDD4 family ubiquitin ligases by WBP1L. We revealed that WBP1L interacts with and increases the activity of multiple NEDD4 family ligases and that the presence of the NEDD4

family binding sites is at least partially responsible for the changes in CXCR4 expression and ubiquitination mediated by WBP1L. Nevertheless, we found that WBP1L function can be compensated for, when WBP1L is lost in the germline. The mechanism of the compensation is unknown but it is of high interest, especially with respect to cancer cells, which can acquire multiple compensatory mutations. Interestingly, we also observed that WBP1L regulates early progenitor and stem cell function. However, the molecular mechanism of the process is at present unknown. Moreover, our observations have implications for the biology of leukemia and other diseases associated with WBP1L transcriptional repressor ETV6.

In the third project we focused on the mechanisms, which lead to the development of autoinflamatory disease in mice deficient in adaptor protein PSTPIP2. We showed that PSTPIP2 regulates ROS production in neutrophils. Using MYD88 PSTPIP2 double deficient mice and several methods to assess the activation of neutrophils we proposed that enhanced production of ROS in neutrophils is independent of inflammatory environment and, therefore, it is cell intrinsic. Nevertheless, the precise mechanism of how PSTPIP2 regulates NADPH activity remains unclear. So far, we know that the mechanism includes hyperphosphorylation of p47 subunit of NADPH oxidase by protein kinase C. Moreover, we showed that in our mouse model of autoinflamatory chronic multifocal osteomyelitis NADPH oxidase activity is responsible for the bone destruction. However, whether this is a common mechanism present also in certain types of human autoinflamatory diseases remains to be discovered.

In the fourth project we have generated detailed protocol describing preparation of bone marrow derived macrophages and dendritic cells expressing fluorescent proteins. The protocol is based on two methods: Retroviral transduction with construct coding for fluorescent fusion protein and differentiation of macrophages and dendritic cells from transduced murine bone marrow cells. The methodical paper covers every detail necessary to establish the method in the laboratory.

8.Contribution

The following text is written for the purpose of my dissertation thesis and, thus, I highlight my contribution to the projects. However, even though I performed majority of experimental work for some of these projects, I feel obligated to clearly state that all the projects were dependent on the close collaboration with my colleagues and my supervisor, who are listed as coauthors on the publications and their contribution was also indispensable.

Differential threshold for sensing Src-family kinase activity by B cell and T cell antigen receptors. I performed majority of the experiments. I also participated in designing the experiments and writing the manuscript. I am listed as the first author on the manuscript.

Transmembrane adaptor protein WBP1L regulates CXCR4 signaling and murine hematopoiesis.

My contributions were similar as in the case of previous project. I performed majority of the experiments, I participated in designing the experiments and writing the manuscript and I am listed as the first author on resulting publication.

Dysregulated NADPH oxidase promotes bone damage in murine model of autoinflammatory osteomyelitis.

I was participating in microscopy analyses of PSTPIP2 localization in neutrophils. I also designed and performed the analysis of cytoskeletal organization in neutrophils. Apart from the experiments, which are included in the publication I also prepared enzyme traps derived from PEST family phosphatases to identify its target proteins in neutrophils and thus to uncover the mechanism of how PSTPIP2 regulates NADPH oxidase. However, this effort has not been successful. I am listed on the publication as a co-author.

Expression of fluorescent fusion proteins in murine bone marrow-derived dendritic cells and macrophages.

I prepared the construct coding for WBP1L fused with GFP and I cloned it into MSCV vector, which we used to demonstrate the method in the paper. I am listed in the publication as a co-author.

Prohlášení o podílu studenta na výsledcích

Prohlašuji, že se Šimon Borna podílel na publikacích uvedených v této dizertační práci v rozsahu uvedeném v kapitole Contribution.

V Praze dne 12.3.2020 Mgr. Tomáš Brdička, Ph.D.

9. References

1. Sadowski, I., J.C. Stone, and T. Pawson, *A noncatalytic domain conserved among cytoplasmic protein-tyrosine kinases modifies the kinase function and transforming activity of Fujinami sarcoma virus P130gag-fps.* Mol Cell Biol, 1986. **6**(12): p. 4396-408.
2. Pawson, T., *Non-catalytic domains of cytoplasmic protein-tyrosine kinases: regulatory elements in signal transduction.* Oncogene, 1988. **3**(5): p. 491-5.
3. Marengere, L.E. and T. Pawson, *Structure and function of SH2 domains.* J Cell Sci Suppl, 1994. **18**: p. 97-104.
4. Overduin, M., et al., *Three-dimensional solution structure of the src homology 2 domain of c-abl.* Cell, 1992. **70**(4): p. 697-704.
5. Siegal, G., et al., *Solution structure of the C-terminal SH2 domain of the p85 alpha regulatory subunit of phosphoinositide 3-kinase.* J Mol Biol, 1998. **276**(2): p. 461-78.
6. Waksman, G., et al., *Binding of a high affinity phosphotyrosyl peptide to the Src SH2 domain: crystal structures of the complexed and peptide-free forms.* Cell, 1993. **72**(5): p. 779-90.
7. Eck, M.J., S.E. Shoelson, and S.C. Harrison, *Recognition of a high-affinity phosphotyrosyl peptide by the Src homology-2 domain of p56lck.* Nature, 1993. **362**(6415): p. 87-91.
8. Cicchetti, P., et al., *Identification of a protein that binds to the SH3 region of Abl and is similar to Bcr and GAP-rho.* Science, 1992. **257**(5071): p. 803-6.
9. Ren, R., et al., *Identification of a ten-amino acid proline-rich SH3 binding site.* Science, 1993. **259**(5098): p. 1157-61.
10. Posern, G., et al., *Development of highly selective SH3 binding peptides for Crk and CRKL which disrupt Crk-complexes with DOCK180, SoS and C3G.* Oncogene, 1998. **16**(15): p. 1903-12.
11. Kay, B.K., M.P. Williamson, and M. Sudol, *The importance of being proline: the interaction of proline-rich motifs in signaling proteins with their cognate domains.* Faseb j, 2000. **14**(2): p. 231-41.
12. Bork, P. and M. Sudol, *The WW domain: a signalling site in dystrophin?* Trends Biochem Sci, 1994. **19**(12): p. 531-3.
13. Andre, B. and J.Y. Springael, *WWP, a new amino acid motif present in single or multiple copies in various proteins including dystrophin and the SH3-binding Yes-associated protein YAP65.* Biochem Biophys Res Commun, 1994. **205**(2): p. 1201-5.
14. Huang, X., et al., *Structure of a WW domain containing fragment of dystrophin in complex with beta-dystroglycan.* Nat Struct Biol, 2000. **7**(8): p. 634-8.
15. Macias, M.J., et al., *Structure of the WW domain of a kinase-associated protein complexed with a proline-rich peptide.* Nature, 1996. **382**(6592): p. 646-9.
16. Ingham, R.J., et al., *WW domains provide a platform for the assembly of multiprotein networks.* Mol Cell Biol, 2005. **25**(16): p. 7092-106.
17. Jung, D. and F.W. Alt, *Unraveling V(D)J recombination; insights into gene regulation.* Cell, 2004. **116**(2): p. 299-311.
18. Alt, F.W. and D. Baltimore, *Joining of immunoglobulin heavy chain gene segments: implications from a chromosome with evidence of three D-JH fusions.* Proceedings of the National Academy of Sciences of the United States of America, 1982. **79**(13): p. 4118-4122.
19. Komori, T., et al., *Lack of N regions in antigen receptor variable region genes of TdT-deficient lymphocytes.* Science (New York, N.Y.), 1993. **261**(5125): p. 1171-1175.
20. Gilfillan, S., et al., *Mice lacking TdT: mature animals with an immature lymphocyte repertoire.* Science (New York, N.Y.), 1993. **261**(5125): p. 1175-1178.
21. Zheng, B., W. Xue, and G. Kelsoe, *Locus-specific somatic hypermutation in germinal centre T cells.* Nature, 1994. **372**(6506): p. 556-559.

22. Berek, C., A. Berger, and M. Apel, *Maturation of the immune response in germinal centers.* Cell, 1991. **67**(6): p. 1121-9.
23. Jacob, J., et al., *Intraclonal generation of antibody mutants in germinal centres.* Nature, 1991. **354**(6352): p. 389-392.
24. Weiss, U. and K. Rajewsky, *The repertoire of somatic antibody mutants accumulating in the memory compartment after primary immunization is restricted through affinity maturation and mirrors that expressed in the secondary response.* The Journal of experimental medicine, 1990. **172**(6): p. 1681-1689.
25. Bransteitter, R., et al., *Activation-induced cytidine deaminase deaminates deoxycytidine on single-stranded DNA but requires the action of RNase.* Proceedings of the National Academy of Sciences of the United States of America, 2003. **100**(7): p. 4102-4107.
26. Dickerson, S.K., et al., *AID mediates hypermutation by deaminating single stranded DNA.* The Journal of experimental medicine, 2003. **197**(10): p. 1291-1296.
27. Rada, C., *Mutagenesis by AID: Being in the Right Place at the Right Time.* PLoS Genet, 2015. **11**(9): p. e1005489.
28. Pieper, K., B. Grimbacher, and H. Eibel, *B-cell biology and development.* J Allergy Clin Immunol, 2013. **131**(4): p. 959-71.
29. Klein, L., et al., *Positive and negative selection of the T cell repertoire: what thymocytes see (and don't see).* Nat Rev Immunol, 2014. **14**(6): p. 377-91.
30. Jeurissen, A., J.L. Ceuppens, and X. Bossuyt, *T lymphocyte dependence of the antibody response to 'T lymphocyte independent type 2' antigens.* Immunology, 2004. **111**(1): p. 1-7.
31. Campbell, K.S., et al., *IgM antigen receptor complex contains phosphoprotein products of B29 and mb-1 genes.* Proc Natl Acad Sci U S A, 1991. **88**(9): p. 3982-6.
32. Campbell, K.S. and J.C. Cambier, *B lymphocyte antigen receptors (mIg) are non-covalently associated with a disulfide linked, inducibly phosphorylated glycoprotein complex.* Embo j, 1990. **9**(2): p. 441-8.
33. Cambier, J.C., *New nomenclature for the Reth motif (or ARH1/TAM/ARAM/YXXL).* Immunol Today, 1995. **16**(2): p. 110.
34. Reth, M., *Pillars article: antigen receptor tail clue. Nature. 1989. 338: 383-384.* J Immunol, 2014. **192**(9): p. 4015-6.
35. Dong, et al., *Structural basis of assembly of the human T cell receptor-CD3 complex.* Nature, 2019. **573**(7775): p. 546-552.
36. Gold, D.P., et al., *Isolation of cDNA clones encoding the 20K non-glycosylated polypeptide chain of the human T-cell receptor/T3 complex.* Nature, 1986. **321**(6068): p. 431-4.
37. Borst, J., et al., *The T3 complex on human T lymphocytes involves four structurally distinct glycoproteins.* J Biol Chem, 1983. **258**(8): p. 5135-41.
38. Borst, J., M.A. Prendiville, and C. Terhorst, *The T3 complex on human thymus-derived lymphocytes contains two different subunits of 20 kDa.* Eur J Immunol, 1983. **13**(7): p. 576-80.
39. Kanellopoulos, J.M., et al., *Biosynthesis and molecular nature of the T3 antigen of human T lymphocytes.* Embo j, 1983. **2**(10): p. 1807-14.
40. Koretzky, G.A., F. Abtahian, and M.A. Silverman, *SLP76 and SLP65: complex regulation of signalling in lymphocytes and beyond.* Nat Rev Immunol, 2006. **6**(1): p. 67-78.
41. Xu, C., et al., *Regulation of T cell receptor activation by dynamic membrane binding of the CD3epsilon cytoplasmic tyrosine-based motif.* Cell, 2008. **135**(4): p. 702-13.
42. Sasmal, D.K., et al., *TCR-pMHC bond conformation controls TCR ligand discrimination.* Cell Mol Immunol, 2019.
43. Artyomov, M.N., et al., *CD4 and CD8 binding to MHC molecules primarily acts to enhance Lck delivery.* Proc Natl Acad Sci U S A, 2010. **107**(39): p. 16916-21.

44. Turner, J.M., et al., *Interaction of the unique N-terminal region of tyrosine kinase p56lck with cytoplasmic domains of CD4 and CD8 is mediated by cysteine motifs.* Cell, 1990. **60**(5): p. 755-65.
45. Palacios, E.H. and A. Weiss, *Function of the Src-family kinases, Lck and Fyn, in T-cell development and activation.* Oncogene, 2004. **23**(48): p. 7990-8000.
46. Chan, A.C., et al., *Differential expression of ZAP-70 and Syk protein tyrosine kinases, and the role of this family of protein tyrosine kinases in TCR signaling.* J Immunol, 1994. **152**(10): p. 4758-66.
47. Mallick-Wood, C.A., et al., *Disruption of epithelial gamma delta T cell repertoires by mutation of the Syk tyrosine kinase.* Proc Natl Acad Sci U S A, 1996. **93**(18): p. 9704-9.
48. Steele, R.E., N.A. Stover, and M. Sakaguchi, *Appearance and disappearance of Syk family protein-tyrosine kinase genes during metazoan evolution.* Gene, 1999. **239**(1): p. 91-7.
49. Chan, A.C., et al., *Activation of ZAP-70 kinase activity by phosphorylation of tyrosine 493 is required for lymphocyte antigen receptor function.* Embo j, 1995. **14**(11): p. 2499-508.
50. Brdicka, T., et al., *Intramolecular regulatory switch in ZAP-70: analogy with receptor tyrosine kinases.* Mol Cell Biol, 2005. **25**(12): p. 4924-33.
51. Mansueto, M.S., et al., *A reevaluation of the spleen tyrosine kinase (SYK) activation mechanism.* J Biol Chem, 2019. **294**(19): p. 7658-7668.
52. Kimura, T., et al., *Conformational changes induced in the protein tyrosine kinase p72syk by tyrosine phosphorylation or by binding of phosphorylated immunoreceptor tyrosine-based activation motif peptides.* Mol Cell Biol, 1996. **16**(4): p. 1471-8.
53. Deindl, S., et al., *Structural basis for the inhibition of tyrosine kinase activity of ZAP-70.* Cell, 2007. **129**(4): p. 735-46.
54. Deindl, S., et al., *Stability of an autoinhibitory interface in the structure of the tyrosine kinase ZAP-70 impacts T cell receptor response.* Proc Natl Acad Sci U S A, 2009. **106**(49): p. 20699-704.
55. Yan, Q., et al., *Structural basis for activation of ZAP-70 by phosphorylation of the SH2-kinase linker.* Mol Cell Biol, 2013. **33**(11): p. 2188-201.
56. Gradler, U., et al., *Structural and biophysical characterization of the Syk activation switch.* J Mol Biol, 2013. **425**(2): p. 309-33.
57. Klammt, C., et al., *T cell receptor dwell times control the kinase activity of Zap70.* Nat Immunol, 2015. **16**(9): p. 961-9.
58. Williams, B.L., et al., *Genetic evidence for differential coupling of Syk family kinases to the T-cell receptor: reconstitution studies in a ZAP-70-deficient Jurkat T-cell line.* Mol Cell Biol, 1998. **18**(3): p. 1388-99.
59. Lo, W.L., et al., *Lck promotes Zap70-dependent LAT phosphorylation by bridging Zap70 to LAT.* Nat Immunol, 2018. **19**(7): p. 733-741.
60. Clements, J.L., et al., *Integration of T cell receptor-dependent signaling pathways by adapter proteins.* Annu Rev Immunol, 1999. **17**: p. 89-108.
61. Yang, J. and M. Reth, *Oligomeric organization of the B-cell antigen receptor on resting cells.* Nature, 2010. **467**(7314): p. 465-9.
62. Yang, J. and M. Reth, *The dissociation activation model of B cell antigen receptor triggering.* FEBS Lett, 2010. **584**(24): p. 4872-7.
63. Takata, M., et al., *Tyrosine kinases Lyn and Syk regulate B cell receptor-coupled Ca2+ mobilization through distinct pathways.* Embo j, 1994. **13**(6): p. 1341-9.
64. Saijo, K., et al., *Essential role of Src-family protein tyrosine kinases in NF-kappaB activation during B cell development.* Nat Immunol, 2003. **4**(3): p. 274-9.
65. Stepanek, O., et al., *Nonredundant roles of Src-family kinases and Syk in the initiation of B-cell antigen receptor signaling.* J Immunol, 2013. **190**(4): p. 1807-18.
66. Mukherjee, S., et al., *Monovalent and multivalent ligation of the B cell receptor exhibit differential dependence upon Syk and Src family kinases.* Sci Signal, 2013. **6**(256): p. ra1.

67. Rolli, V., et al., *Amplification of B cell antigen receptor signaling by a Syk/ITAM positive feedback loop.* Mol Cell, 2002. **10**(5): p. 1057-69.
68. Zoller, K.E., I.A. MacNeil, and J.S. Brugge, *Protein tyrosine kinases Syk and ZAP-70 display distinct requirements for Src family kinases in immune response receptor signal transduction.* J Immunol, 1997. **158**(4): p. 1650-9.
69. Dal Porto, J.M., et al., *B cell antigen receptor signaling 101.* Mol Immunol, 2004. **41**(6-7): p. 599-613.
70. Lanier, L.L., et al., *Immunoreceptor DAP12 bearing a tyrosine-based activation motif is involved in activating NK cells.* Nature, 1998. **391**(6668): p. 703-7.
71. Wu, J., et al., *An activating immunoreceptor complex formed by NKG2D and DAP10.* Science, 1999. **285**(5428): p. 730-2.
72. Buday, L., et al., *A complex of Grb2 adaptor protein, Sos exchange factor, and a 36-kDa membrane-bound tyrosine phosphoprotein is implicated in ras activation in T cells.* J Biol Chem, 1994. **269**(12): p. 9019-23.
73. Sieh, M., et al., *GRB2 and phospholipase C-gamma 1 associate with a 36- to 38-kilodalton phosphotyrosine protein after T-cell receptor stimulation.* Mol Cell Biol, 1994. **14**(7): p. 4435-42.
74. Zhang, W., et al., *LAT: the ZAP-70 tyrosine kinase substrate that links T cell receptor to cellular activation.* Cell, 1998. **92**(1): p. 83-92.
75. Kawabuchi, M., et al., *Transmembrane phosphoprotein Cbp regulates the activities of Src-family tyrosine kinases.* Nature, 2000. **404**(6781): p. 999-1003.
76. Brdicka, T., et al., *Phosphoprotein associated with glycosphingolipid-enriched microdomains (PAG), a novel ubiquitously expressed transmembrane adaptor protein, binds the protein tyrosine kinase csk and is involved in regulation of T cell activation.* J Exp Med, 2000. **191**(9): p. 1591-604.
77. Brdickova, N., et al., *LIME: a new membrane Raft-associated adaptor protein involved in CD4 and CD8 coreceptor signaling.* J Exp Med, 2003. **198**(10): p. 1453-62.
78. Hur, E.M., et al., *LIME, a novel transmembrane adaptor protein, associates with p56lck and mediates T cell activation.* J Exp Med, 2003. **198**(10): p. 1463-73.
79. Brdicka, T., et al., *Non-T cell activation linker (NTAL): a transmembrane adaptor protein involved in immunoreceptor signaling.* J Exp Med, 2002. **196**(12): p. 1617-26.
80. Draber, P., et al., *LST1/A is a myeloid leukocyte-specific transmembrane adaptor protein recruiting protein tyrosine phosphatases SHP-1 and SHP-2 to the plasma membrane.* J Biol Chem, 2012. **287**(27): p. 22812-21.
81. Holzinger, I., et al., *Cloning and genomic characterization of LST1: a new gene in the human TNF region.* Immunogenetics, 1995. **42**(5): p. 315-22.
82. Stepanek, O., P. Draber, and V. Horejsi, *Palmitoylated transmembrane adaptor proteins in leukocyte signaling.* Cell Signal, 2014. **26**(5): p. 895-902.
83. Tsuge, I., et al., *A gene in the H-2S:H-2D interval of the major histocompatibility complex which is transcribed in B cells and macrophages.* Immunogenetics, 1987. **26**(6): p. 378-80.
84. Raghunathan, A., et al., *Functional analysis of B144/LST1: a gene in the tumor necrosis factor cluster that induces formation of long filopodia in eukaryotic cells.* Exp Cell Res, 2001. **268**(2): p. 230-44.
85. Draber, P., et al., *SCIMP, a transmembrane adaptor protein involved in major histocompatibility complex class II signaling.* Mol Cell Biol, 2011. **31**(22): p. 4550-62.
86. Borna, S., et al., *Transmembrane adaptor protein WBP1L regulates CXCR4 signalling and murine haematopoiesis.* J Cell Mol Med, 2020. **24**(2): p. 1980-1992.

87. Hrdinka, M., et al., *PRR7 is a transmembrane adaptor protein expressed in activated T cells involved in regulation of T cell receptor signaling and apoptosis.* J Biol Chem, 2011. **286**(22): p. 19617-29.
88. Zhu, M., et al., *Molecular cloning of a novel gene encoding a membrane-associated adaptor protein (LAX) in lymphocyte signaling.* J Biol Chem, 2002. **277**(48): p. 46151-8.
89. Kralova, J., et al., *The Transmembrane Adaptor Protein SCIMP Facilitates Sustained Dectin-1 Signaling in Dendritic Cells.* J Biol Chem, 2016. **291**(32): p. 16530-40.
90. Luo, L., et al., *SCIMP is a universal Toll-like receptor adaptor in macrophages.* J Leukoc Biol, 2020. **107**(2): p. 251-262.
91. Luo, L., et al., *SCIMP is a transmembrane non-TIR TLR adaptor that promotes proinflammatory cytokine production from macrophages.* Nat Commun, 2017. **8**: p. 14133.
92. Zhang, W., R.P. Trible, and L.E. Samelson, *LAT palmitoylation: its essential role in membrane microdomain targeting and tyrosine phosphorylation during T cell activation.* Immunity, 1998. **9**(2): p. 239-46.
93. Tanimura, N., et al., *Palmitoylation of LAT contributes to its subcellular localization and stability.* Biochem Biophys Res Commun, 2006. **341**(4): p. 1177-83.
94. Levental, I., et al., *Palmitoylation regulates raft affinity for the majority of integral raft proteins.* Proc Natl Acad Sci U S A, 2010. **107**(51): p. 22050-4.
95. Staub, O., et al., *WW domains of Nedd4 bind to the proline-rich PY motifs in the epithelial Na+ channel deleted in Liddle's syndrome.* Embo j, 1996. **15**(10): p. 2371-80.
96. Chen, H.I. and M. Sudol, *The WW domain of Yes-associated protein binds a proline-rich ligand that differs from the consensus established for Src homology 3-binding modules.* Proc Natl Acad Sci U S A, 1995. **92**(17): p. 7819-23.
97. Ingham, R.J., G. Gish, and T. Pawson, *The Nedd4 family of E3 ubiquitin ligases: functional diversity within a common modular architecture.* Oncogene, 2004. **23**(11): p. 1972-84.
98. Zhu, M., et al., *Negative regulation of T cell activation and autoimmunity by the transmembrane adaptor protein LAB.* Immunity, 2006. **25**(5): p. 757-68.
99. Janssen, E., et al., *LAB: a new membrane-associated adaptor molecule in B cell activation.* Nat Immunol, 2003. **4**(2): p. 117-23.
100. Mosquera-Caro, M., *Identification, validation, and cloning of a novel gene (OPAL1) and association of genes highly predictive of outcome in pediatric acute lymphoblastic leukemia using gene expression profiling.* Blood, 2003. **102**: p. 4a.
101. Kanderova, V., et al., *High-resolution Antibody Array Analysis of Childhood Acute Leukemia Cells.* Mol Cell Proteomics, 2016. **15**(4): p. 1246-61.
102. Holleman, A., et al., *Expression of the outcome predictor in acute leukemia 1 (OPAL1) gene is not an independent prognostic factor in patients treated according to COALL or St Jude protocols.* Blood, 2006. **108**(6): p. 1984-90.
103. Moorman, A.V., et al., *Prognostic effect of chromosomal abnormalities in childhood B-cell precursor acute lymphoblastic leukaemia: results from the UK Medical Research Council ALL97/99 randomised trial.* Lancet Oncol, 2010. **11**(5): p. 429-38.
104. Neveu, B., et al., *CLIC5: a novel ETV6 target gene in childhood acute lymphoblastic leukemia.* Haematologica, 2016. **101**(12): p. 1534-1543.
105. Lopez, R.G., et al., *TEL is a sequence-specific transcriptional repressor.* J Biol Chem, 1999. **274**(42): p. 30132-8.
106. Cave, H., et al., *ETV6 is the target of chromosome 12p deletions in t(12;21) childhood acute lymphocytic leukemia.* Leukemia, 1997. **11**(9): p. 1459-64.

107. Montpetit, A., et al., *Mutational and expression analysis of the chromosome 12p candidate tumor suppressor genes in pre-B acute lymphoblastic leukemia.* Leukemia, 2004. **18**(9): p. 1499-504.
108. Noetzli, L., et al., *Germline mutations in ETV6 are associated with thrombocytopenia, red cell macrocytosis and predisposition to lymphoblastic leukemia.* Nat Genet, 2015. **47**(5): p. 535-538.
109. Bejar, R., et al., *Clinical effect of point mutations in myelodysplastic syndromes.* N Engl J Med, 2011. **364**(26): p. 2496-506.
110. Barjesteh van Waalwijk van Doorn-Khosrovani, S., et al., *Somatic heterozygous mutations in ETV6 (TEL) and frequent absence of ETV6 protein in acute myeloid leukemia.* Oncogene, 2005. **24**(25): p. 4129-37.
111. Yoshida, K., et al., *Frequent pathway mutations of splicing machinery in myelodysplasia.* Nature, 2011. **478**(7367): p. 64-9.
112. Hock, H. and A. Shimamura, *ETV6 in hematopoiesis and leukemia predisposition.* Semin Hematol, 2017. **54**(2): p. 98-104.
113. Wang, L.C., et al., *Yolk sac angiogenic defect and intra-embryonic apoptosis in mice lacking the Ets-related factor TEL.* Embo j, 1997. **16**(14): p. 4374-83.
114. Wang, L.C., et al., *The TEL/ETV6 gene is required specifically for hematopoiesis in the bone marrow.* Genes Dev, 1998. **12**(15): p. 2392-402.
115. Hock, H., et al., *Tel/Etv6 is an essential and selective regulator of adult hematopoietic stem cell survival.* Genes Dev, 2004. **18**(19): p. 2336-41.
116. Pei, J. and N.V. Grishin, *Unexpected diversity in Shisa-like proteins suggests the importance of their roles as transmembrane adaptors.* Cell Signal, 2012. **24**(3): p. 758-69.
117. Jackman, J.K., et al., *Molecular cloning of SLP-76, a 76-kDa tyrosine phosphoprotein associated with Grb2 in T cells.* J Biol Chem, 1995. **270**(13): p. 7029-32.
118. Fu, C., et al., *BLNK: a central linker protein in B cell activation.* Immunity, 1998. **9**(1): p. 93-103.
119. Gangi-Peterson, L., et al., *bca: an activation-related B-cell gene.* Mol Immunol, 1998. **35**(1): p. 55-63.
120. Goitsuka, R., et al., *BASH, a novel signaling molecule preferentially expressed in B cells of the bursa of Fabricius.* J Immunol, 1998. **161**(11): p. 5804-8.
121. Wienands, J., et al., *SLP-65: a new signaling component in B lymphocytes which requires expression of the antigen receptor for phosphorylation.* J Exp Med, 1998. **188**(4): p. 791-5.
122. Kohler, F., et al., *A leucine zipper in the N terminus confers membrane association to SLP-65.* Nat Immunol, 2005. **6**(2): p. 204-10.
123. Yablonski, D., T. Kadlecek, and A. Weiss, *Identification of a phospholipase C-gamma1 (PLC-gamma1) SH3 domain-binding site in SLP-76 required for T-cell receptor-mediated activation of PLC-gamma1 and NFAT.* Mol Cell Biol, 2001. **21**(13): p. 4208-18.
124. Ishiai, M., et al., *Cutting edge: association of phospholipase C-gamma 2 Src homology 2 domains with BLNK is critical for B cell antigen receptor signaling.* J Immunol, 1999. **163**(4): p. 1746-9.
125. Yablonski, D., et al., *Uncoupling of nonreceptor tyrosine kinases from PLC-gamma1 in an SLP-76-deficient T cell.* Science, 1998. **281**(5375): p. 413-6.
126. Ishiai, M., et al., *BLNK required for coupling Syk to PLC gamma 2 and Rac1-JNK in B cells.* Immunity, 1999. **10**(1): p. 117-25.
127. Matzinger, P., *Tolerance, danger, and the extended family.* Annu Rev Immunol, 1994. **12**: p. 991-1045.
128. Janeway, C.A., Jr., *Approaching the asymptote? Evolution and revolution in immunology.* Cold Spring Harb Symp Quant Biol, 1989. **54 Pt 1**: p. 1-13.
129. Bianchi, M.E., *DAMPs, PAMPs and alarmins: all we need to know about danger.* J Leukoc Biol, 2007. **81**(1): p. 1-5.

130. Medzhitov, R., P. Preston-Hurlburt, and C.A. Janeway, Jr., *A human homologue of the Drosophila Toll protein signals activation of adaptive immunity.* Nature, 1997. **388**(6640): p. 394-7.
131. Lemaitre, B., et al., *The dorsoventral regulatory gene cassette spatzle/Toll/cactus controls the potent antifungal response in Drosophila adults.* Cell, 1996. **86**(6): p. 973-83.
132. Poltorak, A., et al., *Defective LPS signaling in C3H/HeJ and C57BL/10ScCr mice: mutations in Tlr4 gene.* Science, 1998. **282**(5396): p. 2085-8.
133. Ohnishi, H., et al., *Structural basis for the multiple interactions of the MyD88 TIR domain in TLR4 signaling.* Proc Natl Acad Sci U S A, 2009. **106**(25): p. 10260-5.
134. Oshiumi, H., et al., *TICAM-1, an adaptor molecule that participates in Toll-like receptor 3-mediated interferon-beta induction.* Nat Immunol, 2003. **4**(2): p. 161-7.
135. Medzhitov, R., et al., *MyD88 is an adaptor protein in the hToll/IL-1 receptor family signaling pathways.* Mol Cell, 1998. **2**(2): p. 253-8.
136. Kawai, T., et al., *Unresponsiveness of MyD88-deficient mice to endotoxin.* Immunity, 1999. **11**(1): p. 115-22.
137. Yamamoto, M., et al., *Cutting edge: a novel Toll/IL-1 receptor domain-containing adapter that preferentially activates the IFN-beta promoter in the Toll-like receptor signaling.* J Immunol, 2002. **169**(12): p. 6668-72.
138. Drobek, A., et al., *PSTPIP2, a Protein Associated with Autoinflammatory Disease, Interacts with Inhibitory Enzymes SHIP1 and Csk.* J Immunol, 2015. **195**(7): p. 3416-26.
139. Wu, Y., D. Dowbenko, and L.A. Lasky, *PSTPIP 2, a second tyrosine phosphorylated, cytoskeletal-associated protein that binds a PEST-type protein-tyrosine phosphatase.* J Biol Chem, 1998. **273**(46): p. 30487-96.
140. Yeung, Y.G., S. Soldera, and E.R. Stanley, *A novel macrophage actin-associated protein (MAYP) is tyrosine-phosphorylated following colony stimulating factor-1 stimulation.* J Biol Chem, 1998. **273**(46): p. 30638-42.
141. Grosse, J., et al., *Mutation of mouse Mayp/Pstpip2 causes a macrophage autoinflammatory disease.* Blood, 2006. **107**(8): p. 3350-8.
142. Roberts-Galbraith, R.H. and K.L. Gould, *Setting the F-BAR: functions and regulation of the F-BAR protein family.* Cell Cycle, 2010. **9**(20): p. 4091-7.
143. Sztacho, M., et al., *BAR Proteins PSTPIP1/2 Regulate Podosome Dynamics and the Resorption Activity of Osteoclasts.* PLoS One, 2016. **11**(10): p. e0164829.
144. Chitu, V., et al., *PSTPIP2 deficiency in mice causes osteopenia and increased differentiation of multipotent myeloid precursors into osteoclasts.* Blood, 2012. **120**(15): p. 3126-35.
145. Ferguson, P.J., et al., *A missense mutation in pstpip2 is associated with the murine autoinflammatory disorder chronic multifocal osteomyelitis.* Bone, 2006. **38**(1): p. 41-7.
146. Chitu, V., et al., *Primed innate immunity leads to autoinflammatory disease in PSTPIP2-deficient cmo mice.* Blood, 2009. **114**(12): p. 2497-505.
147. Byrd, L., et al., *Chronic multifocal osteomyelitis, a new recessive mutation on chromosome 18 of the mouse.* Genomics, 1991. **11**(4): p. 794-8.
148. Lukens, J.R., et al., *Dietary modulation of the microbiome affects autoinflammatory disease.* Nature, 2014. **516**(7530): p. 246-9.
149. Lukens, J.R., et al., *Critical role for inflammasome-independent IL-1beta production in osteomyelitis.* Proc Natl Acad Sci U S A, 2014. **111**(3): p. 1066-71.
150. Cassel, S.L., et al., *Inflammasome-independent IL-1beta mediates autoinflammatory disease in Pstpip2-deficient mice.* Proc Natl Acad Sci U S A, 2014. **111**(3): p. 1072-7.
151. Fajner, V., E. Maspero, and S. Polo, *Targeting HECT-type E3 ligases - insights from catalysis, regulation and inhibitors.* FEBS Lett, 2017. **591**(17): p. 2636-2647.
152. Chen, Z., et al., *A Tunable Brake for HECT Ubiquitin Ligases.* Mol Cell, 2017. **66**(3): p. 345-357.e6.

153. Wiesner, S., et al., *Autoinhibition of the HECT-type ubiquitin ligase Smurf2 through its C2 domain.* Cell, 2007. **130**(4): p. 651-62.
154. Mari, S., et al., *Structural and functional framework for the autoinhibition of Nedd4-family ubiquitin ligases.* Structure, 2014. **22**(11): p. 1639-49.
155. Bruce, M.C., et al., *Regulation of Nedd4-2 self-ubiquitination and stability by a PY motif located within its HECT-domain.* Biochem J, 2008. **415**(1): p. 155-63.
156. Riling, C., et al., *Itch WW Domains Inhibit Its E3 Ubiquitin Ligase Activity by Blocking E2-E3 Ligase Trans-thiolation.* J Biol Chem, 2015. **290**(39): p. 23875-87.
157. Gallagher, E., et al., *Activation of the E3 ubiquitin ligase Itch through a phosphorylation-induced conformational change.* Proc Natl Acad Sci U S A, 2006. **103**(6): p. 1717-22.
158. Escobedo, A., et al., *Structural basis of the activation and degradation mechanisms of the E3 ubiquitin ligase Nedd4L.* Structure, 2014. **22**(10): p. 1446-57.
159. Liu, Y., et al., *Abnormal development of the neuromuscular junction in Nedd4-deficient mice.* Dev Biol, 2009. **330**(1): p. 153-66.
160. Yang, B., et al., *Nedd4 augments the adaptive immune response by promoting ubiquitin-mediated degradation of Cbl-b in activated T cells.* Nature immunology, 2008. **9**(12): p. 1356-1363.
161. Marchese, A., et al., *The E3 ubiquitin ligase AIP4 mediates ubiquitination and sorting of the G protein-coupled receptor CXCR4.* Dev Cell, 2003. **5**(5): p. 709-22.
162. Shu, L., et al., *Ubiquitin E3 ligase Wwp1 negatively regulates osteoblast function by inhibiting osteoblast differentiation and migration.* J Bone Miner Res, 2013. **28**(9): p. 1925-35.
163. Subik, K., et al., *The ubiquitin E3 ligase WWP1 decreases CXCL12-mediated MDA231 breast cancer cell migration and bone metastasis.* Bone, 2012. **50**(4): p. 813-23.
164. Perry, W.L., et al., *The itchy locus encodes a novel ubiquitin protein ligase that is disrupted in a18H mice.* Nat Genet, 1998. **18**(2): p. 143-6.
165. Hustad, C.M., et al., *Molecular genetic characterization of six recessive viable alleles of the mouse agouti locus.* Genetics, 1995. **140**(1): p. 255-65.
166. Melino, G., et al., *Itch: a HECT-type E3 ligase regulating immunity, skin and cancer.* Cell Death Differ, 2008. **15**(7): p. 1103-12.
167. Fang, D., et al., *Dysregulation of T lymphocyte function in itchy mice: a role for Itch in TH2 differentiation.* Nat Immunol, 2002. **3**(3): p. 281-7.
168. Feng, Y., et al., *HIV-1 entry cofactor: functional cDNA cloning of a seven-transmembrane, G protein-coupled receptor.* Science (New York, N.Y.), 1996. **272**(5263): p. 872-877.
169. Loetscher, M., et al., *Cloning of a human seven-transmembrane domain receptor, LESTR, that is highly expressed in leukocytes.* The Journal of biological chemistry, 1994. **269**(1): p. 232-237.
170. Federsppiel, B., et al., *Molecular cloning of the cDNA and chromosomal localization of the gene for a putative seven-transmembrane segment (7-TMS) receptor isolated from human spleen.* Genomics, 1993. **16**(3): p. 707-712.
171. Oberlin, E., et al., *The CXC chemokine SDF-1 is the ligand for LESTR/fusin and prevents infection by T-cell-line-adapted HIV-1.* Nature, 1996. **382**(6594): p. 833-835.
172. Bleul, C.C., et al., *The lymphocyte chemoattractant SDF-1 is a ligand for LESTR/fusin and blocks HIV-1 entry.* Nature, 1996. **382**(6594): p. 829-833.
173. Nagasawa, T., et al., *Molecular cloning and characterization of a murine pre-B-cell growth-stimulating factor/stromal cell-derived factor 1 receptor, a murine homolog of the human immunodeficiency virus 1 entry coreceptor fusin.* Proc Natl Acad Sci U S A, 1996. **93**(25): p. 14726-9.
174. Tashiro, K., et al., *Signal sequence trap: a cloning strategy for secreted proteins and type I membrane proteins.* Science, 1993. **261**(5121): p. 600-3.

175. Yu, L., et al., *Identification and expression of novel isoforms of human stromal cell-derived factor 1.* Gene, 2006. **374**: p. 174-9.
176. Janowski, M., *Functional diversity of SDF-1 splicing variants.* Cell Adh Migr, 2009. **3**(3): p. 243-9.
177. Sotsios, Y., et al., *The CXC chemokine stromal cell-derived factor activates a Gi-coupled phosphoinositide 3-kinase in T lymphocytes.* J Immunol, 1999. **163**(11): p. 5954-63.
178. Busillo, J.M. and J.L. Benovic, *Regulation of CXCR4 signaling.* Biochim Biophys Acta, 2007. **1768**(4): p. 952-63.
179. Zou, Y.R., et al., *Function of the chemokine receptor CXCR4 in haematopoiesis and in cerebellar development.* Nature, 1998. **393**(6685): p. 595-9.
180. Ma, Q., D. Jones, and T.A. Springer, *The chemokine receptor CXCR4 is required for the retention of B lineage and granulocytic precursors within the bone marrow microenvironment.* Immunity, 1999. **10**(4): p. 463-71.
181. Nie, Y., Y.C. Han, and Y.R. Zou, *CXCR4 is required for the quiescence of primitive hematopoietic cells.* J Exp Med, 2008. **205**(4): p. 777-83.
182. Egawa, T., et al., *The earliest stages of B cell development require a chemokine stromal cell-derived factor/pre-B cell growth-stimulating factor.* Immunity, 2001. **15**(2): p. 323-34.
183. Balabanian, K., et al., *Proper desensitization of CXCR4 is required for lymphocyte development and peripheral compartmentalization in mice.* Blood, 2012. **119**(24): p. 5722-30.
184. Hernandez, P.A., et al., *Mutations in the chemokine receptor gene CXCR4 are associated with WHIM syndrome, a combined immunodeficiency disease.* Nat Genet, 2003. **34**(1): p. 70-4.
185. McDermott, D.H. and P.M. Murphy, *WHIM syndrome: Immunopathogenesis, treatment and cure strategies.* Immunol Rev, 2019. **287**(1): p. 91-102.
186. Balabanian, K., et al., *WHIM syndromes with different genetic anomalies are accounted for by impaired CXCR4 desensitization to CXCL12.* Blood, 2005. **105**(6): p. 2449-57.
187. Zhan, T., et al., *MIM regulates the trafficking of bone marrow cells via modulating surface expression of CXCR4.* Leukemia, 2016. **30**(6): p. 1327-34.
188. Yu, D., et al., *Mice deficient in MIM expression are predisposed to lymphomagenesis.* Oncogene, 2012. **31**(30): p. 3561-8.
189. Williams, B.L., et al., *Genetic evidence for differential coupling of Syk family kinases to the T-cell receptor: reconstitution studies in a ZAP-70-deficient Jurkat T-cell line.* Molecular and cellular biology, 1998. **18**(3): p. 1388-1399.
190. Latour, S., L.M. Chow, and A. Veillette, *Differential intrinsic enzymatic activity of Syk and Zap-70 protein-tyrosine kinases.* J Biol Chem, 1996. **271**(37): p. 22782-90.
191. Hughes, C.E., et al., *Critical Role for an acidic amino acid region in platelet signaling by the HemITAM (hemi-immunoreceptor tyrosine-based activation motif) containing receptor CLEC-2 (C-type lectin receptor-2).* J Biol Chem, 2013. **288**(7): p. 5127-35.
192. Rowley, R.B., et al., *Syk protein-tyrosine kinase is regulated by tyrosine-phosphorylated Ig alpha/Ig beta immunoreceptor tyrosine activation motif binding and autophosphorylation.* J Biol Chem, 1995. **270**(19): p. 11590-4.
193. El-Hillal, O., et al., *syk kinase activation by a src kinase-initiated activation loop phosphorylation chain reaction.* Proc Natl Acad Sci U S A, 1997. **94**(5): p. 1919-24.
194. Lo, W.L., et al., *Slow phosphorylation of a tyrosine residue in LAT optimizes T cell ligand discrimination.* Nat Immunol, 2019. **20**(11): p. 1481-1493.
195. Stepanek, O., et al., *Coreceptor scanning by the T cell receptor provides a mechanism for T cell tolerance.* Cell, 2014. **159**(2): p. 333-45.
196. Courtney, A.H., W.L. Lo, and A. Weiss, *TCR Signaling: Mechanisms of Initiation and Propagation.* Trends Biochem Sci, 2018. **43**(2): p. 108-123.

197. Heissig, B., et al., *Recruitment of stem and progenitor cells from the bone marrow niche requires MMP-9 mediated release of kit-ligand.* Cell, 2002. **109**(5): p. 625-37.
198. Tsaouli, G., et al., *Notch/CXCR4 Partnership in Acute Lymphoblastic Leukemia Progression.* Journal of immunology research, 2019. **2019**: p. 5601396-5601396.
199. Leung, C.C., I.T.S. Yu, and W. Chen, *Silicosis.* Lancet (London, England), 2012. **379**(9830): p. 2008-2018.
200. Tsugita, M., et al., *SR-B1 Is a Silica Receptor that Mediates Canonical Inflammasome Activation.* Cell Rep, 2017. **18**(5): p. 1298-1311.
201. El-Benna, J., et al., *Priming of the neutrophil respiratory burst: role in host defense and inflammation.* Immunol Rev, 2016. **273**(1): p. 180-93.
202. Miralda, I., S.M. Uriarte, and K.R. McLeish, *Multiple Phenotypic Changes Define Neutrophil Priming.* Front Cell Infect Microbiol, 2017. **7**: p. 217.
203. Crawford, N. and P. Eggleton, *Dynamic changes in neutrophil cytoskeleton during priming and subsequent surface stimulated functions.* Biochem Soc Trans, 1991. **19**(4): p. 1048-55.
204. Muzio, M., et al., *IRAK (Pelle) family member IRAK-2 and MyD88 as proximal mediators of IL-1 signaling.* Science, 1997. **278**(5343): p. 1612-5.
205. Wesche, H., et al., *MyD88: an adapter that recruits IRAK to the IL-1 receptor complex.* Immunity, 1997. **7**(6): p. 837-47.
206. Pollock, J.D., et al., *Mouse model of X-linked chronic granulomatous disease, an inherited defect in phagocyte superoxide production.* Nature genetics, 1995. **9**(2): p. 202-209.
207. Yang, S., et al., *A new superoxide-generating oxidase in murine osteoclasts.* J Biol Chem, 2001. **276**(8): p. 5452-8.
208. Belambri, S.A., et al., *NADPH oxidase activation in neutrophils: Role of the phosphorylation of its subunits.* Eur J Clin Invest, 2018. **48 Suppl 2**: p. e12951.
209. Morita, S., T. Kojima, and T. Kitamura, *Plat-E: an efficient and stable system for transient packaging of retroviruses.* Gene therapy, 2000. **7**(12): p. 1063-1066.
210. Yamashita, M. and M. Emerman, *Retroviral infection of non-dividing cells: old and new perspectives.* Virology, 2006. **344**(1): p. 88-93.

10. Reprints of the publications

1. **Simon Borna**, Matej Fabisik, Kristyna Ilievova, Tomas Dvoracek and Tomas Brdicka *Differential threshold for sensing Src-family kinase activity by B cell and T cell antigen receptors.* Unpublished.

2. **Borna S**, Drobek A, Kralova J, Glatzova D, Splichalova I, Fabisik M, Pokorna J, Skopcova T, Angelisova P, Kanderova V, Starkova J, Stanek P, Matveichuk OV, Pavliuchenko N, Kwiatkowska K, Protty MB, Tomlinson MG, Alberich-Jorda M, Korinek V, Brdicka T: *Transmembrane adaptor protein WBP1L regulates CXCR4 signalling and murine haematopoiesis*. **J Cell Mol Med 2020** *24(2): 1980-1992*., Jan 2020, 10.1111/jcmm.14895

3. Jarmila Kralova, Ales Drobek, Jan Prochazka, Frantisek Spoutil, Matej Fabisik, Daniela Glatzova, **Simon Borna**, Jana Pokorna, Tereza Skopcova, Pavla Angelisova, Martin Gregor, Pavel Kovarik, Radislav Sedlacek, and Tomas Brdicka: *Dysregulated NADPH oxidase promotes bone damage in murine model of autoinflammatory osteomyelitis.* **J Immunol** , 204 (6), 1607-1620, 2020 Mar 15, 10.4049/jimmunol.1900953

4. Kralova J, Glatzova D, **Borna S**, Brdicka T: *Expression of Fluorescent Fusion Proteins in Murine Bone Marrow-derived Dendritic Cells and Macrophages.* **J Vis Exp 2018** (140) e58081, 2018 Oct 30, 10.3791/58081

Differential threshold for sensing Src-family kinase activity by B cell and T cell antigen receptors

Simon Borna[1,2], Matej Fabisik[1,2], Kristyna Ilievova[1], Tomas Dvoracek[1] and Tomas Brdicka[1,2].

[1] Laboratory of Leukocyte Signaling, Institute of Molecular Genetics of the CAS, Prague, Czech Republic

[2] Charles University, Faculty of Science, Department of Cell Biology, Prague, Czech Republic

*Corresponding Author: Tomas Brdicka

E-mail: tomas.brdicka@img.cas.cz

Institute of Molecular Genetics of the Czech Academy of Sciences
Videnska 1083, 14220 Prague
Czech Republic

Phone: +420 241 062 467
Fax: +420 224 310 955

Running title: SFK kinases in BCR and TCR signaling

Keywords: Src-family kinases (SFK), lymphocyte-specific protein tyrosine kinase (Lck), Lck/Yes-related novel protein tyrosine kinase (Lyn) , spleen tyrosine kinase (Syk), 70 kDa zeta-chain associated protein (ZAP-70), B-cell receptor (BCR), T-cell receptor (TCR), SFK inhibitor (PP2), immunoreceptor tyrosine-based activation motif (ITAM), Linker for activation of T-cells family member 1 (LAT).

Abstract

Although signal transduction by immunoreceptors such as T cell antigen receptor (TCR), B cell antigen receptor (BCR) or Fc-receptors uses the same scheme and similar molecules, the threshold and the final tuning are set differently for each receptor. We and others have previously shown that inhibition of Src family kinases (SFK) blocks TCR but not BCR signaling. It has been proposed that SYK, which is downstream from SFKs in B cells, compensates for the loss of SFK activity, while its T cell paralogue ZAP-70 does not. Using SYK deficient B and T cell lines expressing SYK or ZAP-70, we show that SYK is only able to partially compensate for the loss of SFK activity and that structural features of the receptor complexes also play critical roles. Furthermore, we show that separation of LAT from TCR is another important factor setting threshold for SFK activity required to initiate TCR signaling in T cells. Thus, immunoreceptor sensing of SFK activity is regulated at multiple levels.

Introduction

Evolution of receptors and associated signaling pathways have generated a range of different signal transduction systems. However, among this variety, groups of receptors can be distinguished, which utilize common schemes of signal transmission. The multi-usage of similar molecules in similar arrangements is typical for immunoreceptor signaling, including signaling by TCR, BCR, Fc receptors, NK cell receptors and several others. The signaling is initiated by Src family kinases (SFK), which phosphorylate immunoreceptor tyrosine-based activation motifs (ITAM), located within intracellular domains of receptor associated transmembrane adaptor proteins. Phosphorylated ITAM motifs serve as docking sites for SYK family kinases [1, 2]. Their activation is a crucial step in subsequent signal transduction. It results in the recruitment and assembly of a signalosome activating calcium response and other downstream signaling pathways [3, 4].

Several studies have questioned this basic scheme of immunoreceptor signaling by suggesting that at least part of BCR signaling can be triggered independently of SFKs [5-8]. We and others have demonstrated that SFK inhibition by widely used inhibitor PP2 [9, 10] abolished TCR signaling in T cells but was unable to block signaling by BCR in B lymphocytes [8, 11]. Similar observation was later also reported by another group, showing the same effect at the level of SLP65 and SLP76 adaptor protein phosphorylation [12]. It has been proposed that SFK independent signaling in B cells can be explained by unique features of SYK. SYK-family of kinases contains only two members, SYK and ZAP-70. They show different expression patterns. B cells and myeloid cells express mainly SYK and T cells mainly ZAP-70 [13, 14]. Both kinases are in the steady state in the cytoplasm in a closed inactive conformation and upon receptor activation, they are loaded on the phosphorylated ITAM motifs. Binding to ITAMs via their tandem SH domains leads to transition to the active conformation [15-18]. However, to become fully active and/or to stabilize interaction with ITAMs, SYK-family kinases must be further phosphorylated. For ZAP-70 this phosphorylation seems to be more dependent on SFKs than for SYK, which shows higher propensity to autophosphorylate during this step [13, 17-23]. Furthermore, it has been proposed that intense stimulation of B cells with multivalent ligands can trigger SYK to phosphorylate ITAM motifs independently of SFK, while ZAP-70 is thought to lack this ability. However, the data directly demonstrating the SYK-mediated phosphorylation of ITAM motifs were all generated using either recombinant proteins and peptides in vitro or overexpression in non-

hematopoietic cells, such as S2, 293T, or COS cells [5, 8, 23, 24].

In this study, we have re-evaluated these data using human B and T cell lines. We show that SYK mediated ITAM phosphorylation is rather limited and that what may appear as SFK-independent signaling by SYK in studies employing SFK inhibitors can be largely explained by incomplete inhibition of SFKs, coupled to a low threshold for signaling initiation in B cells. Importantly, multiple components of TCR and BCR signaling apparatuses, including antigen receptors themselves, Src- and Syk-family kinases, and LAT appear to be parts of a complex mechanism differentially setting this threshold for signaling by BCR and TCR.

Results

Differences between SYK and ZAP-70 cannot fully explain differential sensitivity of TCR and BCR signaling to SFK inhibition.

First, we calibrated our experimental system using model T cell line Jurkat and B cell line Ramos. In Jurkat T cells, 2μM concentration of PP2 was enough to completely inhibit calcium response initiated by TCR crosslinking with anti TCR antibody C305 (Figure 1A). Consistent with previously published data [8, 11], calcium response in B cell line Ramos stimulated with anti BCR antibody was resistant to at least 20 μM PP2, although it exhibited a delay dependent on the PP2 dose (Figure 1B). The difference can be explained by two alternative hypotheses. First, that downstream B cell kinase SYK but not its T cell paralogue ZAP-70 can initiate receptor signaling by phosphorylating ITAMs independently of SFKs. Second, it is also possible that SFKs are incompletely inhibited by PP2 and their residual activity is sufficient to initiate signaling by BCR but not by TCR.

To start addressing these questions we employed Jurkat-derived T cell line P116, which lacks expression of SYK and ZAP-70 [25]. We reconstituted these cells with SYK, ZAP-70, or empty vector and stimulated these cells with anti TCR antibody C305 and gated on cells with expression of SYK and ZAP-70 similar to their native expression in Jurkat and Ramos cells (Figure 1C and S1). Interestingly, SYK expression somewhat increased TCR signaling resistance to SFK inhibition and these cells responded even in the presence of 5μM PP2. However, 10μM concentration, a standard dose widely used to inhibit SFK activity, completely abolished calcium response in SYK expressing P116 cells (Figure 1D). This result suggested that although it contributes to the resistance of the signaling to SFK inhibition, SYK activity alone cannot explain it.

In order to further dissect the role of SYK, we complemented the experiment in T cells with similar experiment in B cell line Ramos. Using CRISPR-CAS9 technology, we have obtained several clones of Ramos B cells, which lack expression of SYK (Figure 1E). None of the tested clones was responsive to BCR stimulation and all the clones had comparable expression of BCR (Figure 1F and data not shown). For further experiments, we have used one of these clones, hereafter termed R.SYK^{KO}. To avoid clonal bias, we always used SYK reconstituted cells as a control. We transduced R.SYK^{KO} cells with SYK, ZAP-70 and empty vector (Figure 1G) and stimulated the cells with anti BCR antibody in the presence of different doses of PP2. SYK expressing cells were similarly resistant to PP2 inhibition as original Ramos cells. Importantly, ZAP-70 expressing cells were also resistant to 10μM PP2 and the signaling was only inhibited by 20μM concentration (Figure 1H). Such a high resistance of ZAP-70 expressing cells suggests that the differences between ZAP-70 and SYK account only for part of the resistance of BCR signaling to SFK inhibition and

additional mechanisms substantially contribute to this phenomenon.

Both SYK and ZAP-70 can potentiate ITAM phosphorylation.

To test if SYK ability to phosphorylate ITAMs contributes to the BCR resistance to SFK inhibition, we have analyzed tyrosine phosphorylation of CD79a immunoprecipitated from BCR-stimulated R.SYK^{KO} cells reconstituted (or not) with SYK or ZAP-70. We also probed the phosphorylation of tyrosine 182 of CD79a in the whole cell lysates of the same cells to complement immunoprecipitation with an independent method (figure 2A). Expression of both SYK and ZAP-70 increased ITAM phosphorylation detected by both methods. Surprisingly this effect was stronger in ZAP-70 expressing cells (fig. 2A,B). Despite of this, SYK was better able to restore the resistance of BCR signaling to SFK inhibition (Figure 1H), leading to the conclusion that any potentially unique ability of SYK to phosphorylate ITAM motifs is not the reason why BCR better tolerates SFK inhibition. Importantly, ITAM phosphorylation induced by BCR stimulation could be observed even after treatment with 20μM PP2 in the complete absence of SYK or ZAP-70, demonstrating that even high dose of PP2 is not able to completely inhibit ITAM phosphorylation by SFKs. Collectively, these data show that SYK ability to phosphorylate ITAMs does not explain increased resistance of SYK-expressing cells to SFK inhibition. In addition, they also show that there still is a residual SFK activity in PP2-treated cells, which is probably sufficient to trigger BCR mediated signaling.

Structural features of antigen receptors contribute to their differential sensitivity to SFK inhibition.

To address the question if TCR per se is inherently less sensitive than BCR to SFK activity, we transduced our T and B cell lines with chimeric protein composed of extracellular domain of CD16 and full length TCRζ (Figure 3A and 3B). Importantly, CD16 is not expressed in any of the cell lines used in our experiments (Figure 3C). Crosslinking of CD16-ζ on T cells induced strong calcium response similar to the one elicited by TCR stimulation (Figure 3D). Crosslinking of CD16-ζ on B cells induced relatively strong but already delayed calcium response, which was inhibited by 10μM concentration of PP2 (Figure 3E), indicating that antigen receptor composition is important for the resistance to SFK inhibition. To further explore this possibility, we transduced Jurkat T cells with the BCR complex, including IgH, Igα, and Igβ (Figure 4A). We stimulated these cells with anti TCR or anti BCR antibody and treated with different doses of PP2. Interestingly, and analogously to CD16-ζ induced signaling in B cells, BCR signaling in T cells was delayed compared to TCR signaling even in PP2 non-treated cells. However, in spite of this, BCR signaling was still more resistant to PP2 inhibition than TCR signaling in the same cells (Figure 4B and 4C), demonstrating that structural features of BCR contribute to increased sensitivity of BCR to SFK activity.

Ectopic expression of Lyn in T cells modulates the resistance to SFK inhibition.

Even though BCR signaling in Jurkat T cells was more resistant to PP2 inhibition than TCR signaling in the same cells, it still could be completely inhibited by a relatively low dose of PP2 suggesting that other factors are contributing too. We have shown above that SYK activity is one of these factors. Next we

wanted to test if differences between SFK members in T cells and B cells can also be responsible. Therefore, we transduced the Jurkat BCR cells with Lyn, a major B cell member of Src family (Figure 5A). Interestingly, in Jurkat BCR cells, Lyn expression accelerated calcium response both in the absence and in the presence of PP2, which demonstrates certain level of non-redundancy between the T cell and B cell SFK and suggest that Lyn expression also slightly increases the resistance of BCR signaling to PP2. Moreover, the fact that Lyn was able to alter signaling output even in the presence of PP2 further supports the argument that signaling in PP2-treated cells is still initiated by SFKs (Figure 5B).

Bridging LAT to TCR induces strong resistance to SFK inhibition

The data described above suggested that multiple members of antigen receptor signaling apparat cooperate to set the threshold for the amount of SFK activity required for receptor activation. This threshold appears to lower in B cells than in T cells, allowing B cells to respond even to the residual SFK activity surviving in the presence of PP2. When considering the differences between BCR and TCR signaling at the level of organization of the molecules potentially involved in regulating this threshold, we realized that one of the most apparent differences is in the usage of receptor independent transmembrane adaptor LAT by TCR signaling machinery, which serves as a docking domain for assembly of PLCy containing signalosome. It was recently published that bridging the TCR to LAT requires adaptor function of Lck, which is dependent on Lck-mediated phosphorylation of ZAP-70 [18, 20, 26]. We speculated that due to its relative complexity, maintaining this bridge may require comparatively high SFK activity. Moreover using Lck as a mere adaptor cannot employ enzymatic amplification and, thus, requires more Lck molecules to transduce the signal. To test this possibility, we wanted to bring LAT to the proximity of TCR independently of Lck-mediated bridging mechanism. To achieve this, we prepared chimeric protein composed of extracellular domain of CD16 and full length LAT (Figure 6A). It enabled us to co-crosslink TCR with LAT and thus probe the resistance of TCR signaling to SFK inhibition independently of LAT-bridging step. We transduced ZAP-70 or SYK expressing P116 T cells with chimeric construct coding for CD16-LAT (Figure 6B). Strikingly, co-crosslinking of LAT to TCR resulted in resistance of the TCR signaling to 10μM concentration of PP2, which is the highest level of resistance we were so far able to achieve in T cells. As expected, the resistance was more profound in case of SYK expressing cells (Figure 6C). Although, the resistance was still not as strong as in case of B cells the results support the conclusion that LAT loading step is regulated by SFK and that it is important part of the mechanism by which TCR signaling apparat sets the threshold for the amount of SFK activity required for signal propagation.

Discussion

In our work, we analyzed the mechanisms, which make TCR signaling sensitive and BCR signaling resistant to inhibition of SFK. This phenomenon has been observed in previous works. Similar difference in the sensitivity of antigen receptor signaling to PP2-mediated inhibition has been observed in primary mouse T cells and B cells [8, 11]. It was also described in cell lines where SFKs were inhibited genetically by membrane-targeted Csk [11]. Delayed but still robust calcium response has also been observed in LYN-deficient DT-40 cell line [7]. Differences in the sensitivity to SFK inhibition were ascribed either to the unique ability of SYK to phosphorylate ITAMs and thus initiate the signaling independently of

SFKs or to the residual activity of SFKs which initiated signaling in B cells [8, 11]. Here, we re-evaluated these results using SYK and ZAP-70 deficient B and T cell lines reconstituted with SYK or ZAP-70. Notably, we have observed increased ITAM phosphorylation in SYK deficient B cells even in the presence of high concentration of PP2, which suggest that even high concentration of PP2 does not completely inhibit SFK activity.

In line with previously published data, we observed enhanced resistance to SFK inhibition in both B and T cells expressing SYK, when compared to ZAP-70. However, ZAP-70 expressing B cells retained high resistance to SFK inhibition and SYK expressing T cells were still inhibited by relatively low dose of PP2, which indicated that SYK is only a part of the mechanism responsible for the resistance of BCR signaling to SFK inhibition. Moreover, SYK ability to phosphorylate ITAMs could not explain increased resistance of SYK-expressing cells to SFK inhibition, because the phosphorylation of ITAMs was enhanced to a similar extent in both SYK and ZAP-70 expressing cells. Interestingly, enhanced ITAM phosphorylation in the presence of ZAP-70 was also reported previously [27, 28]. The mechanism does not necessarily involve the direct phosphorylation of ITAM motifs by SYK or ZAP-70. It is equally possible, that SH2 domains of SYK and ZAP-70 protect BCR and TCR ITAMs from dephosphorylation by phosphatses and in this way increase the observed phosphorylation [28, 29]. Regardles of the mechanism, our data show that there is no difference between SYK and ZAP-70 in their ability to keep ITAMs phosphorylated and so the mechanism by which SYK increases the resistance to SFK inhibition must be different. It is plausible that trans-autophosphorylation of SYK [21-23], its ability to bind hemi ITAMs [30] or its higher kinase activity give it an advantage over ZAP-70 [31].

Since SYK compensates only partially for the loss of SFK kinase activity we continued to search for other mechanisms responsible for the resistance. We show that CD3ζ signaling in B cells can be inhibited by standard dose of PP2 and that BCR, compared to TCR signaling in T cells, slightly enhances the resistance to SFK inhibition, which suggest that differences in structure and composition of TCR and BCR play additional role in the mechanism of the resistance.

General composition of BCR and TCR is very similar. They use surface receptor for antigen recognition and ITAMs containing transmembrane adaptor proteins associated with the receptors for signaling. However, TCR uses an additional accessory adaptor protein LAT not present in B cells, which does not contain ITAM motives but serves as a docking platform for PLCγ containing signalosome [32]. Moreover, recent papers report on evidence that LAT phosphorylation by ZAP-70 is the rate-limiting step in TCR activation [33] and that loading of LAT to TCR receptor is dependent on phosphorylated ZAP-70 and adaptor function of Lck [26, 34]. Whether SFK kinase activity play any direct or indirect role in LAT loading process was not clear. Here we show that direct bridging of LAT to TCR receptor highly reduces TCR sensitivity to SFK inhibition. It suggests that loading of LAT to the TCR proximity is highly dependent on SFK kinase activity. These data have interesting implications in understanding of affinity discrimination.

Current models of TCR activation, including kinetic proofreading model, posit that there is a threshold which has to be overcome in order to allow for signal propagation, necessary for discrimination between antigens of varying affinity [35-40]. Even in our relatively crude model of antibody-mediated TCR activation this threshold could be observed and investigated. Our data suggest that multiple components of the TCR signaling

apparatus cooperate to set its level, including structure of antigen receptor itself and unique properties of Lck and ZAP-70. Replacing any of these components with their B cell counterparts lowers this threshold. In addition, our data suggest that another important component of this mechanism is LAT and its separation from TCR signaling machinery. Bringing LAT to the proximity of TCR complex also substantially lowers this threshold. Altogether, our data show that TCR and BCR signaling thresholds are not set by a single protein, but rather that multiple components of antigen receptor signaling apparatus are designed to work together to properly set their level.

Materials and methods

Cell culture

Ramos, Jurkat and P116 cells were cultured in RPMI (Thermo Fisher Scientific) and Phoenix cells were cultured in DMEM (Thermo Fisher Scientific). Media were supplemented with 10% fetal bovine serum (FBS, Thermo Fisher Scientific) and antibiotics, further referred to as complete RPMI.

Flow cytometry

For extracellular staining, cells were incubated on ice for 30 min in PBS, washed twice with PBS and analyzed. For intracellular staining, cells were fixed for 20 min in room temperature with 4% formaldehyde in PBS (Thermo Fisher Scientific). Alternatively, cells were stained for surface markers as described above. After fixing and/or staining, excess of formaldehyde was washed with PBS and cells were simultaneously blocked and permeabilized for 40 min using 0.3% Triton X-100 (Merck), 5% BSA (Merck) in PBS. Next, the cells were incubated on ice for 1 hour with primary antibody in 0.3% Triton X-100, 1% BSA in PBS, washed with PBS and analyzed. For calcium measurement, cells in concentration of 1×10^7 per ml were loaded with 4 µg of Fura-Red (Thermo Fisher Scientific) in DMSO (Merck) for 1 hour in complete RPMI in 37°C, washed, and resuspended in complete RPMI in concentration of $6x10^6$ cells per ml and placed on ice. Before stimulation, 0.5 ml of cell suspension was pre-warmed in 37°C with or without PP2 in DMSO. Cells were than measured for 30 sec. without stimulation and then stimulated with 0.5 ml of complete RPMI containing anti-TCR antibody (C305, produced as supernatant in house, approximately 10 µg/ml), 0.5 ml complete RPMI of anti CD16 (MEM-168, produced as supernatant in house, approximately 10 µg/ml), 0.5 ml complete RPMI containing 20 µg of AffiniPure $F(ab')_2$ Fragment Goat Anti-Human IgM, Fc5µ fragment specific (Jackson Immunoresearch), or with combination of 0.25 ml anti CD16 (10 µg/ml), 0.25 ml anti TCR (10 µg/ml) and 10 µg/ml of AffiniPure $F(ab')_2$ Fragment Goat Anti-Mouse IgM, µ chain specific. Cells were analyzed using LSRII cytometer (BD) followed by data analyses using FlowJo (BD).

Western blot and immunoprecipitation

Western blots were performed as described previously [41], visualized using Azure c300 imaging system (Azure Biosystems) and quantified using Aida Image Analysis software (Elysia-raytest). For immunoprecipitation, 2.5×10^7 cells per sample were incubated for 20 min with or without 20µM PP2 in complete RPMI. Cells were stimulated with Goat Anti-Human IgM (10 µg/ml final concentration) and incubated for 3 min. Next, cells were chilled on ice for 1 min, spun and lysed for 1 hour in 500 µl of Lysis buffer (50mM TRIS pH 7.4, 150mM NaCl, 1% NP-40 substitute (AppliChem GmbH), 10mM Chloroacetamide (Merck), Phosphatase inhibitor tablets (PhosSTOP, Roche), Protease Inhibitor Cocktail (Roche), 2mM EDTA (Merck)). Nuclei were spun down and supernatants were incubated overnight with indicated antibodies. Next day, antibodies were isolated from the lysates using protein A/G agarose beads (Santa Cruz Biotechnology), washed and eluted with SDS-PAGE sample buffer.

Cloning, transfection, transduction, cell sorting.

Sequences were amplified by PCR using Q5-polymerase (New England Biolabs) from human PBMC derived cDNA or from Ramos cells derived cDNA. DNA fragments were cloned into plasmids using Invitrogen enzymes as recommended by the manufacturer. Plasmids, inserts and cloning strategies are summarized in Table S1. Sequences of all inserts were verified using Sanger sequencing (Eurofins Genomics). For virus production, Phoenix ampho cells were transfected using Lipofectamine 2000 (Invitrogen). Two days after transfection, virus containing supernatant was collected and spun in the presence of polybrene (Merck) on the cells. Subsequently, infected cells were sorted based on reported gene expression on Influx sorter (BD).

Antibodies

Antibodies used for western blot and flow cytometry are listed in Tables S2 and S3.

Data availability

Representative experiments are shown in the figures. For any additional information, please contact the corresponding author.

Acknowledgments

We would like to thank to Ondřej Štěpánek and Aleš Drobek for discussions and to Jana Pokorná for providing us c305 and MEM-168 antibodies.

Funding and additional information

This study was supported by Charles University Grant Agency project number *1034216*.

Conflict of interest

The authors declare that they have no conflicts of interest with the contents of this article.

References

1. Irving, B. and A. Weiss, *A clue to antigen receptor tails.* J Immunol, 2014. **192**(9): p. 4013-4.
2. Getahun, A. and J.C. Cambier, *Of ITIMs, ITAMs, and ITAMis: revisiting immunoglobulin Fc receptor signaling.* Immunol Rev, 2015. **268**(1): p. 66-73.
3. Packard, T.A. and J.C. Cambier, *B lymphocyte antigen receptor signaling: initiation, amplification, and regulation.* F1000Prime Rep, 2013. **5**: p. 40.
4. Lanier, L.L., *Up on the tightrope: natural killer cell activation and inhibition.* Nat Immunol, 2008. **9**(5): p. 495-502.
5. Rolli, V., et al., *Amplification of B cell antigen receptor signaling by a Syk/ITAM positive feedback loop.* Mol Cell, 2002. **10**(5): p. 1057-69.
6. Saijo, K., et al., *Essential role of Src-family protein tyrosine kinases in NF-kappaB activation during B cell development.* Nat Immunol, 2003. **4**(3): p. 274-9.
7. Takata, M., et al., *Tyrosine kinases Lyn and Syk regulate B cell receptor-coupled Ca2+ mobilization through distinct pathways.* Embo j, 1994. **13**(6): p. 1341-9.
8. Mukherjee, S., et al., *Monovalent and multivalent ligation of the B cell receptor exhibit differential dependence upon Syk and Src family kinases.* Sci Signal, 2013. **6**(256): p. ra1.
9. Hanke, J.H., et al., *Discovery of a novel, potent, and Src family-selective tyrosine kinase inhibitor. Study of Lck- and FynT-dependent T cell activation.* J Biol Chem, 1996. **271**(2): p. 695-701.
10. Zhu, X., et al., *Structural analysis of the lymphocyte-specific kinase Lck in complex with non-selective and Src family selective kinase inhibitors.* Structure, 1999. **7**(6): p. 651-61.
11. Stepanek, O., et al., *Nonredundant roles of Src-family kinases and Syk in the initiation of B-cell antigen receptor signaling.* J Immunol, 2013. **190**(4): p. 1807-18.
12. Fasbender, F., et al., *Differential Requirements for Src-Family Kinases in SYK or ZAP70-Mediated SLP-76 Phosphorylation in Lymphocytes.* Front Immunol, 2017. **8**: p. 789.
13. Mocsai, A., J. Ruland, and V.L. Tybulewicz, *The SYK tyrosine kinase: a crucial player in diverse biological functions.* Nat Rev Immunol, 2010. **10**(6): p. 387-402.
14. Au-Yeung, B.B., et al., *The structure, regulation, and function of ZAP-70.* Immunol Rev, 2009. **228**(1): p. 41-57.
15. Klammt, C., et al., *T cell receptor dwell times control the kinase activity of Zap70.* Nat Immunol, 2015. **16**(9): p. 961-9.
16. Gradler, U., et al., *Structural and biophysical characterization of the Syk activation switch.* J Mol Biol, 2013. **425**(2): p. 309-33.
17. Deindl, S., et al., *Structural basis for the inhibition of tyrosine kinase activity of ZAP-70.* Cell, 2007. **129**(4): p. 735-46.
18. Yan, Q., et al., *Structural basis for activation of ZAP-70 by phosphorylation of the SH2-kinase linker.* Mol Cell Biol, 2013. **33**(11): p. 2188-201.

19. Chan, A.C., et al., *Activation of ZAP-70 kinase activity by phosphorylation of tyrosine 493 is required for lymphocyte antigen receptor function.* Embo j, 1995. **14**(11): p. 2499-508.
20. Brdicka, T., et al., *Intramolecular regulatory switch in ZAP-70: analogy with receptor tyrosine kinases.* Mol Cell Biol, 2005. **25**(12): p. 4924-33.
21. Rowley, R.B., et al., *Syk protein-tyrosine kinase is regulated by tyrosine-phosphorylated Ig alpha/Ig beta immunoreceptor tyrosine activation motif binding and autophosphorylation.* J Biol Chem, 1995. **270**(19): p. 11590-4.
22. El-Hillal, O., et al., *syk kinase activation by a src kinase-initiated activation loop phosphorylation chain reaction.* Proc Natl Acad Sci U S A, 1997. **94**(5): p. 1919-24.
23. Zoller, K.E., I.A. MacNeil, and J.S. Brugge, *Protein tyrosine kinases Syk and ZAP-70 display distinct requirements for Src family kinases in immune response receptor signal transduction.* J Immunol, 1997. **158**(4): p. 1650-9.
24. Tsang, E., et al., *Molecular mechanism of the Syk activation switch.* J Biol Chem, 2008. **283**(47): p. 32650-9.
25. Williams, B.L., et al., *Genetic evidence for differential coupling of Syk family kinases to the T-cell receptor: reconstitution studies in a ZAP-70-deficient Jurkat T-cell line.* Mol Cell Biol, 1998. **18**(3): p. 1388-99.
26. Lo, W.L., et al., *Lck promotes Zap70-dependent LAT phosphorylation by bridging Zap70 to LAT.* Nat Immunol, 2018. **19**(7): p. 733-741.
27. Steinberg, M., et al., *T-cell receptor-induced phosphorylation of the zeta chain is efficiently promoted by ZAP-70 but not Syk.* Blood, 2004. **104**(3): p. 760-7.
28. Iwashima, M., et al., *Sequential interactions of the TCR with two distinct cytoplasmic tyrosine kinases.* Science, 1994. **263**(5150): p. 1136-9.
29. Rotin, D., et al., *SH2 domains prevent tyrosine dephosphorylation of the EGF receptor: identification of Tyr992 as the high-affinity binding site for SH2 domains of phospholipase C gamma.* Embo j, 1992. **11**(2): p. 559-67.
30. Hughes, C.E., et al., *Critical Role for an acidic amino acid region in platelet signaling by the HemITAM (hemi-immunoreceptor tyrosine-based activation motif) containing receptor CLEC-2 (C-type lectin receptor-2).* J Biol Chem, 2013. **288**(7): p. 5127-35.
31. LATour, S., L.M. Chow, and A. Veillette, *Differential intrinsic enzymatic activity of Syk and Zap-70 protein-tyrosine kinases.* J Biol Chem, 1996. **271**(37): p. 22782-90.
32. Balagopalan, L., et al., *The LAT story: a tale of cooperativity, coordination, and choreography.* Cold Spring Harb Perspect Biol, 2010. **2**(8): p. a005512.
33. Lo, W.L., et al., *Slow phosphorylation of a tyrosine residue in LAT optimizes T cell ligand discrimination.* Nat Immunol, 2019. **20**(11): p. 1481-1493.
34. Arbulo-Echevarria, M.M., et al., *A Stretch of Negatively Charged Amino Acids of Linker for Activation of T-Cell Adaptor Has a Dual Role in T-Cell Antigen Receptor Intracellular Signaling.* Front Immunol, 2018. **9**: p. 115.
35. Bielekova, B. and R. Martin, *Antigen-specific immunomodulation via altered peptide ligands.* J Mol Med (Berl), 2001. **79**(10): p. 552-65.
36. Madrenas, J., et al., *Zeta phosphorylation without ZAP-70 activation induced by TCR antagonists or partial agonists.* Science, 1995. **267**(5197): p. 515-8.
37. McKeithan, T.W., *Kinetic proofreading in T-cell receptor signal transduction.* Proc Natl Acad Sci U S A, 1995. **92**(11): p. 5042-6.
38. Courtney, A.H., W.L. Lo, and A. Weiss, *TCR Signaling: Mechanisms of Initiation and Propagation.* Trends Biochem Sci, 2018. **43**(2): p. 108-123.
39. Yousefi, O.S., et al., *Optogenetic control shows that kinetic proofreading regulates the activity of the T cell receptor.* Elife, 2019. **8**.

40. Tischer, D.K. and O.D. Weiner, *Light-based tuning of ligand half-life supports kinetic proofreading model of T cell signaling.* Elife, 2019. **8**.
41. Kralova, J., et al., *Dysregulated NADPH Oxidase Promotes Bone Damage in Murine Model of Autoinflammatory Osteomyelitis.* J Immunol, 2020.

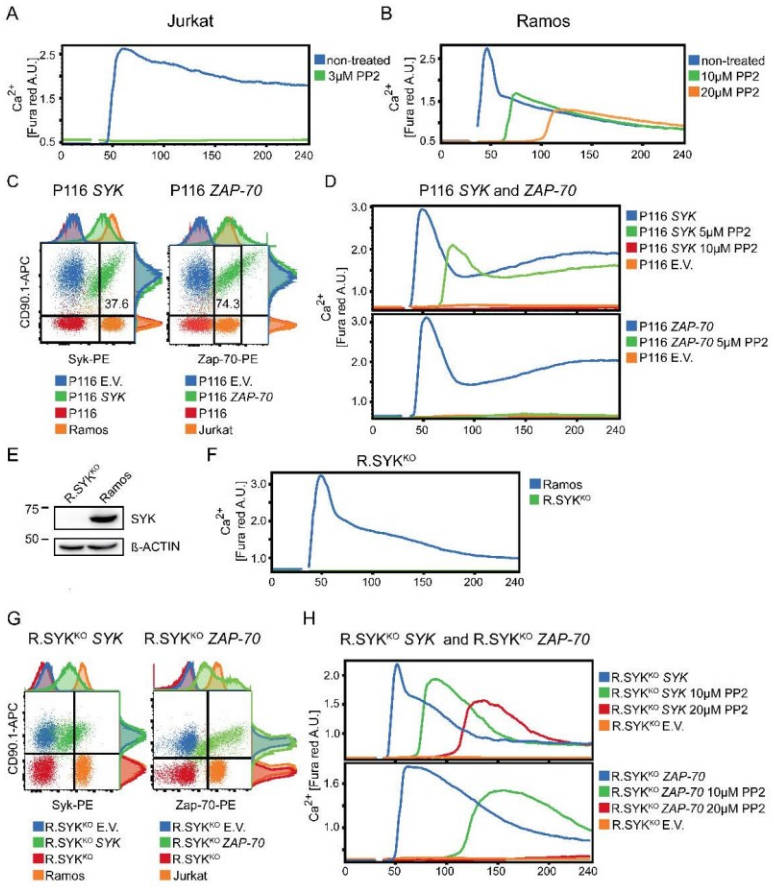

Figure 1. Differences between SYK and ZAP-70 only partially explain higher resistance of BCR signaling to SFK inhibition. (**A, B**) Flow cytometry analysis of calcium response in TCR-stimulated Jurkat T cell line (A) or BCR-stimulated Ramos B cell line (B) in the presence or absence of different concentrations of PP2. (N≥3) (**C**) Flow cytometry analysis of SYK and ZAP-70 expression in P116 cell line transduced with constructs coding for SYK or ZAP-70 followed by IRES-CD90.1. reporter. (**D**) Calcium signaling in P116 SYK or ZAP-70 cells stimulated with anti-TCR antibody C305. See supporting information S1 for gating strategy (N=3). (**E**) Western blot analysis of SYK expression in Ramos and R.SYK^{KO} cells. Beta Actin staining serves as a loading control. (**F**) Calcium signaling in Ramos and R.SYK^{KO} cells stimulated with anti-BCR antibody. (**G**) Flow cytometry analysis of SYK and ZAP-70 expression in R.SYK^{KO} cells transduced with construct coding for SYK or ZAP-70 -IRES-CD90.1. (**H**) Calcium response in

R.SYK^{KO} *SYK* or *ZAP-70* expressing cells stimulated with anti-BCR antibody (N≥3). All data from calcium measurements are depicted as medians of relative calcium concentration in the cells.

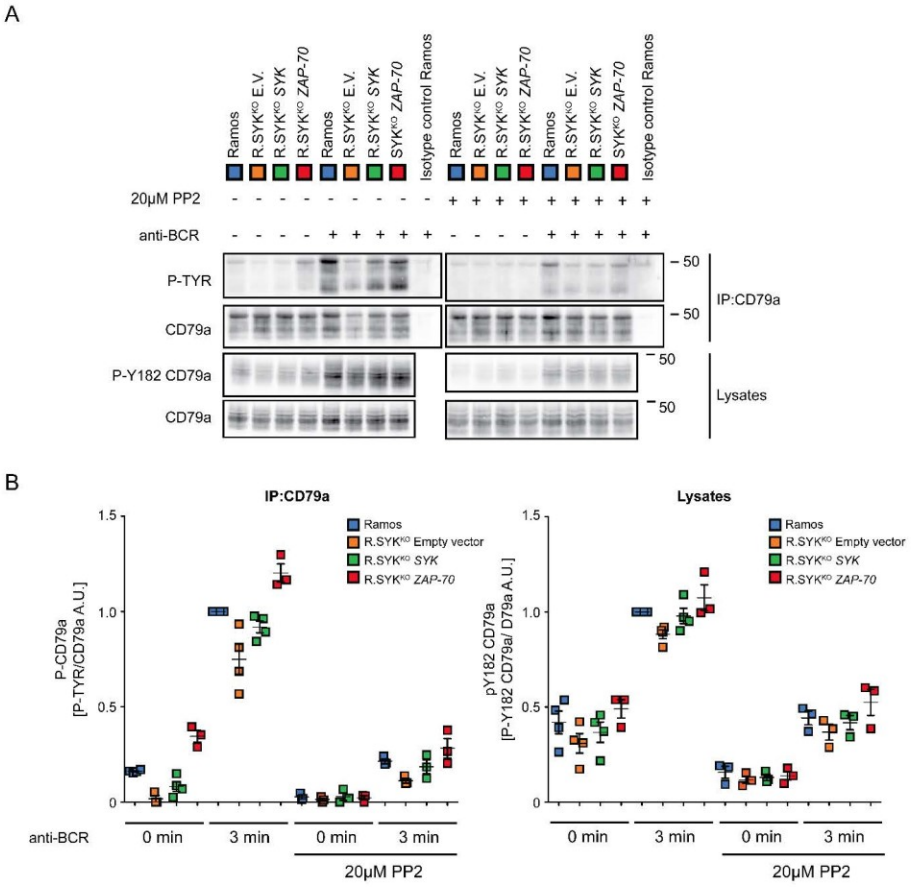

Figure 2. SYK and ZAP-70 facilitate similar increase in ITAM phosphorylation. (**A**) Western blot analysis of CD79a phosphorylation in Ramos cells and R.SYK^{KO} cells, transduced with *SYK*, *ZAP-70* or empty vector. The cells were treated with 20μM PP2, stimulated with anti BCR antibody, lysed and subjected to immunoprecipitation with anti-CD79a or control antibody. CD79a tyrosine phosphorylation in the immunoprecipitates was probed with anti-phosphotyrosine antibody. CD79a phosphorylation in the cell lysates was detected with phospho-specific antibody to tyrosine 182 of CD79a. (**B**) Quantification of multiple experiments from (A). The data were normalized to CD79a and then the background from control immunoprecipitation was subtracted.

To allow for comparison between individual experiments data were normalized to BCR stimulated Ramos cells (N≥3).

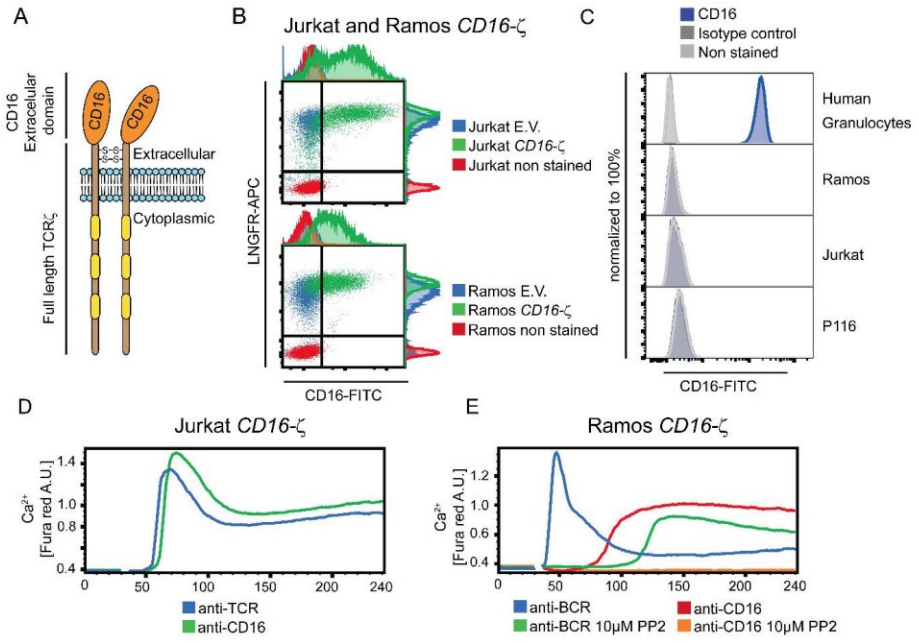

Figure 3. Signaling initiated by crosslinking of CD16-tagged TCRζ molecules (CD16-ζ) in B cells can be inhibited by PP2. (**A**) Schematic representation of chimeric CD16-ζ molecule. (**B**) Flow cytometry analyses of CD16-ζ expression in Jurkat and Ramos cell line transduced with construct coding for CD16-ζ -IRES-LNGFR. (**C**) Flow cytometry analyses of CD16 expression in human granulocytes (gated on SSA-high cells), Ramos Jurkat and P116 cells. (**D**) Calcium response in Jurkat CD16-ζ cells stimulated with anti-CD16 antibody or anti TCR antibody (C305). The experiment was performed similarly as in figure 1A (N=3). (**E**) Calcium response in Ramos CD16-ζ cells stimulated with anti-CD16 antibody or anti TCR antibody in the presence or absence of 10μM concentration of PP2. Experiment was performed similarly as in figure 1A (**E**, N=3).

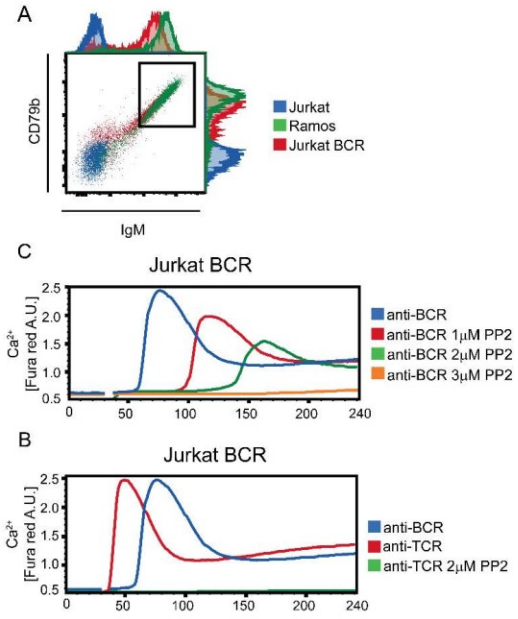

Figure 4. Ectopic expression of BCR in T cells increases the resistance to SFK inhibition. (**A**) Flow cytometry analysis of CD79a and surface IgM expression in Jurkat BCR cells. (**B, C**) Calcium response in Jurkat BCR cells stimulated with antibodies to TCR (B) or BCR (C) in the presence or absence of various concentrations of of PP2. Calcium response measurements were performed as in figure 1A (N≥3).

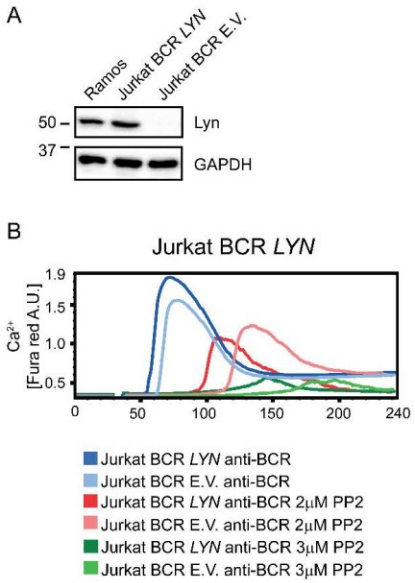

Figure 5. Effects of LYN expression on signaling in Jurkat BCR cells. (**A**) Western blot analysis of LYN expression in Jurkat BCR LYN, Jurkat BCR empty vector or Ramos cells. Similar loading was verified using GAPDH staining. (**B**) Calcium response in anti BCR antibody stimulated Jurkat BCR LYN or Jurkat BCR cells transduced with empty vector (E.V.) in the presence or absence of 2 and 3μM concentration of PP2. Calcium response measurements were performed as in Figure 1A (N=3).

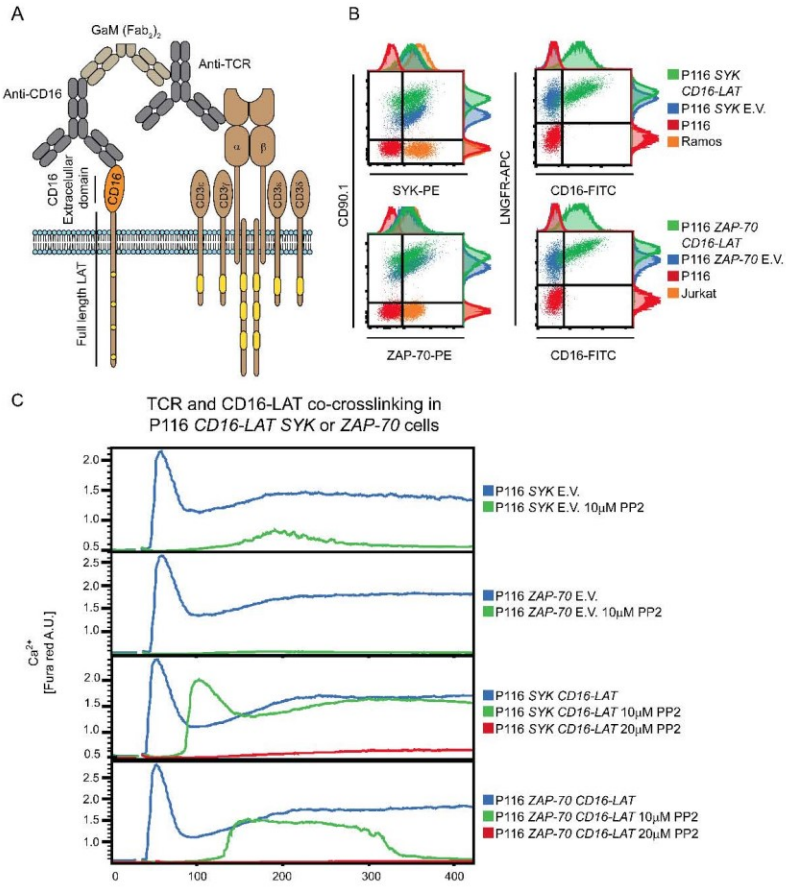

Figure 6. Co-crosslinking of chimeric protein CD16-LAT with TCR induces strong resistance to SFK inhibition. (**A**) Schematic representation of the experimental set up. (**B**) Flow cytometry analysis of SYK, ZAP-70 and CD16-LAT expression in Jurkat, Ramos, P116 and P116 cells transduced with indicated constructs. SYK or ZAP-70 were fused to IRES-CD90.1 reporter and CD16-LAT to IRES-LNGFR reporter. (**C**) Calcium response in P116 cells transduced with indicated constructs and stimulated with anti-CD16 and anti-TCR antibody co-crosslinked with secondary Goat-anti-Mouse IgG antibody in the presence of variable doses of PP2. Calcium measurement was performed as in Figure 1A (N=3).

Supporting information:

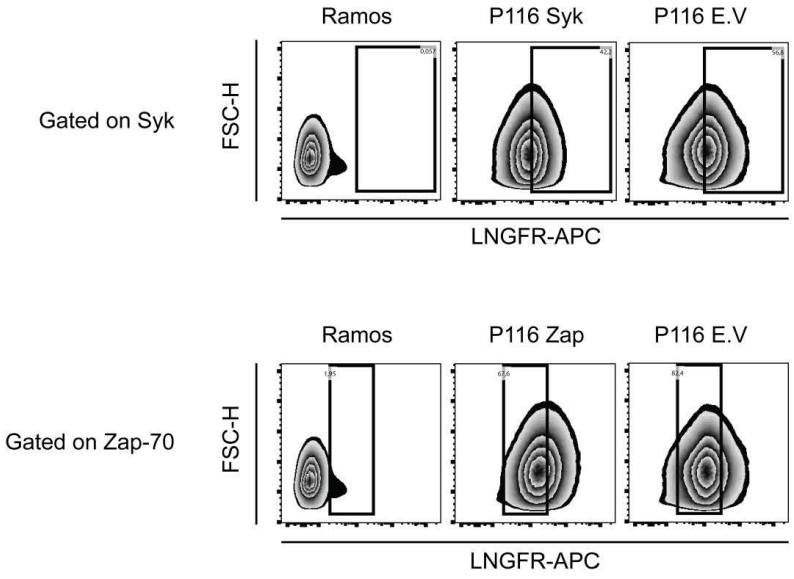

Supporting figure 1. Gating strategy of P116 *SYK*, *ZAP-70* or Empty vector cells from Figure 1D. Ramos cells were used as a negative control.

Inserted sequence	Type of isoform / targeted sequence	Plasmid	Aditional adjustments and comments
Zap-70	Isoform 1	MSCV IRES CD90.1	
Syk	Isoform 1	MSCV IRES CD90.1	Codons of crisper targeting sequence was optimalised to prevent cleavege. Changed nucleotides are capitalised gcTcaTcaTtaTacGatTgaAAgA 5' Untranslated region was syntetised by Eurofins Genomics gctcatgggcgcggtcagcagggcgggccagggcggcggggcgcgacactgggaggaagtgcgggccgcctgcccgggcgcgttaaggaagttgCccaaaatgaggaagagccgcgggcccggcggctgaggccaccccggcggcggctggagagcgaggaggagcgggtggccccgcgctgcgccgccctcgcctcacctggcgcaggtggacacctgcgcaggtgtgtgccctccggcccctgaagc
CD16-CD3ζ	CD16 Isoform 1 CD3ζ isoform 1	MSCV IRES LNGFR	CD16 extracelular fragment 1-208 AA followed by linker Thr,Arg and full length CD3ζ
IgM heavy chain	IgM, VH4	MSCV IRES LNGFR	
CD79a IRES CD79b	CD79a isoform 1 CD79b isoform 1	MSCV	CD79a was cloned to polycloning side of MSCV vector and CD79b inserted after IRES sequence in exchanged for reporter gen
Lyn	Isoform 1	MSCV IRES CD90.2	
CD16 Lat	Lat isoform 2 CD16 isoform 1	MSCV IRES LNGFR	CD16 extracelular fragment 1-208 AA followed by linker Thr,Arg and full length Lat
Syk targeting Crisper	ACACCACTACACC ATCGAGCGGG TCTGGTGATGTGG TAGCTCGCCC	pXPR_001	Genome-scale CRISPR-Cas9 knockout screening in human cells. Shalem O*, Sanjana NE*, Hartenian E, Shi X, Scott DA, Mikkelsen T, Heckl D, Ebert BL, Root DE, Doench JG, Zhang F (2014). Science, 343, 83-7. DOI: 10.1126/science.1247005

Table S1. Summary of constructs and cloning strategy.

Antigen	Clone	Company	Comments
Syk	4D10	Cell Signalling Technology	
Beta actin	13E5	Cell Signalling Technology	
CD79a	D1X5C	Cell Signalling Technology	For western blot staining
CD79a	HM 47	Exbio	For immunoprecipitation
p182 CD79a	Rabbit polyclonal	Cell Signalling Technology	
pTyrosine	4G10	Produced in house	
Lyn	Rabbit polyclonal	Cell Signalling Technology	
Gapdh	Rabbit polyclonal	Merck	
Mouse IgG1 Isotype control	MOPC-21	Exbio	
Mouse Anti-Rabbit IgG Antibody conjugated to peroxidase	M205	Genscript	For immunoprecipitation
Goat anti-Mouse IgG (H+L), conjugated to peroxidase	Polyclonal	Bio-Rad	For lysates
Goat anti-Rabbit IgG (H+L), conjugated to peroxidase	Polyclonal	Bio-Rad	For lysates

Table S2. List of antibodies used for western blot staining and immunoprecipitation.

Antigen	Clone	Conjugate	Company
CD90.1	HIS51	APC	eBioscience
Syk	4D10.2	PE	BioLegend
Zap-70	1E7.2.	PE	Exbio
CD16	MEM-154	FITC	Exbio
LNGFR	ME20.4-1.H4	APC	Miltenyi Biotec
Izotype control	P3.6.2.8.1	FITC	eBioscience
CD79b	Cb3-1	PE	Exbio
IgM, IgG, IgA	Goat polyclonal	FITC	Jackson Immunoresearch

Table S3. List of antibodies used for Flow cytometry analyzes.

Received: 12 July 2019 | Revised: 23 October 2019 | Accepted: 19 November 2019

DOI: 10.1111/jcmm.14895

ORIGINAL ARTICLE

WILEY

Transmembrane adaptor protein WBP1L regulates CXCR4 signalling and murine haematopoiesis

Simon Borna[1,2] | Ales Drobek[1] | Jarmila Kralova[1] | Daniela Glatzova[1,2,3] | Iva Splichalova[4] | Matej Fabisik[1,2] | Jana Pokorna[1] | Tereza Skopcova[1] | Pavla Angelisova[1] | Veronika Kanderova[5] | Julia Starkova[5] | Petr Stanek[6] | Orest V. Matveichuk[7] | Nataliia Pavliuchenko[1,2] | Katarzyna Kwiatkowska[7] | Majd B. Protty[8] | Michael G. Tomlinson[9] | Meritxell Alberich-Jorda[10] | Vladimir Korinek[11] | Tomas Brdicka[1]

[1]Laboratory of Leukocyte Signaling, Institute of Molecular Genetics of the Czech Academy of Sciences, Prague, Czech Republic

[2]Faculty of Science, Charles University, Prague, Czech Republic

[3]Department of Biophysical Chemistry, J. Heyrovsky Institute of Physical Chemistry of the Czech Academy of Sciences, Prague, Czech Republic

[4]Laboratory of Immunobiology, Institute of Molecular Genetics of the Czech Academy of Sciences, Prague, Czech Republic

[5]CLIP - Childhood Leukaemia Investigation Prague and Department of Pediatric Hematology and Oncology, Second Faculty of Medicine, Charles University, Prague, Czech Republic

[6]Second Faculty of Medicine, Charles University, Prague, Czech Republic

[7]Laboratory of Molecular Membrane Biology, Nencki Institute of Experimental Biology, Warsaw, Poland

[8]Institute of Biomedical Research, University of Birmingham, Birmingham, UK

[9]School of Biosciences, University of Birmingham, Birmingham, UK

[10]Laboratory of Hematooncology, Institute of Molecular Genetics of the Czech Academy of Sciences, Prague, Czech Republic

[11]Laboratory of Cell and Developmental Biology, Institute of Molecular Genetics of the Czech Academy of Sciences, Prague, Czech Republic

Correspondence
Tomas Brdicka, Institute of Molecular Genetics of the Czech Academy of Sciences, Videnska 1083, 14220 Prague, Czech Republic.
Email: tomas.brdicka@img.cas.cz

Present address
Majd B. Protty, Sir Geraint Evans Cardiovascular Research Building, Cardiff University, Cardiff, UK

Funding information
European Regional Development Fund, Grant/Award Number: CZ.1.05/1.1.00/02.0109 and OPPK (CZ.2.16/3.1.00/21547); Grantová Agentura České Republiky, Grant/Award Number: 16-07425S and P302-12-G101; H2020 Marie Skłodowska-Curie

Abstract

WW domain binding protein 1-like (WBP1L), also known as outcome predictor of acute leukaemia 1 (OPAL1), is a transmembrane adaptor protein, expression of which correlates with *ETV6-RUNX1* (t(12;21)(p13;q22)) translocation and favourable prognosis in childhood leukaemia. It has a broad expression pattern in haematopoietic and in non-haematopoietic cells. However, its physiological function has been unknown. Here, we show that WBP1L negatively regulates signalling through a critical chemokine receptor CXCR4 in multiple leucocyte subsets and cell lines. We also show that WBP1L interacts with NEDD4-family ubiquitin ligases and regulates CXCR4 ubiquitination and expression. Moreover, analysis of *Wbp1l*-deficient mice revealed alterations in B cell development and enhanced efficiency of bone marrow cell transplantation. Collectively, our data show that WBP1L is a novel regulator of CXCR4 signalling and haematopoiesis.

This is an open access article under the terms of the Creative Commons Attribution License, which permits use, distribution and reproduction in any medium, provided the original work is properly cited.
© 2019 The Authors. *Journal of Cellular and Molecular Medicine* published by Foundation for Cellular and Molecular Medicine and John Wiley & Sons Ltd.

Actions, Grant/Award Number: 665735; Medical Research Council, Grant/Award Number: G0400247; Akademie Věd České Republiky, Grant/Award Number: RVO 68378050; Ministerstvo Školství, Mládeže a Tělovýchovy, Grant/Award Number: LM2015040, LM2015062, NPU I LO1419, NPU I LO1604 and OP RDI CZ.1.05/2.1.00/19.0395; Agentura pro zdravotnický výzkum České republiky (Czech Health Research Council), Grant/Award Number: NV15-28848A; Institute of Molecular Genetics

KEYWORDS

bone marrow homing, bone marrow transplantation, CXCR4, ETV6, haematopoiesis, haematopoietic stem cell, NEDD4 family, OPAL1, RUNX1, WBP1L

1 | INTRODUCTION

WW domain binding protein 1-like (WBP1L) also known as outcome predictor of acute leukaemia 1 (OPAL1) has attracted attention because of a report showing that its elevated expression at mRNA level correlates with favourable outcome in childhood acute lymphoblastic leukaemia (ALL).[1] These data suggested that it could potentially serve as a prognostic marker. Later, it was shown that its levels are particularly increased in B cell progenitor ALL (BCP-ALL) with chromosomal translocation t(12;21)(p13;q22), which results in expression of *ETV6-RUNX1* fusion transcription factor.[2,3] In BCP-ALL, this translocation is associated with good prognosis, which likely explains the correlation between WBP1L expression and favourable outcome.[2] However, it is not known whether WBP1L functionally contributes to it.

ETV6, a fusion partner in *ETV6-RUNX1*, is a transcriptional repressor and *WBP1L* is one of its target genes.[4-6] In general, ETV6 targets are of high interest because of critical importance of ETV6 in haematopoiesis and its involvement in leukaemia. Around 30 fusions of *ETV6* to different partner genes and a number of mutations in *ETV6* have been identified so far, many of them implicated in various haematological malignancies of myeloid and lymphoid origin.[7,8] In addition, its critical role in normal haematopoiesis has been revealed in studies of ETV6-deficient mice, which show profound defects in haematopoietic stem and progenitor cell function and inability of these cells to reconstitute haematopoiesis after bone marrow transplantation.[9,10]

Bioinformatic sequence analysis revealed that WBP1L is a transmembrane adaptor protein with a very short extracellular/luminal part followed by a single transmembrane domain and a larger cytoplasmic tail.[11] Although relatively short, the extracellular/luminal part presumably forms a small compact domain held together by disulphide bridges formed among cysteines in the C*C*CC*CC motif.[11] The cytoplasmic part of WBP1L contains several potential interaction motifs corresponding to the consensus sequence of WW domain binding motifs L-P-X-Y or P-P-X-Y.[11]

Except for the limited bioinformatics analysis, WBP1L protein remained completely uncharacterized. Its physiological function has been unknown and whether it has any functional features that may link it to normal haematopoiesis or neoplasia has never been investigated. Here, we show that it binds several members of the NEDD4-family of ubiquitin ligases and that its deficiency results in enhanced surface expression and signalling of critical chemokine receptor CXCR4. WBP1L deficiency also results in alterations in B cell development and altered dynamics of stem and progenitor cells in the bone marrow. Taken together, we establish the role of WBP1L in CXCR4 signalling and in normal haematopoiesis. These findings also form the basis for further research on its potential role in leukaemia.

2 | MATERIALS AND METHODS

2.1 | Protein isolation, detection and quantification assays

Immunoprecipitations (IP) and immunoblotting were performed essentially as reported with adjustments described in online supplement. Western blot quantifications were carried out using Azure c300 imaging system (Azure Biosystems) and Aida Image Analysis software (Elysia-raytest). WBP1L expression in B cell lines was analysed by size exclusion chromatography-microsphere-based affinity proteomics analysis described in detail here,[3] and the data were quantified using Matlab (MathWorks). Tandem purification of WBP1L was based on the following publication[12] with modifications described in online supplement. WBP1L palmitoylation was analysed using metabolic labelling with palmitic acid analogue 17ODYA followed by reaction with biotin-azide and enrichment on streptavidin-coupled beads as described in detail in online supplement.

2.2 | Antibodies

Antibodies are listed in Tables S1 and S2. WBP1L antisera were generated by immunization of rabbits with KLH-conjugated peptide from WBP1L C-terminus while WBP1L monoclonal antibodies were prepared by standard hybridoma technology after immunization of mice with recombinant C-terminal part of murine WBP1L protein as described in online supplement.

2.3 | Cloning, qPCR, DNA transfection, virus preparation and cell infection

cDNA was generated using Quick-RNA kit (Zymo Research), revert aid reverse transcriptase (Thermo-Fisher) and oligo-dT primer. qPCR reactions were run on LightCycler 480 Instrument II using LightCycler 480 SYBR Green I Master mix (Roche). List of qPCR primers is in Table S3. For construct preparation see online supplement and Table S4. Phoenix cell transfection, virus generation and cell transduction were performed as described.[13] For lentivirus production, the procedure was to a minor extent modified as described in online supplement. Infected cells were sorted on Influx (BD) or selected on G418 (Thermo-Fisher).

2.4 | Mouse experiments, homing assays

Wbp1l$^{-/-}$ mice (*Wbp1l*$^{tm2a(EUCOMM)Hmgu}$) on C57Bl/6J genetic background were obtained from International Mouse Phenotyping Consortium. In these mice, gene trap flanked by FRT sites followed by coding region of exon 5 surrounded by LoxP sites were inserted into *Wbp1l* locus by homologous recombination (*Wbp1l*$^{-/-}$). Mice were bred in specific pathogen free conditions. To obtain inducible *Wbp1l*$^{fl/fl}$*CreERT* mice, we crossed animals of the *Wbp1l*$^{-/-}$ strain to *B6.Cg-Tg (ACTFLPe)9205 Dym/J* mice to remove the gene trap, and subsequently, to *B6.129-Gt(ROSA)26Sor*$^{tm1(cre/ERT2)Tyj}$*/J* animals. Both mouse strains were purchased from the Jackson Laboratory (Bar Harbor). To achieve *Wbp1l* deletion, mice were injected intraperitoneally with five daily doses of 2 mg of tamoxifen (Merck) in corn oil (Merck). For homing and transplantation assays, congenic *Ly5.1* (*C57BL/6NCr*) or *Ly5.1/Ly5.2* (*C57Bl/6J*) heterozygote recipients were sublethally (three Grey) or lethally (seven Grey) irradiated, followed by injection of transplanted cells into the tail vain. For experiments we used 8- to 12–week-old sex and age matched animals. Housing of mice and in vivo experiments were performed in compliance with local legal requirements and ethical guidelines. The Animal Care and Use Committee of the Institute of Molecular Genetics approved animal care and experimental procedures (Ref. No. 69/2014, 6/2016).

2.5 | Transwell migration

1 × 10^5 Cells in DMEM with 0.2% BSA were plated in the upper well of 5µm pore Transwell apparatus (Corning). After 4 hours, migrated cells in the bottom well were counted using a flow cytometer (LSRII; BD).

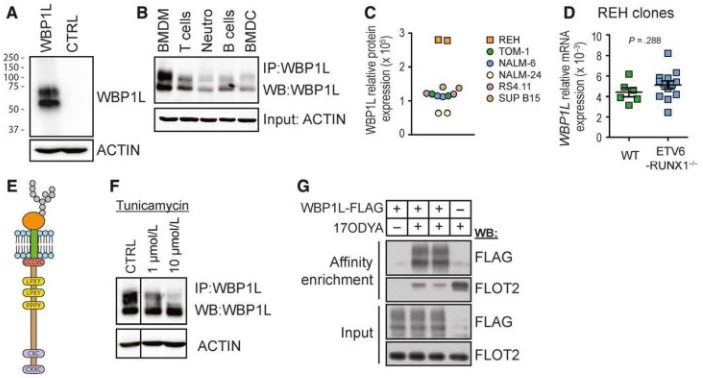

FIGURE 1 WBP1L is a palmitoylated glycoprotein, broadly expressed in haematopoietic cells. (A) Verification of new WBP1L rabbit antisera specificity on the lysates of HEK293 cells transfected or not with WBP1L construct. (B) Western blot analysis of WBP1L expression in murine leucocyte subsets. T cells (CD3$^+$), B cells (CD43$^-$, CD11b$^-$) and neutrophils (Ly6G$^+$) were isolated from the spleen or bone marrow. Bone marrow-derived macrophages (BMDM) and bone marrow-derived dendritic cells (BMDC) were differentiated in vitro from murine bone marrow. N = 3. (C) Expression of WBP1L in BCP-ALL cell lines was probed using size exclusion chromatography-microsphere-based affinity Proteomics method. Expression in *ETV6-RUNX1*$^+$ B cell line REH and *ETV6-RUNX1*$^-$ lines TOM-1, NALM-6, NALM-24, RS4.11 and SUB B15 was probed by two antibody clones to WBP1L (OPAL-01, OPAL-02) and quantified as an area under the curve on parts of chromatograms representing fractions corresponding to WBP1L (N = 1 per antibody clone). (D) Expression of *WBP1L* mRNA in different *ETV6-RUNX1*$^{-/-}$ REH clones from two independent sources of REH cells. Data are plotted as $2^{-\Delta ct}$ (N = 3). (E) Schematic representation of WBP1L structure and conserved sequence motifs (F) Analysis of WBP1L glycosylation in BMDM. BMDM treated or not with 1 or 10 µmol/L tunicamycin (overnight) were subjected to WBP1L immunoprecipitation followed by immunoblotting with WBP1L antisera. β-actin was stained in the corresponding cell lysates (N = 2). Irrelevant lines from the blot image were removed and replaced with a vertical dividing line. (G) Analysis of palmitoylation of WBP1L. HEK293 cells expressing WBP1L-FLAG-STREP were metabolically labelled with palmitate analogue 17ODYA and lysed. 17ODYA labelled proteins were tagged in a click chemistry reaction with biotin-azide, purified on streptavidin-coupled beads and analysed for the presence of WBP1L with anti-FLAG antibody (upper panel) or FLOTILLIN-2 as a representative of endogenous palmitoylated proteins (middle upper panel). WBP1L expression in cell lysates (middle lower panel) and comparable loading were verified by immunoblotting with antibodies to FLAG-tag (WBP1L) or FLOTILLIN-2, respectively (N = 3)

2.6 | Statistics

Results represent means ± SEM. If not specified otherwise, *P*-values were calculated using two-tailed Student's *t* test, one-way ANOVA or *Q* test. N represents number of animals or values per group or number of independent experiments.

3 | RESULTS

3.1 | WBP1L is a palmitoylated glycoprotein broadly expressed in haematopoietic cells

Analysis of WBP1L protein and mRNA expression in murine and human haematopoietic system with a newly generated polyclonal rabbit antibody (Figure 1A) and with Genevestigator tool, respectively, revealed that WBP1L is broadly expressed across multiple human and murine haematopoietic cell subsets (Figure 1B and S1). In addition and in agreement with previous reports of deregulated WBP1L expression in *ETV6-RUNX1*$^{+}$ BCP-ALL, we have found elevated levels of WBP1L protein in REH cell line, which is derived from *ETV6-RUNX1*$^{+}$ BCP-ALL. (Figure 1C and S2A). Interestingly, the genetic deletion of *ETV6-RUNX1* in REH cells (Figure S2B,C) did not alter WBP1L expression in these cells (Figure 1D).

Imaging of murine bone marrow-derived macrophages transduced with retroviral vector coding for murine WBP1L fused to EGFP revealed relatively broad distribution of WBP1L-EGFP within these cells. We have observed co-localization with plasma membrane, Golgi, endoplasmic reticulum, and to a limited extent with lysosomes and/or other acidic organelles (Figure S3). On the other hand, no co-localization with mitochondria could be detected (Figure S3).

The N-terminal part of WBP1L protein is highly conserved among major vertebrate classes (Figure S4). This region contains several conserved motifs, including potential N-glycosylation (NXS) and palmitoylation sites (Figure 1E and S4). Indeed, we could confirm that WBP1L is both glycosylated and palmitoylated (Figure 1F,G).

3.2 | WBP1L interacts with NEDD4-family E3 ubiquitin ligases

Cytoplasmic part of WBP1L contains three WW domain binding motifs ([L/P]PXY) (Figure 1E and S4). It has been speculated that they may interact with WW domains of NEDD4-family ubiquitin ligases.[11]

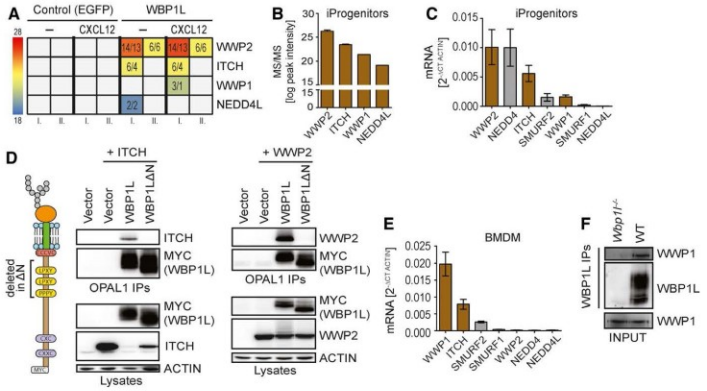

FIGURE 2 WBP1L binds multiple NEDD4-family E3 ubiquitin ligases. (A) Data from two independent mass spectrometry analyses (I. and II.) of WBP1L binding partners. *Wbp1l*$^{-/-}$ monocyte/macrophage progenitors were transduced with the constructs coding for WBP1L-FLAG-STREP or EGFP with the same tag. The cells were stimulated for 2 min with CXCL12 or left untreated. Tagged proteins with their binding partners were isolated by tandem purification and subjected to mass spectrometry analysis. The data are presented as colour-coded intensities obtained by label-free quantification of NEDD4-family E3 ubiquitin ligases. Values represent number of peptides used for intensity calculation/ number of unique peptides. Samples, where no peptides from a particular E3 ligase were detected, are coloured in grey (B) Label-free quantification of interacting E3 ligases from mass spectrometry experiment. Combined average intensities from both CXCR4 stimulated and non-stimulated samples are plotted (experiment I. form (A) only). (C) mRNA expression of NEDD4-family E3 ubiquitin ligases in immortalized monocyte/macrophage progenitors (iProgenitors). Plotted in brown are those ligases that interacted with WBP1L in mass spectrometry experiments (N = 3). (D) WBP1L interaction with NEDD4-family E3 ligases is dependent on WW binding motifs in WBP1L N-terminus. HEK293 cells were transfected with WBP1L-Myc or WBP1LΔN-Myc (with segment containing all WW binding motifs deleted) together with ITCH or WWP2. Following WBP1L immunoprecipitation, the isolated material and the original lysates were immunoblotted with antibody to ITCH or WWP2 and various controls as indicated (N = 3). (E) mRNA expression of NEDD4-family E3 ligases in BMDM. Plotted in brown are those ligases that interacted with WBP1L in mass spectrometry experiment (N = 3). (F) Endogenous interaction of WBP1L with WWP1 in BMDM. WBP1L immunoprecipitates from WT or *Wbp1l*$^{-/-}$ BMDM were immunoblotted with antibody to WWP1 and WBP1L. Input lysates were probed with antibody to WWP1 (N = 3). See also Figure S5

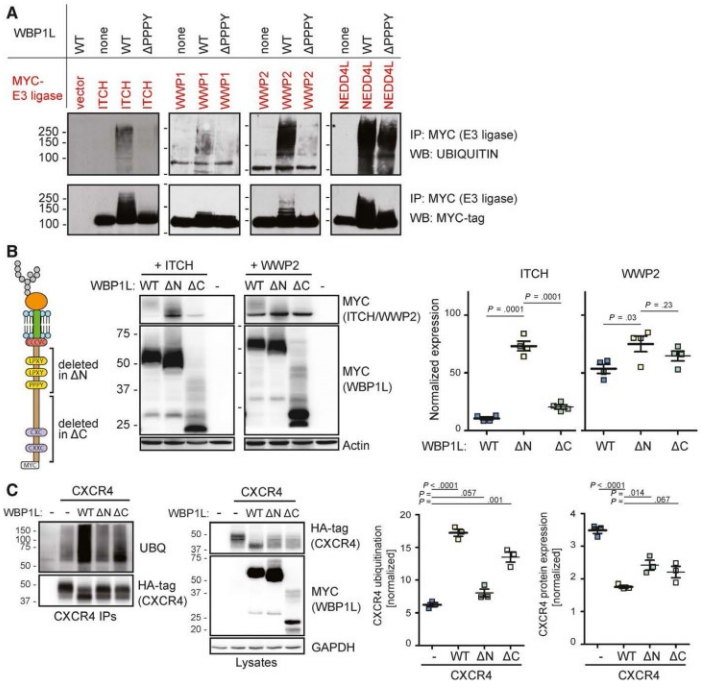

FIGURE 3 WBP1L regulates ubiquitination and expression of NEDD4-family E3 ubiquitin ligases and CXCR4. (A) HEK293 cells were cotransfected with individual Myc-tagged NEDD4-family E3 ubiquitin ligases and non-tagged WBP1L or its mutant lacking PPPY WW domain interacting motif. E3 ligases were immunoprecipitated via the Myc-tag from the lysates of these cells and subjected to immunoblotting with anti-MYC-tag or anti-UBIQUITIN antibody. (B) ITCH and WWP2 stability in HEK293 cells in the presence of WBP1L-MYC, WBP1L ΔC-MYC (deletion of almost entire intracellular part of WBP1L except for WW binding motifs) or WBP1L ΔN-MYC (deletion of WW binding motifs). Lysates from HEK293 cells transfected with ITCH-MYC or WWP2-MYC and WBP1L constructs were immunoblotted with antibody to MYC-tag to visualize ITCH, WWP2 and all forms of WBP1L and with antibody to ACTIN. Quantifications of the data are plotted as values normalized to ACTIN signal and then further normalized to experiment average to allow for comparison among the experiments (N = 3). (C) WBP1L-mediated increase in CXCR4 ubiqutination and down-regulation of CXCR4 protein levels in HEK293 cells. WBP1L-MYC, WBP1LΔC-MYC or WBP1LΔN-MYC were cotransfected with CXCR4-HA followed by CXCR4 imunoprecipitation and immunoblotting with antibodies to ubiquitin or HA-tag. Lysates were probed with antibodies to HA-tag (CXCR4), MYC-tag (WBP1L) or GAPDH (N = 3). For quantification, ubiquitination was normalized to HA-tag (CXCR4) signal (left panel) and CXCR4 expression to GAPDH (right panel). Both were further normalized to experiment average to allow for comparison among the individual experiments

However, this family has nine different members. To investigate whether WBP1L interacts with any of these ligases, we have expressed a FLAG-STREP-tagged WBP1L construct in immortalized monocyte/macrophage progenitors. We have selected this cell type because of a relatively high level of *Wbpl1* mRNA in myeloid progenitors (Figure S1). We isolated the FALG-STREP-tagged construct together with its associated binding partners from the lysates of these cells via a tandem purification on anti-FLAG and Streptactin beads. Mass spectrometry analysis of the isolated material revealed that WBP1L indeed interacts with several members of NEDD4-family. In this particular cell type, WWP2 was the most prominent. However, ITCH, WWP1 and NEDD4L could also be detected in one experiment (Figure 2A). Interestingly, the mass spectrometry signal intensities corresponded to the relative expression levels of these NEDD4-family members in immortalized monocyte/macrophage progenitors (Figure 2B,C). On the other hand, not all NEDD4-family members expressed in these cells could be co-isolated with WBP1L. These data suggest a certain level of WBP1L selectivity for individual NEDD4-family members.

To find out whether NEDD4-family ligases bind WBP1L via its [L/P]PXY WW domain binding motifs we have co-expressed the two highest scoring NEDD4-family ligases from the mass spectrometry experiment, WWP2 or ITCH, with wild-type WBP1L construct or with mutant WBP1LΔN lacking the membrane-proximal WW domain binding sequences (Figure 2D) in HEK293 cells. These cells allow for relatively high level of overexpression, which was ideal for reliable identification of NEDD4 family binding sites in WBP1L. Both E3 ligases could be readily co-immunoprecipitated with wild-type WBP1L but not with WBP1LΔN (Figure 2D). These data were further confirmed in a similar experiment in J774 macrophage-like cell line, which expresses relatively high level of

ITCH (not shown). The endogenous ITCH could be co-isolated with wild-type WBP1L but not with WBP1LΔN from these cells (Figure S5). To confirm the interaction of WBP1L with a NEDD4-family member at the endogenous protein level, we have selected bone marrow-derived macrophages (BMDM) which express the highest levels of WBP1L among the cell types we have tested so far (Figure 1B). WWP1, which is the most abundant NEDD4-family member in this cell type (Figure 2E), could be co-isolated with WBP1L in this experiment (Figure 2F).

3.3 | WBP1L regulates ubiquitination and expression level of NEDD4-family E3 ubiquitin ligases and of CXCR4

Interaction with WW domain binding motifs is known to result in the activation and autoubiquitination of NEDD4-family ubiquitin ligases.[14,15] To test whether WBP1L can activate NEDD4 family members, we have cotransfected WBP1L-interacting (Figure 2A) NEDD4-family ligases with wild-type WBP1L, or its mutant lacking one of the conserved WW domain binding motifs, into HEK293 cells. This analysis demonstrated that cotransfection with wild-type but not mutant WBP1L resulted in a substantial increase in ubiquitination of all these ligases, which is a sign of their activation (Figure 3A). Published work suggests that in the case of ITCH this ubiquitination results in down-regulation of its protein levels, while WWP2 appears relatively resistant to this negative feedback regulation. Thus, to further explore the mechanism of how WBP1L regulates these ubiquitin ligases, we co-expressed wild-type WBP1L, WBP1LΔN or WBP1LΔC (lacking C-terminal region of unknown function) with ITCH or WWP2 in HEK293 cells. Co-expression of ITCH with wild-type WBP1L and WBP1LΔC resulted in significantly reduced ITCH protein level when compared to co-expression with WBP1LΔN. As expected, this effect was much more limited in case of WWP2 (Figure 3B).

One of the best-studied targets of NEDD4-family ubiquitin ligases in the haematopoietic system is the chemokine receptor CXCR4. It is involved in the maintenance of haematopoietic stem and progenitor cells and in promoting niche interactions in the bone marrow. It is also thought to support the survival and treatment resistance of leukaemic cells.[16,17] Based on these features, we have selected CXCR4 for a similar set of experiments to test whether WBP1L regulates its protein expression levels and ubiquitination. Indeed, co-expression of WBP1L with CXCR4 in HEK293 cells resulted in increased ubiquitination of CXCR4 (presumably by an endogenous NEDD4-family ligase). This effect was almost completely abolished by mutation of the WW domain binding motifs (WBP1LΔN) while deletion of the C-terminal sequence (WBP1LΔC) had a more limited effect (Figure 3C). CXCR4 ubiquitination was further accompanied by reduction in CXCR4 protein levels (Figure 3C). We also observed that WBP1L co-expression resulted in a striking increase in CXCR4 electrophoretic mobility (Figure 3C). The reason for this mobility shift is at present unknown.

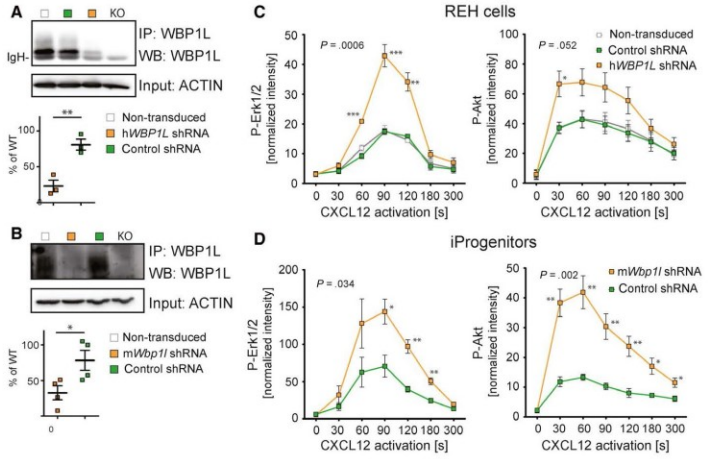

FIGURE 4 ShRNA-mediated down-regulation of WBP1L results in enhanced CXCR4 signalling in human and murine cell lines. (A, B) WBP1L immunoprecipitates from REH cells (A) or immortalized monocyte/macrophage progenitors (B) transduced with *Wbp1l* shRNA were stained with WBP1L antisera to demonstrate WBP1L down-regulation. Equal input of lysates to immunoprecipitation was verified by ACTIN immunoblotting. Quantification of multiple experiments (after normalization to ACTIN signal) was plotted as a percentage of WBP1L expression in non-transduced cells. (C, D) ERK1/2 and AKT phosphorylation downstream of CXCR4 in REH cells (C) and immortalized monocyte/macrophage progenitors (iProgenitors) (D), where WBP1L was down-regulated by shRNA. Cells were stimulated with 100 nmol/L CXCL12, lysed and subjected to Western blot analysis of ERK1/2 and AKT phosphorylation. Data represent mean of fluorescence intensity normalized to GAPDH. The *P*-value was calculated to compare maximum responses of cells transduced with non-silencing control and silencing shRNA. Asterisks denote significant differences in individual time-points. (N = 4)

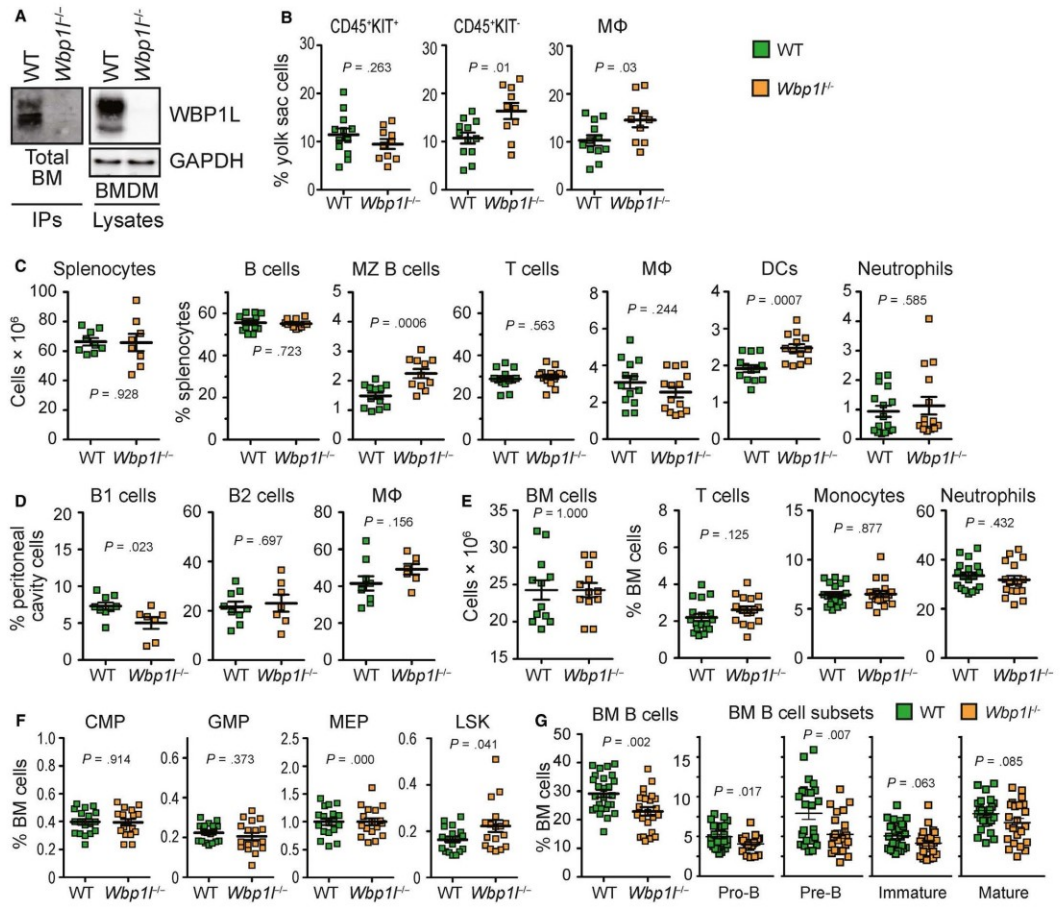

FIGURE 5 Altered leucocyte homeostasis in WBP1L-deficient mice. (A) Western blot analysis of WBP1L immunoprecipitates or whole cell lysates prepared from WT and *Wbp1l*$^{-/-}$ cells. mOPAL-01/03 antibodies were used for immunoprecipitation and WBP1L rabbit antisera for Western blotting. N = 3 (bone marrow), N = 5 (BMDM). (B) Flow cytometry analyses of E10.5 WT and *Wbp1l*$^{-/-}$ yolk sac cell subsets. Primitive macrophages were defined as Ter119^{-} CD11b^{+} F4/80^{+}. (C) Absolute numbers of splenocytes obtained from WT and *Wbp1l*$^{-/-}$ mice and flow cytometry analyses of WT and *Wbp1l*$^{-/-}$ splenocytes defined using the following markers: B cells (B220^{+}), MZ B cells (B220^{+}, AA4.1^{-}, CD23$^{-/low}$, CD1d^{+}), T cells (CD3^{+}), macrophages (F4/80^{+}, CD11b^{int}), DC (CD11c^{+}, LY6C$^{-/low}$) and neutrophils (LY6G^{+}, CD11b^{+}, LY6C^{-}). (D) Flow cytometry analyses of WT and *Wbp1l*$^{-/-}$ leucocytes in the peritoneum, defined using the following markers: B1 cells (SSC^{low}, FSC^{low}, B220^{+}, CD23$^{-/low}$), B2 cells (SSC^{low}, FSC^{low}, B220^{+}, CD23^{+}) and macrophages (large peritoneal macrophages, CD11b^{high},F4/80^{high}). (E) Flow cytometry analyses of WT and *Wbp1l*$^{-/-}$ bone marrow cell subsets, defined using the following markers: T cells (CD3^{+}), monocytes (LY6C^{+}, CD11b^{+}, LY6G^{-}, CD19^{-}, TER119^{-}, CD3^{-}, NK1.1^{-}), neutrophils (KIT^{-}, B220^{-}, TER119^{-}, CD3^{-}, LY6G^{high}) (F) Flow cytometry analyses of stem and progenitor cells in the bone marrow. Cell subsets were defined using following markers: common myeloid progenitors—CMP (lin^{-}, c-kit^{+}, CD34^{+}, CD16/32$^{neg-low}$, SCA1^{-}), granulocyte-monocyte progenitors—GMP (lin^{-}, KIT^{+}, CD34^{+}, CD16/32^{High}, SCA1^{-}), megakaryocyte-erythroid progenitors—MEP (lin^{-}, KIT^{+}, CD34^{-}, CD16/32^{-}, SCA1^{-}) and LSK (lin^{-}, KIT^{+}, SCA1^{+}). (G) Flow cytometry analysis of bone marrow B cell subsets. B cells (B220^{+}), pro-B cells (CD43^{+}, B220^{+}, IgM^{-}), pre-B cells (CD43^{-}, B220^{low}, IgM^{-}), immature B cells (CD43^{-}, B220^{low}, IgM^{+}) and mature B cells (CD43^{-}, B220^{high}, IgM^{+})

3.4 | WBP1L inhibits CXCR4 signalling in murine and human cell lines

To analyse the effects of the endogenous WBP1L on CXCR4, we have selected two cell lines where the expression of WBP1L and/or CXCR4 is highly relevant. These included human leukaemic cell line REH as a representative of *ETV6-RUNX1*$^{+}$ leukaemia, where we have down-regulated WBP1L by a single shRNA specific for human *WBP1L* and immortalized murine monocyte/macrophage progenitors as a representative of bone marrow progenitors, where

we used a different shRNA targeting murine *Wbp1l* (Figure 4A,B). After stimulation with CXCR4 ligand CXCL12, these cells showed enhanced activity of downstream signalling pathways, resulting in increased phosphorylation of ERK1/2 and AKT (Figure 4C,D and S6). CXCR7, another known receptor for CXCL12, did not contribute to the signalling output under these conditions (Figure S7). These data demonstrated that WBP1L is involved in the negative regulation of CXCR4 signalling.

3.5 | Altered haematopoiesis in *Wbp1l*-deficient mice

To further analyse the physiological function of WBP1L, we have acquired *Wbp1l*-deficient mouse strain *Wbp1l*$^{tm2a(EUCOMM)Hmgu}$ (hereafter referred to as *Wbp1l*$^{-/-}$) from the International Mouse Phenotyping Consortium. These mice appeared grossly normal and healthy, were born in normal Mendelian ratios and did not express WBP1L protein (Figure 5A).

To characterize the haematopoietic system in *Wbp1l*$^{-/-}$ mice, we have analysed major cell subset frequencies in adult mice and in embryos. The embryonic haematopoietic cell numbers were grossly normal with small increases in the yolk sac CD45$^+$ KIT$^-$ cells and CD11b$^+$ F4/80$^+$ yolk sac macrophages (Figure 5B). In the peripheral tissues of the adult mice, there was a significant increase in marginal zone B cell fraction in the spleen (Figure 5C) and a reduction in B1 cell percentages in the peritoneal cavity (Figure 5D). We also observed increased frequencies of splenic dendritic cells in *Wbp1l*$^{-/-}$ mice (Figure 5C). Otherwise, the frequencies of other leucocyte subsets found in peripheral tissues were normal (Figure 5C,D). Bone marrows from *Wbp1l*$^{-/-}$ animals showed the same cell counts as wild-type bone marrows (Figure 5E). Most of bone marrow cell subsets were also found in normal numbers, including T cells, monocytes, neutrophils (Figure 5E) and the majority of progenitor populations (Figure 5F). However, there were two notable exceptions. First, the overall B cell percentages in the bone marrow were significantly reduced (Figure 5G). The reduction was most pronounced in early developmental stages (pro- and pre-B cells). At the later stages, including immature and mature B cells a similar trend was observed, but it was outside the threshold for statistical significance (*P*-values .06 and .08, respectively) (Figure 5G). The cell cycle of B cell progenitors was not substantially changed with the exception of a very

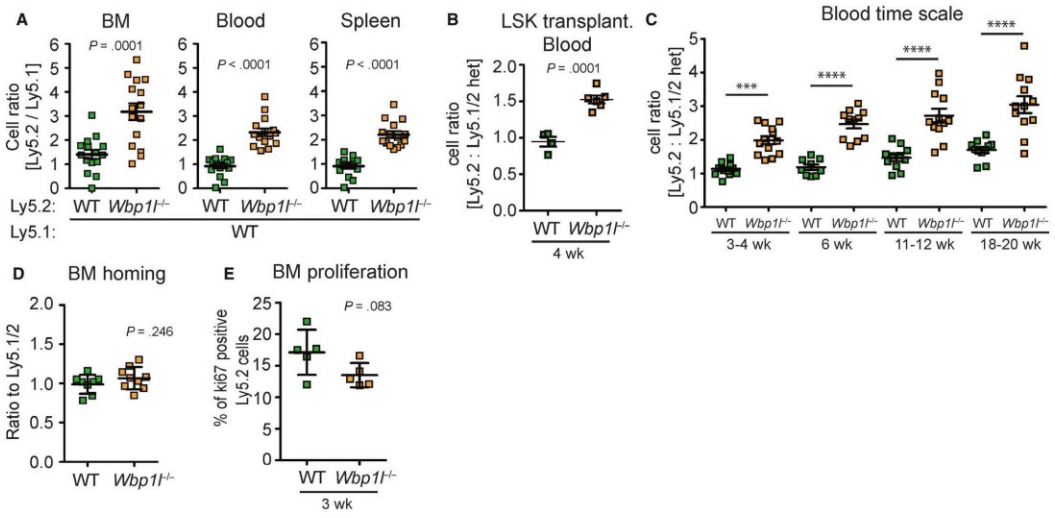

FIGURE 6 Enhanced engraftment of *Wbp1l*$^{-/-}$ bone marrow. (A) Ly5.2$^+$ bone marrow (WT or *Wbp1l*$^{-/-}$) was mixed with Ly5.1$^+$ bone marrow (always WT) in a ratio 1:1 and 2 × 10^6 cells were transplanted into Ly5.1 lethally irradiated mice. Mice were analysed 2 months post-transplantation. Flow cytometry analyses show the ratio between Ly5.2 and Ly5.1 cells in the bone marrow, blood and spleen. (B) LSK cells sorted from Ly5.2$^+$ bone marrow (WT or *Wbp1l*$^{-/-}$) were mixed with LSK from Ly5.1/Ly5.2$^+$ heterozygous bone marrow (always WT) in a ratio 1:1 and 20 000 cells together with support of 0.5 × 10^6 Ly5.1 bone marrow cells were injected into tail vain of Ly5.1 lethally irradiated mice. Data represent the ratio between Ly5.2$^+$ and Ly5.1/Ly5.2$^+$ cells detected in the recipient blood 4 wk post injection. One of two independent experiments is shown (N ≥ 8). (C) Ly5.2$^+$ bone marrow (WT or *Wbp1l*$^{-/-}$) was mixed with Ly5.1/Ly5.2$^+$ heterozygous bone marrow (always WT) in a ratio 1:1 and 2 × 10^6 cells were transplanted into Ly5.1 lethally irradiated mice. At indicated time-points, the ratio between Ly5.2 and Ly5.1/Ly5.2 cells in blood was measured by flow cytometry. (D) Homing of WT and *Wbp1l*$^{-/-}$ bone marrow cells in a competitive set-up. WT or *Wbp1l*$^{-/-}$ bone marrow (Ly5.2$^+$) was each combined with WT bone marrow from Ly5.1/Ly5.2$^+$ heterozygotes in a ratio 1:1 and 2 × 10^6 cells were injected into the tail vain of sublethally irradiated recipient (Ly5.1$^+$). Data represent the ratio between Ly5.2$^+$ and Ly5.1/Ly5.2$^+$ cells detected in the recipient bone marrow 16 h post injection (N ≥ 8). (E) Competitive bone marrow transplantation was performed as in (C) and 3 wk after the transplantation expression of Ki67 proliferation marker was measured in transplanted cells

small but significant increase in G1 phase pre-B cells in *Wbp1l*$^{-/-}$ mice (Figure S8). Second, Lin$^-$SCA1$^+$KIT$^+$ (LSK) cells encompassing early progenitors and stem cells (HSPC) showed slightly but significantly increased percentages in these animals (Figure 5F).

To test their functionality in vivo, we performed a competitive bone marrow transplantation assay, whereby we mixed wild-type or *Wbp1l*$^{-/-}$ Ly5.2 cells with wild-type Ly5.1 bone marrow cells in a 1:1 ratio and transplanted these mixtures into lethally irradiated recipient mice (Ly5.1). Nine weeks later, we have analysed their engraftment. Strikingly, *Wbp1l*$^{-/-}$ bone marrow engrafted significantly better and the ratio between *Wbp1l*$^{-/-}$ and wild-type cells increased from 1:1 to ca 3:1 (Figure 6A), whereas wild-type Ly5.2 and Ly5.1 BM engrafted with equal efficiency. The difference could be observed across all bone marrow leucocyte subsets analysed except for LSK cells, where a similar trend in favour of *Wbp1l*$^{-/-}$ cells was also present but was not statistically significant (Figure S9). The difference was also maintained in the periphery, where the ratio between *Wbp1l*$^{-/-}$ and wild-type cells was roughly 2:1 (Figure 6A). Similar difference in engraftment efficiency was also observed when we transplanted sorted LSK cells in the 1:1 ratio (Figure 6B). Next, we investigated how this ratio changes with time. A significant difference between the engraftment efficiency could be observed as early as 3 weeks after the transplantation and was maintained till at least 18 weeks after the transplantation (Figure 6C). The increased efficiency in the bone marrow engraftment was not the result of increased homing to the bone marrow or increased proliferation, which did not display any alteration (Figure 6D,E). Collectively, these data are showing negative role of WBP1L in HSPC function. Persistence of the engraftment advantage for more than 16 weeks suggests that the haematopoietic system is affected already at the level of haematopoietic stem cells.

3.6 | Compensatory mechanisms restore CXCR4 signalling when WBP1L is lost in the germline, but the effects of WBP1L deficiency on CXCR4 signalling can be observed upon its acute deletion

Part of the data described above are consistent with CXCR4 hyperactivity. However, the same homing capacity of the wild-type and *Wbp1l*$^{-/-}$ bone marrow cells (Figure 6D) is incompatible with enhanced CXCR4 function. These results prompted us to test whether bone marrow cells from *Wbp1l*$^{-/-}$ mice display similar CXCR4 dysregulation as shRNA-treated cell lines. Surprisingly, we did not observe any alterations in CXCL12-triggered ERK phosphorylation in bone marrow cells from *Wbp1l*$^{-/-}$ mice (Figure 7A). This result was in disagreement with our analysis of the effects of shRNA-mediated WBP1L down-regulation in cell lines (Figure 4). To exclude the possibility that enhanced CXCR4 signalling observed there was the result of non-specific off-target effects of *Wbp1l* shRNAs, we expressed shRNA targeting *Wbp1l* in immortalized monocyte/macrophage progenitors from wild-type and *Wbp1l*$^{-/-}$ mice. Because of the absence of WBP1L, only non-specific activity of *Wbp1l* shRNA can be detected in *Wbp1l*$^{-/-}$ progenitors. As expected, *Wbp1l* shRNA significantly enhanced CXCL12-triggered ERK activation in wild-type cells. On the other hand, only negligible insignificant changes were detected in *Wbp1l*$^{-/-}$ cells (Figure 7B). These results demonstrated that the effects of *Wbp1l* shRNA are dependent on *Wbp1l* and, thus, specific. When we used the same cells in an in vivo homing experiment, we observed that WBP1L down-regulation significantly enhanced bone marrow homing of wild-type cells, when compared to *Wbp1l*$^{-/-}$ cells (Figure 7C). This outcome is consistent with the results of our in vitro analyses showing that WBP1L negatively regulates activity of CXCR4.

To definitely prove the validity of our shRNA data, we have generated a mouse strain *Wbp1l*$^{fl/fl}$-*CreERT* where the *Wbp1l* gene can be acutely inactivated upon injection of 4OH-tamoxifen. Acute *Wbp1l* deletion in this model resulted in enhanced ERK phosphorylation in response to CXCL12 stimulation in total bone marrow as well as in several major subsets, including T cells, monocytes and neutrophils, whereas in B cells, the difference was small and not statistically significant (Figure 7D and S10). No effects of WBP1L deficiency on total ERK expression were observed (Figure 7E). The enhanced CXCR4 signalling did not translate to any immediate effect on steady-state numbers of major bone marrow and splenic cell subsets (Figure S11A). However, it is likely that only much more substantial increase in CXCR4 signalling would be needed to alter leucocyte bone marrow retention within this timescale.

The data presented above suggested that the effects of WBP1L down-regulation can only be observed after its acute deletion. To further address this possibility, we have established primary culture of isolated KIT$^+$ bone marrow cells from *Wbp1l*$^{fl/fl}$-*CreERT* mice, where *Wbp1l* could be deleted by 4OH-tamoxifen. Importantly, cells cultured outside the bone marrow are not exposed to continuous CXCL12 stimulation and desensitization and are, thus, having high expression of CXCR4 and stronger signalling capacity. In agreement with our previous observations, after acute *Wbp1l* deletion by CRE recombinase (but not after germline deletion), these progenitors showed increased ERK phosphorylation in response to CXCL12 stimulation (Figure 7F and S11B). *Wbp1l* deletion also resulted in an increase in steady-state CXCR4 surface expression with no other effects on the rate of CXCL12-triggered receptor internalization in these cells (Figure 7G and S11C). The same increase in CXCR4 expression was also observed on KIT$^+$ progenitors from peripheral blood of animals after acute *Wbp1l* deletion (Figure 7H). Similar, though not significant, trend was also observed when CXCR4 was measured on fixed and permeabilized cells (Figure S11D). Finally, cells with acute *Wbp1l* deletion showed increased migration towards CXCR4 ligand CXCL12 in a transwell assay in vitro (Figure 7I) and increased bone marrow homing efficiency in vivo (Figure 7J). These data confirm that WBP1L negatively regulates CXCR4 expression and signalling in primary cells.

4 | DISCUSSION

Expression of the *WBP1L* gene is heightened in *ETV6-RUNX1*$^+$ paediatric BCP-ALL and was shown to correlate with favourable

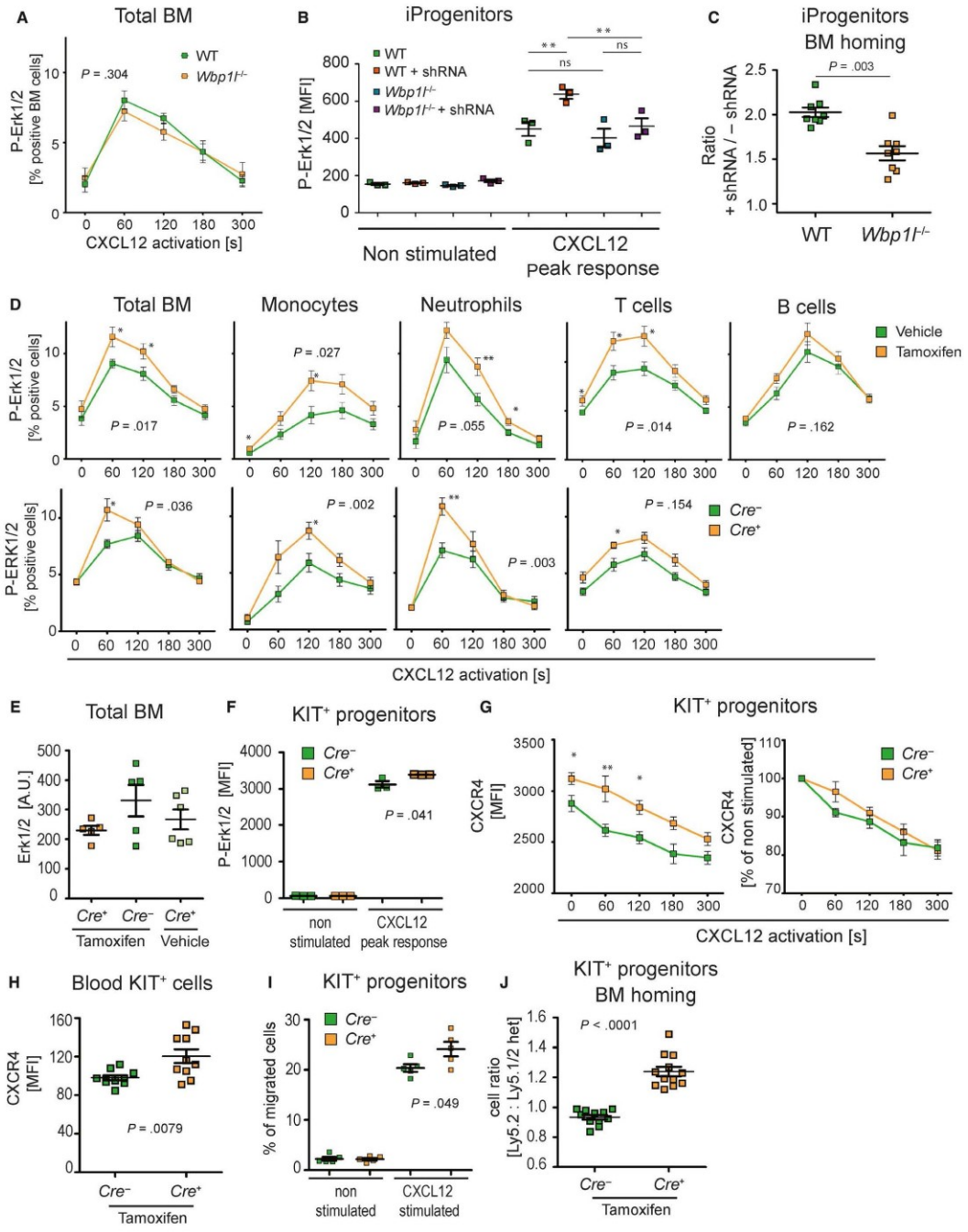

treatment response.[1-3] However, the function of its protein product WBP1L in healthy and leukaemic cells has not been investigated. Here, we attempted to uncover its physiological function. Our initial analysis shows that WBP1L binds several NEDD4-family E3 ubiquitin ligases and its deficiency results in augmented surface expression and signalling of CXCR4, one of their known target proteins.

FIGURE 7 Acute loss of WBP1L results in enhanced CXCR4 signalling but germline deficiency is compensated for. (A) ERK1/2 phosphorylation downstream of CXCR4 in WT and *Wbp1l*$^{-/-}$ (germline deletion) bone marrow cells. Cells were stimulated with 100 nmol/L CXCL12, fixed, stained for phosphorylated ERK1/2 and analysed by flow cytometry. Data represent percentage of responding cells (N = 6). *P*-value was calculated for maximum response of WT and *Wbp1l*$^{-/-}$ cells regardless of the time-point where it was reached. (B) Erk1/2 activation after CXCL12 stimulation (100 nmol/L) of immortalized monocyte/macrophage progenitors (iProgenitors) from WT and *Wbp1l*$^{-/-}$ mice and of the same cells transduced with *Wbp1l* shRNA. Erk phosphorylation was measured by flow cytometry of fixed and permeabilized cells stained with fluorescent P-Erk1/2 antibody. Peak response detected during 5 min measurement is shown. Data are represented as medians of fluorescence intensity (N = 3). *P*-values were calculated using 1way ANOVA with Bonferroni's multiple comparison test. (C) WT cells transduced or not with *Wbp1l* shRNA were mixed 1:1 and their bone marrow homing ability was analysed as in Figure 6D. As a control *Wbp1l*$^{-/-}$ cells transduced or not with *Wbp1l* shRNA and also mixed in a ratio 1:1 were used. Ratios of shRNA transduced and non-transduced cells are plotted for each genotype (n = 8). *P*-value was calculated for the differences between these two ratios. Significant outliers were discarded based on *q* test. As not all cells expressed shRNA containing vector after transduction, the true ratio was lower than 1:1 at the time of injection. The final data were normalized to this true ratio. (D) CXCR4 signalling in bone marrow cell subsets after acute deletion of *Wbp1l*. In the top row, *CreERT* expressing cells treated either with tamoxifen or vehicle (corn oil) are compared. In the bottom row, the comparison is made between tamoxifen-treated *Wbp1l*$^{fl/fl}$-*CreERT* and *Wbp1l*$^{fl/fl}$ (without *CreERT*) bone marrow cells. Cells were stimulated with 100 nmol/L CXCL12, fixed, stained for extracellular markers and intracellular P-ERK and analysed by flow cytometry. Data represent percentage of responding cells from whole bone marrow (N = 7), T cells (CD3$^+$, N = 7/8), monocytes (Ly6C$^+$ Ly6G$^-$, N = 11) and neutrophils (Ly6G$^+$ Ly6C$^-$,N = 7). Significant outliers were discarded based on *q* test. *P*-value was calculated for maximum response (regardless of the time-point at which this maximum was reached). In addition, significant differences in individual time-points are labelled with asterisks. (E) Expression of total ERK1/2 in the bone marrow cells where *Wbp1l* was deleted as in (D). Protein level was measured using Western blot. ERK1 and ERK2 were probed separately and signal was summed and normalized to actin loading control (N ≥ 5) (F). CXCR4 signalling in in vitro 4-hydroxytamoxifen treated KIT$^+$ progenitors isolated from *Wbp1l*$^{fl/fl}$-*CreERT* and *Wbp1l*$^{fl/fl}$ (without *CreERT*) bone marrow. ERK phosphorylation was measured after stimulation with 100 nmol/L CXCL12 by flow cytometry on fixed and permeabilized cells. Peak response detected during 5 min measurement is shown. One of two independent experiments is shown, N = 6. (G) CXCL12-induced changes of CXCR4 surface expression on KIT$^+$ bone marrow progenitors. These cells were isolated from *Wbp1l*$^{fl/fl}$-*CreERT* and *Wbp1l*$^{fl/fl}$ bone marrow, treated with 4-hydroxytamoxifen to induce *Wbp1l* deletion and stimulated with CXCL12 for indicated time intervals. FACS data are plotted as median fluorescence intensities (left graph) or as percentage of expression level on non-stimulated cells (right graph) (n = 7). (H) CXCR4 expression on KIT$^+$ progenitors detected in the blood of tamoxifen-treated *Wbp1l*$^{fl/fl}$-*CreERT* and *Wbp1l*$^{fl/fl}$ mice. Significant outlier was discarded based on *q* test (N = 10). (I) Migration of 4-hydroxytamoxifen-treated KIT$^+$ progenitors from *Wbp1l*$^{fl/fl}$-*CreERT* and *Wbp1l*$^{fl/fl}$ mice towards 500 nmol/L CXCR4 in a transwell assay in vitro (N = 5). (J) Ly5.2$^+$ KIT$^+$ progenitors (from *Wbp1l*$^{fl/fl}$-*CreERT* or *Wbp1l*$^{fl/fl}$ mice, treated with 4-hydroxytamoxifen) were mixed 1:1 with Ly5.1/Ly5.2$^+$ heterozygous KIT$^+$ progenitors from WT mice and 10^7 cells were injected into Ly5.1 sublethally irradiated recipients. After 16 h, the ratio between Ly5.2 and Ly5.1/Ly5.2 cells in the bone marrow was measured by flow cytometry (N ≥ 11)

At the organismal level, WBP1L deficiency resulted in perturbations in B cell development and increased ability of bone marrow stem and progenitor cells to reconstitute haematopoietic system after the bone marrow transplantation. In addition, acute *Wbp1l* deletion resulted in increased progenitor homing to the bone marrow. How much of this phenotype can be attributed to CXCR4 hyperactivity is still an open question. There are at least two other mouse models that show increased CXCR4 activity. One of these strains carries a mutation in CXCR4 that prevents its desensitization and down-regulation (*CXCR4*^{WHiM}). The same mutation in humans causes immunodeficiency known as WHIM syndrome.[18-20] *CXCR4*^{WHiM} mice display a similar selective dysregulation in the bone marrow B cell compartment as *Wbp1l*$^{-/-}$ mice with the reduction in B cell percentages that is most profound at the B cell progenitor level.[20] They also show increase in marginal zone B cell percentages. On the other hand, some of their symptoms were not detected in *Wbp1l*$^{-/-}$ mice, including blood neutropenia and lymphopenia and reduced spleen size.[20] Increased CXCR4 expression and CXCR4-mediated signalling were also observed in mice deficient in the expression of BAR domain containing adaptor protein Missing In Metastasis (MIM). In these animals, leucocyte development and percentages appeared largely normal and no leukopenia has been observed. Rather they showed slightly increased white blood cell counts and splenomegaly.[21,22] Even though MIM deficiency has a number of CXCR4-independent effects, these data show that enhanced CXCR4 activity does not have to lead to leukopenia in the peripheral tissues, nor to major alterations in leucocyte subset numbers and frequencies in the bone marrow. It is possible that the lack of receptor desensitization rather than alterations in peak signal intensity may be the key factor driving peripheral leukopenia in *CXCR4*^{WHiM} mice.

Since in mice with germline *Wbp1l* deletion we have not observed up-regulation in CXCR4 activity, it is difficult to unequivocally answer the question if alterations in *Wbp1l*$^{-/-}$ B cell development are caused by CXCR4 dysregulation. This phenotype is strikingly similar to the one observed in *CXCR4*^{WHiM} animals. It is possible that not all haematopoietic cell subsets are able to compensate for the loss of WBP1L. Early B cell progenitors represent a relatively small population, and their WBP1L expression based on the data from ImmGen consortium[23] is similar to other B cell subsets (not shown). The options to analyse their CXCR4 signalling pathways are relatively limited. Those that can be analysed by flow cytometry, including ERK and STAT3 phosphorylation, as well as calcium response appear to be hypo/non-responsive in this particular cell type despite clearly measurable CXCR4 expression (not shown). As a result, B cell progenitors contribute very little to ERK phosphorylation of the entire B cell pool measured in our experiments where the more mature stages dominated the response. The other pathways we were not able to analyse in this relatively rare subpopulation and so it is still

possible that reduction in B cell progenitor numbers in *Wbp1l*$^{-/-}$ mice is caused by some aspect of CXCR4 signalling, which we could not measure.

WBP1L may also have other functions besides regulation of CXCR4. They may be responsible for a part of the phenotype of WBP1L-deficient cells and animals. WBP1L binds multiple NEDD4 family members and very likely other proteins, which can result in pleiotropic effects on leucocyte biology. It has been shown that in competitive transplantation assay HSPC with only one functional CXCR4 allele perform better than wild-type cells, which perform better than *CXCR4*^{WHIM} cells, clearly showing an inverse correlation between CXCR4 activity and transplantation efficiency.[24,25] This observation is rather counterintuitive and opposite to the results we obtained with *Wbp1l*$^{-/-}$ cells. An explanation suggested in these studies was that CXCR4 promotes haematopoietic stem cell quiescence leading to competitive disadvantage when CXCR4 signalling is up-regulated. This leads to the conclusion that though CXCR4 role cannot be completely excluded by our experiments, effects of WBP1L on transplantation efficiency are likely CXCR4-independent. The molecular mechanism of how WBP1L regulates bone marrow engraftment will have to be addressed in future studies. On the other hand, functional effects of acute down-regulation of WBP1L are more clearly connected to CXCR4, leading to increased surface expression of CXCR4, increased CXCR4 signalling and improved homing efficiency, similar to mouse models with increased CXCR4 activity.

It is at present unclear what is the reason for the unequal effects of the acute and constitutive OPAL1 deletion on CXCR4 signalling. We can speculate that WBP1L may be rather general regulator of expression and/or activity of NEDD4 family ligases. However, there are many additional mechanisms regulating these enzymes. In the majority of cases, these might be able to compensate for the loss of WBP1L in the long-term. However, their ability to rapidly react to acute WBP1L loss would likely be more limited, as it may require changes in the gene expression pattern or other time-consuming adaptations.

Another important question is the role that WBP1L potentially plays in leukaemia. The *WBP1L* gene is a target gene of ETV6, which suppresses its expression.[4] In *ETV6-RUNX1*$^{+}$ BCP-ALL, one allele of *ETV6* is inactivated by fusion with *RUNX1*, while the other is often inactivated as well.[26] This could explain the increase of WBP1L expression in *ETV6-RUNX1*$^{+}$ BCP-ALL. It is also in agreement with our data showing that in REH cells (which already have both *ETV6* alleles inactivated) *ETV6-RUNX1* genetic deletion did not have any further effect on WBP1L expression. *ETV6* inactivation likely represents part of the mechanism leading to the development of leukaemia and defining its features. In principle, WBP1L in this context can have two different functions. First, negative regulation of CXCR4 by WBP1L could dampen the interactions of leukaemic (stem) cells with protective bone marrow niches, making them more sensitive to treatment. Second, WBP1L may also have negative effect on leukaemic stem cells similar to its negative regulatory effects on HSPCs that were revealed in our competitive transplantation experiment. Our data do not specifically address the role of WBP1L in leukaemia. However, the effects of WBP1L deficiency on normal haematopoiesis that we observed here and the fact that WBP1L is an ETV6 target gene make WBP1L a relevant target of future research in this field.

ACKNOWLEDGEMENTS

This study was supported by Czech Science Foundation (GACR), projects 16-07425S and P302-12-G101, and by institutional funding from the Institute of Molecular Genetics, Academy of Sciences of the Czech Republic (RVO 68378050). We also acknowledge core facilities, including the Czech Centre for Phenogenomics (CCP, supported by project no. LM2015040 and OP RDI CZ.1.05/2.1.00/19.0395 'Higher quality and capacity for transgenic models') and Light Microscopy Core Facility, IMG ASCR, Prague, Czech Republic, supported by MEYS (LM2015062), OPPK (CZ.2.16/3.1.00/21547) and NPU I (LO1419). JS was supported by Czech Health Research Council (AZV), project NV15-28848A. JS a V. Kanderova were also supported by Ministry of Education, Youth and Sports of the Czech Republic, project NPU I LO1604. OVM was supported by European Union's Horizon 2020 research and innovation program under the Marie Sklodowska-Curie grant No. 665735, MBP and MGT were supported by a MRC New Investigator Award (G0400247) to MGT We are grateful to Steve Watson from the University of Birmingham for helpful advice and comments. We also acknowledge Karel Harant and Pavel Talacko from Laboratory of Mass Spectrometry core facility, Biocev, Charles University, Faculty of Science, where mass spectrometric analysis was performed. The mass spectrometric facility is supported by the project 'BIOCEV – Biotechnology and Biomedicine Centre of the Academy of Sciences and Charles University' (CZ.1.05/1.1.00/02.0109), from the European Regional Development Fund. The authors would like to thank Dusan Hrckulak from Laboratory of Cell and Developmental Biology IMG ASCR, Prague, for providing us with Cre recombinase construct and Peter Dráber from the Laboratory of Adaptive Immunity IMG ASCR for helping us to establish the method of tandem purification for mass spectrometry analysis. This work benefitted from the data assembled by ImmGen consortium.

CONFLICT OF INTEREST

The authors confirm that there are no conflicts of interest.

AUTHOR CONTRIBUTIONS

SB, A.D and JK with contribution from MF, PA, JP, TS, NP and TB conducted majority of experiments and data analysis. DG performed microscopy analysis. IS carried out analysis of *Wbp1l*$^{-/-}$ embryos. OVM and KK analysed palmitoylation of WBP1L. V. Kanderova provided data on WBP1L expression in B cell lines. JS and PS generated ETV6-RUNX1-deficient REH cell line. MBP and MGT generated rabbit antisera to WBP1L. MAJ contributed to design and analysis of homing and competitive transplantation assays. V. Korinek contributed to the generation of *Wbp1l*-CreERT mouse strain. TB with

contribution from SB and AD conceptualized the study, evaluated the data and wrote the paper.

DATA AVAILABILITY STATEMENT

The data that support the findings of this study are available from the corresponding author upon reasonable request.

ORCID

Orest V. Matveichuk https://orcid.org/0000-0002-4057-7598
Majd B. Protty https://orcid.org/0000-0001-8992-9120
Tomas Brdicka https://orcid.org/0000-0002-1560-4398

REFERENCES

1. Mosquera-Caro M, Helman P, Veroff R, et al. Identification, validation and cloning of a novel gene (OPAL1) and associated genes highly predictive of outcome in pediatric acute lymphoblastic leukemia using gene expression profiling [abstract]. *Blood*. 2003;102:4a.
2. Holleman A, den Boer ML, Cheok MH, et al. Expression of the outcome predictor in acute leukemia 1 (OPAL1) gene is not an independent prognostic factor in patients treated according to COALL or St Jude protocols. *Blood*. 2006;108:1984-1990.
3. Kanderova V, Kuzilkova D, Stuchly J, et al. High-resolution antibody array analysis of childhood acute leukemia cells. *Mol Cell Proteomics*. 2016;15:1246-1261.
4. Neveu B, Spinella J-F, Richer C, et al. CLIC5: a novel ETV6 target gene in childhood acute lymphoblastic leukemia. *Haematologica*. 2016;101:1534-1543.
5. Lopez RG, Carron C, Oury C, Gardellin P, Bernard O, Ghysdael J. TEL is a sequence-specific transcriptional repressor. *J Biol Chem*. 1999;274:30132-30138.
6. Chakrabarti SR, Nucifora G. The leukemia-associated gene TEL encodes a transcription repressor which associates with SMRT and mSin3A. *Biochem Biophys Res Commun*. 1999;264:871-877.
7. De Braekeleer E, Douet-Guilbert N, Morel F, Le Bris MJ, Basinko A, De Braekeleer M. ETV6 fusion genes in hematological malignancies: a review. *Leuk Res*. 2012;36:945-961.
8. Rasighaemi P, Ward AC. ETV6 and ETV7: Siblings in hematopoiesis and its disruption in disease. *Crit Rev Oncol Hematol*. 2017;116:106-115.
9. Wang LC, Swat W, Fujiwara Y, et al. The TEL/ETV6 gene is required specifically for hematopoiesis in the bone marrow. *Genes Dev*. 1998;12:2392-2402.
10. Hock H, Meade E, Medeiros S, et al. Tel/Etv6 is an essential and selective regulator of adult hematopoietic stem cell survival. *Genes Dev*. 2004;18:2336-2341.
11. Pei J, Grishin NV. Unexpected diversity in Shisa-like proteins suggests the importance of their roles as transmembrane adaptors. *Cell Signal*. 2012;24:758-769.
12. Draber P, Kupka S, Reichert M, et al. LUBAC-recruited CYLD and A20 regulate gene activation and cell death by exerting opposing effects on linear ubiquitin in signaling complexes. *Cell Rep*. 2015;13:2258-2272.
13. Kralova J, Glatzova D, Borna S, Brdicka T. Expression of fluorescent fusion proteins in murine bone marrow-derived dendritic cells and macrophages. *J Vis Exp*. 2018;140:e58081. https://doi.org/10.3791/58081
14. Lorenz S. Structural mechanisms of HECT-type ubiquitin ligases. *Biol Chem*. 2018;399:127-145.
15. Mund T, Pelham HRB. Control of the activity of WW-HECT domain E3 ubiquitin ligases by NDFIP proteins. *EMBO Rep*. 2009;10:501-507.
16. Ayala F, Dewar R, Kieran M, Kalluri R. Contribution of bone microenvironment to leukemogenesis and leukemia progression. *Leukemia*. 2009;23:2233-2241.
17. de Lourdes PA, Amarante MK, Guembarovski RL, de Oliveira CEC, Watanabe MAE. CXCL12/CXCR4 axis in the pathogenesis of acute lymphoblastic leukemia (ALL): a possible therapeutic target. *Cell Mol Life Sci*. 2015;72:1715-1723.
18. Hernandez PA, Gorlin RJ, Lukens JN, et al. Mutations in the chemokine receptor gene CXCR4 are associated with WHIM syndrome, a combined immunodeficiency disease. *Nat Genet*. 2003;34:70-74.
19. Kawai T, Malech HL. WHIM syndrome: congenital immune deficiency disease. *Curr Opin Hematol*. 2009;16:20-26.
20. Balabanian K, Brotin E, Biajoux V, et al. Proper desensitization of CXCR4 is required for lymphocyte development and peripheral compartmentalization in mice. *Blood*. 2012;119:5722-5730.
21. Zhan T, Cao C, Li L, Gu N, Civin CI, Zhan X. MIM regulates the trafficking of bone marrow cells via modulating surface expression of CXCR4. *Leukemia*. 2016;30:1327-1334.
22. Yu D, Zhan XH, Zhao XF, et al. Mice deficient in MIM expression are predisposed to lymphomagenesis. *Oncogene*. 2012;31:3561-3568.
23. Heng TS, Painter MW. The Immunological Genome Project: networks of gene expression in immune cells. *Nat Immunol*. 2008;9:1091-1094.
24. McDermott DH, Gao JL, Liu Q, et al. Chromothriptic cure of WHIM syndrome. *Cell*. 2015;160:686-699.
25. Gao JL, Yim E, Siwicki M, et al. Cxcr4-haploinsufficient bone marrow transplantation corrects leukopenia in an unconditioned WHIM syndrome model. *J Clin Invest*. 2018;128:3312-3318.
26. Sundaresh A, Williams O. Mechanism of ETV6-RUNX1 Leukemia. In: Groner Y, Ito Y, Liu P, Neil JC, Speck NA, van Wijnen A, eds. *RUNX Proteins in Development and Cancer*. Singapore: Springer Singapore; 2017:201-216.

SUPPORTING INFORMATION

Additional supporting information may be found online in the Supporting Information section.

How to cite this article: Borna S, Drobek A, Kralova J, et al. Transmembrane adaptor protein WBP1L regulates CXCR4 signalling and murine haematopoiesis. *J Cell Mol Med*. 2020;24:1980–1992. https://doi.org/10.1111/jcmm.14895

Supplemental methods

Cell culture

REH cells were cultured in RPMI (Thermo Fisher Scientific, Waltham, MA), 293T and J774 cells and Phoenix cells were cultured in DMEM (Thermo Fisher), other BCP-ALL cell lines were cultivated as described previously [1]. Media were supplemented with 10% fetal bovine serum (Thermo Fisher) and antibiotics. Immortalized monocyte-macrophage progenitors were cultivated and generated using conditional HOXB8 construct as described previously [2,3]. KIT^+ cells were cultured in IMDM media supplemented with 0.1% IL-6, 0.2% IL-3, 1% SCF, supplied as supernatants from HEK293 cells transfected with constructs coding for respective cytokines. CRE-mediated *Wbp1l* deletion was induced with 1μM 4-hydroxytamoxifen. BMDM were prepared and cultivated as described [4].

Antibody generation

Preparation of the rabbit anti-WBP1L polyclonal antibody was outsourced to Eurogentec (Seraing, Belgium). The QAREHGHPHLPRPPAC peptide, which is close to the WBP1L C-terminus and is identical in the human and mouse sequences, was conjugated to keyhole limpet hemocyanin (KLH) for use as the antigen. The same peptide was used to affinity purify the antibody. OPAL-01 and OPAL-02 antibodies to human WBP1L were described previously [1]. mOPAL-01 and mOPAL-03 mouse monoclonal antibodies to murine WBP1L were generated by standard hybridoma technology using splenocytes of mice (F1 hybrids of BALB/c × B10) immunized with recombinant intracellular part of murine WBP1L protein and Sp2/0 myeloma cells as a fusion partner.

Flow cytometry

For surface staining, cells were incubated with antibodies and Fc-block (Clone 2.4G2) in PBS with 2% FBS for 30 min. For intracellular staining, cells were fixed with 4% formaldehyde (Thermo Fisher), then stained for surface markers, permeabilized with 90% methanol (Lachner, Neratovice, Czechia), blocked with 5% BSA (Merck, Darmstadt, Germany) 0.3% Triton X-100 (Merck) in PBS and stained for intracellular antigens in 1% BSA 0,3% Triton X-100 in PBS. For cell cycle analyses or Ki67 staining, cells were not permeabilized by methanol and after antibody staining were stained with 2 μg/ml Hoechst 33342 (Merck). Data were collected on LSRII flow cytometer (BD Biosciences, San Jose, CA) and analyzed with FlowJo software (FlowJo LLC, Ashland, OR).

Other reagents and their sources

β-estradiol (Merck), 4-Hydroxytamoxifen (Merck), recombinant murine and human SDF1α (Immunotools, Friesoythe, Germany), Lipofectamine 2000 (Thermo Fisher), Protein A/G (Santa Cruz Biotechnology, Dallas, TX), tunicamycin, Lysotracker Red DND-99, ER-Tracker Red, MitoTracker Red (Thermo Fisher), TC14012 (RanD corporation), AMD3100 (Merck).

Analysis of WBP1L palmitoylation

Palmitoylation of WBP1L was analyzed using click reaction-based approach, essentially as described earlier [5]. Briefly, HEK293 cells (5.5 x 10^5 in 60-mm dish) were transfected with 6 µg of WBP1L-FLAG-STREP-bearing pBABE using FuGENE (Promega, Madison, WI) according to manufacturer's instruction. After 24 h, cells were labeled with 50 µM 17-octadecynoic acid (17ODYA) or exposed to 0.05% DMSO carrier (1.5 h, 37 °C). Cells were lysed in a buffer containing 4% SDS and lysates subjected to click reaction with biotin-azide (500 µM biotin-PEG3-azide; Merck). Proteins were precipitated with chloroform:methanol [6] and resupended in the presence of 0.5% SDS and 1% Brij97. Biotin-tagged proteins were enriched on streptavidin-coupled beads (Thermo Fisher), eluted in hot H_2O followed by series of buffers and analyzed by immunoblotting using mouse anti-FLAG IgG (Merck) and rabbit anti-FLOTILLIN-2 IgG (Cell Signaling Technology, Danvers, MA).

Microscopy

BMDM were plated overnight on eight well µ-plate (IBIDi). The next day the cells were directly imaged or stained with organelle specific dye (MitoTracker Red 1:500, LysoTracker Red DND-99 1:1000, ER-tracker Red 1:1000, all Thermo Fisher) and directly imaged, or stained with CD11b-APC (Table S1) and subsequently fixed with 4% formaldehyde (Merck) and stained with Hoechst 33342 (Merck). Sequential 2-color imaging was performed using Leica TCS SP8 laser scanning confocal microscope with a 63×1.4 NA oil-immersion objective. Acquired images were manually thresholded to remove signal noise detected outside of the cell using ImageJ software.

Isolation of cell subsets from organs

Mouse blood was collected by cheek bleeding to EDTA tubes (KABE Labortechnik, Numbrecht-Elsenroth, Germany). B cells and T cells were isolated from splenocyte suspensions and neutrophils and KIT^+ cells from bone marrow cell suspensions using magnetic microbeads (Miltenyi Biotec, Bergisch Gladbach, Germany, see *Supplementary Table S5*) on an AutoMACS magnetic cell sorter (Miltenyi Biotec). Cells from murine embryo proper and yolk sac were isolated by digestion of respective tissue in dispase (1mg/ml, Thermo Fisher) in HBSS for 10 min followed by erythrocyte lysis with ACK buffer.

Knock-out cell line preparation

ETV6-RUNX1$^{-/-}$ REH cell lines were established using CRISPR/Cas9 technology. pLV-U6g-EPCG plasmid (Merck) was used with guide RNA (GTGCCTCGAGCGCTCAGGATGG) against exon 2 of *ETV6* gene. Since the second allele of *ETV6* is deleted in REH cell line, this targeting sequence is specific for fusion gene only. Knockout of *ETV6-RUNX1* gene was confirmed by Sanger sequencing, on mRNA and protein level (Figure S2 and data not shown). As a control, REH cell line transduced with non-targeting CRISPR/Cas9 vector was used.

Tandem purification of WBP1L for mass spectrometry analysis of WBP1L-binding proteins

Cells were lysed in lysis buffer (30mM TRIS, pH 7.4, 120 mM NaCl, 2 mM KCl, 10% Glycerol, 1% β-D-dodecylmaltoside, 10 mM Chloroacetamide, Phosphatase inhibitor tablets (PhosSTOP, Roche, Basel, Switzerland), Protease Inhibitor Cocktail (Roche)) and tagged proteins were immunoprecipated from postnuclear supernatants on anti-flag M2 affinity gel (Merck), eluted with 3x FLAG peptide (Merck), followed by second round of affinity purification on Strep-Tactin sepharose (IBA Lifesciences, Goettingen, Germany) and elution with 2% sodium deoxycholate (Merck) in 50mM TRIS (pH 8.5). Cysteines in eluted proteins were reduced with 5mM final concentration of TCEP (Tris(2-carboxyethyl)phosphine hydrochloride) and blocked with 10mM final concentration of MMTS (methyl methanethiosulfonate). Samples were cleaved with 1µg of trypsin. After digestion, samples were acidified with TFA (Trifluoroacetic acid) to 1% final concentration. Sodium deoxycholate was removed by extraction to ethylacetate [7]. Peptides were desalted on Michrom C18 column.

nLC-MS 2 Analysis

Nano Reversed phase column (EASY-Spray column, 50 cm x 75 µm ID, PepMap C18, 2 µm particles, 100 Å pore size) was used for LC/MS analysis. Mobile phase buffer A was composed of water and 0.1% formic acid. Mobile phase B was composed of acetonitrile and 0.1% formic acid. Samples were loaded onto the trap column (Acclaim PepMap300, C18, 5 µm, 300 Å Wide Pore, 300 µm x 5 mm, 5 Cartridges) for 4 min at 15 µl/min. Loading buffer was composed of water, 2% acetonitrile and 0.1% trifluoroacetic acid. Peptides were eluted with Mobile phase B gradient from 4% to 35% B in 60 min. Eluting peptide cations were converted to gas-phase ions by electrospray ionization and analyzed on a Thermo Orbitrap Fusion (Q-OT- qIT, Thermo Fisher). Survey scans of peptide precursors from 400 to 1600 m/z were performed at 120K resolution (at 200 m/z) with a 5×10^5 ion count target. Tandem MS was performed by isolation at 1.5 Th with the quadrupole, HCD (Higher-energy collisional dissociation) fragmentation with normalized collision energy of 30, and rapid scan MS analysis in the ion trap. The MS 2 ion count target was set to 10^4 and the max injection time was 35 ms. Only those precursors with charge state 2–6 were sampled for MS 2. The dynamic exclusion duration was set to 45 s with a 10 ppm tolerance around the selected precursor and its isotopes. Monoisotopic precursor selection was turned on. The instrument was run in top speed mode with 2 s cycles [8].

Data analysis of mass spectrometry

All data were analyzed and quantified with the MaxQuant software (version 1.5.3.8) [9]. The false discovery rate (FDR) was set to 1% for both proteins and peptides and we specified a minimum length of seven amino acids. The Andromeda search engine was used for the MS/MS spectra search against the *Mus musculus* database (downloaded from Uniprot on March 2018, containing 25 527 entries). Enzyme specificity was set as C-terminal to Arg and Lys, also allowing cleavage at proline bonds and a maximum of two missed cleavages. Dithiomethylation of cysteine was selected as fixed modification and N- terminal protein acetylation and methionine oxidation as variable modifications. The “match between runs” feature of MaxQuant was used to transfer identifications to other LC-MS/MS runs based on their masses and retention time (maximum deviation 0.7 min) and this was also used in quantification experiments. Quantifications were performed with the label-free algorithms described recently [9]. Data analysis was performed using Perseus 1.5.2.4 software.

Protein immunoprecipitation

Cells were lysed in lysis buffer described in the tandem purification method above. In co-Immunoprecipitation experiments 1% β-D-dodecylmaltoside was replaced with 1% NP-40 substitute (AppliChem GmbH) and in WBP1L immunoprecipitation from multiple B cell lines (Figure S2) RIPA buffer (50 mM TRIS pH7.4, 150 mM NaCl, 1% NP-40 substitute, 1% Deoxycholate (Merck), 0.1% SDS (Merck)) with the same protease and phosphatase inhibitors was used. Lysates were incubated with WBP1L monoclonal antibodies followed by isolation of antibody-bound complexes on protein A/G agarose beads (Santa Cruz Biotechnology) and elution with SDS-PAGE sample buffer.

Construct preparation and lentiviral production

If not otherwise specified, inserts were amplified from cDNA using Q5 polymerase (New England BioLabs, Boston, MA). Myc-tagged *WBP1L WT*, *ΔN* (with deletion of the following sequence QQRQHEINLIAYREAHNYSALPFYFRFLPNSLLPPYEEVVNRPPTPPPPYSAFQL deleted) *ΔC* (lacking entire C-terminus starting from PPPPQGGPPGGSPPGAD...) were generated by PCR and cloned into pcDNA3 vector. For WBP1L palmitoylation analysis and tandem purification, *WBP1L* or *EGFP* were cloned into tagging vector (pBABE containing C-terminal 3xFlag-2x Srep-tag-UGA –IRES-G418). For microscopy, *WBP1L* was cloned into MSCV vector in front of *MYC-tag-EGFP-UAA*. *Golgi-mApple* was amplified from mApple-Golgi-7 (mApple-Golgi-7 was a gift from Michael Davidson, Addgene plasmid # 54907) and subcloned into MSCV. E3 ligase cloning is summarized in Table S3. *WBP1L* shRNA (silencing/nonsilencing murine TRCN0000297606/085, human TRCN0000282025/275362) was obtained from Merck. Full length *Cre* (a gift from Dušan Hrčkulák) was cloned into pHIV-EGFP vector (pHIV-EGFP was a gift from Bryan Welm & Zena Werb, Addgene plasmid # 21373 [10]).

For lentiviral transductions HEK293T cells were transfected with Lentiviral Packaging vector (Thermo Fisher) and a vector of interest in ratio 1:2.5 using polyethyleneimine (PEI) (Polysciences, Warrington, PA). Virus was concentrated on centrifugal filter (Amicon 100K, Millipore). Cell infection was performed similarly to retroviruses as described here [4]. After infection with shRNA constructs, the infected cells were sorted based on the reporter (EGFP) expression and used in experiments no later than 3 weeks after the infection.

Table S1. List of flow cytometry antibodies

Antigen	Clone	Species tested	Conjugate	Company
P-ERK	197G	Mus musculus	Alexa 647	Cell Signalling Technology
Ly5.1	A20	Mus musculus	APC, FITC	BioLegend
Ly5.2	104	Mus musculus	PE-Cy7, PB,	BioLegend
CD3	17A2, 1452/C11	Mus musculus	PE, PB	BioLegend
Ly6C	HK1.4	Mus musculus	FITC, PE-Cy7	BioLegend
Ly6G	1A8	Mus musculus	PB, FITC, PB, APC	BioLegend
B220	RA3-6B2	Mus musculus	e450	Thermo-Fisher
IgM	EB121-15F9	Mus musculus	FITC	eBioscience
CD43	eBioR2/60	Mus musculus	PE	eBioscience
KIT	2B8	Mus musculus	PE, FITC	BioLegend
SCA-1	E13-161.7	Mus musculus	APC	BioLegend
CD16/32	93	Mus musculus	FITC	BioLegend
CD19	6D5	Mus musculus	FITC	BioLegend
CD11c	N418	Mus musculus	APC	BioLegend
F4/80	BM8	Mus musculus	PE, FITC, PE-Cy7	BioLegend
CD11b	M1/70	Mus musculus	PE, BV785, A700, APC	BioLegend, Sony
TER119	TER-119	Mus musculus	PB, Qdot605	BioLegend,
CD34	RAM34	Mus musculus	FITC	eBioscience
CD93	AA4.1	Mus musculus	PerCP-Cy5.5	BioLegend
CD23	B3B4	Mus musculus	e660, APC	Thermo-Fisher
CD1d	1B1	Mus musculus	FITC	BioLegend
CD5	57-7.3	Mus musculus	PE	Thermo-Fisher
CD45	30-F11	Mus musculus	PerCP-Cy5.5	Biolegend
Ki67	16A8	Mus musculus	APC	Biolegend
anti-mouse Lineage Cocktail	17A2/RB6-8C5/RA3-6B2/Ter-119/M1/70	Mus musculus	PB	BioLegend
KOMBITEST™ CD3 FITC / CD16+ CD56 + PE / CD45 PerCP / CD19 APC	UCHT1/3G8/LT56/MEM-28/LT19	Homo sapiens	FITC, PE, PerCP, APC	Exbio
CD14	MEM-18	Homo sapiens	FITC	Exbio
CXCR4	2B11	Mus musculus and Homo sapiens	APC	Thermo-Fisher

Table S2. List of antibodies for immunoprecipitation and Western blotting.

Antigen	Clone	Company	Comments
WBP1L	Rabbit polyclonal	Custom made, Eurogentec	Human/mouse WBP1L for Western Blotting
WBP1L	OPAL-01	Made in house	Human WBP1L
WBP1L	OPAL-02	Made in house	Human WBP1L
WBP1L	mOPAL-01	Made in house	Mouse WBP1L
WBP1L	mOPAL-03	Made in house	Mouse WBP1L
β-ACTIN	AC15	Merck	
P-ERK	197G2	Cell Signalling Technology	
ERK 1	MK12	BD Bioscience	
ERK 2	Rabbit polyclonal	Santa Cruz Biotechnology	
P-AKT	D9E	Cell Signalling Technology	
GAPDH	Rabbit polyclonal	Merck	
MYC-tag	9B11	Cell Signalling Technology	
UBIQUITIN	Rabbit polyclonal (A100)	Boston Biochem	
UBIQUITIN	P4D1	Cell Signalling Technology	CXCR4 ubiquitination
ITCH	Rabbit polyclonal	LifeSpan BioSciences	Itch staining in Fig. 5C
ITCH	D8Q6D	Cell Signalling Technology	Itch expression in progenitors
WWP1	Rabbit polyclonal	Abcam	
WWP2	Rabbit polyclonal	Abcam	
CXCR4	2B11	BD Bioscience	
HA-tag	C29F4	Cell Signalling Technology	
FLOTILLIN-2	Rabbit monoclonal	Cell Signalling Technology	Western Blotting
FLAG	M2	Merck	
Mouse Anti-Rabbit IgG Antibody conjugated to peroxidase	M205	Genscript	For I.P.
Goat Anti-Mouse, light chain specific, conjugated to peroxidase	Monoclonal, not specified	Jackson Immunoresearch	For I.P.
Mouse Anti-Rabbit, light chain specific, conjugated to peroxidase	Monoclonal, not specified	Jackson Immunoresearch	For I.P.
Goat anti-Mouse IgG (H+L), conjugated to peroxidase	Polyclonal	Bio-Rad	For lysates
Goat anti-Mouse IgG (H+L), conjugated to peroxidase	Polyclonal	Bio-Rad	For lysates

Table S3. List of qPCR primers

Primer	Sequence	Species tested	Company
WBP1L forward	CTCAGCGCTGCCATTTTATT	Homo sapiens	Merck
WBP1L reverse	GCTGGAAGGCACTGTATGGT	Homo sapiens	Merck
GAPDH forward	CCACATCGCTCAGACACCAT	Homo sapiens	Merck
GAPDH reverse	CCAGGCGCCCAATACG	Homo sapiens	Merck
WBP1L forward	CGTTGCCGTTTTACTTCAGG	Mus musculus	Merck
WBP1L reverse	GAGCTGGAAGGCACTGTACG	Mus musculus	Merck
WWP1 forward	GTTGCTGCCAGACCCAAA	Mus musculus	Merck
WWP1 reverse	TAGGACAGATGATGATTCTCCATTA	Mus musculus	Merck
WWP2 forward	GCCGGTTACCAGCTCAAA	Mus musculus	Merck
WWP2 reverse	TCAAAGATACAGGTCTGCAAGC	Mus musculus	Merck
SMURF2 forward	TTACATGAGCAGGACACACTTACA	Mus musculus	Merck
SMURF2 reverse	GCTGCGTTGTCCTTTGTTC	Mus musculus	Merck
SMURF1 forward	GGGTCAGTGGTGGACTGC	Mus musculus	Merck
SMURF1 reverse	CCAGGGCCTGAGTCTTCATA	Mus musculus	Merck
NEDD4L forward	TGAGCAAGCTCACCTTCCA	Mus musculus	Merck
NEDD4L reverse	CCCGTGACAGTTGACGAAC	Mus musculus	Merck
NEDD4 forward	GCCGGTTACCAGCTCAAA	Mus musculus	Merck
NEDD4 reverse	TCAAAGATACAGGTCTGCAAGC	Mus musculus	Merck
ITCH forward	TTGATGCGAAGGAATTAGAGG	Mus musculus	Merck
ITCH reverse	GGTGTAGTGGCGGTAGATGG	Mus musculus	Merck
β-ACTIN forward	GATCTGGCACCACACCTTCT	Mus musculus	Merck
β-ACTIN reverse	GGGGTGTTGAAGGTCTCAAA	Mus musculus	Merck

Table S4. List of Nedd4-family cDNA constructs.

E3 ligase	Species	Plasmid or insert origin	Recloned to pK-MYC-C1 and thus adding Myc-tag
NEDD4L	Homo sapiens	Addgene, Plasmid: 27000 Gift from Joan Massague [11]	+
ITCH	Mus musculus	Addgene, Plasmid 11427 Gift from Allan Weissman [12]	-
WWP1	Homo sapiens	Gift from Paul Bieniasz, ADARC, NY	+
WWP2	Homo sapiens	Gift from Paul Bieniasz, ADARC, NY	+

Table S5 List of magnetic cell sorting reagents.

Antigen	Clone	Species tested	Conjugate	Company
Ly6G	17A2	Mus musculus	Biotin	BioLegend
CD3	145/2C11	Mus musculus	Biotin	BioLegend
CD11b MicroBeads	M1/70	Mus musculus and Homo sapiens	Coated	MiltenyiBiotec
CD43 (Ly48) MicroBeads	not specified by the company	Mus musculus	Coated	MiltenyiBiotec
KIT	Ack2	Mus musculus	Biotin	In house

Supplemental figures

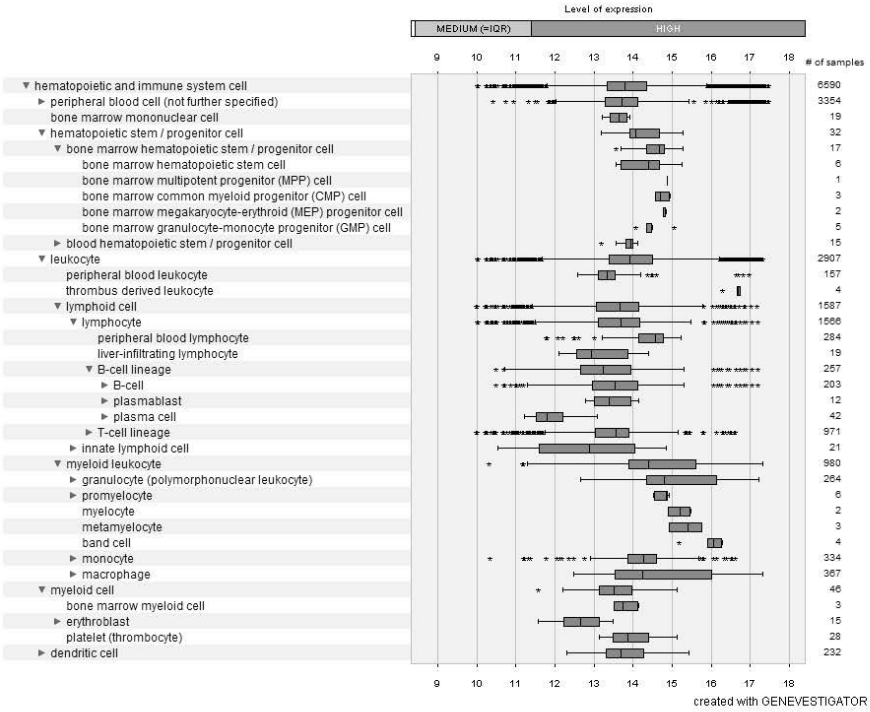

Figure S1. *WBP1L* expression in human leukocytes and leukocyte progenitor subsets. Expression profile of *WBP1L* mRNA generated by Genevestigator gene expression analysis tool, based on manually curated gene expression data from public repositories [13]. The box delimits the area between the upper and lower quartiles. Whiskers represent the lowest or highest data point still within 1.5 times this area in each direction. Stars represent data points outside this range.

A

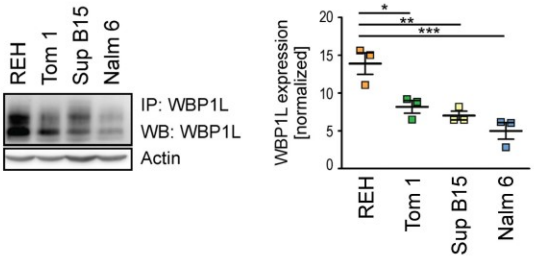

B

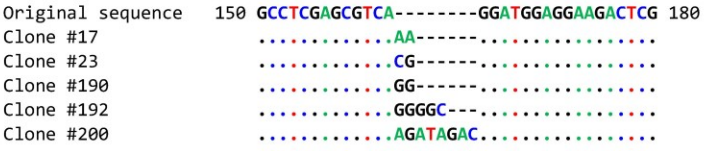

C

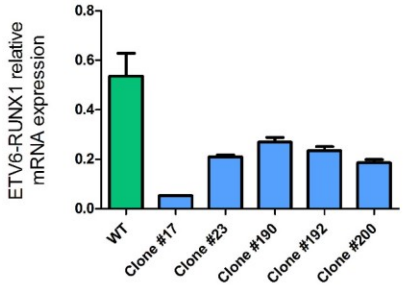

Figure S2. Expression of WBP1L in ETV6-RUNX1^{+} and ETV6-RUNX1^{-} cell lines and deletion of ETV6-RUNX1 in REH cells. (A) WBP1L immunoprecipitates from *ETV6-RUNX1*$^{+}$ B cell line REH and *ETV6-RUNX1*$^{-}$ lines TOM-1, NALM-6, and SUB B15 were immunoblotted with antibody to WBP1L and actin. For quantification, data were normalized in each experiment to actin and then to experiment average to allow comparison among experiments. Statistical significance was calculated using one way ANOVA with Dunnett's post test. (N=3). **(B)** Results of *ETV6* exon2 CRISPR/CAS9 target site sequencing in individual *ETV6-RUNX1*-deficient REH clones. **(C)** *ETV6-RUNX1* mRNA expression in the clones from (B) determined by qPCR. The data are plotted as $2^{-\Delta CT}$.

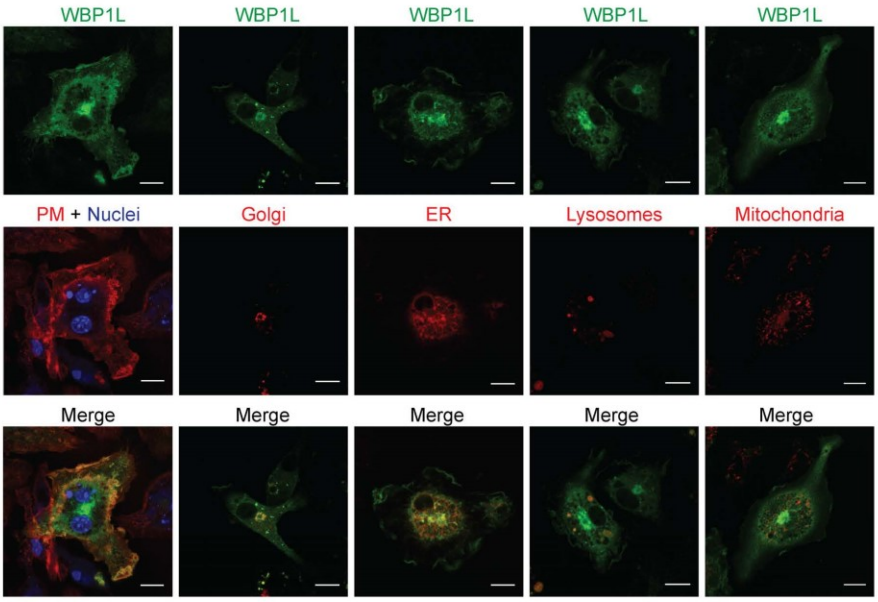

Figure S3. Subcellular localization of WBP1L. Confocal imaging of BMDM from *Wbp1l*$^{-/-}$ mice transduced with WBP1L-EGFP. The following markers were used: Plasma membrane (PM) – CD11b, Nuclei – Hoechst 33342, both on fixed cells; Golgi – Golgi-7-mApple retroviral construct, Endoplasmic reticulum (ER) – ER-Tracker-Red, Lysosomes and other acidic organelles – LysoTracker Red, Mitochondria – MitoTracker Red, all live cell imaging. Bar = 10 µm. N ≥ 3.

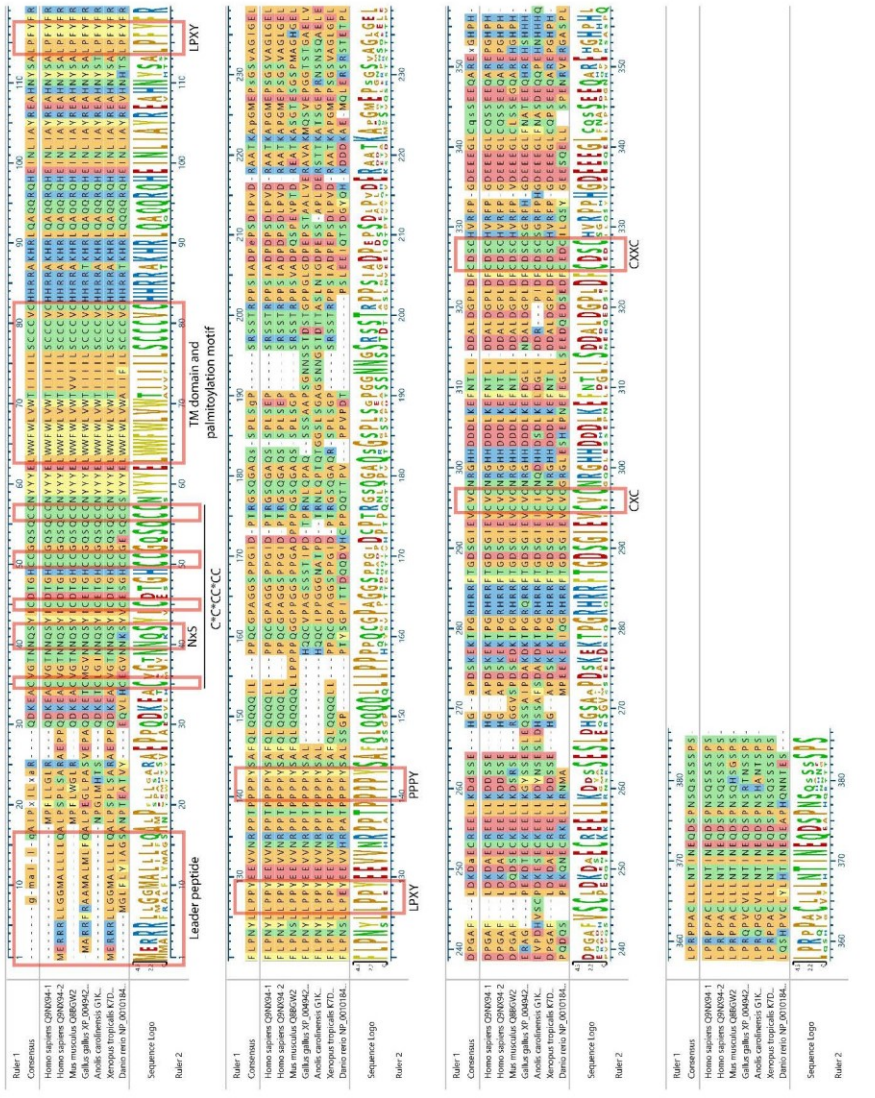

Figure S4. Alignment of WBP1L sequences from representatives of major vertebrate classes. Sequences were aligned with MUSCLE algorithm using MegAlign Pro software from DNASTAR Lasegene suite. Conserved features are highlighted with red boxes.

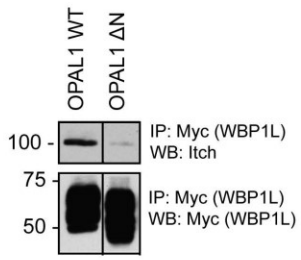

Figure S5. WBP1L interaction with ITCH in J774 macrophage-like cell line. MYC-tag imunoprecipatates from J774 cells stably expressing MYC-tagged WBP1L wild-type form or WBP1LΔN lacking WW domain interacting motifs. Western blots were stained with anti-ITCH antibody and anti MYC-tag antibody. Irrelevant lines from the blot image were removed and replaced with vertical dividing lines. N=2.

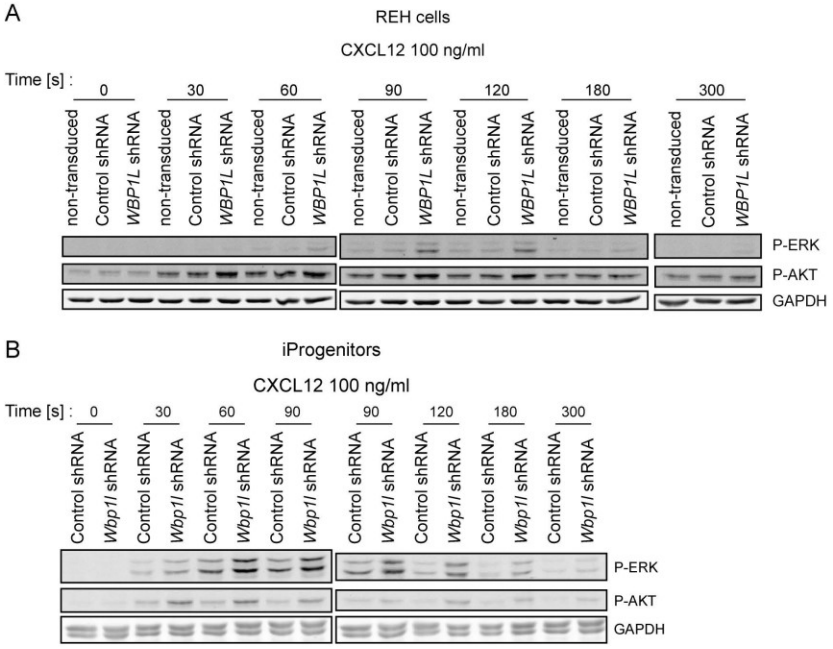

Figure S6. Representative Western blots showing data quantified in Figure 4C (A) and 4D (B).

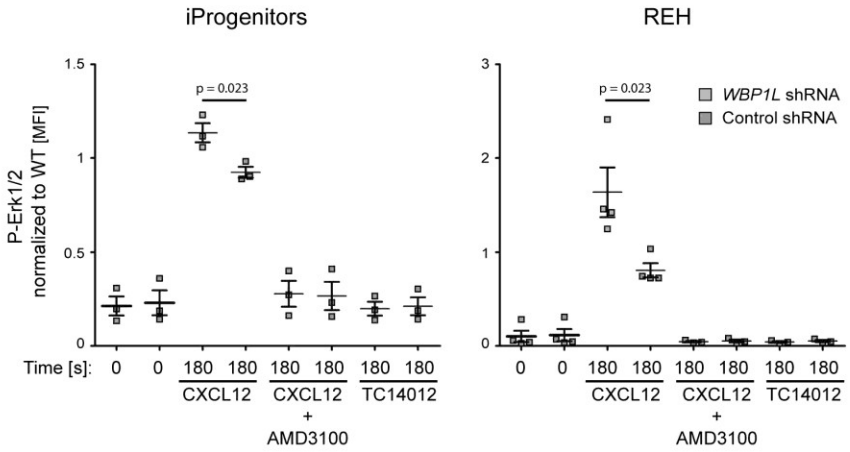

Figure S7. ERK1/2 phosphorylation downstream of CXCR4 or CXCR7 in immortalized monocyte/macrophage progenitors and REH cells transduced with *WBP1L* or control shRNA. Cells were treated with 100 nM CXCL12 alone or together with 1 µg/ml of CXCR4 antagonist AMD3100 or treated with 1 µM specific agonist of CXCR7 TC14012. ERK1/2 phosphorylation was analyzed by flow cytometry. Data are normalized to non-transduced cells (left panel N=3, right panel N=4).

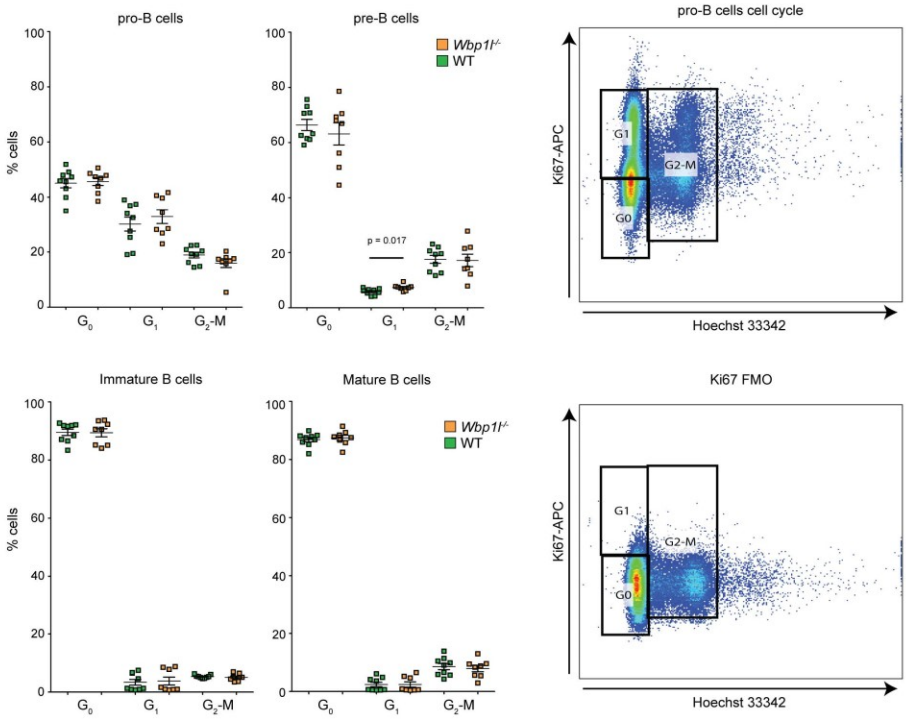

Figure S8. Analysis of cell cycle in bone marrow B cell progenitors from wild-type and *Wbp1l*-deficient mice. Bone marrow cells were fixed, stained for surface markers, permeabilized, and stained with Ki67 and Hoechst 33342. Individual B cell subsets were defined using following markers: Pro-B cells ($CD43^+$, $B220^+$, IgM^-), Pre-B cells ($CD43^-$, $B220^{low}$, IgM^-), Immature B cells ($CD43^-$, $B220^{low}$, IgM^+), Mature B cells ($CD43^-$, $B220^{high}$, IgM^+). The right panel of FACS plots shows gating strategy of cell cycle analyses. Representative FACS plots of stained cells with and without (Ki67 FMO) Ki67 staining are shown.

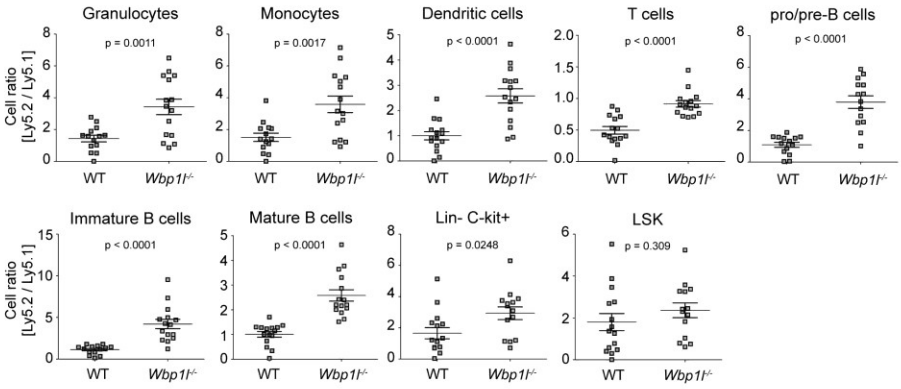

Figure S9. Enhanced engraftment of *Wbp1l*$^{-/-}$ bone marrow. Ly5.2^{+} bone marrow (WT or *Wbp1l*$^{-/-}$) was mixed with Ly5.1^{+} bone marrow (always WT) in a ratio 1:1 and 2 × 10^{6} cells were transplanted into Ly5.1 lethally irradiated mice. Mice were analyzed two months post transplantation. Flow cytometry analyses show the ratio between Ly5.2 and Ly5.1 cells determined for individual bone marrow cell subsets. Individual cell subsets were defined using following markers: Granulocytes (LY6C^{-}, CD11b^{+}, LY6G^{+}), Monocytes (LY6C^{+}, CD11b^{+}, LY6G^{-}), Dendritic cells (CD11c^{+}), T cells (CD3^{+}), Pro/Pre B cells (B220^{low}, IgM^{-}), Immature B cells (B220^{low}, IgM^{+}), Mature B cells (B220^{high}, IgM^{+}), Lin^{-}C-kit^{+} cells (lin^{-}, c-kit^{+}), LSK cells (lin^{-}, c-kit^{+}, SCA1^{+}).

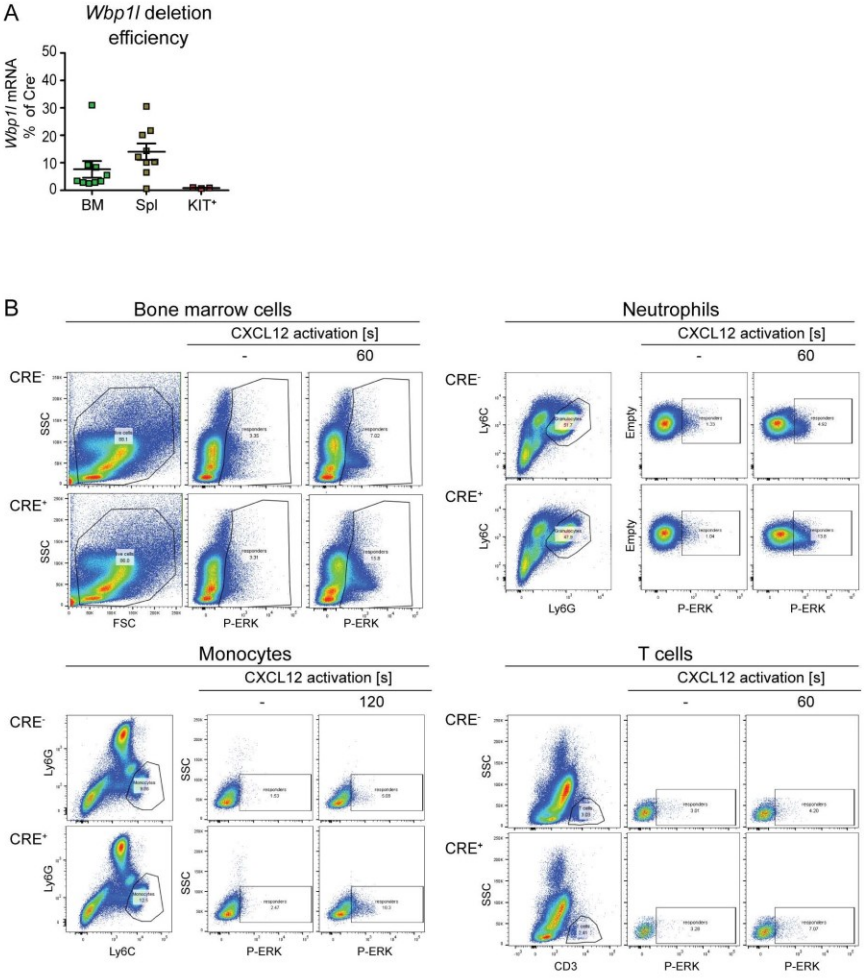

Figure S10. Effects of inducible *Wbp1l* deletion on ERK activation in bone marrow cell subsets. (A) *Wbp1l* mRNA expression after in vitro 4-hydroxytamoxifen induced deletion in samples from Figure 7F compared to 4-hydroxytamoxifen-induced deletion in vivo in the whole bone marrow and spleen from *Wbp1l-CreERT* mice (samples from Figure 7D). (B) Representative FACS plots for data shown in Figure 7D.

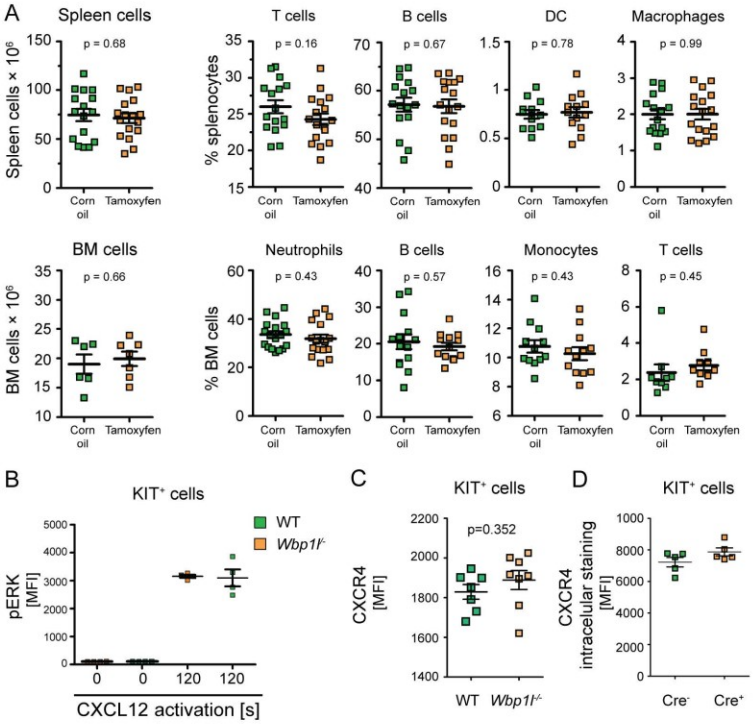

Figure S11. Additional analyses of *Wbp1l*$^{-/-}$ cells. (A) Total numbers of splenocytes and bone marrow cells and percentages of major leukocyte subsets 5-7 days after Tamoxifen-induced deletion of *Wbp1l*. The splenocyte subsets were defined using the following markers: T cells (CD3^{+}), B cells (B220^{+}), DC (CD11c^{+}, Ly6C$^{-/low}$), Macrophages (F4/80^{+}, CD11b^{int}). The bone marrow cell subsets were defined using the following markers: Neutrophils (Ly6C^{int}, CD11b^{+}, Ly6G^{+}), B cells (B220^{+}), Monocytes (Ly6C^{high}, CD11b^{+}, Ly6G^{-}), T cells (CD3^{+}). (B) Similar experiment as in Figure 7F. However, here the cells with constitutive *Wbp1l* inactivation were used (N=4). (C) CXCR4 surface expression was measured in cultured KIT^{+} bone marrow progenitors with constitutive *Wbp1l* inactivation by flow cytometry. One significant outlier was removed based on Q test. (D) Total CXCR4 expression was measured in cultured KIT^{+} bone marrow progenitors with constitutive *Wbp1l* inactivation by flow cytometry of fixed and permeabilized cells.

Supplemental References

1. **Kanderova V, Kuzilkova D, Stuchly J, Vaskova M, Brdicka T, Fiser K, Hrusak O, Lund-Johansen F, Kalina T.** High-resolution Antibody Array Analysis of Childhood Acute Leukemia Cells. *Mol Cell Proteomics*. 2016; 15: 1246-61.
2. **Wang GG, Calvo KR, Pasillas MP, Sykes DB, Hacker H, Kamps MP.** Quantitative production of macrophages or neutrophils ex vivo using conditional Hoxb8. *Nat Methods*. 2006; 3: 287-93.
3. **Drobek A, Kralova J, Skopcova T, Kucova M, Novak P, Angelisova P, Otahal P, Alberich-Jorda M, Brdicka T.** PSTPIP2, a Protein Associated with Autoinflammatory Disease, Interacts with Inhibitory Enzymes SHIP1 and Csk. *J Immunol*. 2015; 195: 3416-26.
4. **Kralova J, Glatzova D, Borna S, Brdicka T.** Expression of Fluorescent Fusion Proteins in Murine Bone Marrow-Derived Dendritic Cells and Macrophages. *J Vis Exp*. 2018; 140: e58081.
5. **Sobocinska J, Roszczenko-Jasinska P, Zareba-Koziol M, Hromada-Judycka A, Matveichuk OV, Traczyk G, Lukasiuk K, Kwiatkowska K.** Lipopolysaccharide Upregulates Palmitoylated Enzymes of the Phosphatidylinositol Cycle: An Insight from Proteomic Studies. *Mol Cell Proteomics*. 2018; 17: 233-54.
6. **Wessel D, Flugge UI.** A method for the quantitative recovery of protein in dilute solution in the presence of detergents and lipids. *Anal Biochem*. 1984; 138: 141-3.
7. **Masuda T, Tomita M, Ishihama Y.** Phase transfer surfactant-aided trypsin digestion for membrane proteome analysis. *J Proteome Res*. 2008; 7: 731-40.
8. **Hebert AS, Richards AL, Bailey DJ, Ulbrich A, Coughlin EE, Westphall MS, Coon JJ.** The one hour yeast proteome. *Mol Cell Proteomics*. 2014; 13: 339-47.
9. **Cox J, Hein MY, Luber CA, Paron I, Nagaraj N, Mann M.** Accurate proteome-wide label-free quantification by delayed normalization and maximal peptide ratio extraction, termed MaxLFQ. *Mol Cell Proteomics*. 2014; 13: 2513-26.
10. **Welm BE, Dijkgraaf GJ, Bledau AS, Welm AL, Werb Z.** Lentiviral transduction of mammary stem cells for analysis of gene function during development and cancer. *Cell Stem Cell*. 2008; 2: 90-102.
11. **Gao S, Alarcon C, Sapkota G, Rahman S, Chen PY, Goerner N, Macias MJ, Erdjument-Bromage H, Tempst P, Massague J.** Ubiquitin ligase Nedd4L targets activated Smad2/3 to limit TGF-beta signaling. *Mol Cell*. 2009; 36: 457-68.
12. **Magnifico A, Ettenberg S, Yang C, Mariano J, Tiwari S, Fang S, Lipkowitz S, Weissman AM.** WW domain HECT E3s target Cbl RING finger E3s for proteasomal degradation. *J Biol Chem*. 2003; 278: 43169-77.
13. **Hruz T, Laule O, Szabo G, Wessendorp F, Bleuler S, Oertle L, Widmayer P, Gruissem W, Zimmermann P.** Genevestigator v3: a reference expression database for the meta-analysis of transcriptomes. *Adv Bioinformatics*. 2008; 2008: 420747.

The Journal of Immunology

Dysregulated NADPH Oxidase Promotes Bone Damage in Murine Model of Autoinflammatory Osteomyelitis

This information is current as of March 12, 2020.

Jarmila Kralova, Ales Drobek, Jan Prochazka, Frantisek Spoutil, Matej Fabisik, Daniela Glatzova, Simon Borna, Jana Pokorna, Tereza Skopcova, Pavla Angelisova, Martin Gregor, Pavel Kovarik, Radislav Sedlacek and Tomas Brdicka

J Immunol 2020; 204:1607-1620; Prepublished online 5 February 2020;
doi: 10.4049/jimmunol.1900953
http://www.jimmunol.org/content/204/6/1607

Supplementary Material **http://www.jimmunol.org/content/suppl/2020/02/04/jimmunol.1900953.DCSupplemental**

References This article **cites 79 articles**, 25 of which you can access for free at:
http://www.jimmunol.org/content/204/6/1607.full#ref-list-1

Why *The JI*? Submit online.

- **Rapid Reviews! 30 days*** from submission to initial decision
- **No Triage!** Every submission reviewed by practicing scientists
- **Fast Publication!** 4 weeks from acceptance to publication

**average*

Subscription Information about subscribing to *The Journal of Immunology* is online at:
http://jimmunol.org/subscription

Permissions Submit copyright permission requests at:
http://www.aai.org/About/Publications/JI/copyright.html

Email Alerts Receive free email-alerts when new articles cite this article. Sign up at:
http://jimmunol.org/alerts

The Journal of Immunology is published twice each month by
The American Association of Immunologists, Inc.,
1451 Rockville Pike, Suite 650, Rockville, MD 20852
Copyright © 2020 by The American Association of Immunologists, Inc. All rights reserved.
Print ISSN: 0022-1767 Online ISSN: 1550-6606.

Downloaded from http://www.jimmunol.org/ at Institute of Physiology ASCR on March 12, 2020

Dysregulated NADPH Oxidase Promotes Bone Damage in Murine Model of Autoinflammatory Osteomyelitis

Jarmila Kralova,[*,1] Ales Drobek,[*,†,1] Jan Prochazka,[‡,§,1] Frantisek Spoutil,[§] Matej Fabisik,[*,¶] Daniela Glatzova,[*,¶] Simon Borna,[*,¶] Jana Pokorna,[*] Tereza Skopcova,[*] Pavla Angelisova,[*] Martin Gregor,[‖] Pavel Kovarik,[#] Radislav Sedlacek,[‡,§] and Tomas Brdicka[*]

Autoinflammatory diseases are characterized by dysregulation of the innate immune system, leading to spontaneous inflammation. *Pstpip2*^{cmo} mouse strain is a well-characterized model of this class of disorders. Because of the mutation leading to the lack of adaptor protein PSTPIP2, these animals suffer from autoinflammatory chronic multifocal osteomyelitis similar to several human syndromes. Current evidence suggests that it is driven by hyperproduction of IL-1β by neutrophil granulocytes. In this study, we show that in addition to IL-1β, PSTPIP2 also negatively regulates pathways governing reactive oxygen species generation by neutrophil NOX2 NADPH oxidase. *Pstpip2*^{cmo} neutrophils display highly elevated superoxide production in response to a range of stimuli. Inactivation of NOX2 NADPH oxidase in *Pstpip2*^{cmo} mice did not affect IL-1β levels, and the autoinflammatory process was initiated with similar kinetics. However, the bone destruction was almost completely alleviated, suggesting that dysregulated NADPH oxidase activity is a key factor promoting autoinflammatory bone damage in *Pstpip2*^{cmo} mice. *The Journal of Immunology*, 2020, 204: 1607–1620.

Autoinflammatory diseases represent a distinct class of disorders of the innate immune system. They are characterized by a pathological inflammation that typically arises spontaneously without detectable extrinsic cause and in the absence of autoantibodies or autoreactive T cells. The symptoms are rather diverse. The most characteristic include periodic fever attacks, skin rashes, arthralgia, myalgia, abdominal pain, arthritis, osteomyelitis, and other signs of systemic or organ specific inflammation (1–3). A number of autoinflammatory diseases are caused by a pathological hyperactivity of IL-1β pathway, either as a result of mutations in single genes affecting inflammasomes and other components of IL-1β activation machinery or from more complex causes in which the underlying genetic lesion is unknown (1, 3).

Bone damage or other types of bone involvement are common in IL-1β–driven autoinflammatory diseases (4). IL-1β promotes osteoclast activity by stimulating RANKL expression in osteoblasts and by direct binding to osteoclasts. This way it likely stimulates inflammatory bone resorption by these cells during the course of the disease (4, 5). Interestingly, different diseases of this group show different and distinct types of bone damage. Moreover, the bone damage is often observed only in a fraction of patients with a particular disease (4, 6, 7). These observations suggest that the character of genetic lesion, genetic modifiers, or other circumstances are critically affecting the outcome (4). However, the identity of these factors and the mechanisms of how they change the clinical picture are largely unknown.

One of the key activators of IL-1β pathway mutated in several autoinflammatory conditions is NLRP3 inflammasome. It is activated by aberrant ion fluxes; lysosomal damage by crystalline matter, such as silica or monosodium urate crystals; mitochondrial damage; presence of reactive oxygen species (ROS); and various microbial products and molecules associated with cellular damage (8–12). Several unifying mechanisms enabling recognition of such a variety of stress agents by a single type of inflammasome have been suggested, but none of them has yet gained universal

*Laboratory of Leukocyte Signalling, Institute of Molecular Genetics of the Czech Academy of Sciences, 14220 Prague, Czech Republic; [†]Laboratory of Adaptive Immunity, Institute of Molecular Genetics of the Czech Academy of Sciences, 14220 Prague, Czech Republic; [‡]Laboratory of Transgenic Models of Diseases, Institute of Molecular Genetics of the Czech Academy of Sciences, 25242 Vestec, Czech Republic; [§]Czech Centre for Phenogenomics, Institute of Molecular Genetics of the Czech Academy of Sciences, 25242 Vestec, Czech Republic; [¶]Faculty of Science, Charles University, 12800 Prague, Czech Republic; [‖]Laboratory of Integrative Biology, Institute of Molecular Genetics of the Czech Academy of Sciences, 14220 Prague, Czech Republic; and [#]Max F. Perutz Laboratories, University of Vienna, 1030 Vienna, Austria

[1]J.K., A.D., and J.P. contributed equally to this work.

ORCIDs: 0000-0003-3017-2666 (J.K.); 0000-0003-1066-9413 (A.D.); 0000-0002-7310-3487 (F.S.); 0000-0002-4742-3196 (D.G.); 0000-0001-8445-2634 (S.B.); 0000-0003-2956-0944 (P.K.); 0000-0002-1560-4398 (T.B.).

Received for publication August 7, 2019. Accepted for publication January 13, 2020.

This work was supported by the Czech Science Foundation (Project 17-07155S). It also benefited from institutional funding by the Czech Academy of Sciences (RVO 68378050). In addition, it was supported by core facilities of the Institute of Molecular Genetics funded by Projects LM2015040 from the Czech Centre for Phenogenomics and LQ1604 NPU II from the Ministry of Education, Youth and Sports of the Czech Republic; Projects CZ.1.05/1.1.00/02.0109 from the Biotechnology and Biomedicine Centre of the Academy of Sciences and Charles University in Vestec and CZ.1.05/2.1.00/19.0395 Higher quality and capacity for transgenic models from the Ministry of Education, Youth and Sports of the Czech Republic and the European Regional Development Fund; Project CZ.02.1.01/0.0/0.0/16_013/0001789 Upgrade of the Czech Centre for Phenogenomics: developing towards translation research by the Ministry of Education, Youth and Sports of the Czech Republic and the European Structural and Investment Funds; the Light Microscopy Core Facility was supported by the Ministry of Education, Youth and Sports of the Czech Republic (LM2015062, CZ.02.1.01/0.0/0.0/16_013/0001775, and LO1419), and Operational Programme Prague - Competitiveness (CZ.2.16/3.1.00/21547). J.K. and D.G. received additional support from the Charles University Grant Agency (Project 923116).

Address correspondence and reprint requests to Dr. Tomas Brdicka, Institute of Molecular Genetics of the Czech Academy of Sciences, Videnska 1083, 14220 Prague, Czech Republic. E-mail address: tomas.brdicka@img.cas.cz

The online version of this article contains supplemental material.

Abbreviations used in this article: BM, bone marrow; CMO, chronic multifocal osteomyelitis; CRMO, chronic recurrent multifocal osteomyelitis; μCT, microcomputed tomography; PKC, protein kinase C; ROS, reactive oxygen species; WT, wild-type.

Copyright © 2020 by The American Association of Immunologists, Inc. 0022-1767/20/$37.50

www.jimmunol.org/cgi/doi/10.4049/jimmunol.1900953

Downloaded from http://www.jimmunol.org/ at Institute of Physiology ASCR on March 12, 2020

acceptance (8, 9, 11–13). Production of ROS represents one such a mechanism that could connect cellular stress to NLRP3 inflammasome activation (for review, see 10, 14). In most of the cell types, there appear to be at least two main sources of ROS, NADPH oxidases, and mitochondria (15). In phagocytes, NOX2 NADPH oxidase is activated downstream of receptors for microbial products and other proinflammatory stimuli. It generates superoxide anion, which can be further converted to a number of additional ROS toxic to microorganisms. Various NADPH oxidases are also part of a broad array of signaling pathways in multiple cell types (16, 17). Mitochondrial ROS are produced mainly as a result of respiratory chain activity, and their generation can be enhanced by stress or mitochondrial damage (18–20). Although initial reports suggested that NADPH oxidase–derived ROS are critical for NLRP3 inflammasome triggering, more recent studies rather support the view that mitochondria are the essential source of ROS required for its activation (21, 22). However, whether NADPH oxidase ROS can contribute to NLRP3 inflammasome activation when deregulated as a result of neutrophil priming or during diseases that result in exaggerated NADPH oxidase-dependent ROS production has not been studied.

Several studies have shown increased production of ROS in monocytes from autoinflammatory disease patients (10, 23–28). In some of these works it has been proposed that these ROS are of mitochondrial origin (10, 23), but there are only limited options of how to study this aspect in patients. The effects of increased ROS production, whether of mitochondrial or NADPH oxidase origin, on the development and/or severity of autoinflammatory diseases is currently unknown.

There are relatively few mouse models of autoinflammatory bone diseases. One of the best characterized is *Pstpip2^{cmo}* mouse strain, which spontaneously develops severe bone and soft tissue inflammation mainly in hind paws and tail. In several aspects, the disease resembles a human condition known as chronic recurrent multifocal osteomyelitis (CRMO) and was thus termed chronic multifocal osteomyelitis (CMO). From there, the strain derives its name *Pstpip2^{cmo}* (29). The disease is caused by a point mutation in the gene coding for the adaptor protein PSTPIP2 (30). As a result, no PSTPIP2 is detectable in these mice at the protein level (31). The mechanism by which PSTPIP2 deficiency leads to CMO disease is only partially understood. It binds several inhibitory molecules, including PEST-family protein tyrosine phosphatases, phosphoinositide phosphatase SHIP1, and inhibitory kinase Csk, which likely mediate its negative regulatory effect on the inflammatory response (32, 33). In addition, it has been reported that osteomyelitis in *Pstpip2^{cmo}* mice is completely dependent on excessive IL-1β production by neutrophilic granulocytes (34–36). Genetic studies suggest a combined involvement of the NLRP3 inflammasome and a poorly characterized mechanism dependent on caspase-8. A relatively limited role of neutrophil proteases has also been demonstrated (36, 37). The involvement of NLRP3 inflammasome suggests that cellular stress and ROS might be involved in CMO disease pathology, especially, when we consider the fact that neutrophils are very potent producers of NADPH oxidase–derived ROS. Moreover, ROS are also activators of osteoclasts (38), a cell type likely responsible for inflammatory bone damage in CMO mice (39). In this study, we show that in *Pstpip2^{cmo}* neutrophils, superoxide generation by NADPH oxidase is profoundly dysregulated and these cells produce substantially increased amounts of superoxide in response to variety of stimuli. Strikingly, the dysregulated superoxide production by these neutrophils does not have a strong effect on IL-1β production and soft tissue inflammation, but rather on the bone inflammation and subsequent bone damage, suggesting that the role of NADPH-oxidase–derived ROS is not in triggering the CMO but rather in directing the damage accompanying this disease to the bones.

Materials and Methods

Abs

Abs to the following murine Ags were used: RAC1/2/3 (catalog no. 2465; Cell Signaling Technology, Danvers, MA); p47phox (D-10) and ERK2 (C-14) (Santa Cruz Biotechnology, Dallas, TX); B220-biotin, TER119-biotin, c-Kit-biotin, CD3ε-biotin, Ly6G-biotin, CD115-biotin, CD11b-allophycocyanin, CD11b-FITC, CD11b-PE, B220-FITC, Ly6C-PE-Cy7, Ly6C-FITC, Ly6G-FITC, Ly6G-allophycocyanin, c-Kit-PE, Sca-1-allophycocyanin, and CD16/32-PE/Cy7 (BioLegend, San Diego, CA); CD34-FITC, DX5-biotin, F4/80-biotin, and Thy1.2-FITC (eBioscience, ThermoFisher Scientific, Waltham, MA); Fc Block (2.4G2) (BD Biosciences, San Jose, CA); and HRP-conjugated goat anti-mouse IgG (Sigma-Aldrich) and HRP-goat anti-rabbit (Bio-Rad, Hercules, CA). The mouse mAb that recognizes murine PSTPIP2 has been described earlier (33). Heat-aggregated IgG was prepared as follows: IgG was purified from mouse serum (Sigma-Aldrich) on protein A–Sepharose (GE Healthcare, Uppsala, Sweden), transferred to PBS, and concentrated to 30 mg/ml on an Amicon Ultracel–30K unit (Millipore, Merck, Darmstadt, Germany). The aggregation was induced by heating to 63°C for 30 min.

Other reagents

In this study we also used luminol, HRP, LPSs from *Escherichia coli* O127:B8, fMLP, PMA, (all from Sigma-Aldrich), L-012 (Wako Chemicals), TNF-α, G-CSF (PeproTech, Rocky Hill, NJ), U0126 (Cell Signaling Technology), and Gö6976 (Calbiochem, Merck). Silica (silicon dioxide crystals) was obtained from Sigma-Aldrich. To enable fluorescent labeling for microscopy, 5 mg/ml silica particles were first coated with nonfat dry milk (2% in PBS, 1 h at room temperature) and then labeled with 5 μM Cell Proliferation Dye eFluor 670 (eBioscience), 30 min at 37°C.

Mice

Pstpip2^{cmo} mouse strain (C.Cg-*Pstpip2^{cmo}*/J) carrying the c.293T→C mutation in the Pstpip2 gene (on BALB/C genetic background) resulting in an L98P change in the PSTPIP2 protein (29, 30), B6.129S-*Cybb^{tm1Din}*/J lacking NADPH oxidase subunit gp91phox (40); MyD88 deficient mouse strain (B6.129P2(SJL)-*MyD88$^{tm1.1Defr}$*/J, derived from *MyD88^{fl}* mice (41); B6.SJL-Ptprca Pepcb/BoyJ (CD45.1^{+}) congenic strain (42), *B6.Cg-Tg(S100A8-cre,-EGFP)1Ilw/J* with granulocyte-specific CRE expression (MRP8-Cre) (43); and *Gt(ROSA)26Sor$^{tm1(DTA)Lky}$*/J strain (44), in which diphtheria toxin expression can be induced by CRE recombinase, were obtained from The Jackson Laboratory (Bar Harbor, ME). *Pstpip2^{cmo}* mouse strain was backcrossed on C57BL/6J background for at least 10 generations and then used in the majority of experiments, with the exception of experiments in Figs. 1E, 4A, 4D–F and Supplemental Fig. 1. For these experiments, the original *Pstpip2^{cmo}* strain on BALB/c genetic background has been selected due to the higher number of neutrophils that could be obtained by the negative selection method and due to the better quality of immortalized granulocyte progenitors derived from this strain. Both genetic backgrounds showed similar disease symptoms and similar dysregulation in superoxide production. The BALB/c and C57BL/6J inbred strains were obtained from the animal facility of Institute of Molecular Genetics, Academy of Sciences of the Czech Republic (Prague, Czech Republic). *Pstpip2^{cmo}-DTA-MRP8-Cre* mouse strain was generated by breeding of the *Pstpip2^{cmo}* mice on C57BL/6J background with *Gt(ROSA)26Sor$^{tm1(DTA)Lky}$*/J strain mouse strain. Breeding this strain to *B6.Cg-Tg(S100A8-cre,-EGFP)1Ilw/J* mice carrying Cre transgene under the control of granulocyte-specific MRP8 promoter resulted in the generation of *Pstpip2^{cmo}-DTA-MRP8-Cre* strain lacking almost all granulocytes (Supplemental Fig. 3B, 3C). Mice were housed and bred in an accredited animal facility at the Institute of Molecular Genetics of the Czech Academy of Sciences (registration number CZ11760038). They were maintained under specific pathogen-free conditions. Animals were fed by standard breeding fortified diet (Altromin) cereal-based (soy, wheat, corn) fixed formula, which is free of alfalfa and fish/animal meal and deficient in nitrosamines, containing 22.6% crude protein, 5% crude fat, 4.5% crude fiber, 7.1% crude ash, autoclavable, and increased vitamin content. The drinking water was purified via reverse osmosis system and chlorinated by chlorine dioxide (ClO_2) as an alternative disinfectant to prevent secondary contamination. The final concentration of active chlorine was maintained between 0.6 and 1.0 ppm (in acid pH 4–5). Experimental cohorts, sex and age matched, were made from both genders, and standard randomization

Downloaded from http://www.jimmunol.org/ at Institute of Physiology ASCR on March 12, 2020

was applied. Unless indicated otherwise, age of animals ranged from 6 to 14 wk. Experiments in this work that were conducted on animals were approved by the Expert Committee on the Welfare of Experimental Animals of the Institute of Molecular Genetics and by the Academy of Sciences of the Czech Republic (registration numbers 69/2014, 62/2015, 50/2016, 66/2016, 45/2018) and were in agreement with local legal requirements and ethical guidelines.

Primary cells and cell lines

All primary cells and cell lines were cultured at 37°C with 5% CO_2 in IMDM supplemented with 10% FCS and antibiotics. For bone marrow (BM) cell isolation, mice were sacrificed by cervical dislocation, BM was flushed with PBS supplemented with 2% FCS, and erythrocytes were lysed in an ACK buffer (150 mM NH_4Cl, 0.1 mM EDTA [disodium salt], 1 mM $KHCO_3$). Murine neutrophils were isolated from BM cells using anti-biotin MicroBeads and LS magnetic columns (Miltenyi Biotec, Bergisch Gladbach, Germany). For negative selection, cells were labeled with biotinylated Abs to B220, F4/80, DX5, c-Kit, CD3ε, CD115, and Ter119 prior to magnetic bead purification. For positive selection, only anti-Ly6G biotin was used. The purity of isolated cells was determined by flow cytometry. Primary murine monocytes were sorted from BM cells as Ly6G negative, Ly6C highly positive, and side scatter–low cells using BD Influx sorter (BD Biosciences). The following cell lines were used in this study: HEK293FT cells (Invitrogen), Platinum Eco cells (Plat-E cells; Cell Biolabs, San Diego, CA), and immortalized granulocyte progenitors. For preparation of immortalized granulocyte progenitors we used a modified version of the protocol for generation of immortalized macrophage progenitors (45). The progenitors were first enriched by the depletion of Mac-1$^+$, B220$^+$, and Thy1.2$^+$ from mouse BM cells and cultured in the presence of IL-3, IL-6, and SCF (supplied as culture supernatants from HEK293FT cells transfected with constructs coding for respective cytokines) for 2 d. Next, progenitors were transduced with ER-HoxB8 construct. The transduced cells were enriched for the GMP progenitor population by FACS (Lin$^-$, Sca-1$^-$, c-Kit$^+$, FcγR$^+$, CD34$^+$) and propagated in a medium containing 1 μM β-estradiol and 1% SCF-containing supernatant. Granulocyte differentiation was induced by β-estradiol withdrawal or by the β-estradiol withdrawal and replacement of SCF for G-CSF (50 ng/ml).

Flow cytometry

Single-cell suspensions of BM cells were incubated with Fc block and fluorophore-conjugated Abs and analyzed on a BD LSR II flow cytometer. For calcium response measurement, single-cell suspensions of BM from 6- to 8-wk-old mice were loaded with 2 μM calcium indicator Fura Red (Invitrogen). Samples were analyzed using a BD LSR II flow cytometer for 30 s at rest and then another 210 s after activation (with fMLP, Silica, or *E. coli* with OD = 0.8). The relative calcium concentration was measured as a ratio of the Fura Red fluorescence intensity elicited by excitation wavelengths of 405 nm (emission measured at 635–720 nm) and 488 nm (emission measured at 655–695 nm). Data were acquired on a BD flow cytometer LSR II. Granulocytes were gated according to forward and side scatter properties. For F-actin detection, BM cells were fixed with 4% formaldehyde and labeled with fluorophore-conjugated Abs to CD11b, Ly6C, and Ly6G. Next, the cells were permeabilized with *l*-α-lysophosphatidylcholine (80 μg/ml; Sigma-Aldrich) and simultaneously stained with Alexa Fluor 488–conjugated phalloidin (Invitrogen). The cell fluorescence was measured on a BD LSR II flow cytometer. Granulocytes were gated as CD11b$^+$, Ly6C^{int}, and Ly6G$^+$. The data were analyzed with FlowJo software (Tree Star, Ashland, OR).

Superoxide detection

Superoxide production in vitro was assessed by luminol-based chemiluminescence assay as published previously (46, 47). BM cells or purified murine neutrophils in IMDM supplemented with 0.2% FCS were plated in a density of 10^6 cells per well into a black 96-well plate (SPL Life Sciences, Naechon-Myeon, Korea). Cells were rested for 30 min at 37°C and 5% CO_2. Then, luminol at final concentration 100 μM and stimuli (100 ng/ml LPS, fMLP 1 μg/ml, TNF-α 10 ng/ml, *E. coli* OD_{600} ~0.8–5× diluted, silica 50 μg/cm^2, heat-aggregated murine IgG 300 μg/ml, PMA 100 ng/ml) were added. Luminescence was measured immediately on an EnVision plate reader (Perkin Elmer, Waltham, MA); each well was scanned every minute for 70 min. For fMLP-induced superoxide production, scanning every 10 s for 5 min was also used as indicated in figure legends. To measure superoxide production by cells in suspension, the cells were kept at 10^7 per 0.9 ml IMDM with 0.2% FCS and 100 μM luminol in an Eppendorf tube at 37°C. After stimulation with 100 μl silica (1 mg/ml), every 5 min a 100-μl aliquot of cell suspension was gently transferred into an empty well of a black 96-well plate and the luminescence was immediately measured on an EnVision plate reader. When fMLP (1 μg/ml) was used as a stimulant, only a single aliquot of 10^6 cells was measured in 10-s intervals in a single well immediately after cell transfer to the plate and activation. For exogenous peroxidase treatment, cells were incubated with HRP (10 μg/ml) for 30 min prior to stimulation with silica.

To assess ROS production in vivo, mice were i.p. injected with luminescence reporter L-012 in final concentration 75 mg/kg (1.8 mg/25 g mouse) dissolved in PBS as previously described (48). Luminescence signal was acquired by Xtreme whole body imager (Bruker, Billerica, MA), with the following settings: binning 8 × 8, exposure time: 5 min. The quantification of photon counts was performed in Molecular Imaging Software (Bruker).

DNA constructs

Generation of MSCV-PSTPIP2-EGFP construct was as follows. The coding sequence of mouse PSTPIP2 was amplified from cDNA of mouse common myeloid progenitors and subcloned into pXJ41-EGFP cloning vector (Chum et al. 2016). IRES and Thy1.1 coding sequence was removed from MSCV-IRES-Thy1.1 retroviral vector (Clontech, Mountain View, CA) by digestion with EcoRI and ClaI followed by blunt ligation. PSTPIP2-EGFP coding sequence was then subcloned into modified MSCV vector using BglII and XhoI restriction sites to generate MSCV-PSTPIP2-EGFP.

Generation of MSCV-mPSTPIP2-TetOn inducible constructs. Wild-type (WT) and mutated sequences (W232A or 3YF) of mouse PSTPIP2 described earlier (33) were fused to C-terminal EGFP by PCR using P2A sequence as a linker. Fusion constructs were cloned into pLVX-Tet3G doxycycline inducible vector (Clontech) using AgeI and BamHI restriction sites. Resulting vectors were used as templates to amplify the Tet-On 3G, TRE3G, and PSTPIP2 sequences by PCR, and the resulting product was cloned into MSCV-IRES-EGFP vector using ClaI and BglII restriction sites.

Retroviral transduction

For confocal microscopy, c-kit+ stem and progenitor cells were obtained from BM of *Pstpip2^{cmo}* (C57BL/6J) mice using magnetic purification (c-kit–biotin Ab, Anti-biotin microbeads). Cells were expanded in IL-3, IL-6, and SCF-supplemented media for 20 h, then infected with PSTPIP2-EGFP retroviral construct. For the production of replication incompetent retrovirus, ecotropic packaging cells (Plat-E) were plated in a 10-cm dish and transfected with 24 μg of plasmid DNA using Lipofectamine 2000 Reagent (Life Technologies) according to the manufacturer's instructions. Virus-containing supernatant was collected, concentrated with Amicon Ultra centrifugal filters with molecular mass cut-off 100 kDa (Merck Millipore), and immediately used to infect the cytokine expanded c-kit+ BM cells. These cells were centrifuged with 150 μl of concentrated virus supernatant and 2.4 μl of Lipofectamine 2000 Reagent (Sigma-Aldrich) at 1250 × *g* for 90 min at 30°C and then incubated for another 4 h at 37°C in 5% CO_2 in a humidified incubator before the exchange of the media. Immortalized granulocyte progenitors were propagated in IMDM with 1 μM β-estradiol and 1% SCF-containing supernatant and then infected with PSTPIP2 mutant constructs using the same procedure described above.

Real-time quantitative PCR

RNA was purified with Zymo Research Quick-RNA Miniprep Plus Kit from neutrophils isolated by positive selection (see above). The reverse transcription was performed with RevertAid First Strand cDNA Synthesis Kit (ThermoFisher Scientific). Real-time quantitative PCR was carried out using LightCycler 480 SYBR Green I Master mix (Roche) and the following primers: 5′-TGTAATGAAAGACGGCACACC-3′ + 5′-TCTTCTTTG-GGTATTGCTTGG-3′ for IL-1β and 5′-GATCTGGCACCACACCTTCT-3′ + 5′-GGGGTGTTGAAGGTCTCAAA-3′ for β-actin on Roche LightCycler 480 Instrument II. The primer functionality was verified on LPS-stimulated BM-derived dendritic cells.

Microscopy

One day postinfection, EGFP-positive cells were sorted on an Influx sorter and injected into sublethally irradiated (6 Gy in a single dose) CD45.1$^+$ recipient mice. After 2 wk, mice were sacrificed, and BM cells isolated and resuspended in IMDM with 0.1% FCS. The cells were activated by 50 μg/cm^2 fluorescent silica (see above) in a 96-well plate for 10 min. The cells were transferred to 4% paraformaldehyde in PBS and fixed at room temperature for 20 min. Cell nuclei were stained with 10 μg/ml Hoechst 33258 (Sigma-Aldrich) for 15 min. Cells were than washed two

Downloaded from http://www.jimmunol.org/ at Institute of Physiology ASCR on March 12, 2020

times with PBS, resuspended in 150 μl of ddH2O, and centrifuged on glass slide at 300 × *g* for 5 min using Centurion Scientific K3 cytospin centrifuge (Centurion Scientific, Stoughton, U.K.). Cell samples were then mounted in 10 μl of DABCO mounting reagent (Sigma-Aldrich) and covered with glass coverslip (Zeiss, Oberkochen, Germany). The microscope setup was as follows: sequential two-color imaging was performed using a Leica TCS SP8 laser scanning confocal microscope (Leica, Wetzlar, Germany) with a 63 × 1.4 numerical aperture oil-immersion objective. Acquired images were manually thresholded to remove signal noise detected outside of the cell using ImageJ software.

Cell activation, lysis, and immunoprecipitation

For Western blotting, the cells were washed and resuspended in IMDM with 0.1% FCS at a concentration of 1–4 × 10^7 cells/ml. Subsequently, the cells were stimulated as indicated at 37°C. The activation of cells was stopped by the addition of an equal volume of a 2× concentrated SDS-PAGE sample buffer (128 mM Tris [pH 6.8], 10% glycerol, 4% SDS, 2% DTT), followed by the sonication and heating of the samples (99°C for 2 min). The samples were analyzed by SDS-PAGE followed by Western blotting. For detection of p47phox phosphorylation, phosphoproteins were isolated from BM cells using PhosphoProtein purification Kit (Qiagen, Hilden, Germany) according to manufacturer's instructions, followed by detection of p47phox by immunoblotting.

RAC activity assay

A total of 2 × 10^7 neutrophils (silica activated or not) were lysed in 1 ml lysis buffer (25 mM HEPES [pH 7.2], 150 mM NaCl, 10 mM $MgCl_2$, 1 mM EDTA, 1% NP-40, 10% glycerol, 100 × diluted Protease Inhibitor Cocktail Set III [Calbiochem, Merck]) containing 5 μg PAK-RBD-GST (RAC-binding domain from PAK1 fused to GST, isolated from *E. coli* strain BL21 transformed with corresponding expression plasmid). After preclearing the lysate by centrifugation, the complexes of active RAC and PAK-RBD-GST were isolated on Glutathione Sepharose (GE Healthcare). RAC was then detected by immunoblotting.

Anesthesia

Mice for in vivo imaging were anesthetized by i.m. injection of Zoletil (20 mg/ml)–Xylazine (1 mg/ml) solution with Zoletil dose 100 mg/kg and Xylazine dose 1 mg/kg.

X-ray microcomputerized tomography

Hind paws were scanned in in vivo x-ray microcomputed tomography (μCT) Skyscan 1176 (Bruker). Scanning parameters were voltage, 50 kV; current, 250 μA; filter, 0.5 mm aluminum; voxel size, 8.67 μm; exposure time, 2 s; rotation step, 0.3° for 180° total; object to source distance, 119.271 mm; and camera to source distance, 171.987 mm; with time of scanning, 30 min. Reconstruction of virtual slices was performed in NRecon software 1.6.10 (Bruker) with setup for smoothing = 3, ring artifact correction = 4, and beam hardening correction = 36%. Intensities of interest for reconstruction were in the range of 0.0045 to 0.0900. For reorientation of virtual slices to the same orientation, the DataViewer 1.5.2 software (Bruker) was used.

For μCT data analysis, CT Analyzer 1.16.4.1 (Bruker) was used. The volume of interest was chosen there containing the distal part of hind paw starting from the half of metatarsus. Based on differences of x-ray absorption, three parts were analyzed separately: the whole volume of interest, the newly formed bone connected mostly with arthritis, and the area inhabited by the original bone of phalanges and metatarsi. The total volume was recorded for all three parts. For original and new bone, other parameters from two-dimensional and three-dimensional analysis were recoded to describe changes in the structure, namely, surface of the bone, surface/volume ratio, number of objects, closed porosity, mean fractal dimension, mean number of objects per slice, mean closed porosity per slice, and mean fractal dimension per slice. Scans with technical artifacts caused by spontaneous movements of animals were excluded from the analysis. Raw data are available upon request.

Cytokine detection

Murine paws were homogenized in 1 ml RIPA lysis buffer (20 mM TRIS [pH 7.5], 150 mM NaCl, 1% Nonidet P-40, 1% sodium deoxycholate, 0.1% SDS) containing 5 mM iodoacetamide (Sigma-Aldrich) and 100 × diluted Protease Inhibitor Cocktail Set III (Calbiochem, Merck) using Avans AHM1 Homogenizer (30 s, speed 25). Any insoluble material was removed by centrifugation (20,000 × *g*, 5 min, 2°C), and concentration of the proteins in the samples were normalized to the same level using Bradford solution (AppliChem). Concentrations of IL-1β in the samples were determined by Ready-SET-Go! ELISA kits from eBioscience according to the instructions of the manufacturer.

Histology

The paws were fixed in 10% formol solution for 24 h and decalcified in Osteosoft (Merck) solution for 1 wk, followed by paraffin embedding and histological cutting. The slides were stained in automatic system Ventana Symphony (Roche), and slides were scanned in Axio Scan.Z1 (Zeiss). The image postprocessing and analysis was done in Zen software (Zeiss).

Statistical analysis

The *p* values were calculated in GraphPad Prism software (GraphPad Software, La Jolla, CA) using unpaired *t* test (two-tailed) for data in Figs. 2B–G, 2I, 3C, 5E; one-way ANOVA with Tukey–Kramer or Bonferroni multiple comparison posttest for data in Figs. 1E, 4A, 6E, 7B, and 7D; Mann–Whitney *U* test for Fig. 5C; and Gehan–Breslow–Wilcoxon test for disease-free curve in Fig. 6C. Symbol meanings are as follows: n.s. $p > 0.05$, $*p \leq 0.05$, $**p \leq 0.01$, $***p \leq 0.001$, $****p \leq 0.0001$. Unless stated otherwise, "*n*" in figure legends represent number of experiment repeats, points in column scatter plots represent biological replicates (in most cases animals), error bars in these plots show median with interquartile range, and points and error bars in superoxide production time course curves (arbitrary luminescence intensity curves) represent mean ± SEM values obtained from two to eight technical replicates.

Results

Pstpip2^{cmo} neutrophils produce substantially more superoxide in response to inflammasome activator silica than WT neutrophils

Disease development in *Pstpip2^{cmo}* mice is, in part, dependent on NLRP3 inflammasome (37). Because ROS are involved in the NLRP3 inflammasome regulation, we tested if their production was dysregulated in *Pstpip2^{cmo}* BM cells. We isolated these cells from WT C57BL/6 and *Pstpip2^{cmo}* mice (backcrossed to the same genetic background) and stimulated these cells with silica particles, a well-established activator of NLRP3 inflammasome (49) employed in previous studies of *Pstpip2^{cmo}* mice (33–35). Strikingly, this stimulation led to a substantially higher superoxide production by *Pstpip2^{cmo}* cells, when compared with their WT counterparts (Fig. 1A). This assay was performed in a 96-well plate, where the response could be affected by adhesion of the cells to plastic. Therefore, we carried out a similar measurement on the cells maintained strictly in suspension. This resulted in signals of lower intensity. However, the dysregulation of superoxide production by *Pstpip2^{cmo}* cells could still be observed (Fig. 1B).

Because superoxide generation is a characteristic feature of neutrophils, which form a large fraction of BM leukocytes (Fig. 1C), we have isolated these cells for further testing. Silica stimulation of adherent neutrophils, isolated by negative selection, led to even higher production of superoxide when compared with the full BM. Moreover, the difference between WT and *Pstpip2^{cmo}* cells was still preserved (Fig. 1D). In our experiments, negatively selected neutrophils were typically more than 90% pure. However, a large fraction of the contaminating cells were monocytes. Because these cells are also known to respond by ROS production to a variety of stimuli, we have analyzed superoxide generation by purified monocytes. To determine the impact of these cells on our results, we have adjusted the quantity of monocytes to 10% of the neutrophil numbers, which is similar to the amount of monocytes contaminating our neutrophil samples prepared by negative selection. We compared the response of these monocytes with the superoxide production by neutrophils isolated by positive selection on Ly6G. This purification resulted in virtually pure (more than 99%) neutrophils. The response of purified monocytes was almost two orders of magnitude lower than that of purified neutrophils, and there was no significant difference between WT and

Downloaded from http://www.jimmunol.org/ at Institute of Physiology ASCR on March 12, 2020

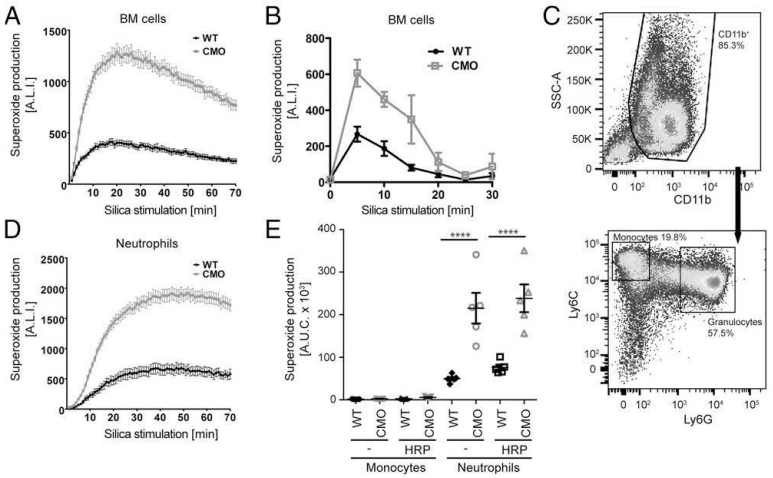

FIGURE 1. Pstpip2^{cmo} neutrophils produce higher amounts of superoxide. (**A**) Superoxide production by silica-stimulated *Pstpip2^{cmo}* (CMO) and WT BM cells measured in 1-min intervals by luminol-based chemiluminescence assay (for quantification of multiple experiments, see Fig. 2B). (**B**) Similar measurement as in (A) performed on BM cells held in suspension (5-min intervals; for quantification of multiple experiments, see Fig. 2C). (**C**) Representative flow cytometry dot plot showing percentages of monocytes and neutrophils in Pstpip2^{cmo} BM ($n > 5$). (**D**) Similar experiment as in (A) performed on neutrophils purified by negative selection (for quantification of multiple experiments, see Fig. 2B). (**E**) The superoxide production by silica-stimulated neutrophils purified by positive selection (10^6 per well) is compared with superoxide production by FACS-sorted (Ly6C$^+$, Ly6G$^-$) monocytes (10^5 per well) stimulated in the same manner in the presence or absence of HRP ($n = 3$). ****$p \leq 0.0001$. A.L.I., arbitrary luminescence intensity; A.U.C., area under the curve.

Pstpip2^{cmo} cells (Fig. 1E). Addition of exogenous peroxidase (HRP) to compensate for lower myeloperoxidase expression in monocytes (50) did not substantially alter the results (Fig. 1E). These data demonstrated that in the neutrophil samples prepared by negative selection, the monocyte contribution to the measured superoxide production is negligible. They also lead to the conclusion that even in nonseparated BM, the vast majority of superoxide originated from neutrophils and that neutrophils are responsible for enhanced superoxide production by *Pstpip2^{cmo}* BM cells.

Higher superoxide production by Pstpip2^{cmo} neutrophils is observed across a range of conditions

To find out how universal the superoxide overproduction in *Pstpip2^{cmo}* neutrophils is, we treated either BM cells or purified neutrophils with silica, PMA, live *E. coli* bacteria, heat-aggregated mouse IgG (as a model of immunocomplexes), TNF-α, LPS, or fMLP. All these experiments demonstrated dysregulated superoxide production in *Pstpip2^{cmo}* BM cells (Fig. 2A–D, 2F) and purified neutrophils (Fig. 2B, 2E). The same dysregulation was also observed in the BM cells with *Pstpip2^{cmo}* mutation on BALB/c genetic background (Supplemental Fig. 1A). These results show that PSTPIP2 deficiency renders neutrophils more sensitive and prone to produce more ROS than WT cells. Interestingly, unstimulated BM cells from *Pstpip2^{cmo}* mice produced low but detectable levels of superoxide even in the absence of any stimulus. This constitutive production has not been observed in WT BM (Fig. 2A, 2G). It also was not observed in both WT and *Pstpip2^{cmo}* cells maintained in suspension (data not shown). In addition, nonadherent cells also did not show any superoxide production in response to treatment with LPS, TNF-α, and fMLP when measured in 5-min intervals (data not shown). However, in the case of fMLP, rapid transient response was detectable within the first 5 min of the measurement (Fig. 2H). Maximum superoxide production was not significantly altered in *Pstpip2^{cmo}* BM cells. However, it was more sustained, and total superoxide production was thus higher than in WT cells (Fig. 2I).

Pstpip2^{cmo} neutrophils do not produce excessive superoxide as a consequence of ongoing inflammation and do not show the signs of spontaneous priming

Higher superoxide production under resting conditions and after activation with a wide range of stimuli demonstrates general dysregulation of pathways leading to superoxide production in *Pstpip2^{cmo}* neutrophils. This dysregulation could be cell intrinsic because of PSTPIP2 deficiency or a side effect of ongoing bone inflammation, which could prime BM neutrophils located in the proximity of the inflamed tissue. It has previously been reported that autoinflammation in *Pstpip2^{cmo}* mice is completely dependent on IL-1β and its receptor (34, 35). Signaling through this receptor is critically dependent on MyD88 adaptor protein (51). To determine whether the observed overproduction of ROS in *Pstpip2^{cmo}* neutrophils is not just the effect of ongoing inflammation, we crossed *Pstpip2^{cmo}* mice with MyD88-deficient strain to block IL-1β signaling. As expected, *Pstpip2^{cmo}* mice were in the absence of MyD88 completely protected from the disease development as determined by visual inspection (Fig. 3A) and x-ray μCT of hind paws (Fig. 3B). MyD88-deficient *Pstpip2^{cmo}* BM cells displayed the same dysregulation in superoxide production triggered by a variety of stimuli as *Pstpip2^{cmo}* cells. Treatments with LPS or *E. coli* were the only exceptions where the response was substantially lower in both *Pstpip2^{cmo}/MyD88$^{-/-}$* and *MyD88$^{-/-}$* cells, probably due to the higher dependence of signaling triggered by these activators on the TLR/MyD88 pathway. Nevertheless, even in *MyD88*-deficient cells, the *cmo* mutation gave rise to a stronger response to these two stimuli when compared with *MyD88*-deficient cells without the *cmo* mutation (Fig. 3C, Supplemental Fig. 1B). These results demonstrate the cell-intrinsic dysregulation of NADPH oxidase machinery that is not caused by chronic exposure to the inflammatory environment.

Another potential explanation for the observed dysregulation of superoxide generation is that *Pstpip2^{cmo}* neutrophils are in a constitutively primed state. Increased superoxide production is

Downloaded from http://www.jimmunol.org/ at Institute of Physiology ASCR on March 12, 2020

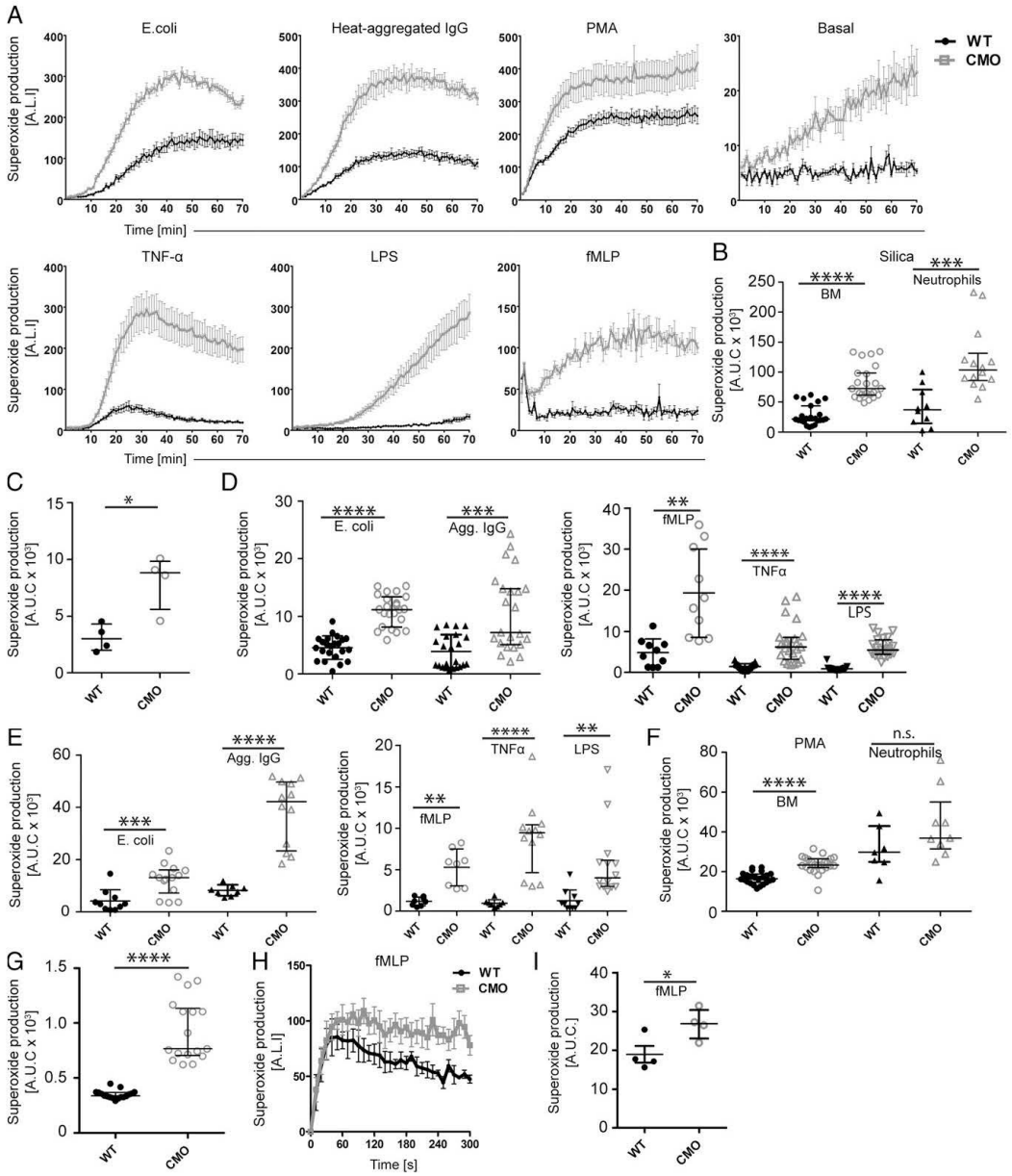

FIGURE 2. Increased superoxide production by *Pstpip2*^{cmo} neutrophils is triggered by a variety of stimuli. (**A**) Superoxide production by adherent *Pstpip2*^{cmo} (CMO) and WT BM cells treated with indicated agents (for quantification of multiple experiments, see **D–G**). (**B**) Quantification of superoxide production by adherent BM cells and neutrophils after silica treatment ($n = 4$ for BM and $n = 5$ for neutrophils). (**C**) Quantification of superoxide production by BM cells activated by silica in suspension ($n = 2$). (D) Quantification of superoxide production by adherent BM cells treated with live *E. coli* bacteria (E.coli), mouse aggregated IgG (IC), fMLP, TNF-α, and LPS ($n = 4$). (E) Similar analysis as in (D), performed on neutrophils purified by negative selection ($n = 5$ for *E. coli* and $n = 3$ for aggregated [Agg.] IgG). (F) Quantification of superoxide production by adherent BM cells and neutrophils after treatment with PMA ($n = 4$). (G) Quantification of basal superoxide production by nonstimulated adherent BM cells. (**H**) Superoxide production by nonadherent *Pstpip2*^{cmo} (CMO) and WT BM cells treated with fMLP. Measurement was performed in 10-s intervals, and data were normalized to basal ROS production. (**I**) Quantification of data in **H** ($n = 2$). "*n*" represents the number of independent experiments that were combined to generate the scatter plots in (B)–(I), and points in scatter plots represent biological replicates (i.e., cells from individual mice). *$p \leq 0.05$, **$p \leq 0.01$, ***$p \leq 0.001$, ****$p \leq 0.0001$. A.L.I., arbitrary luminescence intensity; A.U.C., area under the curve; n.s., $p > 0.05$.

Downloaded from http://www.jimmunol.org/ at Institute of Physiology ASCR on March 12, 2020

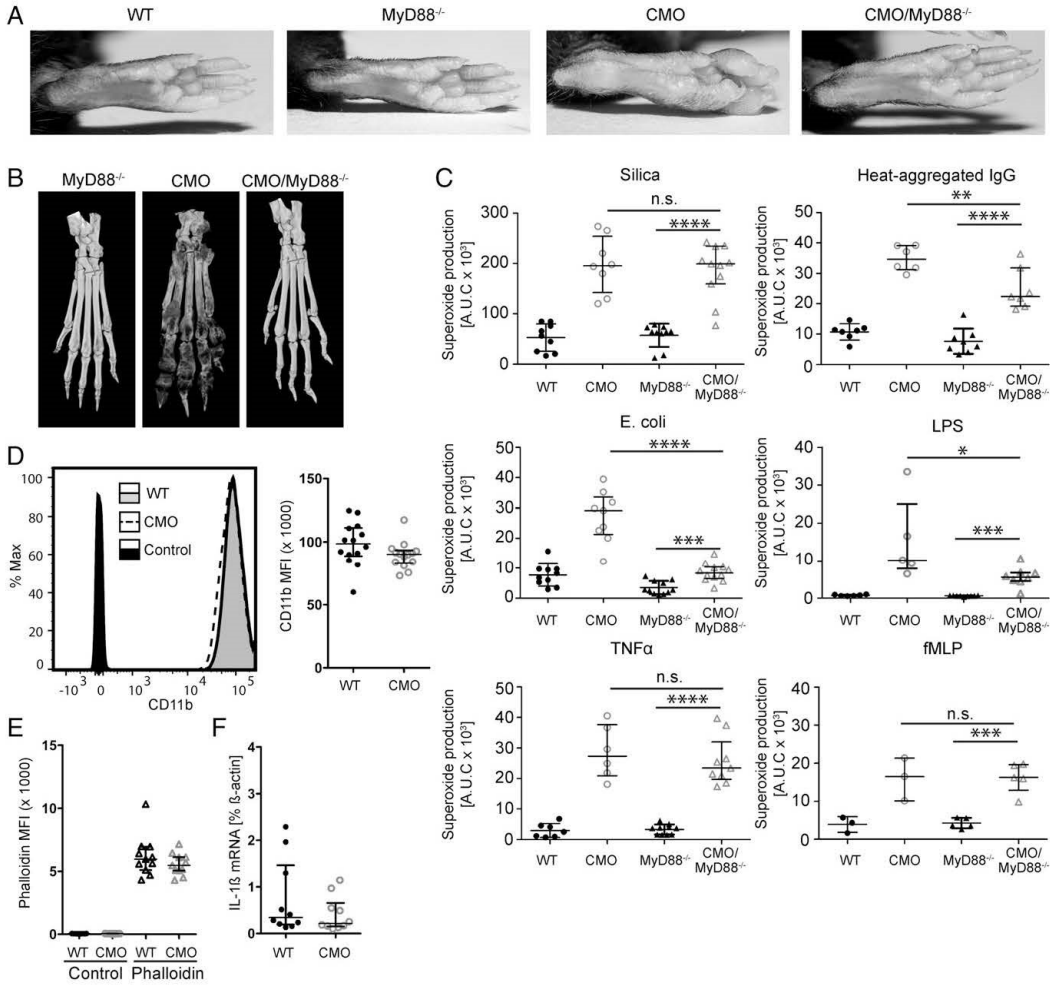

FIGURE 3. Overproduction of superoxide is not triggered by ongoing inflammation. (**A**) Representative hind paw photographs of 23- to 26-wk-old WT, *MyD88*$^{-/-}$, *Pstpip2*^{cmo} (CMO), and *Pstpip2*^{cmo}*/MyD88*$^{-/-}$ (CMO/MyD88$^{-/-}$) mice. (**B**) Representative x-ray μCT scans of hind paws from *MyD88*$^{-/-}$, *Pstpip2*^{cmo}, and *Pstpip2*^{cmo}*/MyD88*$^{-/-}$ mice, 14 wk old (n = 5 for *Pstpip2*^{cmo}*/MyD88*$^{-/-}$ and n = 3 for *MyD88*$^{-/-}$). (**C**) Quantification of superoxide production by BM cells isolated from WT, *MyD88*$^{-/-}$, *Pstpip2*^{cmo}, and *Pstpip2*^{cmo}*/MyD88*$^{-/-}$ mice and treated with indicated stimuli. For silica, n = 5; aggregated [Agg.] IgG, LPS, TNF-α, n = 4; *E. coli*, n = 6; fMLP, n = 3. (**D**) CD11b surface expression in resting neutrophils gated as Ly6G^{+} Ly6C^{+} (see Fig. 1B) measured by flow cytometry. Representative FACS plot and quantification of mean fluorescence intensities (MFI) measured in multiple experiments are shown (n = 3). (**E**) F-actin content in resting neutrophils gated as Ly6G^{+}Ly6C^{+} measured by flow cytometry with the use of fluorescent phalloidin on fixed and permeabilized cells. In controls, phalloidin staining was omitted (n = 3). (**F**) Real-time quantitative PCR quantification of IL-1β mRNA in resting neutrophils (n = 3). $^{*}p \leq 0.05$, $^{**}p \leq 0.01$, $^{***}p \leq 0.001$, $^{****}p \leq 0.0001$. n.s., $p > 0.05$.

one of the hallmarks of neutrophil priming. However, number of other changes also characterize primed neutrophils, including increased CD11b surface expression, actin cytoskeleton reorganization, and increase in IL-1β promoter activity (52–58). We have analyzed all these parameters, but we could not detect any alterations in these features (Fig. 3D–F).

Superoxide hyperproduction in Pstpip2^{cmo} neutrophils is suppressed by PSTPIP2 binding partners and is accompanied by hyperphosphorylation of p47phox

To elucidate the mechanism of how PSTPIP2 suppresses superoxide production, we employed conditionally immortalized *Pstpip2*^{cmo} granulocyte progenitors (45) we had established previously (33) and reconstituted these cells with doxycycline-inducible retroviral constructs coding for WT PSTPIP2 and its mutated versions unable to bind PEST-family phosphatases (W232A) and SHIP1 (3YF) (32, 33). After maturation of these progenitors into neutrophils and induction of PSTPIP2 expression with doxycycline, we treated these cells with silica and measured superoxide production. We observed around 50% reduction of superoxide generation in cells expressing WT PSTPIP2. In contrast, both mutated versions of PSTPIP2 were unable to substantially inhibit silica-induced superoxide production (Fig. 4A), despite similar expression levels of these constructs (Fig. 4B).

Downloaded from http://www.jimmunol.org/ at Institute of Physiology ASCR on March 12, 2020

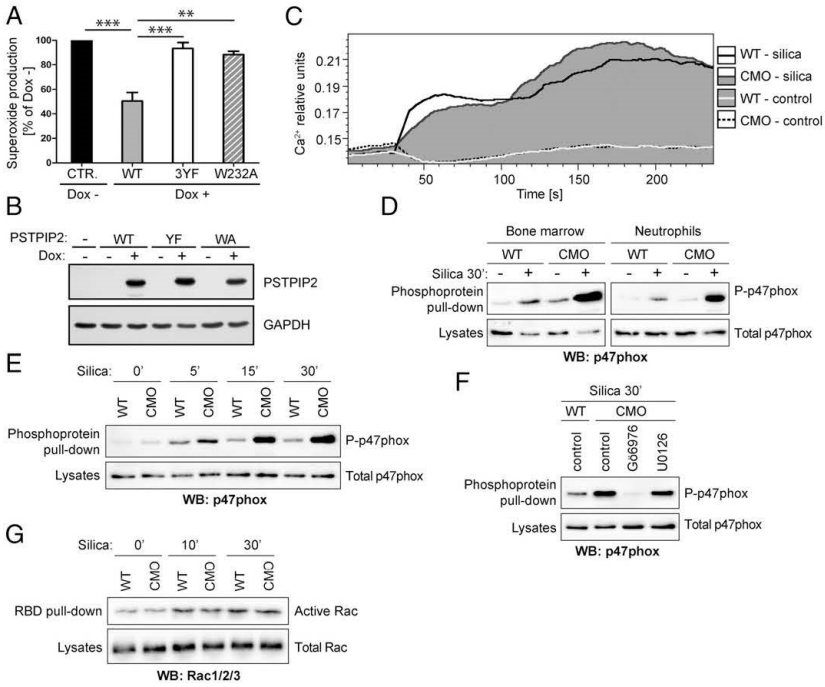

FIGURE 4. PSTPIP2-mediated suppression of superoxide production in neutrophils is dependent on PSTPIP2 binding partners and involves negative regulation of p47phox phosphorylation. (**A**) Suppression of superoxide production by WT and mutant PSTPIP2 in mature granulocytes differentiated from conditionally immortalized granulocyte progenitors. Expression of PSTPIP2 was triggered by overnight incubation with doxycycline. On the vertical axis, percentage of superoxide response by doxycycline-treated cells when compared with doxycycline nontreated cells is shown. Error bars represent SEM of three biological replicates. (**B**) Equal expression levels of PSTPIP2 variants from (A) after induction with doxycycline. (**C**) Calcium response of WT and Pstpip2^{cmo} neutrophils (gated from full BM) after silica treatment ($n = 3$). (**D**) Phosphorylation of p47phox in WT and Pstpip2^{cmo} BM cells and neutrophils after 30 min incubation with silica. To detect p47phox phosphorylation, total phosphoproteins were isolated from cell lysates followed by p47phox detection by immunoblotting ($n = 3$). (**E**) P47phox phosphorylation in BM cells at various time points. The phosphorylation was detected as in (D) ($n = 3$). (**F**) Phosphorylation of p47phox in Pstpip2^{cmo} neutrophils treated for 30 min with silica together with PKC inhibitor Gö6976 or MEK inhibitor U0126. Phosphorylation of p47phox was detected as in (D) ($n = 4$ for Gö6976 and $n = 2$ for U0126). (**G**) RAC activation in WT and Pstpip2^{cmo} neutrophils. Active RAC was isolated using PAK1-RBD-GST (RBD pull-down) and detected by immunoblotting with Ab to all three RAC proteins (RAC1/2/3) ($n = 2$). $^{**}p \leq 0.01$, $^{***}p \leq 0.001$.

To analyze subcellular localization of PSTPIP2 during silica stimulation, we isolated BM progenitors from *Pstpip2^{cmo}* mice and transduced these cells with retroviral construct coding for PSTPIP2 fused to EGFP. Next, we transplanted these cells into lethally irradiated mice, and after 2 wk, we collected neutrophils expressing PSTPIP2-EGFP for microscopy analysis. In neutrophils, PSTPIP2 showed diffuse distribution throughout the cytoplasm, with occasional formation of speckles in a small fraction of cells (Supplemental Fig. 2, left panel, see an arrowhead). After addition of fluorescently labeled silica particles, neutrophils interacted with these particles and phagocytosed some of them (Supplemental Fig. 2, right panel, see an arrowhead). However, we did not observe any changes in PSTPIP2 subcellular localization during this process (Supplemental Fig. 2). This result suggests that large-scale redistribution of PSTPIP2 inside the cells is not part of the mechanism of how PSTPIP2 controls neutrophil activity during the treatment with silica.

To identify the dysregulated process leading to superoxide overproduction at the biochemical level, we measured the calcium response in WT and *Pstpip2^{cmo}* BM cells. Cells were loaded with Fura Red dye and stimulated with silica particles. We observed the same calcium response in both WT and *Pstpip2^{cmo}* cells (Fig. 4C), indicating that proximal signaling steps leading to calcium response are not responsible for increased ROS production in *Pstpip2^{cmo}* cells.

One of the major events further downstream is phosphorylation of NADPH oxidase cytosolic subunits by members of protein kinase C (PKC) family, including phosphorylation of p47phox, which then serves as an assembly hub for building the active NADPH oxidase complex (16, 59). To detect p47phox phosphorylation, we isolated phosphoproteins from untreated and silica-treated BM cells or purified neutrophils and detected p47phox in the isolated material by immunoblotting. In both *Pstpip2^{cmo}* BM cells and neutrophils, we found substantially stronger phosphorylation of p47phox when compared with WT cells (Fig. 4D). This difference was observed as early as 5 min after stimulation and was maintained for at least 30 min (Fig. 4E).

Although PKCs are critical for p47phox activation, costimulatory effects of other kinases have also been demonstrated (59, 60). Of these, ERK MAP kinase was shown to be dysregulated in silica-treated CMO neutrophils (33). To assess the roles of PKCs and ERK pathway in p47phox dysregulation, we have treated *Pstpip2^{cmo}* neutrophils either with PKC inhibitor Gö6976 or MEK1/MEK2 inhibitor U0126 prior to activation with silica.

Downloaded from http://www.jimmunol.org/ at Institute of Physiology ASCR on March 12, 2020

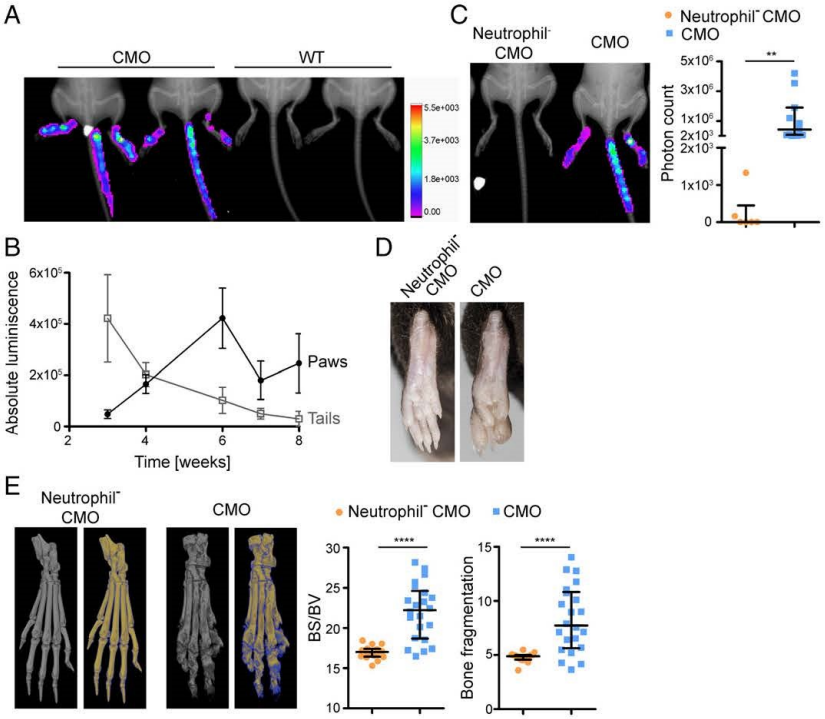

FIGURE 5. Neutrophil-dependent superoxide production in vivo precedes the onset of the disease. (**A**) Representative in vivo measurement of superoxide in 4-wk-old anesthetized WT and Pstpip2^{cmo} (CMO) mice injected i.p. with L-012 chemiluminescent probe. Superoxide-induced luminescence is shown as a heat-map in artificial colors on the background of an x-ray image. (**B**) Time course quantification of absolute L-012 luminescence driven by in vivo ROS production in Pstpip2^{cmo} mice. The luminescence was quantified separately for paws and tails ($n = 6$ per time point, mean ± SEM). (**C**) Representative in vivo measurement of ROS production in anesthetized 4-wk-old Pstpip2^{cmo}-DTA mice where neutrophils were depleted or not via MRP8-CRE-dependent expression of diphtheria toxin (Neutrophil^{-}). The left panel shows quantification of in vivo ROS production in multiple mice of both genotypes (3–4 wk old). (**D**) Representative photographs of hind paws of 26-wk-old mice of the same genotypes as in (C). (**E**) Representative x-ray μCT scans of bones from 20-wk-old mice of the same genotypes as in (C). Gray images represent visualization of total bone tissue. Pseudocolor images distinguish between old (in yellow) and newly formed (in blue) bone mass. Quantification of bone surface/bone volume ratio (BS/BV) and bone fragmentation in paw bones of multiple mice is shown on the right. $^{**}p \leq 0.01$, $^{****}p \leq 0.0001$.

Only the treatment with PKC inhibitor led to specific block of p47phox phosphorylation (Fig. 4F).

Small G-protein RAC is another critical component of active NADPH oxidase. We have tested the activation status of RAC after silica treatment of BM cells, but no difference between WT and *Pstpip2^{cmo}* cells has been observed (Fig. 4G).

Collectively, these data suggest that PSTPIP2 via its binding partners suppresses pathways leading to PKC-mediated p47phox phosphorylation and that this is the mechanism by which PSTPIP2 attenuates NADPH oxidase activity and superoxide production.

Unprovoked ROS production by neutrophils in vivo precedes the onset of the disease

To analyze the ROS production in vivo during the disease development, we used luminol derivative L-012 to visualize ROS generation in living anesthetized mice. Very interestingly, we observed a strong luminescent signal already in freshly weaned 3-wk-old mice that were otherwise asymptomatic (Supplemental Fig. 3A). The signal was mostly localized along the tail and with weaker intensity in the hind paws. Visualization at later time points revealed that at 4 wk of age, the ROS production was equally intensive in the tail and paws (Fig. 5A, 5B) and gradually moved to the hind paws during the weeks 6–8. At this age, ROS production became predominant in hind paws with more restricted focal localization (Fig. 5B, Supplemental Fig. 3A).

To test if neutrophils are the source of dysregulated ROS observed in vivo, we have generated *Pstpip2^{cmo}* mouse strain where the majority of neutrophils were deleted via MRP8-CRE-dependent expression of Diphtheria toxin (*Pstpip2^{cmo}-DTA-MRP8-CRE*, Supplemental Fig. 3B, 3C). In vivo ROS imaging revealed that ROS production in the tails and hind paws of these mice was almost completely abolished (Fig. 5C). In addition, these mice also did not show any symptoms of autoinflammatory disease, whether determined by visual inspection (Fig. 5D) or by x-ray μCT analysis (Fig. 5E). These data strongly support the idea that increased ROS production preceding the onset of the disease originates in neutrophils and, at the same time, confirm that neutrophils are critical for the development of disease symptoms (36).

NADPH oxidase deficiency has specific effects on bone destruction

Strong unprovoked production of ROS in very young mice preceding visible symptoms weeks before their demonstration suggested that ROS may act upstream of IL-1β in osteomyelitis development. To determine the contribution of high in vivo ROS

Downloaded from http://www.jimmunol.org/ at Institute of Physiology ASCR on March 12, 2020

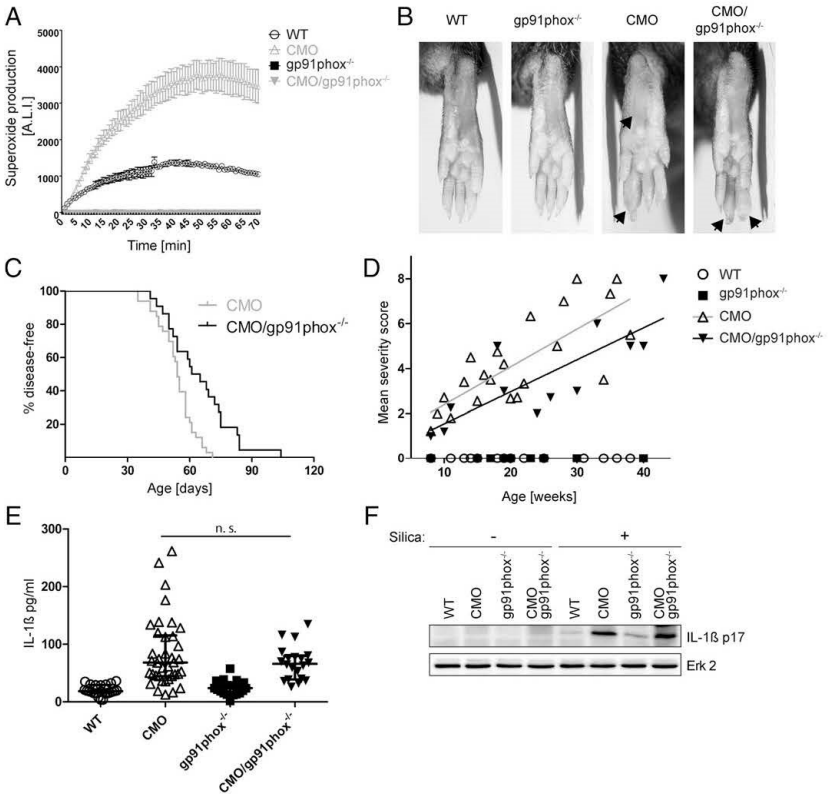

FIGURE 6. Limited effect of gp91phox deficiency on visible symptom development and IL-1β production. (**A**) In vitro superoxide generation induced by silica treatment in BM cells from 13- to 16-wk-old WT, Pstpip2^{cmo}, gp91phox$^{-/-}$, and Pstpip2^{cmo}/gp91phox$^{-/-}$ mice. Representative of two independent experiments. (**B**) Representative photographs of hind paws of 18- to 19-wk-old WT, Pstpip2^{cmo}, gp91phox$^{-/-}$, and Pstpip2^{cmo}/gp91phox$^{-/-}$ mice. (**C**) Disease-free curve comparing the time of disease appearance in Pstpip2^{cmo} and Pstpip2^{cmo}/gp91phox$^{-/-}$ mice. Development of visible symptoms was evaluated two to three times per week. (**D**) Disease severity was scored (scale from 0 to 8) by visual inspection of photographs of the hind paws collected over the course of this study. Each point represents mean value for the mice of the same age and genotype. Lines were generated using linear regression. (**E**) ELISA analysis of IL-1β from hind paw lysates. Samples were adjusted to the same protein concentration before analysis. Bars represent median with interquartile range. (**F**) Presence of processed IL-1β in the lysates from BM cells treated for 60 min (or not) with silica was detected by immunoblotting ($n = 4$). n.s., $p > 0.05$.

generation to disease development, we crossed *Pstpip2^{cmo}* mice to gp91phox-deficient mouse strain. In the absence of gp91phox, we were unable to detect any superoxide production upon silica, *E. coli*, or aggregated IgG stimulation even in *Pstpip2^{cmo}* cells (Fig. 6A, data not shown). These data confirm that NADPH oxidase was responsible for the dysregulated ROS production in *Pstpip2^{cmo}* neutrophils. Surprisingly, *Pstpip2^{cmo}* mice lacking gp91phox developed similar disease symptoms as *Pstpip2^{cmo}* mice (Fig. 6B) and with similar, only slightly delayed, kinetics (Fig. 6C). Blind scoring of the disease severity by visual inspection of hind paw photographs collected throughout various experiments revealed that the symptoms of the disease are only partially alleviated in gp91phox-deficient animals, by approximately one to two points on 8-point scale (Fig. 6D). Moreover, ELISA analysis detected comparable amount of IL-1β in hind paw extracts from *Pstpip2^{cmo}* and *Pstpip2^{cmo}/gp91phox$^{-/-}$* animals (Fig. 6E), and similar amount of processed IL-1β p17 was found in the lysates of silica-stimulated BM cells by immunoblot (Fig. 6F).

These data demonstrated that the phagocyte NADPH oxidase is dispensable for autoinflammatory disease initiation, but it affects the severity of the disease. We also noticed that the character of the hind paw edema was somewhat different in *Pstpip2^{cmo}/gp91phox$^{-/-}$* mice. Typically, the swelling was most serious at the distal part of phalanges and only rarely affected metatarsal area in *Pstpip2^{cmo}/gp91phox$^{-/-}$* animals, whereas in *Pstpip2^{cmo}* mice, metatarsi were frequently enlarged and the phalanges were often most seriously affected in their central parts (Fig. 6B).

To find out if these differences were caused by different character of bone inflammation, we performed x-ray μCT analysis of *Pstpip2^{cmo}* and *Pstpip2^{cmo}/gp91phox$^{-/-}$* mice. Very surprisingly, bone destruction in *Pstpip2^{cmo}/gp91phox$^{-/-}$* animals was almost entirely missing, whereas in *Pstpip2^{cmo}* mice substantial bone damage could be observed (Fig. 7A). To support this observation with a quantitative analysis, we calculated bone surface to volume ratio and bone fragmentation from the x-ray μCT data. *Pstpip2^{cmo}*/gp91phox$^{-/-}$ mice showed similar values to WT, whereas values for *Pstpip2^{cmo}* mice were substantially higher (Fig. 7B). Timeline x-ray μCT scans of hind paws revealed progressive bone lesion formation in *Pstpip2^{cmo}* mice whereas

Downloaded from http://www.jimmunol.org/ at Institute of Physiology ASCR on March 12, 2020

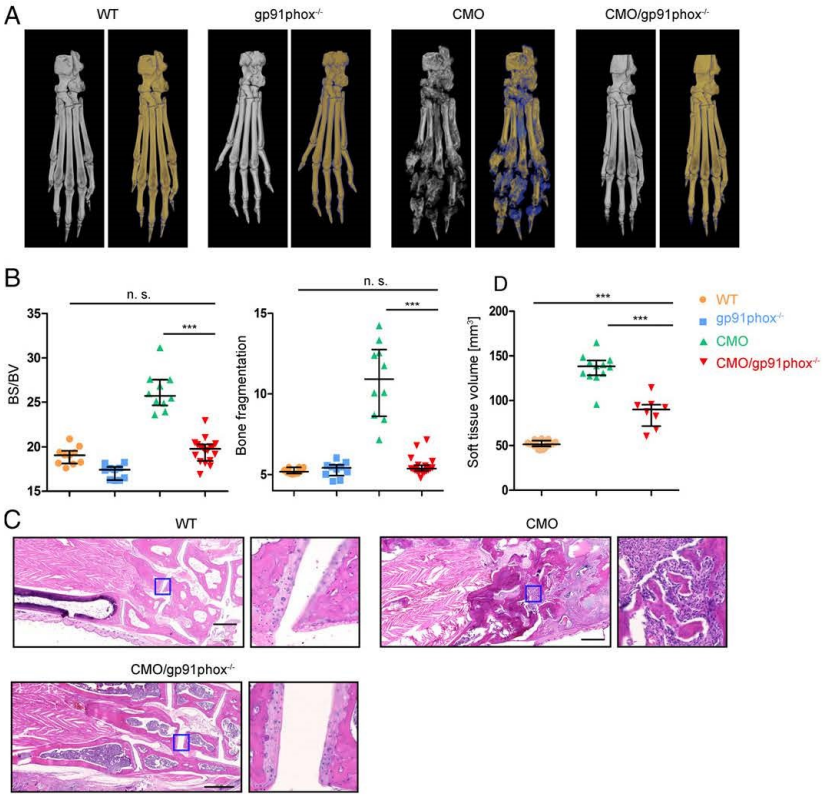

FIGURE 7. Almost complete absence of bone damage in gp91phox-deficient PSTPIP2^{cmo} mice. (**A**) Representative x-ray μCT scans of bones from 14-wk-old mice. Gray images represent visualization of total bone tissue. Pseudocolor images distinguish between old (in yellow) and newly formed (in blue) bone mass. (**B**) Quantification of bone surface/bone volume ratio (BS/BV) and bone fragmentation in paw bones of 14-wk-old mice. Bars represent median with interquartile range. (**C**) Sections of paraffin embedded tissue from tarsal area of hind paw stained with H&E. Scale bars, 500 μm. The regions in the blue squares are magnified and shown at the right of each image. (**D**) Volume of soft tissue in hind paws calculated as a total paw volume from which the bone volume has been subtracted. Values were calculated from x-ray μCT data. ***$p \leq 0.001$. n.s., $p > 0.05$.

Pstpip2^{cmo} gp91phox$^{-/-}$ littermates remained largely protected (Supplemental Fig. 4).

The lack of bone damage can also be demonstrated on tissue sections from tarsal area of hind paws (Fig. 7C). The CMO mice show very high level of osteolysis of tarsal bones, with almost missing joint cartilages due to arthritic changes accompanied with robust granulomatous infiltration. The WT mice have normally developed and structurally well-defined tarsal bones with undamaged joint cartilages with no infiltration of immune cells and no adverse changes in the BM. The *Pstpip2^{cmo}/gp91phox$^{-/-}$* mice show a rescue effect in ossified parts of tarsal bones with no or minimal signs of bone damage by immune cells, and the soft tissue infiltration in the metatarsal area is minimal compared with CMO mice. The cartilages are also well shaped and are covering the joint areas comparably with WT animals. The difference from WT animals is in hypercellular structure of BM resulting in decreased volume of ossified tissue.

To address protection potential of gp91phox deficiency in old *Pstpip2^{cmo}* mice, we performed x-ray μCT scans on 7-mo-old mice. Old *Pstpip2^{cmo}* mice suffered from strong bone destruction and remodeling but *Pstpip2^{cmo}/gp91phox$^{-/-}$* mice were still protected from adverse effects of osteomyelitis (Supplemental Fig. 4). To gain a quantitative insight into the level of soft tissue inflammation, we have performed computational reconstruction of soft tissues from x-ray μCT scans described above in Fig. 7B and calculated soft tissue volume. This measurement revealed that soft tissues in *Pstpip2^{cmo}/gp91phox$^{-/-}$* hind paws were significantly enlarged, albeit not to the same extent as in *Pstpip2^{cmo}* mice (Fig. 7D). Collectively, these data demonstrate that despite significant swelling that can be detected in the hind paw soft tissues of *Pstpip2^{cmo}/gp91phox$^{-/-}$* mice, bones remain largely protected in the absence of NADPH oxidase activity.

Discussion

Monogenic autoinflammatory diseases develop as a result of dysregulation of the innate immune system. Although the specificity of this branch of the immune system is relatively limited, these diseases still show tissue and organ selectivity. The mechanisms of this selectivity are often poorly understood (3). *Pstpip2^{cmo}* mice represent an important model of tissue-selective IL-1β–driven autoinflammatory disease that affects mainly bones and surrounding tissue in hind paws and tails (29–31). Our current studies demonstrate that IL-1β pathway is not the only pathway dysregulated in these animals. Superoxide production by neutrophil NADPH oxidase is also substantially enhanced, independently of IL-1β activity. Moreover, our data suggest that dysregulated ROS

Downloaded from http://www.jimmunol.org/ at Institute of Physiology ASCR on March 12, 2020

production is a critical part of the selectivity mechanisms directing inflammatory damage to the bones.

Increased superoxide generation by neutrophil NADPH oxidase is one of the major consequences of neutrophil priming. It is a state of enhanced responsiveness attained after an exposure to priming agents such as LPS or TNF-α. These agents typically do not elicit superoxide production by themselves but rather increase its generation triggered by other substances (53, 54). To find out if *Pstpip2^{cmo}* neutrophils are spontaneously constitutively primed, we have tested several additional parameters known to be associated with neutrophil priming, including increased expression of integrin subunit CD11b, changes in cytoskeleton organization, and IL-1β promoter activity (52–58). However, none of these traits were altered in *Pstpip2^{cmo}* neutrophils.

Neutrophil adhesion is also often considered a priming stimulus, because it results in similar phenotypic changes and is able to elicit enhanced superoxide production, even in response to solely priming agents such as TNF-α (54, 61). Accordingly, whereas we observed TNF-α– and LPS-induced superoxide production by adherent neutrophils, cells in suspension did not show any response, regardless of the genotype. The reaction to silica and fMLP was also substantially attenuated in nonadherent cells. However, the deregulation of responses in *Pstpip2^{cmo}* neutrophils could still be detected under these conditions. These data support the conclusion that dysregulation of NADPH oxidase activity in *Pstpip2^{cmo}* neutrophils is independent of adhesion. They also show that *Pstpip2^{cmo}* neutrophils are not fully primed and can still undergo priming.

Collectively, our data do not support the idea of spontaneous priming of *Pstpip2^{cmo}* neutrophils. They rather suggest dysregulation of pathways controlling NADPH oxidase activity. However, it should be noted that different priming agents elicit varying sets of phenotypic changes in neutrophils (53), and some specific form of constitutive priming cannot be completely disregarded.

We found that increased ROS production in *Pstpip2^{cmo}* mice was associated with p47phox hyperphosphorylation, leading to the conclusion that one or more pathways governing p47phox phosphorylation are negatively regulated by PSTPIP2. MAP kinase ERK was shown to have a supporting role in p47phox activation by phosphorylating Ser 345 and 348 (62, 63). We have shown previously that ERK is also hyperactive in silica-treated CMO neutrophils (33). However, in this study we found that ERK pathway inhibition did not have any substantial effect on p47phox phosphorylation, whereas this phosphorylation could be almost completely abolished by inhibition of PKC (Fig. 4E). These data suggest that PSTPIP2 deficiency mainly affects the phosphorylation of p47phox that is PKC mediated. However, the precise mechanism is still unclear.

To our knowledge, genetically determined hyperactivation of NADPH oxidase has not yet been described or studied in the context of IL-1β activation or in autoinflammatory disease. Our observations show that elevated NADPH oxidase activity does not affect IL-1β pathway but rather the inflammatory bone damage in CMO. These data are in agreement with several other reports that disprove the role of NADPH oxidase–generated ROS in IL-1β processing by inflammasome. They are mainly based on analyses of monocytes and macrophages from NADPH oxidase–deficient patients and mice, where IL-1β production is not altered or it is even enhanced (64–67). In a single study on human neutrophils, NADPH oxidase deficiency also did not lead to reduction of NLRP3 inflammasome activity (68). In contrast, inhibition of mitochondrial ROS production in monocytes/macrophages results in an impairment of IL-1β production in these cells (19, 69), showing that the majority of ROS supporting inflammasome activation in these cell types is generated by mitochondria.

The roles of IL-1β and ROS in CMO pathophysiology appear to be different form each other. Whereas dysregulated IL-1β production is a critical trigger of the disease development, enhanced ROS production modifies the outcome. However, ROS are not able to initiate the disease on their own in the absence of IL-1β signaling. It is documented by our experiments with *MyD88*-deficient *Pstpip2^{cmo}* mice, which displayed the same ROS dysregulation as *Pstpip2^{cmo}* mice and yet they did not develop any symptoms of autoinflammation. These data also demonstrate that enhanced ROS production is not downstream of IL-1β because MyD88 is critical for signaling by IL-1R (70).

ROS are known to play a key role in differentiation and activity of osteoclasts. These cells are responsible for physiological bone resorption during bone remodeling processes. They are also involved in pathological bone damage in a number of disease states (71). *Pstpip2^{cmo}* mice exhibited increased osteoclastogenesis and osteoclast hyperactivity, suggesting that osteoclasts are responsible for inflammatory bone damage in these mice (39). Our data show that the bone damage can be almost completely abolished when phagocyte NADPH oxidase is inactivated by deletion of its gp91phox subunit. One possibility is that deficiency in osteoclast gp91phox results in defects in their differentiation and activity and reduced bone damage. However, in *gp91phox$^{-/-}$* mice, no bone abnormalities have been observed. In addition, gp91phox-deficient osteoclasts differentiate normally and have normal bone resorption activity (72–74). These results show that gp91phox expressed in osteoclasts is dispensable for differentiation and activity of these cells. In fact, other NADPH oxidases were shown to be more important for their function (72, 75). In contrast, exogenous ROS generated in culture media after addition of xanthine oxidase were shown to upregulate osteoclast numbers and activity in bone cultures in vitro (76). Our data together with published results thus favor the explanation that exogenous ROS originating from hyperactive neutrophils, ample production of which we observed in *Pstpip2^{cmo}* mice in vivo, lead either directly or indirectly to increased differentiation and/or activity of osteoclasts and resulting bone damage.

PSTPIP2 mutations in humans have not yet been described. However, PSTPIP2 gene has been sequenced only in a limited number of CRMO patients and patients with closely related SAPHO syndrome (77–79). CRMO and SAPHO form a rather heterogeneous disease spectrum, which may in fact represent a number of distinct disorders in which various defects at the molecular level may lead to similar outcome, and so PSTPIP2 mutations in some of these patients may still be discovered in the future. The data on ROS production in these diseases are also largely missing. We are aware of only a single study in which the superoxide production by neutrophils was analyzed in two SAPHO patients from a single family without any mutations in PSTPIP2 gene. These data showed reduced superoxide generation after activation with multiple activators, including PMA, fMLP, and TNF-α, when compared with healthy controls (77). However, from the information provided, it was unclear whether the patients were undergoing anti-inflammatory treatment that could suppress the response at the time of analysis. Further studies are needed to fully understand the role of PSTPIP2 and ROS in CRMO, SAPHO, and other inflammatory bone diseases in humans.

Inflammatory bone damage is a serious problem accompanying a number of human disorders. Full understanding of possible mechanisms that can govern its development is critical for designing successful therapeutic interventions. Our data reveal how dysregulated ROS production results in bone damage in the specific

Downloaded from http://www.jimmunol.org/ at Institute of Physiology ASCR on March 12, 2020

case of CMO. However, these findings may represent a more general mechanism with broader validity for other syndromes where inflammatory bone damage is involved, and analysis of ROS production in other instances of inflammatory bone damage may prove beneficial.

Acknowledgments

We thank the staff of Institute of Molecular Genetics core facilities for excellent support and help.

Disclosures

The authors have no financial conflicts of interest.

References

1. Manthiram, K., Q. Zhou, I. Aksentijevich, and D. L. Kastner. 2017. The monogenic autoinflammatory diseases define new pathways in human innate immunity and inflammation. [Published erratum appears in 2017 *Nat.* Immunol. 18: 1271.] *Nat. Immunol.* 18: 832–842.
2. Masters, S. L., A. Simon, I. Aksentijevich, and D. L. Kastner. 2009. Horror autoinflammaticus: the molecular pathophysiology of autoinflammatory disease (*). *Annu. Rev. Immunol.* 27: 621–668.
3. de Jesus, A. A., S. W. Canna, Y. Liu, and R. Goldbach-Mansky. 2015. Molecular mechanisms in genetically defined autoinflammatory diseases: disorders of amplified danger signaling. *Annu. Rev. Immunol.* 33: 823–874.
4. Bader-Meunier, B., E. Van Nieuwenhove, S. Breton, and C. Wouters. 2018. Bone involvement in monogenic autoinflammatory syndromes. *Rheumatology (Oxford)* 57: 606–618.
5. Takayanagi, H. 2007. Osteoimmunology: shared mechanisms and crosstalk between the immune and bone systems. *Nat. Rev. Immunol.* 7: 292–304.
6. Houx, L., E. Hachulla, I. Kone-Paut, P. Quartier, I. Touitou, X. Guennoc, G. Grateau, M. Hamidou, B. Neven, J. M. Berthelot, et al. 2015. Musculoskeletal symptoms in patients with cryopyrin-associated periodic syndromes: a large database study. *Arthritis Rheumatol.* 67: 3027–3036.
7. Tunca, M., S. Akar, F. Onen, H. Ozdogan, O. Kasapcopur, F. Yalcinkaya, E. Tutar, S. Ozen, R. Topaloglu, E. Yilmaz, et al; Turkish FMF Study Group. 2005. Familial Mediterranean fever (FMF) in Turkey: results of a nationwide multicenter study. *Medicine (Baltimore)* 84: 1–11.
8. Gong, T., Y. Yang, T. Jin, W. Jiang, and R. Zhou. 2018. Orchestration of NLRP3 inflammasome activation by ion fluxes. *Trends Immunol.* 39: 393–406
9. Lawlor, K. E., and J. E. Vince. 2014. Ambiguities in NLRP3 inflammasome regulation: is there a role for mitochondria? *Biochim. Biophys. Acta* 1840: 1433–1440.
10. Carta, S., S. Tassi, L. Delfino, A. Omenetti, S. Raffa, M. R. Torrisi, A. Martini, M. Gattorno, and A. Rubartelli. 2012. Deficient production of IL-1 receptor antagonist and IL-6 coupled to oxidative stress in cryopyrin-associated periodic syndrome monocytes. *Ann. Rheum. Dis.* 71: 1577–1581.
11. Hughes, M. M., and L. A. J. O'Neill. 2018. Metabolic regulation of NLRP3. *Immunol. Rev.* 281: 88–98.
12. Broz, P., and V. M. Dixit. 2016. Inflammasomes: mechanism of assembly, regulation and signalling. *Nat. Rev. Immunol.* 16: 407–420.
13. Zhen, Y., and H. Zhang. 2019. NLRP3 inflammasome and inflammatory bowel disease. *Front. Immunol.* 10: 276.
14. Abais, J. M., M. Xia, Y. Zhang, K. M. Boini, and P. L. Li. 2015. Redox regulation of NLRP3 inflammasomes: ROS as trigger or effector? *Antioxid. Redox Signal.* 22: 1111–1129.
15. Holmström, K. M., and T. Finkel. 2014. Cellular mechanisms and physiological consequences of redox-dependent signalling. *Nat. Rev. Mol. Cell Biol.* 15: 411–421.
16. Brandes, R. P., N. Weissmann, and K. Schröder. 2014. Nox family NADPH oxidases: molecular mechanisms of activation. *Free Radic. Biol. Med.* 76: 208–226.
17. Sumimoto, H. 2008. Structure, regulation and evolution of Nox-family NADPH oxidases that produce reactive oxygen species. *FEBS J.* 275: 3249–3277.
18. West, A. P., G. S. Shadel, and S. Ghosh. 2011. Mitochondria in innate immune responses. *Nat. Rev. Immunol.* 11: 389–402.
19. Zhou, R., A. S. Yazdi, P. Menu, and J. Tschopp. 2011. A role for mitochondria in NLRP3 inflammasome activation. [Published erratum appears in 2011 *Nature* 475: 122.] *Nature* 469: 221–225.
20. Brookes, P. S., Y. Yoon, J. L. Robotham, M. W. Anders, and S.-S. Sheu. 2004. Calcium, ATP, and ROS: a mitochondrial love-hate triangle. *Am. J. Physiol. Cell Physiol.* 287: C817–C833.
21. Swanson, K. V., M. Deng, and J. P. Ting. 2019. The NLRP3 inflammasome: molecular activation and regulation to therapeutics. *Nat. Rev. Immunol.* 19: 477–489.
22. Chen, Y., Z. Zhou, and W. Min. 2018. Mitochondria, oxidative stress and innate immunity. *Front. Physiol.* 9: 1487.
23. Bulua, A. C., A. Simon, R. Maddipati, M. Pelletier, H. Park, K. Y. Kim, M. N. Sack, D. L. Kastner, and R. M. Siegel. 2011. Mitochondrial reactive oxygen species promote production of proinflammatory cytokines and are elevated in TNFR1-associated periodic syndrome (TRAPS). *J. Exp. Med.* 208: 519–533.
24. van der Burgh, R., L. Nijhuis, K. Pervolaraki, E. B. Compeer, L. H. Jongeneel, M. van Gijn, P. J. Coffer, M. P. Murphy, P. G. Mastroberardino, J. Frenkel, and M. Boes. 2014. Defects in mitochondrial clearance predispose human monocytes to interleukin-1β hypersecretion. *J. Biol. Chem.* 289: 5000–5012.
25. Borghini, S., S. Tassi, S. Chiesa, F. Caroli, S. Carta, R. Caorsi, M. Fiore, L. Delfino, D. Lasiglié, C. Ferraris, et al. 2011. Clinical presentation and pathogenesis of cold-induced autoinflammatory disease in a family with recurrence of an NLRP12 mutation. *Arthritis Rheum.* 63: 830–839.
26. Tassi, S., S. Carta, L. Delfino, R. Caorsi, A. Martini, M. Gattorno, and A. Rubartelli. 2010. Altered redox state of monocytes from cryopyrin-associated periodic syndromes causes accelerated IL-1beta secretion. *Proc. Natl. Acad. Sci. USA* 107: 9789–9794.
27. Omenetti, A., S. Carta, L. Delfino, A. Martini, M. Gattorno, and A. Rubartelli. 2014. Increased NLRP3-dependent interleukin 1β secretion in patients with familial Mediterranean fever: correlation with MEFV genotype. *Ann. Rheum. Dis.* 73: 462–469.
28. Carta, S., F. Penco, R. Lavieri, A. Martini, C. A. Dinarello, M. Gattorno, and A. Rubartelli. 2015. Cell stress increases ATP release in NLRP3 inflammasome-mediated autoinflammatory diseases, resulting in cytokine imbalance. *Proc. Natl. Acad. Sci. USA* 112: 2835–2840.
29. Byrd, L., M. Grossmann, M. Potter, and G. L. Shen-Ong. 1991. Chronic multifocal osteomyelitis, a new recessive mutation on chromosome 18 of the mouse. *Genomics* 11: 794–798.
30. Ferguson, P. J., X. Bing, M. A. Vasef, L. A. Ochoa, A. Mahgoub, T. J. Waldschmidt, L. T. Tygrett, A. J. Schlueter, and H. El-Shanti. 2006. A missense mutation in pstpip2 is associated with the murine autoinflammatory disorder chronic multifocal osteomyelitis. *Bone* 38: 41–47.
31. Chitu, V., P. J. Ferguson, R. de Bruijn, A. J. Schlueter, L. A. Ochoa, T. J. Waldschmidt, Y. G. Yeung, and E. R. Stanley. 2009. Primed innate immunity leads to autoinflammatory disease in PSTPIP2-deficient cmo mice. *Blood* 114: 2497–2505.
32. Wu, Y., D. Dowbenko, and L. A. Lasky. 1998. PSTPIP 2, a second tyrosine phosphorylated, cytoskeletal-associated protein that binds a PEST-type protein-tyrosine phosphatase. *J. Biol. Chem.* 273: 30487–30496.
33. Drobek, A., J. Kralova, T. Skopcova, M. Kucova, P. Novák, P. Angelisová, P. Otahal, M. Alberich-Jorda, and T. Brdicka. 2015. PSTPIP2, a protein associated with autoinflammatory disease, interacts with inhibitory enzymes SHIP1 and Csk. *J. Immunol.* 195: 3416–3426.
34. Cassel, S. L., J. R. Janczy, X. Bing, S. P. Wilson, A. K. Olivier, J. E. Otero, Y. Iwakura, D. M. Shayakhmetov, A. G. Bassuk, Y. Abu-Amer, et al. 2014. Inflammasome-independent IL-1β mediates autoinflammatory disease in Pstpip2-deficient mice. *Proc. Natl. Acad. Sci. USA* 111: 1072–1077.
35. Lukens, J. R., J. M. Gross, C. Calabrese, Y. Iwakura, M. Lamkanfi, P. Vogel, and T. D. Kanneganti. 2014. Critical role for inflammasome-independent IL-1β production in osteomyelitis. *Proc. Natl. Acad. Sci. USA* 111: 1066–1071.
36. Lukens, J. R., P. Gurung, P. Vogel, G. R. Johnson, R. A. Carter, D. J. McGoldrick, S. R. Bandi, C. R. Calabrese, L. Vande Walle, M. Lamkanfi, and T.-D. Kanneganti. 2014. Dietary modulation of the microbiome affects autoinflammatory disease. *Nature* 516: 246–249.
37. Gurung, P., A. Burton, and T. D. Kanneganti. 2016. NLRP3 inflammasome plays a redundant role with caspase 8 to promote IL-1β-mediated osteomyelitis. *Proc. Natl. Acad. Sci. USA* 113: 4452–4457.
38. Callaway, D. A., and J. X. Jiang. 2015. Reactive oxygen species and oxidative stress in osteoclastogenesis, skeletal aging and bone diseases. *J. Bone Miner. Metab.* 33: 359–370.
39. Chitu, V., V. Nacu, J. F. Charles, W. M. Henne, H. T. McMahon, S. Nandi, H. Ketchum, R. Harris, M. C. Nakamura, and E. R. Stanley. 2012. PSTPIP2 deficiency in mice causes osteopenia and increased differentiation of multipotent myeloid precursors into osteoclasts. *Blood* 120: 3126–3135.
40. Pollock, J. D., D. A. Williams, M. A. Gifford, L. L. Li, X. Du, J. Fisherman, S. H. Orkin, C. M. Doerschuk, and M. C. Dinauer. 1995. Mouse model of X-linked chronic granulomatous disease, an inherited defect in phagocyte superoxide production. *Nat. Genet.* 9: 202–209.
41. Hou, B., B. Reizis, and A. L. DeFranco. 2008. Toll-like receptors activate innate and adaptive immunity by using dendritic cell-intrinsic and -extrinsic mechanisms. *Immunity* 29: 272–282.
42. Shen, F. W., Y. Saga, G. Litman, G. Freeman, J. S. Tung, H. Cantor, and E. A. Boyse. 1985. Cloning of Ly-5 cDNA. *Proc. Natl. Acad. Sci. USA* 82: 7360–7363.
43. Passegué, E., E. F. Wagner, and I. L. Weissman. 2004. JunB deficiency leads to a myeloproliferative disorder arising from hematopoietic stem cells. *Cell* 119: 431–443.
44. Voehringer, D., H. E. Liang, and R. M. Locksley. 2008. Homeostasis and effector function of lymphopenia-induced "memory-like" T cells in constitutively T cell-depleted mice. *J. Immunol.* 180: 4742–4753.
45. Wang, G. G., K. R. Calvo, M. P. Pasillas, D. B. Sykes, H. Häcker, and M. P. Kamps. 2006. Quantitative production of macrophages or neutrophils ex vivo using conditional Hoxb8. *Nat. Methods* 3: 287–293.
46. Goodridge, H. S., C. N. Reyes, C. A. Becker, T. R. Katsumoto, J. Ma, A. J. Wolf, N. Bose, A. S. Chan, A. S. Magee, M. E. Danielson, et al. 2011. Activation of the innate immune receptor Dectin-1 upon formation of a 'phagocytic synapse'. *Nature* 472: 471–475.
47. Bedouhène, S., F. Moulti-Mati, M. Hurtado-Nedelec, P. M. Dang, and J. El-Benna. 2017. Luminol-amplified chemiluminescence detects mainly superoxide anion produced by human neutrophils. *Am. J. Blood Res.* 7: 41–48.
48. Kielland, A., T. Blom, K. S. Nandakumar, R. Holmdahl, R. Blomhoff, and H. Carlsen. 2009. In vivo imaging of reactive oxygen and nitrogen species in

Downloaded from http://www.jimmunol.org/ at Institute of Physiology ASCR on March 12, 2020

inflammation using the luminescent probe L-012. *Free Radic. Biol. Med.* 47: 760–766.
49. Cassel, S. L., S. C. Eisenbarth, S. S. Iyer, J. J. Sadler, O. R. Colegio, L. A. Tephly, A. B. Carter, P. B. Rothman, R. A. Flavell, and F. S. Sutterwala. 2008. The Nalp3 inflammasome is essential for the development of silicosis. *Proc. Natl. Acad. Sci. USA* 105: 9035–9040.
50. Aratani, Y. 2018. Myeloperoxidase: its role for host defense, inflammation, and neutrophil function. *Arch. Biochem. Biophys.* 640: 47–52.
51. Adachi, O., T. Kawai, K. Takeda, M. Matsumoto, H. Tsutsui, M. Sakagami, K. Nakanishi, and S. Akira. 1998. Targeted disruption of the MyD88 gene results in loss of IL-1- and IL-18-mediated function. *Immunity* 9: 143–150.
52. Condliffe, A. M., E. R. Chilvers, C. Haslett, and I. Dransfield. 1996. Priming differentially regulates neutrophil adhesion molecule expression/function. *Immunology* 89: 105–111.
53. Miralda, I., S. M. Uriarte, and K. R. McLeish. 2017. Multiple phenotypic changes define neutrophil priming. *Front. Cell. Infect. Microbiol.* 7: 217.
54. Vogt, K. L., C. Summers, E. R. Chilvers, and A. M. Condliffe. 2018. Priming and de-priming of neutrophil responses in vitro and in vivo. *Eur. J. Clin. Invest.* 48(Suppl. 2): e12967.
55. Crawford, N., and P. Eggleton. 1991. Dynamic changes in neutrophil cytoskeleton during priming and subsequent surface stimulated functions. *Biochem. Soc. Trans.* 19: 1048–1055.
56. Yao, Y., H. Matsushima, J. A. Ohtola, S. Geng, R. Lu, and A. Takashima. 2015. Neutrophil priming occurs in a sequential manner and can be visualized in living animals by monitoring IL-1β promoter activation. *J. Immunol.* 194: 1211–1224.
57. Jennings, R. T., M. Strengert, P. Hayes, J. El-Benna, C. Brakebusch, M. Kubica, and U. G. Knaus. 2014. RhoA determines disease progression by controlling neutrophil motility and restricting hyperresponsiveness. *Blood* 123: 3635–3645.
58. Liu, Z., T. Yago, N. Zhang, S. R. Panicker, Y. Wang, L. Yao, P. Mehta-D'souza, L. Xia, C. Zhu, and R. P. McEver. 2017. L-selectin mechanochemistry restricts neutrophil priming in vivo. *Nat. Commun.* 8: 15196.
59. Belambri, S. A., L. Rolas, H. Raad, M. Hurtado-Nedelec, P. M.-C. Dang, and J. El-Benna. 2018. NADPH oxidase activation in neutrophils: role of the phosphorylation of its subunits. *Eur. J. Clin. Invest.* 48(Suppl. 2): e12951.
60. El-Benna, J., P. M. Dang, M. A. Gougerot-Pocidalo, J. C. Marie, and F. Braut-Boucher. 2009. p47phox, the phagocyte NADPH oxidase/NOX2 organizer: structure, phosphorylation and implication in diseases. *Exp. Mol. Med.* 41: 217–225.
61. Dapino, P., F. Dallegri, L. Ottonello, and C. Sacchetti. 1993. Induction of neutrophil respiratory burst by tumour necrosis factor-alpha; priming effect of solid-phase fibronectin and intervention of CD11b-CD18 integrins. *Clin. Exp. Immunol.* 94: 533–538.
62. Dang, P. M., A. Stensballe, T. Boussetta, H. Raad, C. Dewas, Y. Kroviarski, G. Hayem, O. N. Jensen, M. A. Gougerot-Pocidalo, and J. El-Benna. 2006. A specific p47phox -serine phosphorylated by convergent MAPKs mediates neutrophil NADPH oxidase priming at inflammatory sites. *J. Clin. Invest.* 116: 2033–2043.
63. El Benna, J., J. Han, J. W. Park, E. Schmid, R. J. Ulevitch, and B. M. Babior. 1996. Activation of p38 in stimulated human neutrophils: phosphorylation of the oxidase component p47phox by p38 and ERK but not by JNK. *Arch. Biochem. Biophys.* 334: 395–400.
64. van de Veerdonk, F. L., S. P. Smeekens, L. A. Joosten, B. J. Kullberg, C. A. Dinarello, J. W. van der Meer, and M. G. Netea. 2010. Reactive oxygen species-independent activation of the IL-1beta inflammasome in cells from patients with chronic granulomatous disease. *Proc. Natl. Acad. Sci. USA* 107: 3030–3033.
65. van Bruggen, R., M. Y. Köker, M. Jansen, M. van Houdt, D. Roos, T. W. Kuijpers, and T. K. van den Berg. 2010. Human NLRP3 inflammasome activation is Nox1-4 independent. *Blood* 115: 5398–5400.
66. Meissner, F., R. A. Seger, D. Moshous, A. Fischer, J. Reichenbach, and A. Zychlinsky. 2010. Inflammasome activation in NADPH oxidase defective mononuclear phagocytes from patients with chronic granulomatous disease. *Blood* 116: 1570–1573.
67. Meissner, F., K. Molawi, and A. Zychlinsky. 2008. Superoxide dismutase 1 regulates caspase-1 and endotoxic shock. *Nat. Immunol.* 9: 866–872.
68. Gabelloni, M. L., F. Sabbione, C. Jancic, J. Fuxman Bass, I. Keitelman, L. Iula, M. Oleastro, J. R. Geffner, and A. S. Trevani. 2013. NADPH oxidase derived reactive oxygen species are involved in human neutrophil IL-1β secretion but not in inflammasome activation. *Eur. J. Immunol.* 43: 3324–3335.
69. Nakahira, K., J. A. Haspel, V. A. Rathinam, S. J. Lee, T. Dolinay, H. C. Lam, J. A. Englert, M. Rabinovitch, M. Cernadas, H. P. Kim, et al. 2011. Autophagy proteins regulate innate immune responses by inhibiting the release of mitochondrial DNA mediated by the NALP3 inflammasome. *Nat. Immunol.* 12: 222–230.
70. Deguine, J., and G. M. Barton. 2014. MyD88: a central player in innate immune signaling. *F1000Prime Rep.* 6: 97.
71. Okamoto, K., T. Nakashima, M. Shinohara, T. Negishi-Koga, N. Komatsu, A. Terashima, S. Sawa, T. Nitta, and H. Takayanagi. 2017. Osteoimmunology: the conceptual framework unifying the immune and skeletal systems. *Physiol. Rev.* 97: 1295–1349.
72. Lee, N. K., Y. G. Choi, J. Y. Baik, S. Y. Han, D. W. Jeong, Y. S. Bae, N. Kim, and S. Y. Lee. 2005. A crucial role for reactive oxygen species in RANKL-induced osteoclast differentiation. *Blood* 106: 852–859.
73. Yang, S., P. Madyastha, S. Bingel, W. Ries, and L. Key. 2001. A new superoxide-generating oxidase in murine osteoclasts. *J. Biol. Chem.* 276: 5452–5458.
74. Sasaki, H., H. Yamamoto, K. Tominaga, K. Masuda, T. Kawai, S. Teshima-Kondo, K. Matsuno, C. Yabe-Nishimura, and K. Rokutan. 2009. Receptor activator of nuclear factor-kappaB ligand-induced mouse osteoclast differentiation is associated with switching between NADPH oxidase homologues. *Free Radic. Biol. Med.* 47: 189–199.
75. Goettsch, C., A. Babelova, O. Trummer, R. G. Erben, M. Rauner, S. Rammelt, N. Weissmann, V. Weinberger, S. Benkhoff, M. Kampschulte, et al. 2013. NADPH oxidase 4 limits bone mass by promoting osteoclastogenesis. *J. Clin. Invest.* 123: 4731–4738.
76. Garrett, I. R., B. F. Boyce, R. O. Oreffo, L. Bonewald, J. Poser, and G. R. Mundy. 1990. Oxygen-derived free radicals stimulate osteoclastic bone resorption in rodent bone in vitro and in vivo. *J. Clin. Invest.* 85: 632–639.
77. Ferguson, P. J., M. A. Lokuta, H. I. El-Shanti, L. Muhle, X. Bing, and A. Huttenlocher. 2008. Neutrophil dysfunction in a family with a SAPHO syndrome-like phenotype. *Arthritis Rheum.* 58: 3264–3269.
78. Hurtado-Nedelec, M., S. Chollet-Martin, D. Chapeton, J. P. Hugot, G. Hayem, and B. Gérard. 2010. Genetic susceptibility factors in a cohort of 38 patients with SAPHO syndrome: a study of PSTPIP2, NOD2, and LPIN2 genes. *J. Rheumatol.* 37: 401–409.
79. Jansson, A., E. D. Renner, J. Ramser, A. Mayer, M. Haban, A. Meindl, V. Grote, J. Diebold, V. Jansson, K. Schneider, and B. H. Belohradsky. 2007. Classification of non-bacterial osteitis: retrospective study of clinical, immunological and genetic aspects in 89 patients. *Rheumatology (Oxford)* 46: 154–160.

Downloaded from http://www.jimmunol.org/ at Institute of Physiology ASCR on March 12, 2020

Supplementary figures

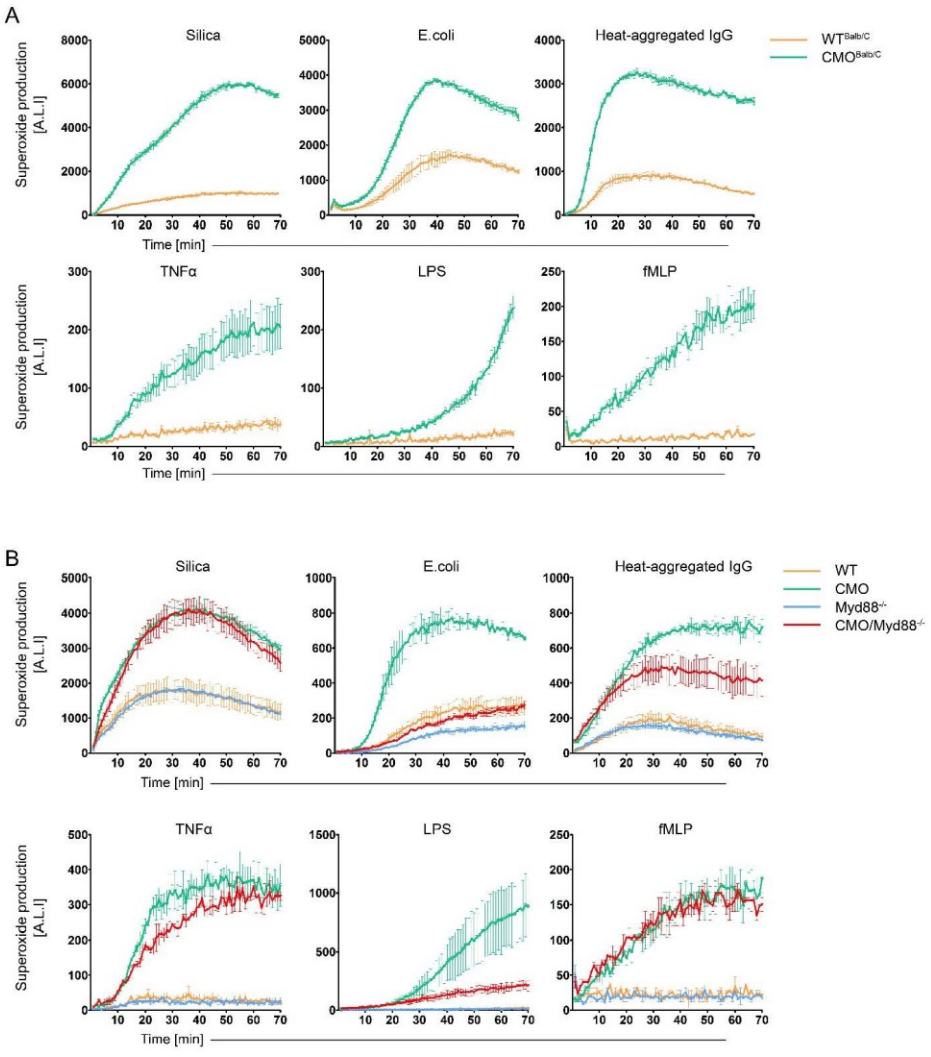

Supplemental Figure 1. Dysregulated superoxide production by bone marrow cells from *Pstpip2*^{cmo} mice of Balb/c (**A**) or MyD88$^{-/-}$ (**B**) genetic background. Superoxide production was detected by Luminol-based assay, exactly as described in Figure 2A.

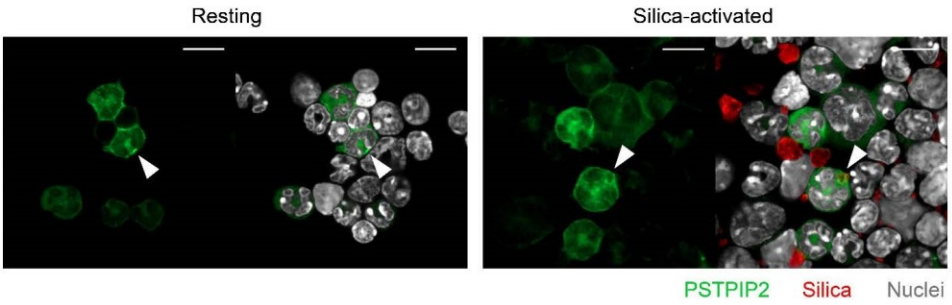

Supplemental Figure 2. Subcellular localization of PSTPIP2 in primary murine neutrophils. Neutrophils differentiated in vivo from bone marrow cells transduced with retroviral PSTPIP2-EGFP construct (green) were activated or not by silica (red) and imaged by confocal microscopy. Bar = 10 μm.

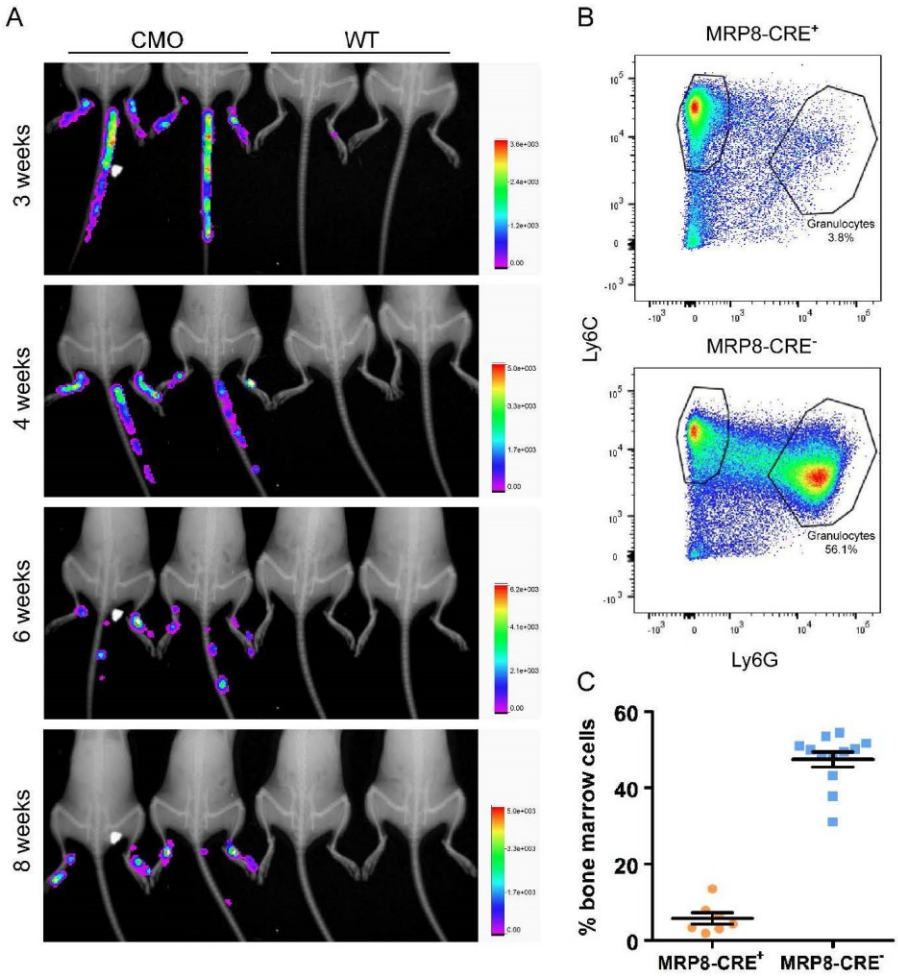

Supplemental Figure 3. Neutrophil-dependent ROS production in vivo. (**A**) In vivo ROS production in WT and *Pstpip2*^{cmo} (CMO) mice of various ages: representative images of the animals that were part of the analysis in Figure 5B. (**B**) Neutrophils were depleted in Pstpip2^{cmo}-DTA mice via MRP8-CRE-dependent expression of Diphtheria toxin (MRP8-CRE^{+}) or left untouched in the absence of MRP8-CRE (MRP8-CRE^{-}). Representative FACS plots of CD11b^{+} cells further gated for granulocytes (Ly6G^{High}, Ly6C^{Low}) and monocytes (Ly6G^{-}, Ly6C^{High}) are shown. (**C**) Efficiencies of granulocyte depletion in multiple animals. Shown are the percentages of granulocytes gated as in (B).

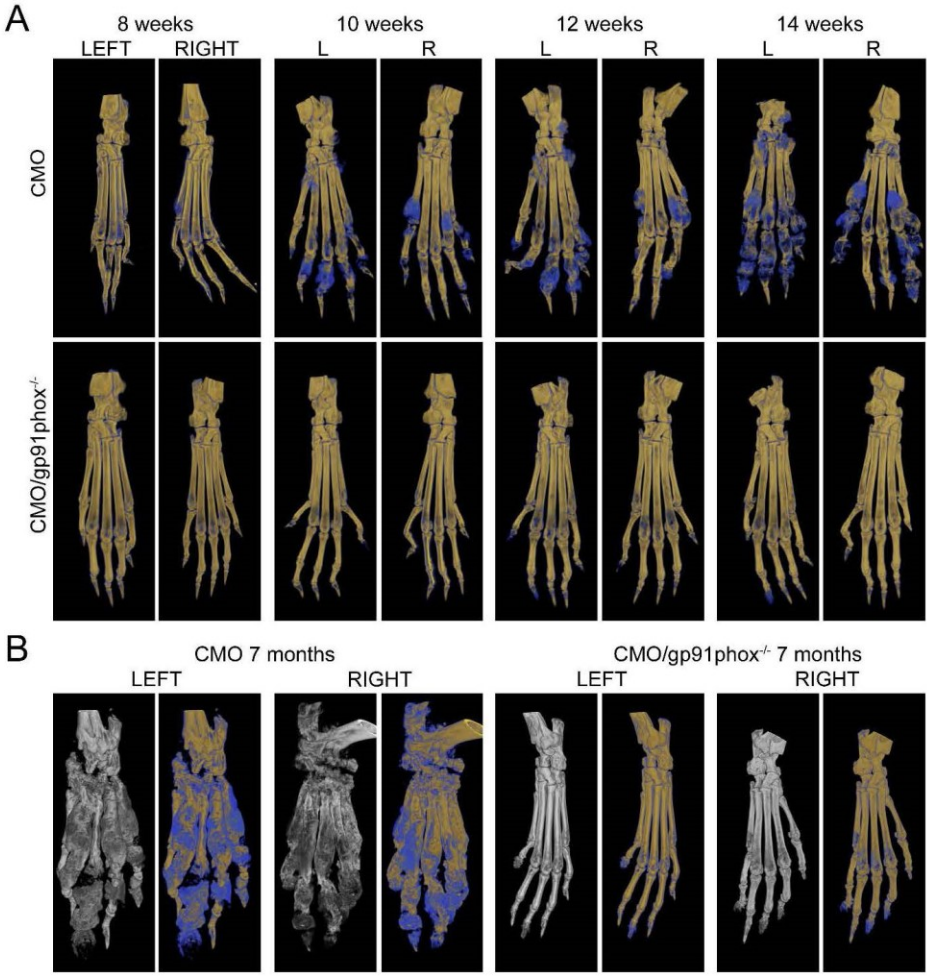

Supplemental Figure 4. Time course of bone damage development in *Pstpip2^{cmo}* and *Pstpip2^{cmo}/gp91phox$^{-/-}$* mice. (**A**) Mice at 8, 10, 12, and 14 weeks of age were anesthetized and their hind paw bones were imaged on X-ray µCT scanner. (**B**) The same analysis performed on 7 months old animals. Grey images represent visualization of total bone tissue. Pseudocolor images distinguish between old (in yellow) and newly formed (in blue) bone mass.

Video Article

Expression of Fluorescent Fusion Proteins in Murine Bone Marrow-derived Dendritic Cells and Macrophages

Jarmila Kralova[1,2], Daniela Glatzova[1,2,3], Simon Borna[1,2], Tomas Brdicka[1]

[1]Laboratory of Leukocyte Signalling, Institute of Molecular Genetics of the ASCR

[2]Faculty of Science, Charles University

[3]Department of Biophysical Chemistry, J. Heyrovsky Institute of Physical Chemistry ASCR

Correspondence to: Tomas Brdicka at tomas.brdicka@img.cas.cz

URL: https://www.jove.com/video/58081
DOI: doi:10.3791/58081

Keywords: Biology, Issue 140, Dendritic cells, macrophages, myeloid cells, differentiation, murine bone marrow cells, cytokines, M-CSF, GM-CSF, viral infection, GFP tagged protein

Date Published: 10/30/2018

Citation: Kralova, J., Glatzova, D., Borna, S., Brdicka, T. Expression of Fluorescent Fusion Proteins in Murine Bone Marrow-derived Dendritic Cells and Macrophages. *J. Vis. Exp.* (140), e58081, doi:10.3791/58081 (2018).

Abstract

Dendritic cells and macrophages are crucial cells that form the first line of defense against pathogens. They also play important roles in the initiation of an adaptive immune response. Experimental work with these cells is rather challenging. Their abundance in organs and tissues is relatively low. As a result, they cannot be isolated in large numbers. They are also difficult to transfect with cDNA constructs. In the murine model, these problems can be partially overcome by *in vitro* differentiation from bone marrow progenitors in the presence of M-CSF for macrophages or GM-CSF for dendritic cells. In this way, it is possible to obtain large amounts of these cells from very few animals. Moreover, bone marrow progenitors can be transduced with retroviral vectors carrying cDNA constructs during early stages of cultivation prior to their differentiation into bone marrow derived dendritic cells and macrophages. Thus, retroviral transduction followed by differentiation *in vitro* can be used to express various cDNA constructs in these cells. The ability to express ectopic proteins substantially extends the range of experiments that can be performed on these cells, including live cell imaging of fluorescent proteins, tandem purifications for interactome analyses, structure-function analyses, monitoring of cellular functions with biosensors and many others. In this article, we describe a detailed protocol for retroviral transduction of murine bone marrow derived dendritic cells and macrophages with vectors coding for fluorescently-tagged proteins. On the example of two adaptor proteins, OPAL1 and PSTPIP2, we demonstrate its practical application in flow cytometry and microscopy. We also discuss the advantages and limitations of this approach.

Video Link

The video component of this article can be found at https://www.jove.com/video/58081/

Introduction

Myeloid cells represent an indispensable part of our defense mechanisms against pathogens. They are able to rapidly eliminate microbes, as well as dying cells. In addition, they are also involved in regulating tissue development and repair and in maintaining homeostasis[1,2,3]. All myeloid cells differentiate from common myeloid progenitors in the bone marrow. Their differentiation into many functionally and morphologically distinct subsets is to a large extent controlled by cytokines and their various combinations[4]. The most intensively studied myeloid cell subsets include neutrophilic granulocytes, macrophages and dendritic cells. Defects in any of these populations lead to potentially life-threatening consequences and cause severe dysfunctions of the immune system in humans and mice[1,2,3,5,6].

Unlike neutrophilic granulocytes, dendritic cells and macrophages are tissue resident cells and their abundance in immune organs is relatively low. As a result, the isolation and purification of primary dendritic cells and macrophages for experiments requiring a large number of these cells is expensive and often impossible. To solve this problem, protocols have been developed to obtain large amounts of homogenous macrophages or dendritic cells *in vitro*. These approaches are based on the differentiation of murine bone marrow cells in the presence of cytokines: macrophage colony-stimulating factor (M-CSF) for macrophages and granulocyte-macrophage colony-stimulating factor (GM-CSF) or Flt3 ligand for dendritic cells[7,8,9,10,11,12]. Cells generated by this method are commonly described in the literature as bone marrow derived macrophages (BMDMs) and bone marrow derived dendritic cells (BMDCs). They have more physiological properties in common with primary macrophages or dendritic cells than with corresponding cell lines. Another major advantage is the possibility of obtaining these cells form genetically modified mice[13]. Comparative studies between wild-type cells and cells derived from genetically modified mice are often critical for uncovering novel functions of genes or proteins of interest.

Analysis of subcellular localization of proteins in living cells requires the coupling of a fluorescent label to the protein of interest *in vivo*. This is most commonly achieved by expressing genetically encoded fusion construct composed of an analyzed protein coupled (often via a short linker) to a fluorescent protein (*e.g.*, green fluorescent protein (GFP))[14,15,16]. The expression of fluorescently tagged proteins in dendritic cells or macrophages is challenging. These cells are generally difficult to transfect by standard transfection procedures and the efficiencies tend to be very low. Moreover, the transfection is transient, it generates cellular stress and achieved intensity of fluorescence might not be sufficient for

Copyright © 2018 Journal of Visualized Experiments

microscopy[17]. In order to obtain a reasonable fraction of these cells with a sufficient level of transgene expression, the infection of bone marrow progenitor cells with retroviral vectors and their subsequent differentiation into BMDMs or BMDCs has become a very efficient approach. It has allowed for the analysis of the proteins of myeloid origin in their native cellular environment, both in a steady state or during processes that are critical for immune response such as phagocytosis, immunological synapse formation or migration. Here, we describe a protocol that allows stable expression of fluorescently tagged proteins of interest in murine bone marrow derived macrophages and dendritic cells.

Protocol

All methods described here have been approved by the Expert Committee on the Welfare of Experimental Animals of the Institute of Molecular Genetics and by the Academy of Sciences of the Czech Republic.

1. Reagent Preparation

1. Prepare the ammonium-chloride-potassium (ACK) buffer. Add 4.145 g of NH_4Cl and 0.5 g of $KHCO_3$ to 500 mL of ddH_2O, then add 100 µL of 0.5 M ethylenediaminetetraacetic acid (EDTA) and filter-sterilize.
2. Prepare polyethylenimine (PEI) solution. Add 0.1 g of PEI to 90 mL of ddH_2O. While stirring, add 1 M HCl dropwise until the pH is lower than 2.0. Stir for up to 3 h until PEI is dissolved and then adjust pH to 7.2 with 1 M NaOH. Adjust the volume to 100 mL with ddH_2O and filter-sterilize. Make 1–2 mL aliquots and store at -20 °C.
   NOTE: After thawing, PEI can be stored at 4 °C for up to 2 weeks but should not be re-frozen.
3. Prepare cell culture supernatants containing M-CSF or GM-CSF. These supernatants can be made in advance and stored in -80 °C. To make these supernatants, grow the cytokine-producing cells (J558 cells for GM-CSF [18] or CMG 14-12 cells for M-CSF [19]) in a 10 cm Petri dish in Dulbecco's modified Eagle's medium (DMEM) with 10% fetal bovine serum (FBS) to confluence. Then transfer all cells to 200 mL of media in T150 tissue culture flask and culture for additional 4 days at 5% CO_2/37 °C. Collect the supernatant and filter over 0.2 µm sterilization filter. Make aliquots and store these at -80 °C.
4. Prepare 100 mL of cell culture medium: DMEM supplemented with 10% heat inactivated FBS and cell culture supernatants from cells secreting GM-CSF (for BMDC differentiation) or M-CSF (for BMDM differentiation).
   NOTE: The amount of cytokines in these supernatants can vary and the working concentration has to be determined empirically. Typically, 2–3% supernatant from cell lines producing GM-CSF (the recommended starting concentration is 2%) or 5–10% supernatant from CMG 14–12 cells producing M-CSF (the recommended starting concentration is 10%) is used. Alternatively, purified commercially available M-CSF at 10 ng/mL and GM-CSF at 20 ng/mL can be used with results virtually identical to cytokine-containing supernatants, *i.e.*, without any effect on the rate of differentiation, infection efficiency and subcellular localization of EGFP-tagged constructs. Antibiotics, including penicillin G (100 IU/mL), streptomycin (100 µg/mL), and gentamicin (40 µg/mL), can be used for cell culture at any step of the protocol unless otherwise stated.

2. Production of Retrovirus

CAUTION: Although retroviral vectors are relatively safe when compared to other types of viral vectors, they still pose a potential safety hazard. Therefore, it is crucial to work with the utmost care and appropriate protective equipment, and to adhere to all safety regulations and legal requirements for working with viral particles.

1. Plate a single cell suspension of Platinum-Eco (Plat-E) packaging cells in a 10 cm Petri dish and cultivate in 15 mL of DMEM containing 10% FBS until 50-60 % confluent (24 h). Cells should grow in a monolayer and should not form clumps in culture.
2. Pipette 20 µg of retroviral construct (*e.g.*, the construct expressing the fluorescently tagged protein of interest in the pMSCV vector) and 10 µg of pCL-Eco packaging vector[20] into 1 mL of DMEM (without serum and antibiotics) and gently mix.
3. To a second tube, add 75 µL of PEI in 1 mL of DMEM (without serum and antibiotics). Incubate 5 min at room temperature (RT) and then mix the contents of both tubes together and incubate for additional 10 min at RT.
   NOTE: Addition of pCL-Eco is optional. It is coding for the ecotropic viral receptor and may increase the virus titer.
4. Carefully replace the medium on Plat-E cells with 8 mL of fresh DMEMsupplemented with 2% FBS. Pre-warm the medium to 37 °C before use. Do not use antibiotics during transfection, since antibiotics may reduce the transfection efficiency.
5. Carefully add (in drops) the mixture prepared in Step 2.3 on the Plat-E cells, and incubate for 4 h at 37 °C.
6. After the incubation, exchange the medium on Plat-E cells for 10 mL of pre-warmed DMEM containing 10% FBS, and cultivate the cells for 24 h at 37 °C. During this incubation, Plat-E cells will produce virus into the media.
7. After 24 h, collect the medium containing retroviral particles from Platinum Eco cells using a 5 mL pipette and transfer it to a 15 mL centrifuge tube (= "supernatant 1" containing ecotropic retroviral particles).
8. To avoid contamination by Plat-E cells in viral supernatants, spin the collected virus at 1250 × g for 5 min at 4 °C. For the best results, the virus should be used immediately for infection.
   NOTE: Aliquots of virus can also be stored at -80 °C for later use. However, it will result in certain reduction in transduction efficiency. Avoid repetitive freezing/thawing of the virus, since it leads to virus degradation.
9. Add 10 mL of pre-warmed DMEM with 10% FBS to Plat-E cells and cultivate for another 24 h at 37 °C.
10. Repeat steps 2.7. and 2.8. to obtain "supernatant 2".

3. Murine Bone Marrow Cell Isolation

1. Sacrifice the mouse using cervical dislocation or other approved method. Spray the mouse with 70% ethanol.
2. Using tweezers and scissors, remove the skin as well as part of muscles from hind legs. Carefully dislodge the acetabulum from the hip joint without breaking the femur. Cut the paw in the ankle joint. Spray the bones (femur connected to tibia) with 70% ethanol and remove the rest of the muscles using a paper towel.

Copyright © 2018 Journal of Visualized Experiments

3. Place the bones in a 5 cm Petri dish containing sterile phosphate buffered saline (PBS) with 2% FBS (PBS-FBS). If preparing more bones, keep the Petri dish on ice until processed.
4. For securing cultivation sterility, perform all the following steps in a tissue culture hood.
5. Separate the femur from the tibia without breaking the bone ends (bend in the knee joint and carefully cut with scissors).
6. Process the bones one by one. Cut off a very small part of the epiphyses (approximately 1–2 mm) with scissors while holding the bone in tweezers.
7. Use a 30 G needle and a 2 or 5 mL syringe filled with PBS-FBS to flush the bone marrow cells from both ends of the bone into a 15 mL centrifuge tube. Move the needle inside the bone during the flushing in order to remove all the cells. If the needle gets clogged, change it.
   NOTE: Bones should turn from red to white during flushing. This indicates that the majority of the cells were removed from the bone. Use approximately 2–3 mL of PBS-FBS per bone.
8. Centrifuge the cells at 500 x g for 5 min at 4 °C.
9. Discard the supernatant and lyse the red blood cells by resuspending the pellet in 2.5 mL of ACK buffer for 2–3 min at room temperature. During the lysis, filter the bone marrow cells through a 100 µm cell strainer into a fresh 15 mL centrifug tube. Restore the tonicity by adding 12 mL of PBS-FBS.
   NOTE: Do not exceed 5 min of hypotonic lysis with ACK buffer to avoid cell death.
10. Centrifuge immediately at 500 x g for 5 min at 4 °C.

4. Bone Marrow Cell Differentiation into Bone Marrow Derived Macrophages

1. Resuspend the pellet of bone marrow cells in DMEM supplemented with 10 % FBS and antibiotics (see the note after Step 1.4. for antibiotic concentration) and count the cells. For differentiation into BM derived macrophages, plate 5–10 x 10^6 of bone marrow cells in a 10 cm non-tissue culture treated (bacterial) Petri dish with 10 mL of pre-prepared DMEM media with serum and M-CSF from Step 1.4.
   NOTE: The yield of the bone marrow cells is approximately 4 x 10^7 per 6–8 week-old C57BL/6J mouse.
2. Incubate the cells in cell culture incubator for 3 days at 5% CO_2, 37 °C.
   NOTE: During the first 2 days, cells do not look very vital, as a large number of apoptotic cells is present (cells unable to differentiate into myeloid cells and terminally differentiated cells).
3. After 3 days, the bone marrow cell culture begins to look vital and clusters of dividing cells are formed. First adherent cells can already be observed. At this point, supplement the cells with fresh cytokine media.
4. Add 10 mL of pre-warmed DMEM media with serum and M-CSF (from Step 1.4) into each 10 cm Petri dish and return it in the cell culture incubator. There is no need to remove the old media during this step.
   NOTE: Bone marrow macrophages are fully differentiated after 5–7 days in culture. The best time for harvesting is at day 6–8, where majority of cells are adherent and the Petri dish is completely covered.
5. At day 5, take the Petri dish into the cell culture hood and incline the dish until the media is almost reaching the edge of the dish. Carefully take out 15 mL of the media from the surface near the edge, and the cells tend to stay in the middle of the dish. Add the same volume of pre-warmed media with M-CSF and place the dish back into the incubator.
   NOTE: If media is aspirated slowly and carefully, almost no cells are lost. However, it is also possible to centrifuge the aspirated media and add the cells back to the culture, to ensure that no non-adherent (*i.e.*, incompletely differentiated) cells are lost.
6. For experiments, only adherent cells (macrophages) are used. To harvest cells, on day 6 or 7, remove all media and floating cells. Wash the dish once with pre-warmed PBS without serum.
7. Add 5 mL of 0.02% EDTA in PBS, and incubate for 3–5 min at 37 °C in tissue culture incubator.
8. Using a 5 mL pipette, remove the cells from the dish by a stream of PBS-EDTA and place them in a 50 mL centrifuge tube with 25 mL of PBS. If needed, pool more dishes together.
9. Centrifuge immediately at 500 x g for 5 min at 4 °C.
10. Resuspend the macrophage pellet in DMEM media and count the cells. Verify the expression of macrophage surface differentiation markers (CD11b and F4/80) by flow cytometry.
11. For experiments requiring the cells to be in suspension, *e.g.*, flow cytometry experiments, qPCR or western blot analysis, use the macrophages directly. For experiments with adherent macrophages, plate the cells in the tissue culture plate according to the experimental setup.
12. The cells are already fully differentiated. Keep them in the media suitable for the intended experiment or in the original growth and differentiation media with M-CSF.
    NOTE: For working with adherent macrophages, transfer them into a new plate at least 6 h before use (ideally overnight) to allow for the full adhesion to the new surface. The small fraction of floating cells can be removed before experiment.

5. Bone Marrow Cell Differentiation into Bone Marrow Derived Dendritic Cells

1. Follow the protocol for BMDMs with adjustments specific for BMDCs described below in steps 5.2–5.4.
2. Resuspend the obtained pellet of bone marrow cells in DMEMsupplemented with 10% FBS and antibiotics and count the cells (by following Step 4.1 of macrophage protocol). For differentiation into dendritic cells, plate 1–1.5 x 10^7 bone marrow cells in a 10 cm non-tissue culture treated (bacterial) Petri dish in 10 mL of pre-prepared DMEM media with serum and GM-CSF (from Step 1.4.).
3. Follow the same cultivation steps as in BMDM protocol (steps 4.3–4.5. of macrophage protocol). Use DMEM media with serum and GM-CSF instead of M-CSF. Since for BMDCs the cultivation time is longer (typically 10–12 days), add 1–2 additional feedings in 3 day intervals (by removing the supernatant and adding a new cultivation media as described in Step 4.5.).
4. This part of the protocol is virtually the same as the corresponding part of the macrophage protocol (Steps 4.6–4.12. of macrophage protocol). For experiments use only adherent cells. On day 10-12, collect the cells using EDTA, count and plate them on a new surface. Verify the expression of surface differentiation markers of dendritic cells (CD11c+, CD11b+, F4/80-) by flow cytometry.

Copyright © 2018 Journal of Visualized Experiments

6. Production of BMDMs and BMDCs Expressing EGFP-tagged Protein of Interest

1. Resuspend the pellet of bone marrow cells obtained in Step 3.10. in DMEM supplemented with 10 % FBS and antibiotics and count the cells. For the infection, use 2–5 x 10^6 of BM cells per well of a 6-well tissue culture treated plate.
2. Plate the cells in 1 mL of the prepared DMEM media per well, supplemented either with M-CSF for differentiation into BMDMs or with GM-CSF for differentiation in BMDCs. Keep the cells for 4–6 h in a tissue culture incubator with 5% CO_2 at 37 °C.
3. Add 2 mL of freshly collected virus ("supernatant 1") supplemented with polybrene (12 µg/mL, final concentration 8 µg/mL after addition to the cells).
   NOTE: Frozen aliquot of the virus-containing supernatant can also be used, but efficacy will be lower.
4. Centrifuge the plate at 1,250 x g for 90 min at 30 °C (with slow acceleration and deceleration). Then, incubate for 4 h with 5% CO_2 at 37 °C.
5. Optional: Replace 2 mL of the culture media with fresh medium containing respective cytokine (M-CSF or GM-CSF) and culture with 5% CO_2 at 37 °C. On the second day, remove 2 mL of culture media and repeat the whole infection procedure (Step 6.3–6.4) with 2 mL of freshly collected virus ("supernatant 2").
   NOTE: This step may increase infection efficacy. Improvement after the second infection is dependent on the cell type and target protein and in our experience can vary from 30% increase in efficiency to no improvement at all.
6. Collect the non-adherent cells, transfer to a 15 mL centrifuge tube, and spin at 500 x g for 5 min (4 °C). Discard the supernatant.
7. Resuspend the cell pellet in 10 mL of culture media with M-CSF or GM-CSF, place the cells into a 10 cm non-tissue culture treated Petri dish and culture at 37 °C, 5% CO_2. Optimal number of cells for a 10 cm dish is 5–10 x 10^6 for BM-derived macrophages and 10–15 x 10^6 for BM-derived dendritic cell.
   NOTE: Smaller dishes or plates can be used, but cell numbers must be adjusted accordingly.
8. Follow the macrophage and dendritic cell cultivation and differentiation protocol described in step 4 and 5.

Representative Results

Signaling adaptor proteins are usually small proteins without any enzymatic activity. They possess various interaction domains or motifs, which mediate binding to other proteins involved in signal transduction, including tyrosine kinases, phosphatases, ubiquitin ligases and others[21]. For the demonstration of the functionality of this protocol myeloid cell adaptors PSTPIP2 and OPAL1 were selected. PSTPIP2 is a well characterized protein involved in the regulation of inflammatory response[22]. It is a cytoplasmic protein which can also be recruited to cellular membranes via its F-bar domain. Second protein is a transmembrane adaptor OPAL1, expected to be associated with cellular membranes. Its physiological function is still unknown. However, in acute lymphoblastic leukemia, expression of OPAL1 is associated with better prognosis[23].

cDNA constructs coding for PSTPIP2 or OPAL1 fused via a short linker (GSGGGS or Myc-tag, respectively) to EGFP at the C-terminus were cloned into the pMSCV retroviral vector using standard methods of cDNA cloning. This construct was then transfected into Plat-E cells together with the packaging vector pCL-Eco. The resulting supernatants containing retroviruses were used for the transduction of bone marrow cells, followed by the differentiation into BMDMs and BMDCs. The efficacy of Plat-E transfection was evaluated by flow cytometry after the collection of the second virus-containing supernatant. Mean transfection efficiency was 62% for PSTPIP2-EGFP and 53% for OPAL1 and the results were highly reproducible (**Figure 1A, B**). OPAL1 construct seemed to be more toxic for Plat-E cells (assessed by the appearance of floating/dying cells in culture), resulting in a reduction in the percentages of transfected cells.

Differentiation status of the bone marrow derived macrophages and dendritic cells (transduced with PSTPIP2-EGFP and OPAL1-EGFP retroviral constructs) was assessed by flow cytometry. Mature macrophage population is defined by CD11b and F4/80 expression, while dendritic cells express the CD11c lineage marker. More than 90% of cells in both types of culture were positive for their respective markers (**Figure 2A, B**). Finally, we determined the expression level of PSTPIP2-EGFP and OPAL1-EGFP constructs in BMDMs and BMDCs by a simple flow cytometry measurement of EGFP fluorescence. The mean percentage of EGFP-positive macrophages was 71% for PSTPIP2-EGFP and 62% for OPAL1-EGFP (**Figure 3A**). In case of dendritic cells, the efficiency was lower, 32% for PSTPIP2 and 9% for OPAL1 (**Figure 3B**). The results of multiple experiments demonstrate the reproducibility of this method (**Figure 3C**).

We typically do not determine the virus concentration in the supernatants that we use in infections. We prefer to use the virus supernatants fresh, immediately after collection, while the virus titer determination requires three additional days. As a result, the information on virus titer can only be obtained *ex post*. However, it can still be useful when addressing technical issues and problems. To assess the virus concentration in supernatants from Plat E cells transfected with PSTPIP2-EGFP and OPAL1-EGFP constructs, we incubated NIH-3T3 cells with serially diluted virus-containing supernatants collected from these transfected Plat-E cells and determined virus titer exactly as described by Zjablovskaja *et al* in previously published JoVE article[24]. In three independent experiments, the virus titer ranged from 1.1 x 10^6 to 4.4 x 10^6 TU/mL. We did not observe any substantial differences between PSTPIP1-EGFP and OPAL1-EGFP constructs and between supernatants from day 1 and day 2. When these supernatants were used for bone marrow cell infections according to the protocol we are describing in this article, the multiplicity of infection (MOI) ranged from 1.1 to 4.4. Interestingly, within this range, we did not observe any correlation between MOI and infection efficiency.

In **Figure 4**, PSTPIP2-EGFP and OPAL1-EGFP expressed in BMDMs and BMDCs were visualized by confocal microscopy. Fully differentiated macrophages and dendritic cells have a characteristic shape. The change in morphology from small rounded progenitor cells to the large cells of irregular shapes confirms successful differentiation. In macrophages, PSTPIP2 was cytoplasmic with partial localization at the plasma membrane. OPAL1 appeared to be also partially targeted to the plasma membrane. The rest was likely associated with intracellular membranes, such as the endoplasmic reticulum and Golgi complex. However, to confirm this localization, specific organelle markers would have to be used. In dendritic cells, the membrane localization was less apparent.

Copyright © 2018 Journal of Visualized Experiments

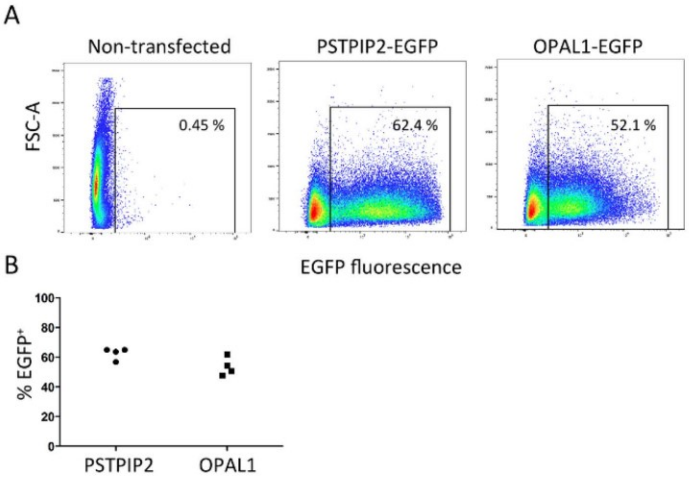

Figure 1: Efficiency of Plat-E cell transfection. For transfection of Plat-E cells, two constructs encoding adaptor proteins PSTPIP2 and OPAL1 fused with EGFP (PSTPIP2-EGFP and OPAL1-EGFP) were cloned into the pMSCV vector. Standard PEI transfection was performed. The efficacy of transfection was evaluated by flow cytometry of the Plat-E cells after the collection of the second viral supernatant. (**A**). Representative flow cytometry plot. (**B**). Graph showing results of four independent experiments. Please click here to view a larger version of this figure.

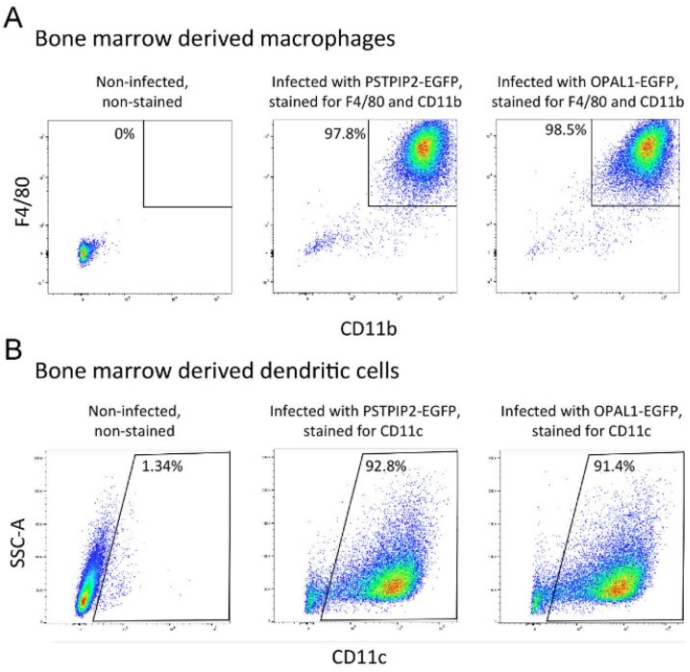

Figure 2: Assessment of the differentiation status of BMDMs (A) and BMDCs (B). Surface expression of specific macrophage and dendritic cell lineage markers was measured by flow cytometry at day 8 of cultivation. Dead cells were gated out based on their side and forward scatter properties and staining with Hoechst 33258. The results are representative of at least 3 independent experiments. Please click here to view a larger version of this figure.

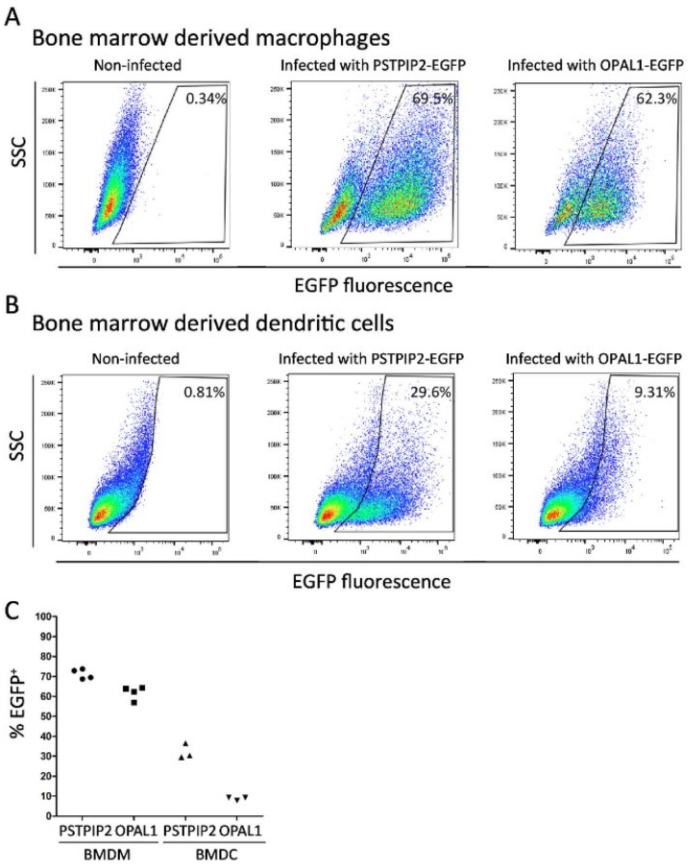

Figure 3: Assessment of the expression of PSTPIP2-EGFP and OPAL1-EGFP. EGFP fluorescence in BMDMs (**A**) and BMDCs (**B**) retrovirally transduced with PSTPIP2-EGFP and OPAL1-EGFP constructs was measured by flow cytometry at day 8 of cultivation. (**C**). Graph showing the results of multiple independent experiments. BMDMs and BMDCs were gated as in **Figure 2**. Please click here to view a larger version of this figure.

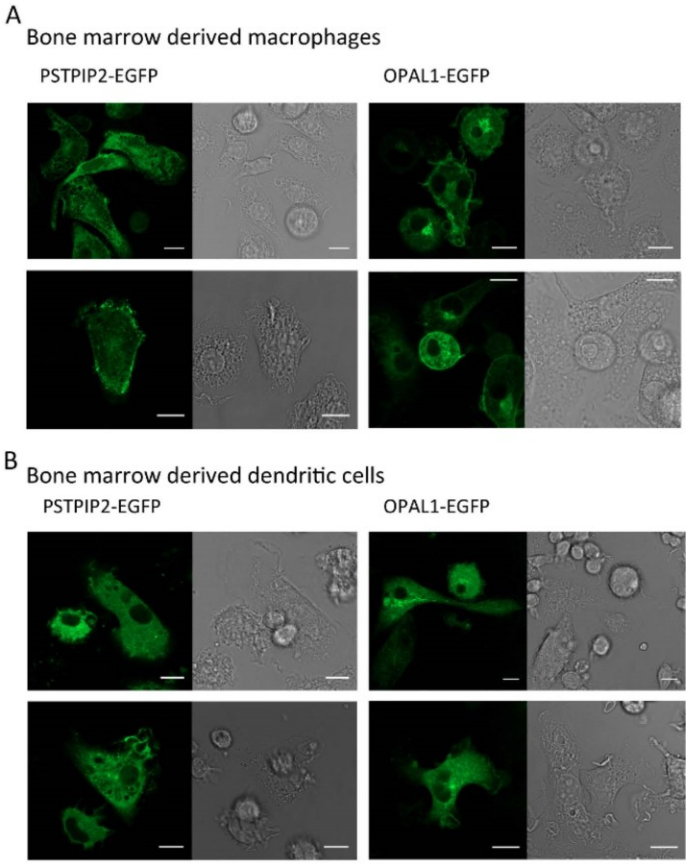

Figure 4: Representative images of macrophages and dendritic cells expressing PSTPIP2 or OPAL1. BMDMs (**A**) and BMDCs (**B**) expressing PSTPIP2 and OPAL1 were visualized by live imaging confocal microscopy. EGFP fluorescence in green is shown on the left side of each panel, bright field image on the right. Scale bar = 10 µm. The results are representative of at least three independent experiments. Please click here to view a larger version of this figure.

Discussion

The expression of protein of interest in target cells is a key step in many types of biological studies. Differentiated macrophages and dendritic cells are difficult to transfect by standard transfection and retroviral transduction techniques. Bypassing the transfection of these differentiated cells with retroviral transduction of bone marrow progenitors, followed by differentiation when they already carry the desired construct, is a critical step allowing the expression of ectopic cDNAs in these cell types. An example of successful use of this method can be found in our recent publication[25]. Here, we provide a cost-effective protocol for achieving stable expression of the construct of choice in bone marrow-derived dendritic cells and macrophages using this approach. The procedure we present is relatively inexpensive and simple, yet delivering very good results. Reagents used in this protocol allow for its routine use even under a relatively restrictive budget. The protocol for Plat-E transfection employs PEI as a transfection reagent. Compared to other chemical transfection agents, PEI is of a very low cost, while its efficiency is similar to the majority of other widely used compounds. However, PEI can be replaced with many different commercially available transfection reagents in this step without any loss of efficiency. As a guiding principle, transfection protocols known to work with commonly used HEK293 cells typically perform well with Plat-E cells, too. Another cost-effective measure is the utilization of cytokine-containing supernatants instead of purified recombinant cytokines. The use of these supernatants requires some optimization. However, when the standard protocol for their preparation is established and followed, the variability between individual batches of these supernatants becomes very low, usually requiring no changes in working concentrations between individual lots. The efficiencies of BMDM and BMDC differentiation with these supernatants are, in our experience, identical to purified cytokines.

In addition to retroviral transduction, other well-established methods of mammalian cell transfection exist, including chemical transfection (typically using cationic lipids or cationic polymers forming complexes with DNA), electroporation and the use of other types of viral vectors,

Copyright © 2018 Journal of Visualized Experiments

mainly adenoviral and lentiviral systems[26,27,28,29,30]. Although very high titers and efficiencies can be achieved with adenovirus-based gene delivery, the preparation of corresponding plasmids and viral particles are more difficult and time-consuming than in the case of retroviral systems[29]. In addition, adenovirus elicits inflammatory response in dendritic cells and macrophages[29,31,32] and for optimum performance in murine hematopoietic cells mouse strain carrying transgenic adenovirus receptor is required[33]. On the other hand, the generation of lentiviral particles carrying the gene of interest is a relatively simple process, virtually identical to the one utilized for retroviruses. In contrast to the ecotropic retroviral vectors used in this protocol, lentiviruses are capable of infecting non-proliferating cells of multiple species, including humans[34]. This may be an important advantage under specific experimental conditions. However, this feature also greatly compromises the safety of these vectors. In our opinion, for gene delivery to BMDMs and BMDCs, retroviruses provide the best balance of efficiency, safety and ease of use. Retroviral DNA constructs can be easily prepared using simple standard molecular cloning techniques. Virus is produced by packaging the cell lines directly to the culture supernatant and further virus purification is usually not necessary. Ecotropic retroviruses also do not readily infect human cells, which makes their use relatively safe. However, there also are some general disadvantages associated with the use of retroviral vectors. The major limiting factor is that these viruses infect only proliferating cells[35]. This feature does not significantly affect the protocol described here, but it limits the range of applications where retroviral vectors can be used. The size of the gene of interest that can be cloned into these vectors is also limited and the viral particle titer decreases with increasing insert size. With pMSCV vectors, we usually start seeing effects of insert size at around 3 kbp. With further increases in insert size, the infection efficiency gradually declines.

The chemical transfection and electroporation are easier to use, safer and less time-consuming than any of the virus-based procedures[26,27,28,30]. However, in BMDMs and BMDCs, they can stimulate responses to foreign nucleic acids[31] and they generate more cellular stress. In addition, some chemical transfection reagents increase cell auto-fluorescence that may interfere with flow cytometry or microscopy analyzes. Due to the transient nature of expression, they can only be used with mature differentiated BMDMs or BMDCs. In contrast, the sequences introduced with retroviral vectors are permanently integrated into the genome of the target cells and allow for a stable long-lasting expression compatible with the time scale of the differentiation protocols[34,35]. However, this feature also increases the risk of insertional mutagenesis. Due to the relatively random nature of the vector integration, its effects on large populations of cells are limited. However, they may be visible at the level of individual cells. Additional problems may arise when a construct expressed from the retroviral vector affects dendritic cell or macrophage differentiation, resulting in failure to generate differentiated BMDMs or BMDCs from the infected progenitors. To some extent, this may be overcome by adjusting the infection conditions to achieve low expression levels (*e.g.*, by reducing the virus titer) or through the use of an inducible expression system. The use of EGFP fused to the protein of interest or as a reporter also allows for sorting of cells with expression level corresponding to experiment goals and limitations. Finally, we should also mention problems common to all transfection/transduction procedures. These include mainly overexpression artefacts, such as protein misfolding, mislocalization and toxicity[36]. Protein toxicity could be the reason why OPAL1 was relatively difficult to express. Its example clearly illustrates that the nature of the expressed protein can substantially affect the effectiveness of this method. However, despite this, we were able to obtain sufficient quantities of OPAL1-EGFP expressing cells for microscopy analysis with this method, demonstrating its usefulness even when dealing with difficult targets. In addition, it would be possible to increase the percentages of transduced cells by FACS sorting if required by a particular application. The low infection efficiency can also be partially overcome by increasing viral particle concentration using various methods or ready-to-use kits. In our hands, ultrafiltration of the viral supernatant on centrifugal filters with a molecular weight cut off of 100 kDa has proven to provide the best balance between efficiency and required effort.

Bone marrow derived macrophages and dendritic cells are widely used tools in phagocyte immunology. They are more physiologically relevant than available cell lines. They can be generated in relatively high numbers and, at the same time, lack the genetic heterogeneity and instability characteristic of cell lines. Another advantage is that they can be generated from genetically modified mice to study the effects of genetic modification on a relatively abundant and homogenous cell population. This is particularly useful in biochemical studies, where relatively large amounts of cells are typically required. The ability to transduce these cells with cDNA constructs opens up additional possibilities of research based on the reconstitution or complementation of genetic defects in these cells and structure-function analysis.

Disclosures

The authors have nothing to disclose.

Acknowledgements

This work was supported by Czech Science Foundation (GACR) (project number 16-07425S), by Charles University Grant Agency (GAUK) (project number 923116) and by institutional funding from the Institute of Molecular Genetics, Academy of Sciences of the Czech Republic (RVO 68378050).

References

1. Moghaddam, A. S. *et al.* Macrophage plasticity, polarization and function in health and disease. *Journal of Cellular Physiology.* (2018).
2. Qian, C., & Cao, X. Dendritic cells in the regulation of immunity and inflammation. *Seminars in Immunology.* **35** 3-11, (2018).
3. Amulic, B., Cazalet, C., Hayes, G. L., Metzler, K. D., & Zychlinsky, A. Neutrophil function: from mechanisms to disease. *Annual Review of Immunology.* **30** 459-489, (2012).
4. Kondo, M. Lymphoid and myeloid lineage commitment in multipotent hematopoietic progenitors. *Immunological Reviews.* **238** (1), 37-46, (2010).
5. Andrews, T., & Sullivan, K. E. Infections in patients with inherited defects in phagocytic function. *Clinical Microbiology Reviews.* **16** (4), 597-621, (2003).
6. Wynn, T. A., Chawla, A., & Pollard, J. W. Macrophage biology in development, homeostasis and disease. *Nature.* **496** (7446), 445-455, (2013).
7. Austin, P. E., McCulloch, E. A., & Till, J. E. Characterization of the factor in L-cell conditioned medium capable of stimulating colony formation by mouse marrow cells in culture. *Journal of Cellular Physiology.* **77** (2), 121-134, (1971).

Copyright © 2018 Journal of Visualized Experiments

8. Scheicher, C. *et al.* Recombinant GM-CSF induces in vitro differentiation of dendritic cells from mouse bone marrow. *Advances in Experimental Medicine and Biology.* **329** 269-273, (1993).
9. Stanley, E. R. The macrophage colony-stimulating factor, CSF-1. *Methods in Enzymology.* **116** 564-587, (1985).
10. Weischenfeldt, J., & Porse, B. Bone Marrow-Derived Macrophages (BMM): Isolation and Applications. *Cold Spring Harbor Protocols.* **2008** pdb prot5080, (2008).
11. Lutz, M. B. *et al.* An advanced culture method for generating large quantities of highly pure dendritic cells from mouse bone marrow. *Journal of Immunological Methods.* **223** (1), 77-92, (1999).
12. Inaba, K. *et al.* Generation of large numbers of dendritic cells from mouse bone marrow cultures supplemented with granulocyte/macrophage colony-stimulating factor. *Journal of Experimental Medicine.* **176** (6), 1693-1702, (1992).
13. Chamberlain, L. M., Godek, M. L., Gonzalez-Juarrero, M., & Grainger, D. W. Phenotypic non-equivalence of murine (monocyte-) macrophage cells in biomaterial and inflammatory models. *Journal of Biomedical Materials Research Part A.* **88** (4), 858-871, (2009).
14. Remington, S. J. Green fluorescent protein: a perspective. *Protein Science.* **20** (9), 1509-1519, (2011).
15. Hoffman, R. M. Strategies for In Vivo Imaging Using Fluorescent Proteins. *Journal of Cellular Biochemistry.* **118** (9), 2571-2580, (2017).
16. Telford, W. G., Hawley, T., Subach, F., Verkhusha, V., & Hawley, R. G. Flow cytometry of fluorescent proteins. *Methods.* **57** (3), 318-330, (2012).
17. Zhang, X., Edwards, J. P., & Mosser, D. M. The expression of exogenous genes in macrophages: obstacles and opportunities. *Methods in Molecular Biology.* **531** 123-143, (2009).
18. Zal, T., Volkmann, A., & Stockinger, B. Mechanisms of tolerance induction in major histocompatibility complex class II-restricted T cells specific for a blood-borne self-antigen. *Journal of Experimental Medicine.* **180** (6), 2089-2099, (1994).
19. Takeshita, S., Kaji, K., & Kudo, A. Identification and Characterization of the New Osteoclast Progenitor with Macrophage Phenotypes Being Able to Differentiate into Mature Osteoclasts. *Journal of Bone and Mineral Research.* **15** (8), 1477-1488, (2000).
20. Naviaux, R. K., Costanzi, E., Haas, M., & Verma, I. M. The pCL vector system: rapid production of helper-free, high-titer, recombinant retroviruses. *Journal of Virology.* **70** (8), 5701-5705, (1996).
21. Janssen, E., & Zhang, W. Adaptor proteins in lymphocyte activation. *Current Opinion in Immunology.* **15** (3), 269-276, (2003).
22. Ferguson, P. J., & Laxer, R. M. New discoveries in CRMO: IL-1beta, the neutrophil, and the microbiome implicated in disease pathogenesis in Pstpip2-deficient mice. *Seminars in Immunopathology.* **37** (4), 407-412, (2015).
23. Holleman, A. *et al.* Expression of the outcome predictor in acute leukemia 1 (OPAL1) gene is not an independent prognostic factor in patients treated according to COALL or St Jude protocols. *Blood.* **108** (6), 1984-1990, (2006).
24. Zjablovskaja, P., Danek, P., Kardosova, M., & Alberich-Jorda, M. Proliferation and Differentiation of Murine Myeloid Precursor 32D/G-CSF-R Cells. *Journal of Visualized Experiments: JoVE.* (132), (2018).
25. Kralova, J. *et al.* The Transmembrane Adaptor Protein SCIMP Facilitates Sustained Dectin-1 Signaling in Dendritic Cells. *Journal of Biological Chemistry.* **291** (32), 16530-16540, (2016).
26. Maess, M. B., Wittig, B., & Lorkowski, S. Highly efficient transfection of human THP-1 macrophages by nucleofection. *Journal of Visualized Experiments: JoVE.* (91), e51960, (2014).
27. Bowles, R., Patil, S., Pincas, H., & Sealfon, S. C. Optimized protocol for efficient transfection of dendritic cells without cell maturation. *Journal of Visualized Experiments: JoVE.* (53), e2766, (2011).
28. Siegert, I. *et al.* Electroporation of siRNA into mouse bone marrow-derived macrophages and dendritic cells. *Methods in Molecular Biology.* **1121** 111-119, (2014).
29. Lee, C. S. *et al.* Adenovirus-Mediated Gene Delivery: Potential Applications for Gene and Cell-Based Therapies in the New Era of Personalized Medicine. *Genes & Diseases.* **4** (2), 43-63, (2017).
30. Jin, L., Zeng, X., Liu, M., Deng, Y., & He, N. Current progress in gene delivery technology based on chemical methods and nano-carriers. *Theranostics.* **4** (3), 240-255, (2014).
31. Muruve, D. A. *et al.* The inflammasome recognizes cytosolic microbial and host DNA and triggers an innate immune response. *Nature.* **452** (7183), 103-107, (2008).
32. Yang, Y., Li, Q., Ertl, H. C., & Wilson, J. M. Cellular and humoral immune responses to viral antigens create barriers to lung-directed gene therapy with recombinant adenoviruses. *Journal of Virology.* **69** (4), 2004-2015, (1995).
33. Tallone, T. *et al.* A mouse model for adenovirus gene delivery. *Proceedings of the National Academy of Sciences of the United States of America.* **98** (14), 7910-7915, (2001).
34. Milone, M. C., & O'Doherty, U. Clinical use of lentiviral vectors. *Leukemia.* (2018).
35. McTaggart, S., & Al-Rubeai, M. Retroviral vectors for human gene delivery. *Biotechnology Advances.* **20** (1), 1-31, (2002).
36. Gibson, T. J., Seiler, M., & Veitia, R. A. The transience of transient overexpression. *Nature Methods.* **10** (8), 715-721, (2013).

Copyright © 2018 Journal of Visualized Experiments

Materials List for:

Expression of Fluorescent Fusion Proteins in Murine Bone Marrow-derived Dendritic Cells and Macrophages

Jarmila Kralova[1,2], Daniela Glatzova[1,2,3], Simon Borna[1,2], Tomas Brdicka[1]

[1]Laboratory of Leukocyte Signalling, Institute of Molecular Genetics of the ASCR

[2]Faculty of Science, Charles University

[3]Department of Biophysical Chemistry, J. Heyrovsky Institute of Physical Chemistry ASCR

Correspondence to: Tomas Brdicka at tomas.brdicka@img.cas.cz

URL: https://www.jove.com/video/58081
DOI: doi:10.3791/58081

Materials

Name	Company	Catalog Number	Comments
DMEM	Thermo Fisher Scientific, Waltham, MA, USA	15028	
Fetal bovine serum (FBS)	Thermo Fisher Scientific, Waltham, MA, USA	10270	For media suplementation
$KHCO_3$	Lachema, Brno, Czech Republic	N/A	
NH_4Cl	Sigma-Aldrich (Merck, Kenilworth, NJ, USA)	A9434	
Penicillin	BB Pharma AS, Prague, Czech Republic	N/A	PENICILIN G 1,0 DRASELNÁ SOL' BIOTIKA
Streptomycin	Sigma-Aldrich (Merck, Kenilworth, NJ, USA)	S9137	Streptomycin sulfate salt powder
Gentamicin	Dr. Kulich Pharma, Hradec Králové, Czech Republic	N/A	
Polyethylenimine, linear, MW 25,000	Polyscience, Warrington, PA, USA	23966	
Polybrene	Sigma-Aldrich (Merck, Kenilworth, NJ, USA)	H9268	
EDTA	Sigma-Aldrich (Merck, Kenilworth, NJ, USA)	E5134	
PBS	Prepared in-house by media facility of IMG ASCR, Prague, Czech Republic	N/A	
APC anti-mouse/human CD11b Antibody, clone M1/70	BioLegend (San Diego, CA, USA)	101212	flow cytometry analysis
PE anti-mouse F4/80 Antibody, clone BM8	BioLegend (San Diego, CA, USA)	123110	flow cytometry analysis
APC anti-mouse CD11c Antibody, clone N418	BioLegend (San Diego, CA, USA)	117310	flow cytometry analysis
M-CSF	PeproTech (Rocky Hill, NJ, USA)	315-02	
GM-CSF	PeproTech (Rocky Hill, NJ, USA)	315-03	
Hoechst 33258	Thermo Fisher Scientific, Waltham, MA, USA	H1398	flow cytometry analysis use at 1-2 µg/mL

Copyright © 2018 Journal of Visualized Experiments